SOME OPTICAL AND MAGNETO-OPTICAL STUDIES

ON THIN ABSORBING FILMS

by

A. J. Taylor, B.Sc.

A thesis submitted for the degree of Doctor of Philosophy in the University of London.

R. H. C. LIBRARY
CLASS No. BPJ Tay
ACC. No. 108312
DATE ACQ Apr 72

Department of Physics,
Royal Holloway College.

August, 1971.

ProQuest Number: 10123888

All rights reserved

INFORMATION TO ALL USERS
The quality of this reproduction is dependent upon the quality of the copy submitted.

In the unlikely event that the author did not send a complete manuscript
and there are missing pages, these will be noted. Also, if material had to be removed,
a note will indicate the deletion.

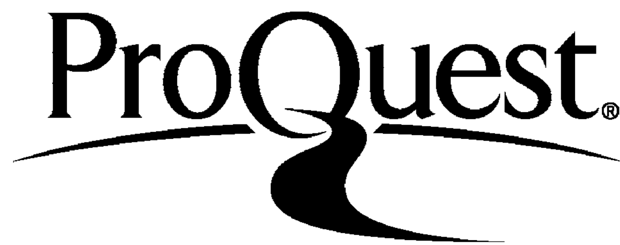

ProQuest 10123888

Published by ProQuest LLC(2016). Copyright of the Dissertation is held by the Author.

All rights reserved.
This work is protected against unauthorized copying under Title 17, United States Code.
Microform Edition © ProQuest LLC.

ProQuest LLC
789 East Eisenhower Parkway
P.O. Box 1346
Ann Arbor, MI 48106-1346

CONTENTS

		Page
ABSTRACT		1
CHAPTER 1	A review of the uses and methods of determining optical constants	3
1.1	Introduction	3
1.2	The relevance of optical constants to present day physics.	5
1.3	Optical constants of absorbing materials.	7
1.4	Methods of determining n and k for opaque absorbing films.	8
1.4.1	Ellipsometry: reflection polarimetry.	9
1.4.2	Reflectometry: non-polarimetric methods.	12
1.5	Methods of determining the optical constants of thin partially transparent absorbing films.	16
1.5.1	The ellipsometric method of determining n_2 and k_2 for thin films.	18
1.5.2	Normal incidence methods of determining n_2 and k_2 for thin films.	20
1.5.3	Some non-normal incidence methods of determining n_2 and k_2 for partially transparent thin absorbing films.	23
1.6	The methods adopted.	27
1.6.1	Opaque absorbing films.	27
1.6.2	Partially-transparent absorbing films.	30
CHAPTER 2	Optimization of, and errors arising from, a reflection method of obtaining n and k for opaque, absorbing films.	32
Abstract		32
2.1	Introduction.	32
2.2	The analytical solution to the Fresnel reflectance equations.	33

Page

2.3	A computer study of the boundary in $(R_{//}, R_{\perp}, \theta)$ space, enclosing values of n and k which satisfy Fresnel's equations.	34
2.4	A brief description of the analytical solution to the boundary evaluation.	36
2.5	Optimization and sensitivity of n and k to $R_{//}$, $R_{\perp}$ and θ.	40
2.6	A more detailed study of the errors involved when the $R_{//}$, $R_{\perp}$ method is used to obtain n and k.	44
2.7	The method of error investigation.	45
2.8	The computer results.	47
2.8.1	Angular dependence of σ.	47
2.8.2	Variation of σ with ΔR.	52
2.9	The case of normal incidence.	55
2.10	General conclusions.	58
CHAPTER 3	Studies of a new optimized reflection ratio method of obtaining n_2 and k_2 for thin films.	60
Abstract		60
3.1	Introduction	60
3.2	The method of resultant waves to obtain an expression for $R_{//}/R_{\perp}$.	62
3.3	Application of the reflection ratio method to thin films.	66
3.4	Optimization of the reflection ratio method.	74
3.5	The precision required for measurements of d/λ.	86
3.6	The precision required for measurements of the ratio $R_{//}/R_{\perp}$.	90
3.7	An investigation of the possible use of the optimized, ratio method for weakly absorbing films.	98
3.8	Summary	99

		Page
CHAPTER 4	A reflectometer for determining the optical constants of opaque and partially transparent absorbing films.	101
Abstract		101
4.1	A review of previous instrumentation.	101
4.2	Description of reflectometer.	105
4.2.1	The reflectometer.	105
4.2.2	The substrate holder for measurements in air.	110
4.2.3	The graded wavelength filter attachment.	112
4.2.4	The optical cell for measurements at low temperatures.	114
4.3	Method of use and some typical results.	118
CHAPTER 5	Specimen preparation.	130
Introduction		130
5.1	Substrates and their preparation.	132
5.1.1	Float glass.	132
5.1.2	Mica substrates for electron microscopy.	137
5.2	Ordinary high vacuum (O.H.V.) preparation of films.	139
5.2.1	The 12" evaporation system for use with tungsten boats and filaments.	139
5.2.2	The electron ring-gun evaporation system.	144
5.3	Ultra-high vacuum (U.H.V.) preparation of films.	146
5.3.1	General description of U.H.V. system.	146
5.3.2	Details of the main service chamber.	149
5.3.3	Details of the U.H.V. pumping group.	151
5.3.4	Details of the U.H.V. electronic controls and power units.	152

		Page
5.3.5	U.H.V. pressure measurement and the ionization gauge.	153
5.3.6	Residual gas analysis inside the U.H.V. system.	155
5.3.7	Evaporation assembly.	157
5.4	U.H.V. pump-down and evaporation procedures.	160
5.4.1	Pump-down procedure.	160
5.4.2	Evaporation procedure.	161
CHAPTER 6	A review of the rare earth metals and some proposed experimental studies.	163
Abstract		163
6.1	Introduction - a brief review of the rare-earth metals.	163
6.1.1	Electronic configuration of the rare-earth metals.	164
6.2	The optical and magneto-optical properties of the rare-earth metals.	165
6.2.1	Band structure calculations for the rare-earth metals.	171
6.2.2	The optical properties of Gd and Tb.	173
6.3	The optical properties of rare-earth oxides.	174
CHAPTER 7	Experimentally observed optical and magneto-optical properties of evaporated films of Ni, Gd, Tb and terbium oxide.	177
Abstract		177
7.1	Optical properties of thin films of Ni grown in U.H.V.	177
7.2	Optical and structural properties of opaque films of Gd grown in U.H.V.	181
7.2.1	The optical constants of Gd in the paramagnetic state.	188

		Page
7.2.2	Some low temperature optical measurements.	200
7.2.3	Some magneto-optical measurements on Gd films.	203
7.3	Optical properties of Tb films grown in O.H.V.	206
7.3.1	Tb films deposited onto mica substrates.	208
7.3.2	Optical constants of Tb films deposited onto glass substrates in O.H.V.	214
7.3.3	The optical properties of terbium oxide thin films.	224
7.4	Overall conclusions and further work.	230
APPENDIX I	List of symbols	234
APPENDIX II	Computer programme for generating 'Calcomp' curves of n_2 against $(R_{//} / R_{\perp})$ for the method of Chapter 3.	237
APPENDIX III	Electropolishing of stainless steel.	243
REFERENCES		244
ACKNOWLEDGMENTS		250

ABSTRACT

An up-to-date review of methods of determining optical constants n and k of optically absorbing material in bulk and film form is given.

It is shown in this thesis that an analytical method which involves measuring $R_{\parallel}$ and $R_{\perp}$ at an angle of incidence θ is capable of yielding n and k values accurate to ± 0.05 providing $R_{\parallel}$ and $R_{\perp}$ are measured to ± 0.004 at values of θ close to 74°. At angles other than 74° the method can become very insensitive to changes in n and k, particularly at normal incidence.

For a thin absorbing film supported by a dielectric substrate, an optimized reflection ratio method for determining optical constants has been devised. Measurement of $(R_{\parallel}/R_{\perp})$ is made at two values of θ and the film thickness d is determined independently. Optimum values of θ are given for $1 \leqslant n \leqslant 4$, $0.2 \leqslant k \leqslant 4$, $0.05 \leqslant d/\lambda \leqslant 0.25$. Accuracies in n and k of ± 0.05 can be obtained if $(R_{\parallel}/R_{\perp})$ is measured to ± 0.01 and d/λ to ± 0.005.

A simple reflectometer is described to measure $R_{\parallel}$ and $R_{\perp}$ to ± 0.006 at non-normal incidence in the wavelength range 400-700nm. An optical cell and a Helmholtz coil system are described which facilitate low temperature optical constants and megneto-optical measurements.

The optical constants of U.H.V. deposited Ni films are reported for film thicknesses 25 to 60nm, and are shown to have very little thickness dependence.

Optically opaque, polycrystalline Gd films deposited in U.H.V. onto float-glass substrates are shown to be almost completely orientated with the c-axis perpendicular to the plane of the film. Dispersion curves of $\sigma(\omega)$ are reported for the paramagnetic and ferromagnetic phases of such films, and are similar to previous work. Some observed

secondary $\sigma(\omega)$ structure at $\sim$ 2.6eV. appears to have previously gone unobserved. The results of preliminary, transverse ferromagnetic Kerr effect measurements on Gd films are also reported.

Electron microscopy and optical constants studies of Tb and Tb_4O_7 films evaporated at $\leqslant 9 \times 10^{-6}$ torr, are presented and shown to be in accordance with a previous study of the terbium oxide system. A $\sigma(\omega)$ dispersion curve is also given for a metallic Tb film.

CHAPTER 1

A REVIEW OF THE USES, AND METHODS OF DETERMINING OPTICAL CONSTANTS

1.1 Introduction

The interactions of electromagnetic radiation with matter form one of the fundamental and continuing concerns of physics, and are the basis of innumerable technological devices. Since the days of Newton, the macroscopic optical behaviour of materials has been studied and classified in terms of measureable quantities, such as refractive index, absorption, reflection and transmission coefficients. With the advent of classical electromagnetic theory (Maxwell), and modern quantum electrodynamics, these so called 'optical constants' assumed a central role in evaluating basic electronic processes in materials. Further, as materials technology developed precise knowledge of optical constants permitted the production of specific devices, such as optical multilayer filters and anti-reflection coatings. Optical constants are therefore of fundamental theoretical and practical interest and it is of prime importance that they be measured to as high a degree of accuracy as possible.

The purpose of this thesis has been to show that by using optimization techniques it is possible to evaluate accurate methods of determining optical constants. In addition, some well established methods have been shown to be inherently inaccurate. Using the optimized experimental methods optical constants of some rare earth metals have been determined.

R.H.C.
LIBRARY

This thesis concerns itself with the optical constants of isotropic material. The optical constants of interest are the real part n and imaginary part k, of the complex refractive index $\hat{n} = n-ik$ of the material. The optical constants n and k are related to the real and imaginary parts of the complex dielectric constant $\hat{\epsilon} = \epsilon_1 - i\epsilon_2$ by means of the equations,

$$\epsilon_1 = n^2-k^2 \qquad (1.1)$$

$$\epsilon_2 = 2nk \qquad (1.2)$$

The optical conductivity $\sigma(\omega)$, which is the electrical conductivity of a solid when made to conduct by the oscillating electrical field of a light wave, is related to n and k and the optical frequency by the equation,

$$\sigma(\omega) = nk\omega/2\pi \qquad (1.3)$$

For ferromagnetic solids, the interaction with electromagnetic radiation may be characterized by a complex magneto-optical parameter M which is written in terms of real and imaginary M_1 and M_2 respectively.

A definitive list of symbols used in this thesis is given in Appendix I.

The optical constants n and k may be used to investigate the optical properties of thin absorbing films, such as metals and semiconductors, in which k is appreciably greater than zero. The interest in films rather than bulk material is largely a matter of convenience; good surfaces may be obtained for optical studies of metals which are difficult to polish in bulk form. In addition films have a large number of technological applications and so it is of interest to catalogue as much information about material in thin film form as possible. Thin films often show properties which do

not occur in material of bulk form, and these are of great interest in their own right. We shall be primarily interested in the optical properties of metal films for wavelengths in the visible range (400 to 700nm), although the work in Chapters 2 and 3 applies to all wavelengths. Thin absorbing films may be roughly divided into those thin enough to transmit visible light and those so thick that they are effectively opaque. Both types of film are considered in this thesis.

1.2 The relevance of optical constants to present day physics

The importance of the optical constants both of bulk material and thin absorbing films to physics in general and solid state physics in particular, may be illustrated by quoting a number of examples:

(i) In recent years there has been a renewed interest in the optical properties of metals. This is largely due to the development of accurate electronic band structure calculations, (Callaway, 1958). From a knowledge of n and k at a number of known wavelengths an optical absorption curve ($\sigma(\omega)$ against photon energy) characteristic of the material can be obtained. Such a curve may be used to substantiate the electronic band structure calculations for the material or *vice-versa*. Now that techniques are readily available for preparing clean, film surfaces in ultra-high vacuum many of the hazards previously associated with such correlations are removed (Heavens, 1955). Good quantitative work of this sort on both bulk and thin film material has been carried out for nickel by Shiga and Pells (1969), for barium, strontium, europium and ytterbium by Endriz and Spicer (1970), and for opaque films of gadolinium

by Hodgson and Cleyet (1970). The problem remains, however, that films frequently display optical properties which not only deviate from those of the bulk material, but are also thickness dependent. Care must therefore be exercised when comparing experimental results with theoretical predictions.

(ii) The electronic band structure calculations for ferromagnetic materials may also be checked by measuring the magneto-optical parameters as a function of incident light energy. Krinchik (1959, 1964, 1968, 1969) has measured the magneto-optical parameters of polished bulk specimens of iron, nickel and cobalt, using the ferromagnetic Kerr effect, and has obtained quantitative agreement between his results and the theoretical band structure calculations.

(iii) The optical constants, n and k, of thin films of metals, such as silver, gold and platinum, and dielectrics such as MgF_2, ZnS, BiO_2 and TiO_2, are needed in the design of multi-layer thin film filters, anti-reflection coatings, beam splitters, laser end mirrors and thin film polarizers. Anders (1967) describes in detail the optical applications of thin films.

(iv) Recently, experimental (Edmond, 1966; Donovan, 1969; Spicer and Donovan, 1970) and theoretical (Herman and Van-Dyke, 1968; Davis and Mott, 1970; Davis and Shaw, 1970; Dow and Redfield, 1970) investigations have been made into the optical properties of amorphous materials in bulk and thin film form. Experimentally the function $\epsilon_2(\omega)$ is determined as a function of incident photon energy over a wide range (0.5-8eV), for the crystalline and amorphous form of the material. The $\epsilon_2(\omega)$ (absorption) spectra can

thus be compared for the two forms, and differences in the electronic density of states N(E) can be calculated. Amorphous germanium both in bulk and thin films has been extensively studied in this way and there is now a reasonable understanding of the electronic states present. It appears from this work that the density of states and electronic energy gaps do not change radically on going from the crystalline to amorphous condition.

1.3 Optical constants of absorbing materials

The optical constants of absorbing materials can be determined by measurements on light transmitted through thin film specimens, light reflected from either thin film or bulk specimens, or by a combination of reflection and transmission measurements on suitably thin films. A review of the appropriate experimental techniques is given in Chapter 4.

The optical properties of an absorbing material can be characterized by certain measurable quantities, e.g. reflection coefficients, and these quantities are related to the constants n and k via the generalized Fresnel reflectance equations, (Heavens, 1955). Until recently (Querry, 1969; Ditchburn, 1955) it was thought impossible to obtain n and k explicitly in terms of measured quantities, even for the case of reflection at a single interface. Consequently, a variety of procedures have been adopted to extract n and k values from the experimental data, e.g. graphical, numerical and curve-fitting methods. A review of some of these methods, which are especially useful for absorbing materials will be given in Section 1.4 of this Chapter. Chapter 2 describes in detail an optimized method for determining n and k based on the analytical solution of the

generalized Fresnel equations, which is superior to all existing methods.

Reflection from two surfaces, that is a thin semi-transparent film supported by an infinitely thick substrate, involves multiple internal reflections, and formulae for the reflection and transmission coefficients in terms of n and k have been derived (Heavens, 1964). There is no published work expressing n and k in terms of the reflection and transmission coefficients and, consequently many methods are in use for determining n and k from the existing equations. Such methods are reviewed in Section 1.5 of this Chapter. Chapter 3 describes how optimization techniques have been applied for the first time to the problem of determining n and k for thin absorbing layers on dielectric substrates, and how this leads to a new method of deducing n and k from measurements of reflected light at non-normal angles of incidence.

Chapter 7 of this thesis describes how the new optimized methods of determining n and k have been used to determine the optical constants of gadolinium (Gd) and terbium (Tb): rare earth metals which have previously received only scant attention from workers in the field of optical studies. Measurements of n and k for an oxide of Tb are also reported in Chapter 7. An attempt is made to explain the variation of the optical constants with photon energy for these films by means of existing band structure calculations. This is described at the end of Chapter 7.

1.4 Methods of determining n and k for opaque absorbing films

For opaque films, and bulk specimens, of absorbing materials it is necessary to use reflection techniques to deduce n and k.

Experimentally, light of a known wavelength is allowed to fall onto the specimen surface and some characteristic of the reflected light is measured. By a suitable choice of measurement sufficient information can be obtained from the reflected light to determine n and k from the generalized Fresnel reflectance equations.

There are two basic ways of analyzing the reflected light from the surface of an absorbing specimen:

(i) Polarimetry, which is the measurement of the effect of reflection on the state of polarization of the light used. Such measurements may be interpreted to yield n and k for the reflecting material.

(ii) Reflectometry, which is the determination of n and k from measurements of reflection coefficients. A reflection coefficient is the ratio of the reflected intensity to the incident intensity, and will depend on the conditions of incidence and light polarization. This thesis is primarily concerned with such methods.

1.4.1 Ellipsometry: reflection polarimetry

A brief review of polarimetric methods of determining n and k is given because, historically, they were the first methods used to investigate optical properties of materials, and they can yield more information about a surface, often with greater accuracy, than methods relying solely on reflection coefficient measurements. However, the rest of this Chapter will show that polarimetric methods when compared with non-polarimetric methods, are experimentally more cumbersome

if dispersion measurements are required, are certainly more expensive and require slightly more computation, when only the optical constants n and k are required.

Reflection polarimetry concerns the reflection of monochromatic, collimated, polarized light from the specimen surface. The state of polarization of the light reflected is specified by the phase and amplitude relationships between the two component plane waves into which the electric field oscillation may be resolved. One wave designated $//$, is parallel to the plane of incidence. The other, designated $\perp$, is perpendicular to the plane of incidence. If the $\perp$ and $//$ components are in phase the resultant wave is plane polarized, but a difference in phase corresponds to a resultant elliptical polarization. Reflection at the surface of an absorbing medium causes a phase change in the $\perp$ and $//$ components, and a change in the ratio of their amplitudes. The change in phase is characterized by an angle Δ, and the change in the amplitude ratio is $\tan\psi$. The ellipsometer measures Δ and ψ at some angle of incidence θ. McCrackin (1963) and Winterbottom (1955) have given general treatments of ellipsometry and previous reviews (Heavens, 1960; Vasicek, 1960; Abeles, 1963) concerning the measurement of n and k have also described ellipsometric methods.

The principle of the measurement of Δ and ψ will be explained in general terms: the incident monochromatic beam is transmitted in sequence by a collimator, a polarizer and a compensator (either a mica quarter-wave plate or a Babinet-Soleil compensator (Ellenbrock, 1927; Pfestorf, 1926; Herschkowitsch, 1931; Ives and Briggs, 1936)). The azimuthal orientations of these devices determine the amplitude ratio and phase difference of the $\perp$ and $//$ components of the incident beam. These orientations are adjusted so that the difference in

phase thereby produced just compensates that which results from reflection. Δ is thus measured. The plane polarized reflected beam is then transmitted through an analyzer to a telescope and finally to a detector. With the polarizer and compensator oriented as described, the analyzer can be rotated by an angle to extinguish the reflected beam. Experimental details of methods for analyzing the reflected light have been given by, Kent and Lawson (1937), O'Bryan (1936) and Archard et al., (1952). Archard et al., dispensed with the conventional compensator but used instead a considerable quantity of electronics.

Prior to 1955 explicit equations for n and k in terms of Δ, ψ and θ did not exist. Instead, approximation, graphical and curve fitting methods were employed to evaluate n and k. Such methods as those of Drude (1890), Tool (1910), Leberknight and Lustman (1934) fall into this category and are adequately described, along with others, by Heavens (1955). In 1955 Ditchburn obtained expressions for n and k as functions of Δ, ψ and θ for an isotropic, film free, surface in an ambient medium with a refractive index of unity. The equations are given below:

$$n^2-k^2 = t^2 \frac{(\cos^2 2\psi - \sin^2 2\psi \sin^2\Delta)}{(1+\sin 2\psi \cos\Delta)^2} + \sin^2\theta \qquad (1.4.1)$$

$$2nk = t^2 \frac{\sin 4\psi \sin\Delta}{(1+\sin 2\psi \cos\Delta)^2} \qquad (1.4.2)$$

$$t = \sin\theta \tan\theta \qquad (1.4.3)$$

If the reflecting surface is contaminated by a thin film of foreign material (e.g. a thin oxide film on a metal surface), then the above equations are only approximations. The Fresnel reflection coefficients for a film-covered surface are given by Heavens (1955),

and expressions for Δ and ψ as functions of θ, λ, the optical constants of the film and substrate, and the film thickness have been evaluated (Archer, 1962). Graphical solution of the equations is necessary.

The order of precision to be expected from ellipsometric determinations of n and k is illustrated by the work of Meyer (1962): n and k were obtained for annealed iron films on glass substrates, to an accuracy of about $\pm$ 0.02. (A very accurate ellipsometer at the National Physical Laboratory can yield n and k accurate to $\pm$ 0.005.)

1.4.2 Reflectometry: Non polarimetric methods

The determination of n and k from measurements of reflected intensities alone has been described in general terms by Tousey (1939). Broadly reflectometry involves measuring some characteristic intensity or intensity ratio for light reflected from a surface at various angles of incidence θ_1, θ_2 etc., for incident light which is plane polarized at some azimuth ϕ. Then, from the appropriate Fresnel equation for the reflection, the measured characteristics R_1, R_2, etc., can be expressed as functions of n, k, θ, and ϕ, as shown in the equations below:

$$R_1 = F(n,k,\theta_1,\phi) \qquad (1.4.4)$$

$$R_2 = F(n,k,\theta_2,\phi) \qquad (1.4.5)$$

The characteristic most generally chosen for measurement is the simple reflection coefficient. Reflection coefficients can be defined and measured using either unpolarized or polarized light. In the latter case it is experimentally and arithmetically easier to choose ϕ to be either 0 or $\pi/2$ with respect to the plane of incidence. The determination of n and k from measurements of

reflection coefficients for polarized light has been described by Collins and Bock (1943), and has been discussed in detail by Simon (1951). Experimentally all that is required is a collimated beam of incident light, perhaps a polarizer, some form of photo-detector, and a means of measuring angles of incidence.

From the reflection coefficients $R_{\parallel}$, $R_{\perp}$ and combinations $R_{\parallel}/R_{\perp}$, and $(R_{\parallel}+R_{\perp})/2$, together with knowledge of angles of incidence, various pairs of measurements may be chosen to determine n and k. Humphreys-Owen (1961) has listed and compared nine possible methods:

(i) Reflection coefficient measurements at two angles of incidence using unpolarized incident light.

(ii) Measurement of $R_{\parallel}$ at two angles of incidence.

(iii) Measurement of $R_{\perp}$ at two angles of incidence.

(iv) The ratio $R_{\parallel}/R_{\perp}$ measured at two angles of incidence.

(v) The reflection coefficients $R_{\parallel}$ and $R_{\perp}$ both measured at the same angle of incidence.

In the four methods which follow a reflection coefficient is measured at any angle of incidence, and then the Brewster angle is measured, thus supplying the second independent equation which is necessary to determine n and k. The Brewster angle is defined at that angle for which the function $R_{\parallel}(\theta)$ is a minimum. The methods are given below:

(vi) θ_B is measured and $R_{\parallel}$ is measured at θ_B.

(vii) θ_B is measured and $R_{\perp}$ is measured at θ_B.

(viii) The ratio $R_{\parallel}/R_{\perp}$ is measured at θ_B, which is also determined.

(ix) θ_B is measured and either $R_{\parallel}$, $R_{\perp}$ or the ratio $R_{\parallel}/R_{\perp}$ is measured at any other angle.

A comparison of the methods (i)-(ix) was made by Humphreys-Owen (1961) by preparing sensitivity charts in which the two measured quantities formed the axes. Because these two quantities fix n and k, a point in the plane of a chart establishes an (n,k) pair. The resultant chart connects some of these points by intersecting curves of constant n and k at fixed intervals. Sensitivity may be estimated from the spaces between such curves: large spacing indicates high sensitivity, i.e. a small change in n and k ($\pm$ 0.2 say) produces a correspondingly large change in the measured values.

A comparison of the methods will now be given. Method (i) has been used by Simon (1951) and has the advantage that it may be used at any wavelength because polarizers are not required. Polarization of light is difficult for certain regions of the ultra-violet and infra-red. Methods (i), (ii) and (iii) have been investigated in some detail by Hunter (1965), who used numerical computation to investigate the errors which can result when such methods are used. He concluded that for a given n and k, method (ii) was the most and method (iii) the least sensitive. To keep sensitivity high for methods (i) and (ii) reflection coefficients should be measured for angles of incidence in the region of 80°. The effect of a $\pm 1\%$ error in the reflection measurements on the accuracy of n and k was pictorially represented for angles of incidence 20° and 70° for $0.3 \leqslant k \leqslant 3.5$, $0.3 \leqslant n \leqslant 3.0$.

Method (iv) had been used by Avery (1952). It surmounts some of the experimental difficulties associated with measurements of reflection coefficients, notably the effect of sample size on the limiting aperture, the effect of image movement on the detector as a function of θ, and the effects arising from long fluctuations in light

source and detector characteristics. The method has a good sensitivity chart, and Avery obtained n and k to $\pm$ 4% when the ratio $R_{\parallel}/R_{\perp}$ was measured to 1 or 2%. Avery's graphical method of extracting n and k from the experimental measurements has been criticized by Lindquist and Ewald (1963). They assert that because the graphs used by Avery have been prepared for only a limited number of angles, (30°, 45°, 60° 73°), that this limits the usefulness of the method because an unrestricted range of angles (Θ) is essential for the greatest accuracy. In an attempt to solve this problem they use geometric constructions which yield n and k directly. An investigation by the present author revealed, however, that the scale to which the constructions must be made to yield accurate values of n and k is the true criterion for their usefulness. In fact, for the values $R_{\parallel}/R_{\perp} > 0.3$ (values often occurring for metals, even near the Brewster angle), the geometric construction would require a scale of many metres to obtain n and k to a reasonable accuracy.

Methods (vii) and (viii) were shown by Humphreys-Owen to be very sensitive and he derived explicit equations for them to extract n and k. Method (viii) has been used by Potter (1965), who also obtained expressions for n and k in the presence of a single layer film on the specimen surface.

Until 1969 Querry (1969), no explicit equations had been derived for the evaluation of n and k from the measured quantities, other than for methods (vii) and (viii). Querry showed that, contrary to previous assertions (Tousey, 1939; Collins and Bock, 1943; Simon, 1951; Humphreys-Owen, 1961; Hunter, 1965; Avery, 1952; Lindquist and Ewald, 1963; Potter, 1965; Abelès, 1952), explicit equations for n and k could be obtained in terms of $R_{\parallel}$ and $R_{\perp}$ and θ, and that the

host of numerical, graphical and curve-fitting methods were not strictly necessary for this case. Miller, Taylor and Julien (1970) extended Querry's analysis to show that n and k are most precisely obtained when $R_{\parallel}$ and $R_{\perp}$ are measured in the region of 74° incidence. The uncertainty in n and k arising from experimental errors in $R_{\parallel}$, $R_{\perp}$ and θ were also studied in detail by Miller, Julien and Taylor (1971), and the relevant work contained in the latter two references is described in Chapter 2 of this thesis.

Reflection coefficient measurements made at or near normal incidence may also be used to determine n and k, but for $\theta = 0^{\circ}$ the Fresnel reflectance equations no longer yield two independent equations because $R_{\parallel} = R_{\perp}$. For the majority of n and k values the difference between $R_{\parallel}$ and $R_{\perp}$ for non-zero values of θ up to about 5°, is less than the experimental precision in reflection coefficient measurements, and a single value of reflection coefficient R is assumed. An ancillary relationship between R and ω, such as the Kramers-Kronig (K-K) dispersion relation (Bode, 1945), must then be used in order to obtain n and k. This method and its associated errors has been discussed by Miller, Julien and Taylor (1971) and is further reported in Chapter 2.

1.5 Some methods of determining the optical constants (n_2 and k_2) of thin, partially transparent absorbing films

The ability to transmit electromagnetic radiation at optical wavelengths characterizes a thin, partially transparent absorbing film. Such films are usually supported by dielectric substrates for the purposes of optical studies. It is important to be aware that thin films deposited onto even an ideally flat substrate are very rarely uniform parallel-sided sheets and that the thickness measured is generally an average thickness. Optically, this is important, because the

application of electromagnetic theory to the problem of reflection from a thin film assumes the film to have parallel plane faces. For optical studies it is, therefore, necessary to know by how much the geometrical properties of a film differ from the ideal. Thickness variations, as small as ± 1nm, may be detected using multiple beam interferometry (Tolansky, 1947). The degree of continuity of thin films varies considerably depending on the film/substrate combination and this is best studied using electron microscopy. For example, gold vacuum deposited onto rock salt at 300°C is not continuous until the average thickness is about 80nm. However, gold deposited onto a clean silver surface at 270°C is continuous for average thicknesses greater than 10nm, (Hirsch et al., 1965). Some aspects of film growth and structure are discussed in Chapter 5.

Optically, the ideal thin film is bounded by plane, parallel surfaces, which form two interfaces:

(i) The interface formed by the ambient medium of refractive index n_1 (usually air or vacuum), and the front face of the film, which, if absorbing, will have optical constants n_2 and k_2.

(ii) The interface formed by the back surface of the film and the supporting dielectric substrate of refractive index n_3.

Using electromagnetic theory and applying boundary conditions at the interfaces, $R_{/\!/}$ and $R_{\perp}$ and corresponding transmission coefficients $T_{/\!/}$ and $T_{\perp}$ may be defined for the thin absorbing film supported by a dielectric substrate (Bornand Wolf, 1965). These expressions are obtained in terms of: $n_1, \theta, n_2, k_2, d, \lambda$ and n_3. For an absorbing film on an absorbing substrate, e.g. a metal film on another metal film or a bulk metal surface, the refractive index of the substrate is complex, i.e. $n_3 - ik_3$. In general there will be little or no

transmission for such a film substrate combination. Expressions for R have been obtained for the special case of normal incidence (Born and Wolf, 1965; Heavens, 1964). The author of this thesis has not been able to find any reference to expressions for $R_{//}$ and $R_{\perp}$ at non-normal incidence for this film/substrate combination. However, such expressions do exist for the case of an absorbing film/dielectric/totally absorbing substrate system (Hadley and Dennison, 1947), i.e. metal film/dielectric/metal mirror. This thesis only considers the case of thin absorbing films (e.g. metals or metallic oxides) supported by dielectric substrates (e.g. glass).

The basis of some methods of determining n and k for a thin film of known thickness are as follows:

(i) Ellipsometry

(ii) Measurements at normal incidence of a suitable combination of any two of the following:- R, R^1, T, ϕ_R, $\phi_{R'}$, ϕ_T, where the primed quantities denote reflection from the back face of the film.

(iii) Measurements at non-normal incidence of a suitable combination of any two of the following:- Ro, $R_{\perp}$, $R_{//}$, To, $T_{\perp}$ and $T_{//}$, or a measurement of any one of these at two angles of incidence, where Ro and To denote reflection and transmission at normal incidence.

1.5.1 The ellipsometric method of determining n_2 and k_2 for thin films

It is possible to relate the ellipsometric quantities Δ and ψ to the optical constants of a film covering the surface of a substrate of known optical constants. The Fresnel reflection coefficients can be derived (Heavens, 1955) by considering the interference between the

multiplicity of beams resulting from reflection in the film. Equations for Δ and ψ can be formed explicitly as functions of θ, λ, n_2, k_2, n_3 and d. The resulting equations are arithmetically complicated and they have not been solved for n_2 and k_2. Measurements of Δ and ψ are made in the usual way (see Section 1.4.1 of this Chapter), and d is determined independently (e.g. by multiple beam interferometry). It appears that the only method of extracting n_2 and k_2 that has been used, requires sets of curves of Δ against ψ for a number of possible combinations of n_2 and k_2 for given values of θ, λ, n_3 and d. This method has been used for weakly absorbing films ($k_2 \simeq 0.05$) on a silicon substrate (Archer, 1962). Ellipsometry appears to be only useful and sensitive for thin, ($d < 10nm$) weakly absorbing ($k \leqslant 1.0$) films (Heavens, 1964). However, it is fairly easy to obtain the optical constants and thickness of such films on absorbing substrates (Menard, 1962). Electron microscopic studies of such thin films should also be made if accurate interpretation of the ellipsometric measurements is required, because the surfaces of such films are likely to be far from plane. Berreman (1970) has shown how Δ and ψ for a given material can vary for a variety of thin film geometries, from the ideal flat film to the half submerged spherical particles. He showed that for a thin film of Ag_2S ($\hat{n} = 3.0 + 0.45i$) on a bulk silver substrate, large errors ($\sim$100%) in the deduced optical constants for the film could arise if the effects of the film structure were ignored. For thin metal films ($d \sim 10nm$) on a flat dielectric substrate Berreman concludes that Drude's ellipsometric equations (Drude, 1890) giving the thickness of such films may be very inaccurate when the films are not planar and continuous. The particle shapes must be known and corrections applied for cases such as above.

1.5.2 Normal incidence methods of determining n_2 and k_2 for thin films

This section deals with some methods for determining the optical constants of thin absorbing films supported by dielectric substrates by means of normally incident radiation.

Ward and Nag (1967) have investigated the sensitivities of some methods of measuring n_2 and k_2 and the optical thickness d/λ for films on rocksalt (n_3 = 1.53). In order to determine all three characteristics of the film, it is necessary to measure at least three parameters for a given wavelength. Ward and Nag expressed the six measurables R, R^1, T, ϕ_R, $\phi_{R'}$ and ϕ_T in terms of the optical constants n_1, n_2, k_2 and n_3 and the optical thickness d/λ. They used a computer to calculate the values of the measurables for n_1 = 1.00, n_3 = 1.53 and a range of values of n_2 and k_2 between 0 and 10 and the values of d/λ of 0.01, 0.02, 0.05 and 0.10 (e.g. d = 6-60nm for λ = 600nm).

Quantitative estimates of the sensitivity of the measured quantities to n_2 and k_2 were based on the changes produced in n_2 and k_2 or d/λ by experimental uncertainties in R, R^1 or T of $\pm$ 0.01, or uncertainties in ϕ_R, $\phi_{R'}$ or ϕ_T of $\pm$ 1°. If the change in n_2 and k_2 was less than 0.15 or that in d/λ was less than 0.003, the method was deemed to be acceptably sensitive for those particular values of n_2, k_2 or d/λ. Seven pair-combinations of the measurables were considered namely:

(ϕ_R,R), (ϕ_R,T), (ϕ_T,R), (ϕ_T,T), (ϕ_R,ϕ_T), (R,T) and (R,R^1)

Some idea of the values of n_2 and k_2 and d/λ for which the various methods are sensitive will now be given. For complete details refer to Ward and Nag (1967). Table 1.5.1 summarises the findings of Ward and Nag. The combination giving the highest overall accuracy in the determination of the three quantities n_2, k_2 and d/λ is (R,T,ϕ_T).

Table 1.5.1 Regions of overall high sensitivity for seven pairs of measurables

$\Delta R = \pm 0.01$, $\Delta T = \pm 0.01$, $\Delta\phi = \pm 1.0^{\circ}$, $\Delta n_2 \leqslant \pm 0.15$, $\Delta k_2 \leqslant \pm 0.15$

Measurables	Values of k_2	Values of n_2	Values of d/λ
ϕ_R, R	0-2	3-4	0.01-0.05
ϕ_R, T	0-2 1-2	4 0-1	0.01-0.05 0.05-0.10
ϕ_T, R	2-4 4-6	0-2 0-2	0.02-0.05 0.02
ϕ_T, T	2-4 4-6	0-2 2	0.02-0.05 0.01-0.02
ϕ_R, ϕ_T	0-1 0-3	3-5 0-1	0.02-0.05 0.10
R, T	3	0-1	0.01-0.05
R, R^1	0-0.5 0-0.5	3-4 2-3	0.02-0.05 0.05-0.10

The reflection and transmission coefficients are measured in the usual way (see Section 1.4), and the phase change ϕ can be measured in the same way as for ellipsometry (see Section 1.4). The triple combination (R, R^1, T) has been used (Malé, 1950) to determine n_2, k_2 and d. Although this has the advantage that only light intensity measurements are required, it is, however, insensitive to n_2, k_2 and d/λ, especially for $k_2 > 0.5$. All six measurables are used in Schopper's (1952) method. This is a general and useful method because the maximum available sensitivity for a given n_2, k_2 may be utilized by choosing the appropriate combination of measurables; it also has the advantage of yielding explicit equations for $n_2 + k_2$ in terms of the observables. The extraction of n_2 and k_2 from the measured quantities is difficult because of the complexity of the equations involved. A computer is essential for such work if much labour is to be avoided. The author of this thesis has not found any other method of determining n_2 and k_2 other than that of Schopper (1952) which has explicit equations for the optical constants in terms of the observables. Instead, numerical, graphical and curve fitting techniques are used all of which usually require much preparatory work. For the (R,T) method Hadley has prepared a set of curves of R and T against d/λ with n_2 a parameter for a number of values of k_2. The use of these curves is described by Heavens (1964). The complicated equations for R and T for a thin absorbing film on an absorbing substrate have been simplified somewhat by Tomlin (1968). Tomlin's work has made less complicated the programming for a computer solution to the equations. Given experimental values for $(1 \pm R)/T$, d, λ, n_1, n_3, k_3, a simple numerical technique is used to write suitable computer subroutines to solve the equations for n_2 and k_2.

If the film surface is far from ideal, i.e. it consists of pits

or bumps, then corrections must be applied to the measured value of R if realistic values of n_2 and k_2 are to be deduced (Berreman, 1970). At normal incidence these corrections are only important for photon energies greater than about 5 e.V.

1.5.3 Some non-normal incidence methods of determining n_2 and k_2 for partially-transparent, thin absorbing films

Measurements, at non-normal incidence, of reflection coefficients $R_{\parallel}$ and $R_{\perp}$ or transmission coefficients $T_{\parallel}$ and $T_{\perp}$, or a pair combination of reflection and transmission coefficients, can be used to determine the optical constants n_2 and k_2. Expressions for $R_{\parallel}$, $R_{\perp}$ and $T_{\parallel}$, $T_{\perp}$ have been derived by Born and Wolf (1965) and Hadley and Dennison (1947) in terms of θ, λ, d, n_1, n_2, k_2 for films supported by dielectric substrates. The expressions given by Born and Wolf are not easy to code into FORTRAN IV computer language, whereas those given by Hadley and Dennison are more easily coded. The expressions are quite cumbersome. In Chapter 3 expressions suitable for writing into a computer programme are given for $R_{\parallel}$ and $R_{\perp}$ for thin films on a dielectric substrate.

The more general case of a thin film (of complex refractive index) supported by a substrate of complex refractive index is not dealt with in this thesis. Hadley and Dennison (1947) give expressions for $R_{\parallel}$ and $R_{\perp}$ for the case of a metal film/dielectric/metal mirror combination. These expressions are in a form suitable for computation.

Ward and Nag (1967) have investigated the sensitivities of fifteen methods of measuring n_2 and k_2 for thin films on a dielectric substrate of refractive index 1.53. Miller and Taylor (1971) have extended Avery's method (Avery, 1952) of determining optical constants for use with thin films. Chapter 3 describes this work.

Ward and Nag (1967) investigated pair combinations of $R_\perp$, $R_{//}$, $T_\perp$ and $T_{//}$ for a number of angles of incidence - 30°, 45°, 60°, 75°. They also investigated methods involving the measurement of one coefficient at two angles of incidence. For a particular pair of observables for example $R_{//}$, $R_\perp$, sensitivities were estimated by calculating the changes produced in n_2, k_2 for a given d/λ by changes in $R_{//}$ and $R_\perp$ of $\pm$ 0.01. The sensitivity with respect to d/λ was also calculated. A particular method was deemed to have high sensitivity if changes produced were as follows:- $\Delta n_2 \leqslant 0.15$, $\Delta k_2 \leqslant 0.15$, $\Delta(d/\lambda) \leqslant 0.003$. Values of n_2 and k_2 from 0 to 10 were investigated and the values of d/λ = 0.01, 0.02, 0.03, 0.04, 0.05. A summary of the values of n_2 and k_2 relevant to metals and d/λ for which the various methods are sensitive is given in Table 1.5.2. For complete details refer to Ward and Nag (1967), in whose work it will be found that other regions of high sensitivity occur for large $n_2 (n_2 \gtrsim 2)$ and small $k_2 (k_2 \lesssim 1)$, i.e. values typical of dielectric materials. There are two methods which show the best overall sensitivity, providing d/λ is known precisely. They are: $(T_{//}, T_\perp)$ and $(R_\perp, T_{//})$ at $\theta = 45^o$-75°, d/λ = 0.01-0.02 and for $0 < n_2 < 3.0$, $0 < k_2 < 3.0$.

Miller and Taylor (1971) investigated the sensitivity of a reflection ratio method of determining the optical constants of thin partially-transparent absorbing films. From an experimental point of view methods which measure ratios of reflection or transmission coefficients are superior to those requiring separate intensity measurements. This method involves the measurement of the ratio of two reflection coefficients $(R_{//}/R_\perp)$ at two angles of incidence. The quantity d/λ is determined independently. The method was shown to have good sensitivity if the measurements could be obtained at certain

Table 1.5.2 Regions of overall high sensitivity for some non-normal incidence methods of measuring n_2 and k_2

$\Delta R = \pm 0.01$, $\Delta T = \pm 0.01$, $\Delta n_2 \leqslant \pm 0.15$, $\Delta k_2 \leqslant \pm 0.15$

Measurables	Θ^o	Values of n_2	Values of k_2	Values of d/λ
$(R_{\parallel}, T_{\parallel})$	30	0-1	5-7	0.01
	30	0-1	2-4	0.05
	45	0-1	6-8	0.01
	45	0-1	1-2	0.05
	60	0-2	0-1	0.05
	75	0-1	0-1	0.02
$(R_{\perp}, T_{\parallel})$	30	0-2	3-7	0.01
	30	0-1	2-5	0.05
	45	0-1	3-7	0.01
	45	0-1	1-3	0.05
	60	0-1	3-7	0.01
	60	0-1	1-3	0.05
	75	0-0.5	1-2	0.05
$(R_{\perp}, T_{\parallel})$	30	0-1	4-7	0.01
	45	0-2	0-3	0.01
	45	0-1	6-7	0.01
	45	0-1	3-4	0.04
	60	0-3	0-4	0.01
	75	0-3	0-4	0.01
	75	0-1	0-1	0.05
$(R_{\parallel}, T_{\perp})$	30	0-2	4-7	0.01
	45	0-1	4-7	0.01
	45	0-1	1-4	0.05
	60	0-1	3-7	0.01
$(T_{\parallel}, T_{\perp})$	30	0-1	0-2	0.02
	45	0-2	0-4	0.01
	45	0-1	0-1	0.05
	60	0-3	0-4	0.01
	60	0-1	0-2	0.05
$(T_{\parallel}\ 30^o, T_{\parallel}\ 60^o)$		0-2	0-4	0.01
$(R_{\parallel}, R_{\perp})$	60	0-1	0-2	0.05
	75	0-2	0-3	0.05
$(R_{\parallel}\ 30^o, R_{\parallel}\ 60^o)$		0-1	0-2	0.05

optimum angles of incidence. These optimum angles are given in Chapter 3. Values of n_2 and k_2 in the ranges $1.0 \leqslant n_2 \leqslant 4.0$, $1.0 \leqslant k_2 \leqslant 4.0$ can be determined to within about $\pm$ 0.05 for values of $d/\lambda \geqslant 0.05$. To obtain this accuracy θ must be measured to better than $\pm\ 0.1^o$, $(R_{//} / R_{\perp})$ measured to better than $\pm$ 0.01 and d/λ measured to at least $\pm$ 0.005. Further work, also reported in Chapter 3, showed that the method was useful for films of dielectric material in which $k_2 < 1$. The errors involved are about the same.

The equations for $R_{//}$, $R_{\perp}$, $T_{//}$ and $T_{\perp}$ in terms of the properties of the film are even more complicated than those for R and T at normal incidence because terms in θ must be included. Simplification and approximation of the equations at non-normal incidence are difficult. It is not, therefore, surprising that there are apparently no non-normal incidence methods involving two measurables which have explicit equations for the evaluation of n_2 and k_2 from the measured quantities. Numerical values of n_2 and k_2 can, however, always be obtained by applying graphical techniques. This involves preparing graphs of the two measurables, each plotted against n_2 (say), with k_2 as a parameter, for known values of θ and d/λ. From such graphs and the experimentally determined values many (n_2,k_2) pairs, which satisfy the equations of the method can be obtained. Two curves, therefore, result for each pair of measured quantities when the (n_2,k_2) pairs are plotted on a graph of n_2 against k_2. In general these two curves intersect at one point, which gives the unique values of n_2 and k_2 corresponding to the two measured quantities. This graphical technique is illustrated in the work of Heavens (1964) and Avery (1952) and Chapter 3. Computers and computer plotters are almost necessary for preparing the graphs. However, it is shown in Chapter 3 that it is possible to use the

"graphical" technique in a computer programme, without actually plotting the graphs. The disadvantage of this method is that the required computing time to yield one (n_2,k_2) pair can be as large as 300 seconds using a C.D.C. 6600 computer.

At non-normal incidence the effect of pits and bumps on the surface of the film is to introduce a perturbation into the equations for $R_{//}$ and $R_{\perp}$. Equations for this perturbation have been derived by Berreman (1970) for $R_{//}$ and $R_{\perp}$. The perturbation is inversely proportional to λ^2 and proportional to the sum of absolute values of the volumes of all bumps or pits per unit area. The bumps and pits are assumed to be approximate figures of revolution about an axis normal to the film surface. In addition the perturbation is proportional to a form factor which is a function of θ and other things, and depends on the state of polarization of the incident light. These perturbation equations apply to a surface only, and thus do not include the film thickness, but do include the optical constants of the film. The effects of surface roughness on reflected visible light is discussed in Chapter 5.

1.6 The methods adopted

It was desirous that the methods to be used for determining optical constants should be capable of high precision with the minimum of experimental complexity, because only a small equipment budget was available.

1.6.1 Opaque absorbing films

The methods chosen for determining the optical constants of opaque absorbing films in the wavelength range 400-700nm were, (a) that due to Avery (1952) and (b) the $(R_{//}, R_{\perp})$ method at the

optimum angle of incidence (Miller et al., 1970) for the following reasons:-

Avery's Method

(i) Experimentally the method has many advantages. It requires only a calibrated polarizer and a means of measuring light intensity and angles of incidence. Light source stability over long time periods is not critical and the method is applicable to small samples. Ellipsometers, which in general are capable of greater accuracy, are more complex in use and more expensive. (An ellipsometer manufactured by Gaertner Scientific Corporation, U.S.A. retails at over £2,000.)

(ii) Humphreys-Owen (1961) has shown that the method has good sensitivity for a large range of n and k ($0 < n < 4$, $0 < k < 3$) if measurements of the ratio $(R_{\parallel} / R_{\perp})$ are obtained at angles of incidence close to 60° and 80°. Avery estimated that n and k can be determined accurate to about $\pm$ 4%, for an error in $(R_{\parallel} / R_{\perp})$ of some 1 to 2%, and θ need only be determined to 0.5°. The method is, therefore, applicable for measuring n and k of many metals in the visible range of wavelengths. Only modest accuracy is required for the measurements to obtain acceptably accurate values of n and k.

(iii) The method of extracting n and k from the equations of the method and the measured quantities is straightforward. Only two charts need be prepared of n against $(R_{\parallel} / R_{\perp})$ for parameterized k although as an additional check a third should be prepared for a value of θ between the values used in the

two above mentioned charts. Values of n and k can then be obtained from the charts for the measured values of $(R_{\parallel}/R_{\perp})$ and curves of n versus k plotted to obtain a common point of intersection, the coordinates of which are the optical constants of the specimen.

The $(R_{\parallel}, R_{\perp})$ method

(i) Explicit equations for n and k in terms of the measurable quantities $R_{\parallel}$, $R_{\perp}$, θ, now exist (Querry, 1969). The method is, therefore, attractive because a direct computation to deduce n and k from the measured quantities is possible. The use of a computer to do the arithmetic involved saves considerable labour. However, a slide rule could, in fact, be used given sufficient time.

(ii) Because explicit equations now exist for n and k, the boundary in $R_{\parallel}$, $R_{\perp}$, θ space enclosing all values of n and k can be explicitly determined. The method can, therefore, be optimized with regard to θ and once this optimum value of θ has been obtained determinations of n and k can be most sensitively made. The optimum value of θ appears to be close to 74° (refer to Miller, Taylor and Julien, 1970 and Chapter 2 of this thesis).

(iii) Only modest accuracy in $R_{\parallel}$, $R_{\perp}$ and θ is required to obtain n and k $(0 < n < 3.0,\ 0 < k < 3.2)$ accurate to $\pm$ 0.05, (Miller, Taylor and Julien, 1970; Miller, Julien and Taylor, 1971 and Chapter 2).

(iv) The $(R_{\parallel}, R_{\perp})$ method requires only simple equipment; a light source capable of maintaining a stable output over the

time required to obtain four light intensity readings, i.e. $I_o^{\parallel}$, $I_o^{\perp}$, $R_{\perp}$, $R_{\parallel}$, a collimator and a polarizer, a simple monochromator are all that is required. A reflectometer designed for use with this method is described in Chapter 4.

(v) The method is ideally suited for insitu measurements from opaque metal films grown in ultra-high vacuum. Modern ultra-high vacuum systems are made of stainless steel to which expensive optical ports must be added if insitu optical measurements are required. The ($R_{\parallel}$, $R_{\perp}$) requires only three optical ports - two in line so that $I_o^{\perp}$ and $I_o^{\parallel}$ may be measured, and one at about 148°-150° to the optical axis of the other two so that $R_{\parallel}$ and $R_{\perp}$ may be measured close to the optimum angle of incidence.

1.6.2 Partially-transparent absorbing films

The method chosen for determining the optical constants (n_2, k_2) of absorbing films thin enough to transmit appreciably ($>$1% transmission) in the wavelength range 400-700 nm was that of Miller and Taylor (1971) (see Chapter 3). This method was chosen for the following reasons:-

(i) The method requires measurements of ($R_{\parallel}$ /$R_{\perp}$) at two angles of incidence and, therefore, has all the experimental advantages outlined by Avery (1952) (also see Section 1.6.1).

(ii) An advantage of the method is that good sensitivity can be achieved with only modest experimental accuracy if certain optimum angles of incidence are chosen.

(iii) The ranges of n_2 and k_2 for which an accuracy of $\pm$ 0.05 may be maintained are approximately $1.0<n_2<3.0$, $1.0<k_2<4.0$ when

the film thickness is determined independently to an accuracy of about $\pm$ 2nm.

(iv) The same reflectometer may be used for this method and the methods chosen for opaque films.

(v) The method does not require any transmission coefficient measurements and so may be used for films too thick for such measurements to be accurately made. In addition, minute pinholes in the film tend to cause systematic errors in transmission measurements (Miller, 1965). The effect of pinholes on reflection coefficient measurements is smaller (Anders pp.105-106, 1965).

(vi) The method seems promising as a means of obtaining n_2 and k_2 for insitu measurements grown in ultra-high vacuum, although the minimum number of optical ports required is four. Only two optical ports would be needed if the ($T_{\parallel}$, $T_{\perp}$) method was used, (see Section 1.5.3 and Table 1.5.2 for information on this method).

CHAPTER 2

OPTIMIZATION OF AND ERRORS ARISING FROM A REFLECTION METHOD OF OBTAINING n AND k FOR OPAQUE ABSORBING FILMS

Abstract

This Chapter is concerned with the $(R_{//}, R_{\perp})$ method of obtaining the optical constants of a single reflecting surface. The shape of the boundary enclosing analytical solutions to the generalized Fresnel reflectance equations for n and k in terms of $R_{//}$, $R_{\perp}$ and θ has been investigated using computer techniques and the optimum angle of incidence for experimental measurements determined for a number of values of n and k. The overall optimum value of θ is about 74° for $0 \leqslant n \leqslant 3.0$ and $0 \leqslant k \leqslant 3.2$. Values of n and k in this range can be determined to within $\pm$ 0.05 if experimental values of $R_{//}$ and $R_{\perp}$, measured to an accuracy of about $\pm$ 0.005 are obtained at $\theta \simeq 74^{o}$. In addition, it is shown that large errors in n and k may arise from errors in $R_{//}$ and $R_{\perp}$ when the latter are measured at angles of incidence other than 74°. Measurements of $R_{//}$ and $R_{\perp}$ at values of θ close to 0°, the region of 'near-normal' incidence, can give rise to large, inherent errors in n and k. Previously the possibility of such errors arising has gone unnoticed.

2.1 Introduction

In order to investigate the wavelength dependence of n and k of some metals, it was preferable to use the $(R_{//}, R_{\perp})$ method. The generalized Fresnel reflectance equations correlating these two quantities with n, k and θ have been solved by Querry (1969) for all angles except $\theta = 0^{o}$ and 45°. One can use Querry's results to evaluate n and k as required.

The experimental method consists of measuring $R_{//}$ and $R_{\perp}$ for a given θ. It is, therefore, of interest (a) to determine which value or values of θ give the best sensitivity to changes in n and k, and (b) for what ranges of n and k the method is experimentally useful. Querry's analysis was used to examine the boundary values for $R_{//}$, $R_{\perp}$ and θ which satisfy Fresnel's equations for all n and k, i.e. $0 \leqslant n \leqslant \infty$, $0 \leqslant k \leqslant \infty$. The useful range of n and k to which the method can be applied, that is the sensitive range of n and k was obtained by plotting $R_{//}$ against $R_{\perp}$ for a series of fixed n and k for 74°.

A more detailed study was made of how changes in the values deduced for n and k, produced by small changes in $R_{//}$ and $R_{\perp}$, depend on θ. Computer programmes in FORTRAN IV written for a C.D.C. 6600 computer, allowed a study of a large number of combinations of the parameters concerned. In particular, it was shown that reflection coefficients measured at near normal incidence are insensitive to changes in n and k, i.e. a large change in n and k produces a small change in $R_{//}$ and $R_{\perp}$ of the order of experimental error.

2.2 The analytical solution to the Fresnel reflectance equations

Querry's solution to the Fresnel reflectance equations may be summarized as follows:

Making the substitutions

$$F = \frac{(R_{\perp} + 1)}{(R_{\perp} - 1)} \qquad 2.2.1$$

$$G = \frac{(R_{//} + 1)}{(R_{//} - 1)} \qquad 2.2.2$$

and putting

$$Q = \frac{(F-G)\mathrm{Sin}\theta\mathrm{Cot}2\theta}{GF+(1-F^2)\mathrm{Cos}^2\theta-1} \qquad 2.2.3$$

$$P^2 = -Q^2-2FQ\mathrm{Cos}\theta-\mathrm{Cos}^2\theta \qquad 2.2.4$$

into Fresnel's reflectance equations in the form

$$R_{\perp} = \frac{(Q-\cos\theta)^2+P^2}{(Q+\cos\theta)^2+P^2} \qquad 2.2.5$$

$$R_{/\!/} = R_{\perp}\frac{(Q-\sin\theta\tan\theta)^2+P^2}{(Q+\sin\theta\tan\theta)^2+P^2} \qquad 2.2.6$$

then

$$(Q^2 - P^2) = n^2 - k^2 - \sin^2\theta \qquad 2.2.7$$

and

$$QP = nk \qquad 2.2.8$$

F and G are functions of the observables $R_{/\!/}$ and $R_{\perp}$ only. Therefore, Q and P, from equations 2.2.3 and 2.2.4, can be calculated for a given θ, and by substituting in 2.2.7 and 2.2.8 n and k are obtained.

The equations for n and k are:

$$n = \left(\tfrac{1}{2}\left[(Q^2-P^2+\sin^2\theta)\right] + \sqrt{(Q^2-P^2+\sin^2\theta)^2+4Q^2P^2}\right)^{\frac{1}{2}} \qquad 2.2.9$$

$$k = \left(\tfrac{1}{2}\left[-(Q^2-P^2+\sin^2\theta)\right] + \sqrt{(Q^2-P^2+\sin^2\theta)^2+4Q^2P^2}\right)^{\frac{1}{2}} \qquad 2.2.10$$

2.3 A computer study of the boundary, ($R_{/\!/}$, $R_{\perp}$, θ) space, enclosing values of n and k which satisfy Fresnel's equations

The necessary mathematical analysis used in the computer programme is given first. A flowchart of the programme, which was written in FORTRAN IV, is then presented.

We observe that

$$R_{/\!/} < R_{\perp} \quad \text{for } 0 < \theta < \pi/2 \qquad 2.3.1$$

and

$$R_{\perp} \neq 0 \qquad 2.3.2$$

Moreover, $R_{/\!/} = 0$ only at the Brewster angle, for a perfect dielectric, i.e. when $k = 0$.

It follows from 2.3.1 and 2.3.2 that F is always more negative than G, and therefore

$$(F - G) < 0 \qquad 2.3.3$$

Also, because G and F are both negative

$$GF > 0 \qquad 2.3.4$$

for all $\theta < 90^{o}$.

Consider now equation (2.2.3):

$$\text{Cot}2\theta > 0 \quad \text{for} \quad 0 < \theta < 45^{o}$$

$$\text{Cot}2\theta < 0 \quad \text{for} \quad 45^{o} < \theta < 90^{o} \qquad 2.3.5$$

$$\text{Also Sin}\theta > 0 \quad \text{for} \quad 0 < \theta < 90^{o} \qquad 2.3.6$$

The numerator of the righthand side of (2.2.3) is, therefore, negative for $0 < \theta < 45^{o}$, and positive for $45^{o} < \theta < 90^{o}$.

The denominator can take on either sign depending whether

$$GF + (1 - F^2)\,\text{Cos}^2\theta - 1 > 0$$

$$\text{or} < 0 \qquad 2.3.7$$

Q can therefore be either positive or negative, changing sign through $\pm\infty$. Consider now equation (2.2.4) when $Q < 0$.

In this case

$$\left.\begin{array}{r} Q^2 > 0 \\ 2FQ\text{Cos}\theta > 0 \\ \text{Cos}^2\theta > 0 \end{array}\right) \qquad 2.3.8$$

therefore $P^2 < 0$ and P is imaginary.

Equation (2.2.3) shows Q to be real, and therefore real n and k are only obtained for real P in (2.2.8). It follows that solutions satisfying the Fresnel equations are only obtained for

$$Q > 0, \quad P^2 \geqslant 0 \qquad 2.3.9$$

The condition $P^2 = 0$ delineates a boundary for these solutions.

The inequalities (2.3.1) and (2.3.9) were used as criteria in the computer programme to find valid solutions to the Fresnel

reflectance equations. Figure 2.3.1 shows a flowchart, summarizing the computer programme, named POL. Output from POL could either be graphical or tabulated; graphical output was found to be the most useful. For a fixed value of θ the graphical output consisted of a pattern of equally spaced dots in the $R_{//}$, $R_{\perp}$ plane, each dot representing a $R_{//}$, $R_{\perp}$ pair giving values of n and k which satisfy Fresnel's reflectance equations. Thus for each value of θ $(1^{o} \leqslant \theta \leqslant 89^{o})$ the valid region in $R_{//}$, $R_{\perp}$ space was mapped out. The boundary of each region representє the $P^2 = 0$ condition or a very close approximation to it because of the finite step size (0.01) by which $R_{//}$ and $R_{\perp}$ were incremented. The step size could not be reduced for graphical output because the line width of the computer printer was limited to 136 characters.

Figure 2.3.2 shows sections of the boundary within which solutions for real n and k exist for a number of values of θ in the range $1^{o} \leqslant \theta \leqslant 89^{o}$ obtained from the computer produced graphs.

The shapes of the boundaries shown in Figure 2.3.2 are everywhere smooth and continuous and this suggested that it might be possible to derive analytically the equation of the boundary in terms of F, G and θ. This would not only provide a check of the graphical output from programme POL, but would enable the shape of the boundary to be determined precisely.

2.4 A brief description of the analytical solution to the boundary evaluation

The equation $P^2 = 0$ delineates a boundary in $(R_{//} , R_{\perp})_{\theta}$ space enclosing all real and positive values of n and k. Another equation for P^2 can be obtained by substituting Q, equation 2.2.3, into equation 2.2.4,

Figure 2.3.1 Flowchart of computer programme to generate valid solutions to the Fresnel reflectance equations.

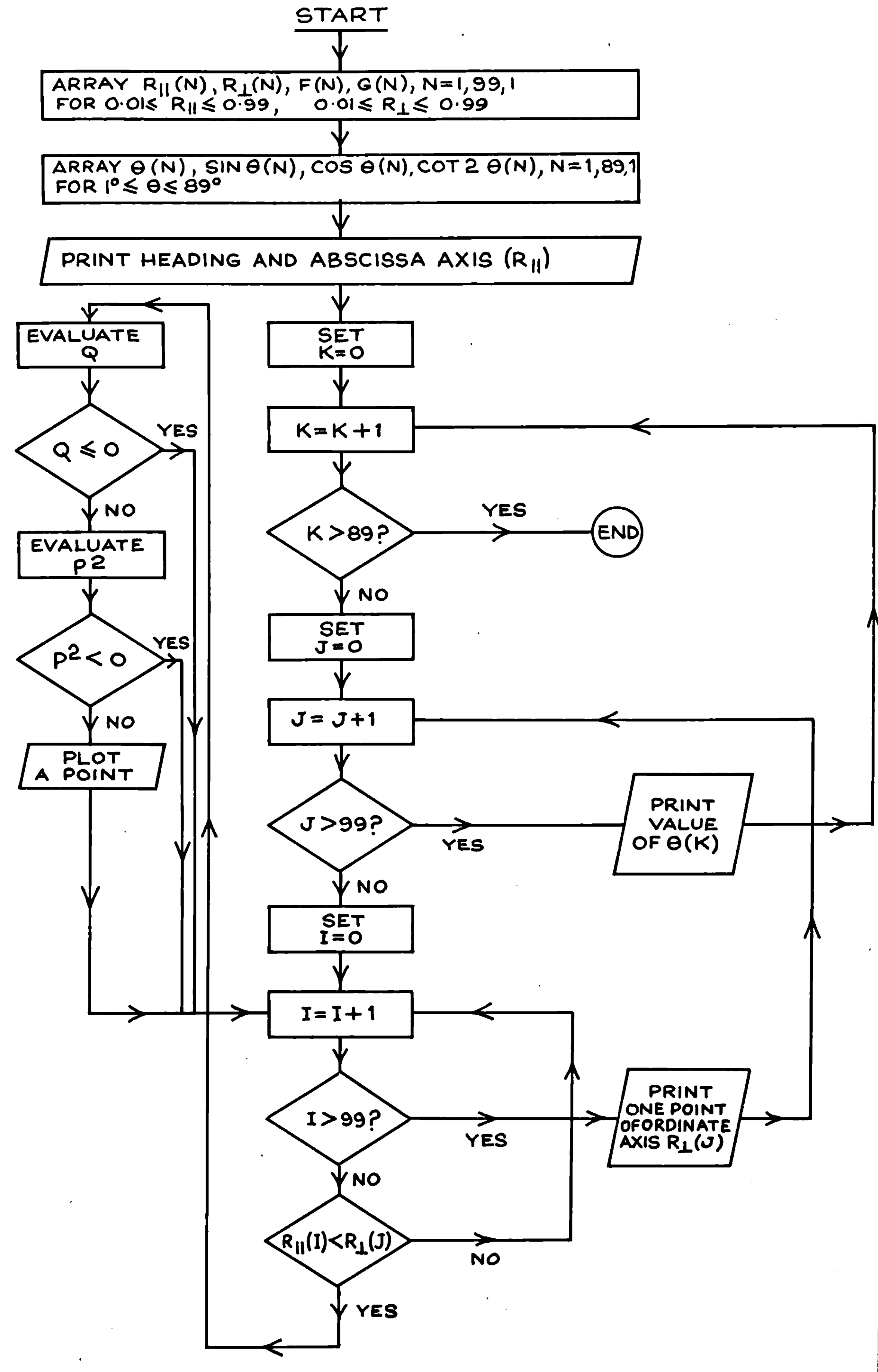
START
ARRAY R||(N), R⊥(N), F(N), G(N), N=1,99,1
FOR 0·01≤ R||≤ 0·99, 0·01≤ R⊥≤ 0·99
ARRAY θ(N), SIN θ(N), COS θ(N), COT 2 θ(N), N=1,89,1
FOR 1°≤ θ≤ 89°
PRINT HEADING AND ABSCISSA AXIS (R||)
EVALUATE Q
Q ≤ 0
YES
NO
EVALUATE P2
P2 < 0
YES
NO
PLOT A POINT
SET K=0
K=K+1
K>89?
YES
END
NO
SET J=0
J=J+1
J>99?
YES
PRINT VALUE OF θ(K)
NO
SET I=0
I=I+1
I>99?
YES
PRINT ONE POINT OFORDINATE AXIS R⊥(J)
NO
R||(I)<R⊥(J)
NO
YES

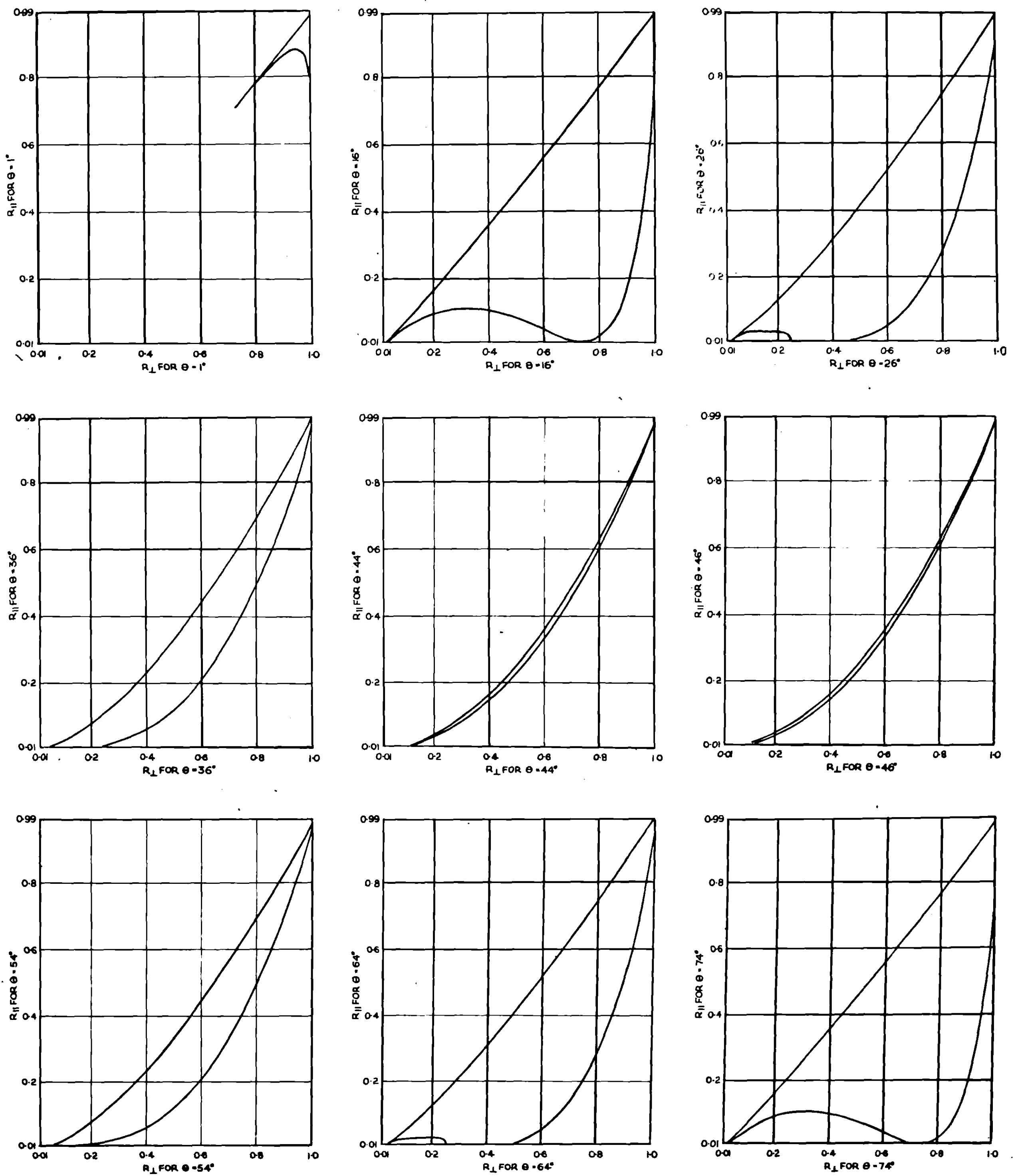

Figure 2.3.2 Boundaries enclosing all possible solutions to the Fresnel reflectance equations.

$$P^2 = -\left(\frac{(F-G)\sin\theta\cot 2\theta}{GF+(1-F^2)\cos^2\theta-1}\right)^2 - \frac{2F\cos\theta(F-G)\sin\theta\cot 2\theta}{GF+(1-F^2)\cos^2\theta-1} - \cos^2\theta \qquad 2.4.1$$

It is easy to see that,

$$\begin{aligned} P^2 &= G^2\left\{\sin^2\theta\cot^2 2\theta + F^2\cos\theta\left[\cos\theta - 2\sin\theta\cot 2\theta\right]\right\} \\ &+ G\left\{2F\cos\theta\left[\cos\theta-\sin\theta\cot 2\theta\right]\left[(1-F^2)\cos^2\theta-1\right]\right. \\ &\qquad \left. + 2F\sin\theta\cot 2\theta\left[F^2\cos\theta-\sin\theta\cot 2\theta\right]\right\} \\ &+ F^2\sin^2\theta\cot^2 2\theta + 2F^2\cos\theta\sin\theta\cot 2\theta\left[(1-F^2)\cos^2\theta-1\right] \\ &+ \cos^2\theta\left[(1-F^2)\cos^2\theta-1\right]^2 \end{aligned} \qquad 2.4.2$$

P^2 is thus a quadratic function of G, which changes sign when

$$aG^2 + bG + c = 0 \qquad 2.4.3$$

where a, b and c are the functions of F and θ indicated by equation 2.4.2. The solutions of 2.4.3, when transformed to $(R_{/\!/}, R_{\perp}, \theta)$ space, via equations 2.2.1 and 2.2.2, bound the region for which all real n and k values may be obtained. This boundary also represents the condition k = 0 because if

$$P^2 = \tfrac{1}{2}\left\{\left[(n^2-k^2-\sin^2\theta)^2+4n^2k^2\right]^{\frac{1}{2}} - (n^2-k^2-\sin^2\theta)\right\}$$

$$= 0 \qquad 2.4.4$$

then

$$4n^2k^2 = 0$$

and therefore $k = 0$, assuming $n > 0$. 2.4.5

Equation 2.4.5 means that the boundary values of $R_{/\!/}$ and $R_{\perp}$ are those corresponding to perfect dielectrics.

A computer programme was used, for use with the C.D.C. 6600 computer to evaluate the shapes of the boundaries for the values of θ used in programme POL. The shapes derived by the two methods were the same.

2.5 Optimization and sensitivity of n and k to $R_{\parallel}$, $R_{\perp}$ and θ

In order to investigate the sensitivity of the ($R_{\parallel}$, $R_{\perp}$) method and to obtain possible optimum values of θ at which to obtain the measurements, it was necessary to investigate the distribution of n and k values within the $R_{\parallel}$, $R_{\perp}$ boundaries.

Loci were plotted by hand, using the tabulated output from programme POL, of $R_{\parallel}$ and $R_{\perp}$ values for which n and k were fixed. It was found that the distribution of these loci were similar within the two ranges $1^{\circ} < \theta < 45^{\circ}$ and $45^{\circ} < \theta < 89^{\circ}$. Some of these fixed n and k loci are shown in Figures 2.5.1 and 2.5.2 for $\theta = 16^{\circ}$ and 74° respectively. From graphs such as these it was found that the 'bunching' of the fixed n and k loci, which occurs near the upper boundary for $1^{\circ} < \theta < 45^{\circ}$, changed to the lower boundary for $45^{\circ} < \theta < 89^{\circ}$ as the value of θ passed through 45°. This 'bunching' is associated with the high values of n and arises from the rapid approach of Q to $+\infty$ as Q changes sign, according to the equation:

$$(Q^2)_{P^2=0} = n^2 - k^2 - \sin^2\theta \qquad 2.5.1$$

If the Q > 0 boundary is close to one of the $P^2 = 0$ solutions, then $k^2 \longrightarrow 0$ in 2.5.1. For $(Q^2)_{P^2=0}$ to go to $+\infty$, n^2 must tend to $+\infty$. The direction from which Q approaches $+\infty$ changes as θ goes through 45° as indicated by equation 2.3.5. There was no localized 'bunching' of the fixed n and k loci anywhere else within the bounded regions investigated.

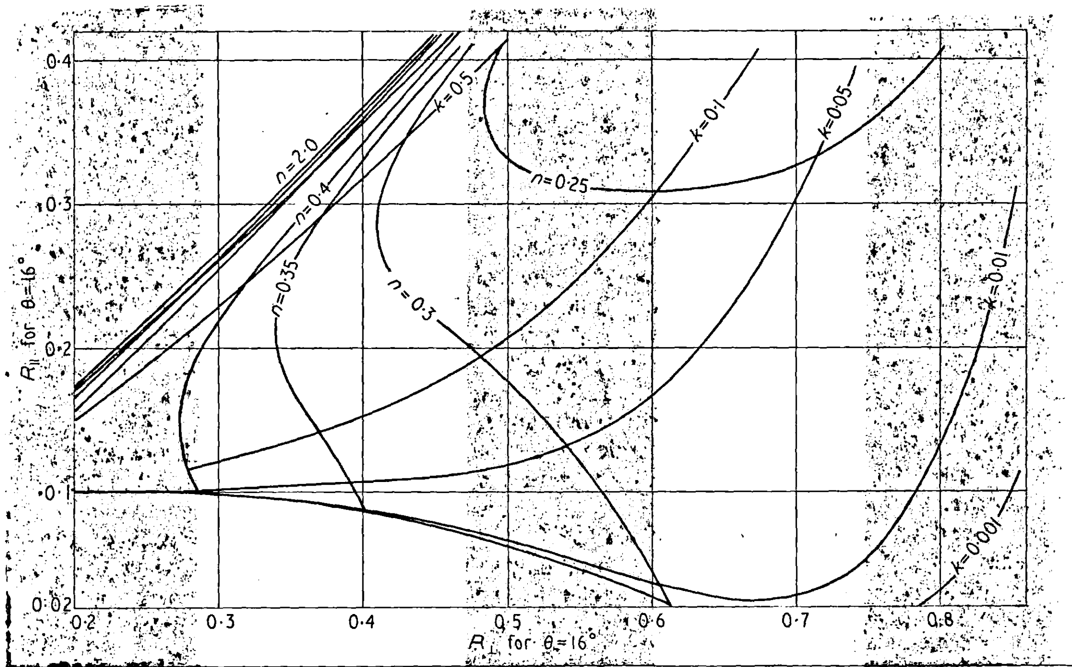

Figure 2.5.1 Distribution of n and k loci for $\Theta = 16^{\circ}$.

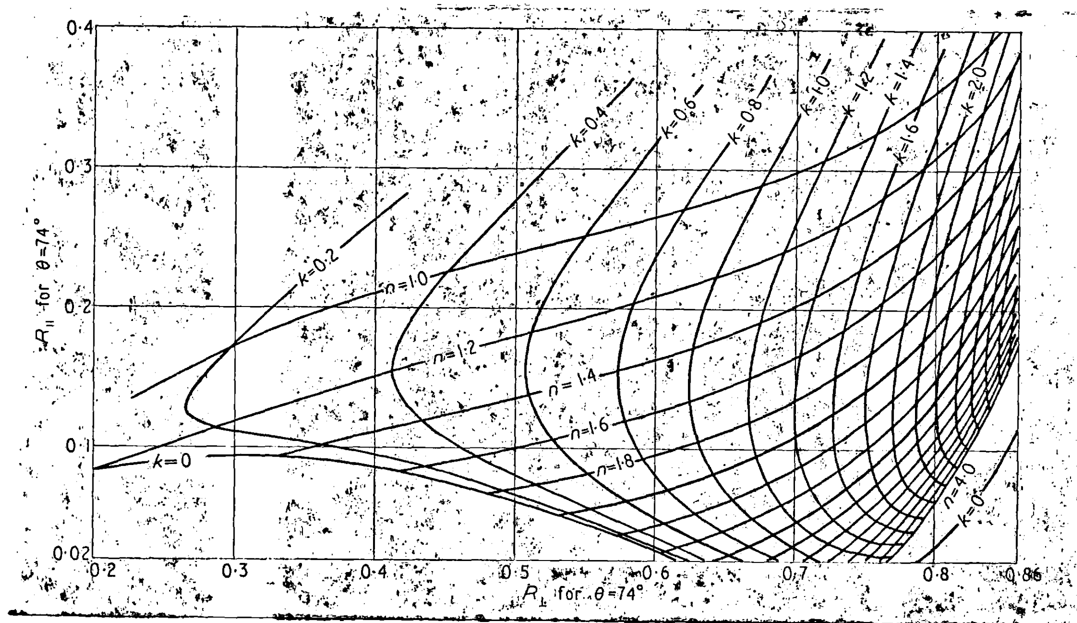

Figure 2.5.2 Distribution of n and k loci for $\Theta = 74^{\circ}$.

The most sensitive measurements of n and k can, therefore, be performed for angles θ such that the area enclosed by the $P^2 = 0$ boundary (transformed to the $R_{/\!/}$, $R_{\perp}$ plane) is largest, because the largest change in $R_{/\!/}$ and $R_{\perp}$ will be produced at these angles for a given change in n and k. Numerical integration was used to evaluate the areas of the bounded regions for the values of θ used in programme POL. To do this POL was modified in two ways: (a) to increase the accuracy in determining the areas, the step size was reduced to 0.001 so that the $R_{/\!/}$ and $R_{\perp}$ values were incremented by this amount; (b) for each value of θ, ($R_{/\!/}$, $R_{\perp}$) pairs, which gave real and positive values of n and k, were counted and the sum total formed. This sum represents very closely the area of the bounded region enclosing all possible n and k. Output from this modified programme was in the form of a table of values of θ, each with its associated area composed of valid ($R_{/\!/}$, $R_{\perp}$) pairs. From this table it was seen that there were two maximum areas of equal area occurring at $\theta = 16^{\circ}$ and $\theta = 74^{\circ}$, (see Figure 2.3.2). These angles are, therefore, the angles of incidence at which determinations of n and k may be most sensitively made. Empirical observation, rather than exact analysis, had previously indicated the most sensitive angle to be about 70°, (Humphreys-Owen, 1961). It was found from the table of θ and area values that the area of the bounded region is, in any case, very nearly stationary in respect of θ at 16° and 74° and, therefore, small changes in θ ($\leqslant 0.5^{\circ}$) near these values will not greatly affect the results.

The distributions of n and k loci within the bounded regions at the best angles demonstrate the ranges of n and k to which the ($R_{/\!/}$, $R_{\perp}$) method may be usefully applied. In Figure 2.5.1 for $\theta = 16^{\circ}$, the loci corresponding to values of n and k which are of practical interest (n is usually > 1) are so close together that

accurate determinations of n and k from measurements of $R_{//}$ and $R_{\perp}$ are impossible. Figure 2.5.2 shows 74° to be practically useful, the distribution being such that changes in $R_{//}$ and $R_{\perp}$ produce only small changes in the n and k values usually observed.

The precise range of n and k for which the ($R_{//}$, $R_{\perp}$) method is acceptably sensitive can be found by determining the $R_{//}$, $R_{\perp}$ values for which an acceptable uncertainty in n and k produces a typical experimental uncertainty in $R_{//}$ and $R_{\perp}$. Assuming n and k are required within $\pm$ 0.05 and $R_{//}$ and $R_{\perp}$ are measurable to within $\pm$ 0.004 visual inspection of Figure 2.5.2 showed the method to be applicable for $0 < n < 3.0$ and $0 < k < 3.2$. This region of usefulness is delineated in the Figure.

From Figure 2.3.2 it can be seen that the area enclosed by the $P^2 = 0$ boundary is very small for $\theta = 1^{o}$ i.e. the region of near normal-incidence. Even at 16° incidence the values of n and k which are of practical interest are tightly 'bunched' at the upper boundary. Measurements of $R_{//}$ and $R_{\perp}$ at near normal-incidence should, therefore, give rise to large errors in the deduced values of n and k. In order to investigate this point more fully and to determine precisely the errors involved in the deduced values of n and k arising from errors in $R_{//}$, $R_{\perp}$ and θ, a further computer study was made of the sensitivity of the ($R_{//}$, $R_{\perp}$) method at values of $1^{o} \leqslant \theta \leqslant 89^{o}$.

2.6 A more detailed study of the errors involved when the ($R_{//}$, $R_{\perp}$) method is used to obtain n and k

Sections 2.7 to 2.10 describe in more detail how changes in the values deduced for n and k, produced by small changes in the measured reflection coefficients $R_{//}$ and $R_{\perp}$, depend on the angle of incidence θ. Special attention was paid to values of θ close to 0° and the overall optimum value of 74°. The values of n and k were selected to be in

the ranges $1.0 \leqslant n \leqslant 4.0$, $1.0 \leqslant k \leqslant 4.0$ because these are the values relevant to the optical properties of many metals in the visible wavelength region. Computer programmes, written for the C.D.C. 6600 computer facilitated a study of a large number of combinations of the parameters concerned. In particular, reflection coefficients measured near normal incidence were shown to be insensitive to changes in n and k; a fact which hitherto has not been noticed by those who have deduced optical constants from measurements of reflectance at or near normal incidence.

2.7 The method of error investigation

The basis of the method is shown in Figure 2.7.1. This method was suggested by the form of the sensitivity diagram shown in Figure 2.5.2 where quadrilaterals having approximately linear sides are formed by the constant n and k loci.

For an arbitrary value of θ the bounded region in the $(R_{\parallel}, R_{\perp})$ plane includes all values of $R_{\parallel}$ and $R_{\perp}$ which will give solutions to the Fresnel equations, (see Sections 2.3 and 2.4). A point O within this boundary is related to unique values of the optical constants n_0 and k_0 via the generalized Fresnel reflectance equations, (see Section 2.2). If there is an uncertainty in the reflection coefficients of $\pm\Delta R$, then the deviant values of optical constants n and k will be obtained from points lying on the perimeter of a square of edge $2\Delta R$ drawn with O as centre. Furthermore, extreme deviant values will occur. A computer subroutine was written, making use of the equations in Section 2.2, to calculate the deviant values n and k for 400 equally spaced points on the perimeter of the square for

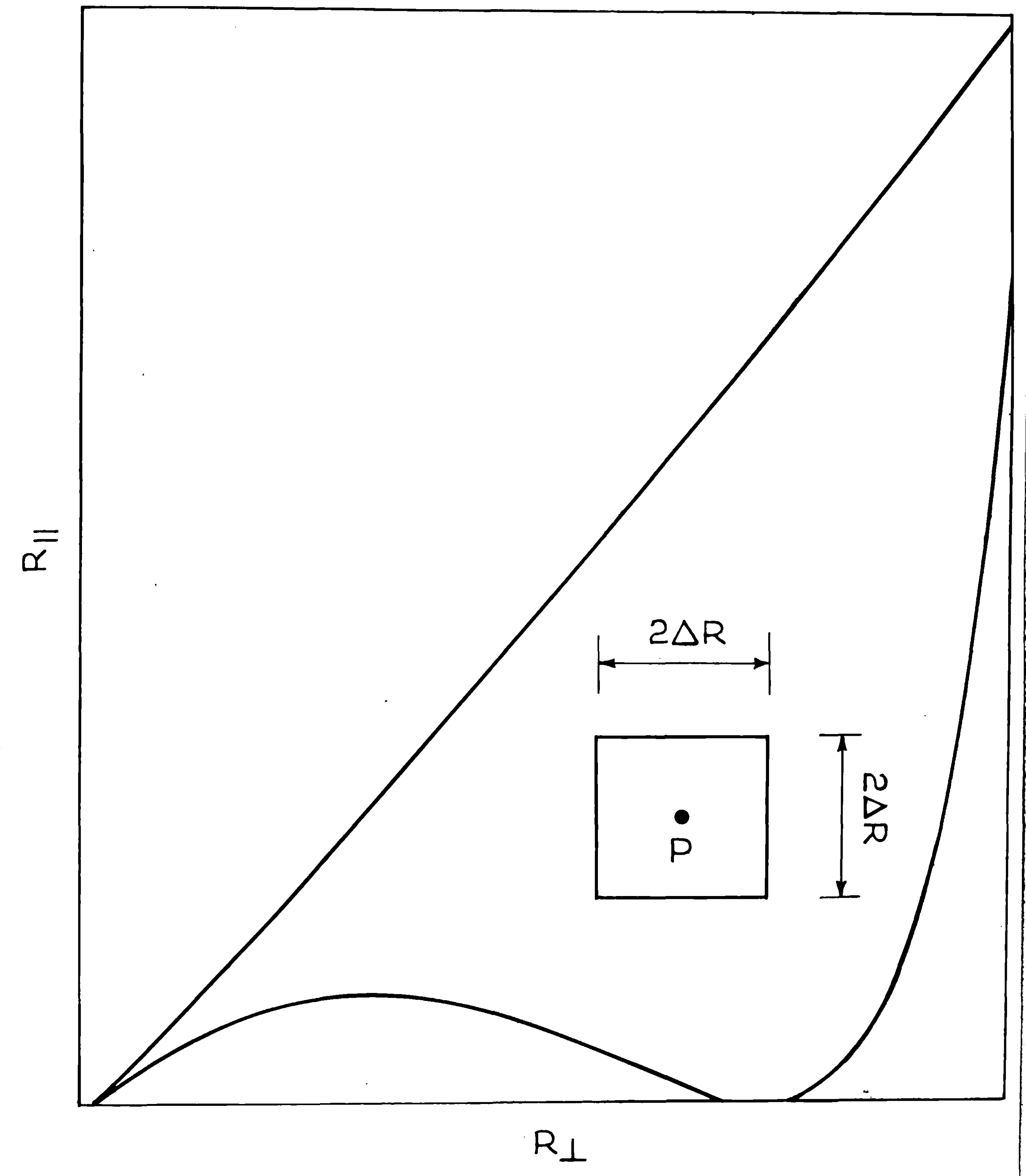

Figure 2.7.1 Boundary enclosing all possible solutions to the Fresnel reflectance equations, for an arbitrary value of Θ.

given values of θ, ΔR, n_o and k_o. It was assumed that $\Delta R = \Delta R_{/\!/} = \Delta R_{\perp}$ and that these values were independent of $R_{/\!/}$ and $R_{\perp}$.

The product of the optical constants (nk) and ($n_o k_o$) was chosen as a suitable parameter for the investigations because of its relevance to electronic band structure calculations, (see Section 1.1). The fractional error in the product ($n_o k_o$) for a point on the square is given by

$$\sigma = \frac{(n_o k_o) - (nk)}{(n_o k_o)}$$

Products (nk) for which σ took the largest positive and negative values were determined using a computer sorting technique. This sorting was set up using another computer subroutine. For the first point on the perimeter of the square a value of σ was evaluated; this was stored. The next point on the perimeter produced another value of σ. This latter value of σ was compared with the first; if it was greater than the first value of σ then it replaced the first σ value in the store. After the 400th value of σ had been calculated, the value of σ residing in the store was printed out as being the largest positive deviant value. The process was repeated to find the largest negative deviant value of σ. In this way, for a given ΔR, n_o and k_o, two values of σ ($\pm\sigma$) were obtained for each value of θ investigated. These values of σ represent the maximum positive and negative errors resulting from uncertainties, $\pm\Delta R$, in the reflection coefficients.

2.8 The computer results

The output from the computer calculations was in tabular form from which graphs were drawn by hand.

2.8.1 Angular dependence of σ

The computational methods described in Section 2.7 were used to

calculate σ for a number of combinations of n_0 and k_0 in the ranges $1.0 \leqslant n_0 \leqslant 4.0$, $1.0 \leqslant k_0 \leqslant 4.0$ and for angles of incidence in the range $0 < \theta < \pi/2$, $(\theta \neq \pi/4)$. The values $n_0 = 2.00$ and $k_0 = 3.00$ are used to typify the results obtained. These values are relevant to the experimental work described in Chapter 7. The point $n_0 = 2.00$ and $k_0 = 3.00$ lies close to the upper boundary of the valid region in $(R_{//}, R_{\perp})$ space for values of $\theta < \pi/4$, and close to the lower boundary for values of $\theta > \pi/4$, (see Figures 2.5.1 and 2.5.2).

Figure 2.8.1 shows the variation with θ of the largest positive and negative percentage errors in the product $(n_0 k_0)$, $\sigma \times 100\%$, for $\Delta R = \pm 0.00005$. The value $\Delta R = \pm 0.00005$ appears to be the best accuracy currently obtained in reflectance measurements (Sell, 1970). The two broad minima (Figure 2.8.1) are in accordance with the results shown in Section 2.5 which identified two regions of maximum sensitivity at $\theta = 16^\circ$ and 74°. Furthermore, the shallower of the two minima occurs for large θ, shown in Section 2.5 to be that region of θ most sensitive for the determination of optical constants from measurements of $R_{//}$ and $R_{\perp}$, in the range $0 \leqslant n_0 \leqslant 3.0$ and $0 \leqslant k_0 \leqslant 3.2$. This broad shallow minimum indicates the existence of a large range of θ at which accurate determinations of n_0 and k_0 may be made: further evidence that the sensitivity of the method is almost stationary with respect to θ at 74°. Catastrophic behaviour occurs as θ approaches 0° and 45°: σ increases significantly and, beyond the points at which the curves are discontinued, a strong possibility exists of measured values of $R_{//}$ and $R_{\perp}$ within the range of $\pm\Delta R$ to produce non-valid solutions to the Fresnel equations, e.g. negative values for k. The catastrophes at 0° and 45° are not surprising when Figure 2.3.2 is viewed, which shows the small area of the valid region in $(R_{//}, R_{\perp})$ space, at 1°, 44° and 46°.

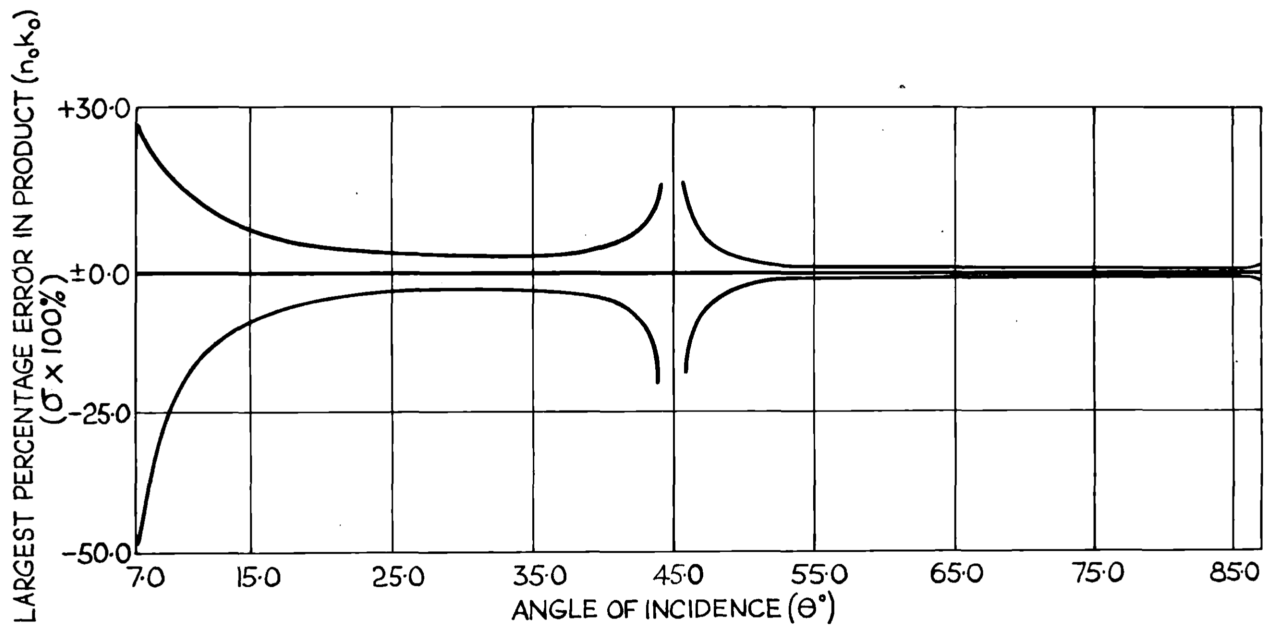

Figure 2.8.1 Angular dependence of the largest percentage error in the product $n_o k_o$ (i.e. σ x 100%) for $\Delta R = \pm 0.00005$, $n_o = 2.00$ and $k_o = 3.00$.

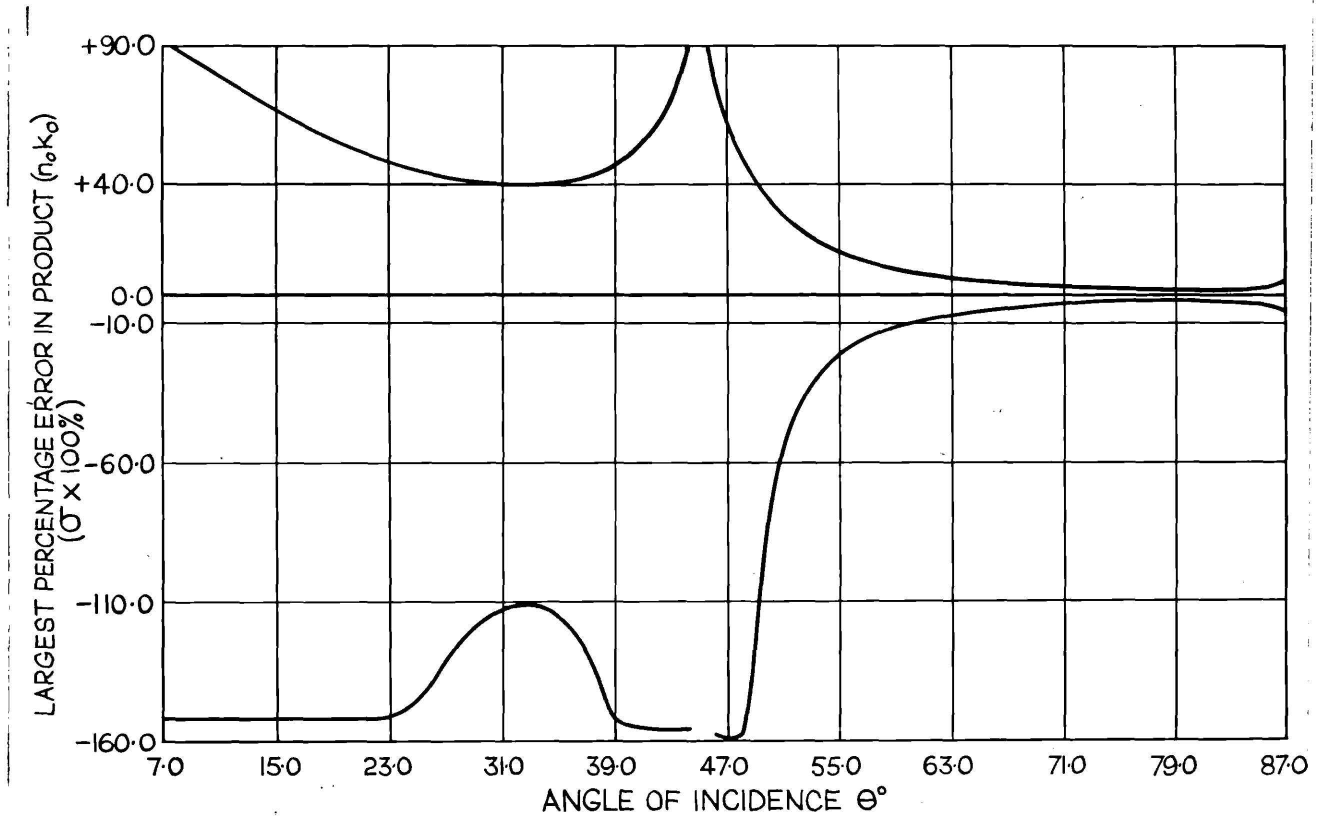

Figure 2.8.2 Angular dependence of the largest percentage error in the product $n_o k_o$ (i.e. σ x 100%) for $\Delta R = \pm 0.001$, $n_o = 2.00$, $k_o = 3.00$.

For a modest degree of accuracy $\Delta R = \pm 0.001$, and the same optical constants $n_o = 2.00$ and $k_o = 3.00$, Figure 2.8.2 shows a shape similar to Figure 2.8.1. However, the minima have sharpened, and there is a dramatic increase in $\pm\sigma$ as θ approaches 0° and 45°. Parts of the negative curve in Figure 2.8.2 show little variation with σ for $\theta < 45^o$. This fact may be explained in the following way. From Figure 2.5.1, for $\theta = 16^o$ the point $n_o = 2.00$, $k_o = 3.00$ will be near to a boundary in the $R_{//}$, $R_{\perp}$ plane. It was shown in Section 2.5 that close to such a boundary $n \longrightarrow \infty$, $k \longrightarrow 0$, It was expected, therefore, that the product (nk) should pass through a maximum near to this boundary. Attempts to prove this analytically from the facts $n \longrightarrow \infty$ and $k \longrightarrow 0$ were unsuccessful. Further numerical work by Julien (1971) showed that the product (nk) did pass through a maximum near to the boundary. For $\Delta R = \pm 0.001$, $n_o = 2.00$, $k_o = 3.00$ the perimeter of the test square approaches the ($R_{//}$, $R_{\perp}$) boundary and, therefore, the computer sorting technique locates the above maximum for certain values of θ. From Figure 2.8.2 it is seen that the maximum in the (nk) product maintains a fairly constant value in the range of $\theta < 45^o$. Even so, the individual errors associated with n_o and k_o may still increase rapidly as $\theta \longrightarrow 0^o$. From Figure 2.8.1 for $\Delta R = \pm 0.00005$ the flattening of the σ versus θ curve does not occur in this region of θ. This is because the perimeter of the test square does not approach the boundary sufficiently closely for the values $n_o = 2.00$ and $k_o = 3.00$. Consequently, for the above (nk) product, the maximum is never located. For different values of n_o and k_o the computer results indicated that the general shape of the σ versus θ curves remain the same, differing only in detail. Curves

of σ versus θ for all combinations of n_o and k_o in the ranges studied were not produced.

It was shown in Section 2.5 that $\theta = 74^o$ is the best angle for determining optical constants from measurements of $R_{//}$ and $R_{\perp}$. In Figure 2.8.3 the angular positions ($\theta > 45^o$), at which minimum σ can occur, have been plotted for a number of combinations of n_o and k_o for $\Delta R = \pm 0.001$. If, for example, $n_o = 2.00$ and $k_o = 3.00$, Figure 2.8.3 shows 80.5^o to be the angle of incidence giving greatest sensitivity. If this angle is used instead of the overall optimum 74°, Figure 2.8.2 shows the gain in accuracy in ($n_o k_o$) to be only 0.5%. For $\Delta R = \pm 0.005$, errors relevant to the experimental work described in Chapter 7, the range of θ, for which minima in σ occur, is considerably smaller.

2.8.2 Variation of σ with ΔR

It was of practical interest to see how the value of the largest percentage error in ($n_o k_o$), i.e. σ x 100%, varied with known errors, ΔR, in the reflection coefficient. Figure 2.8.4 shows the results of this study for the optimum angle 74° and for $n_o = 2.00$ and $k_o = 3.00$. For $\Delta R < 0.005$ the positive and negative portions of the graph are symmetrically placed about the line $\sigma = 0$, and σ varies almost linearly with ΔR. Above this value of ΔR, the negative portion of the curve varies more rapidly owing to the 'bunching' effect of the constant n and k curves shown on a plot of $R_{//}$ against $R_{\perp}$ at 74°, (see Figure 2.5.2). As ΔR increases, so more of the perimeter of the test square centred about $n_o = 2.00$ and $k_o = 3.00$ comes into the 'bunched' region giving rise to large deviant values of the product (nk).

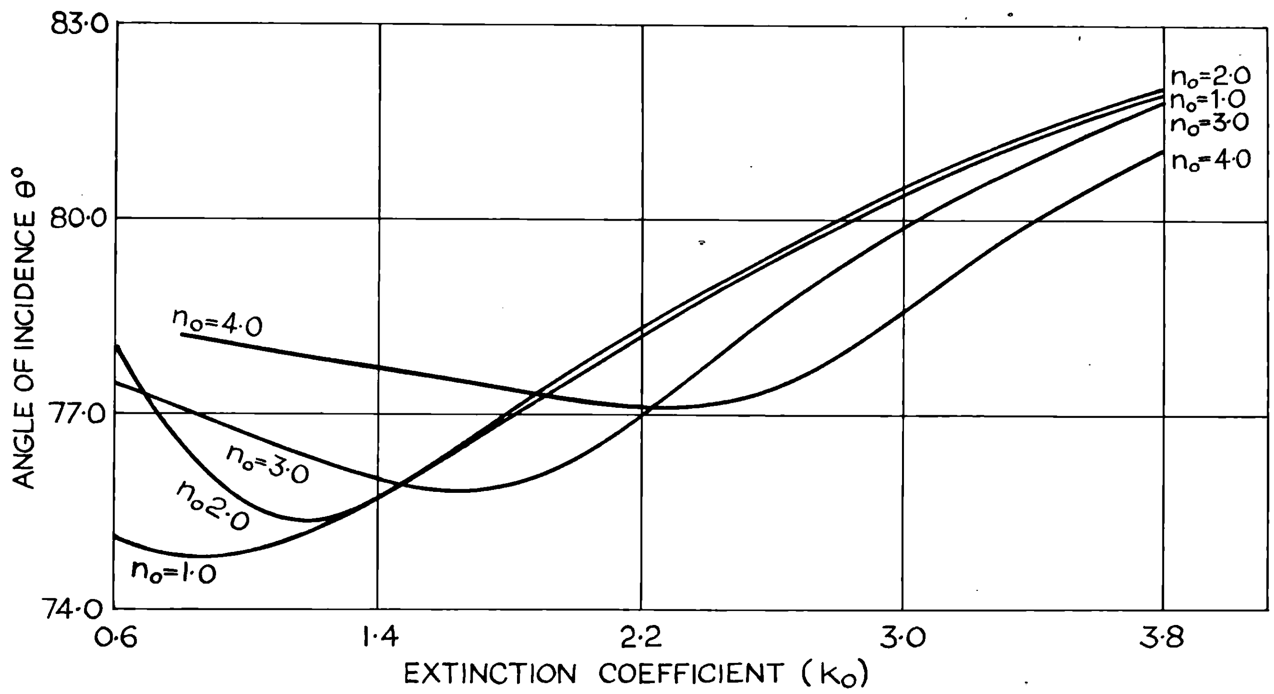

Figure 2.8.3 Angles for which the value of σ is smallest for $\Delta R = \pm 0.001$.

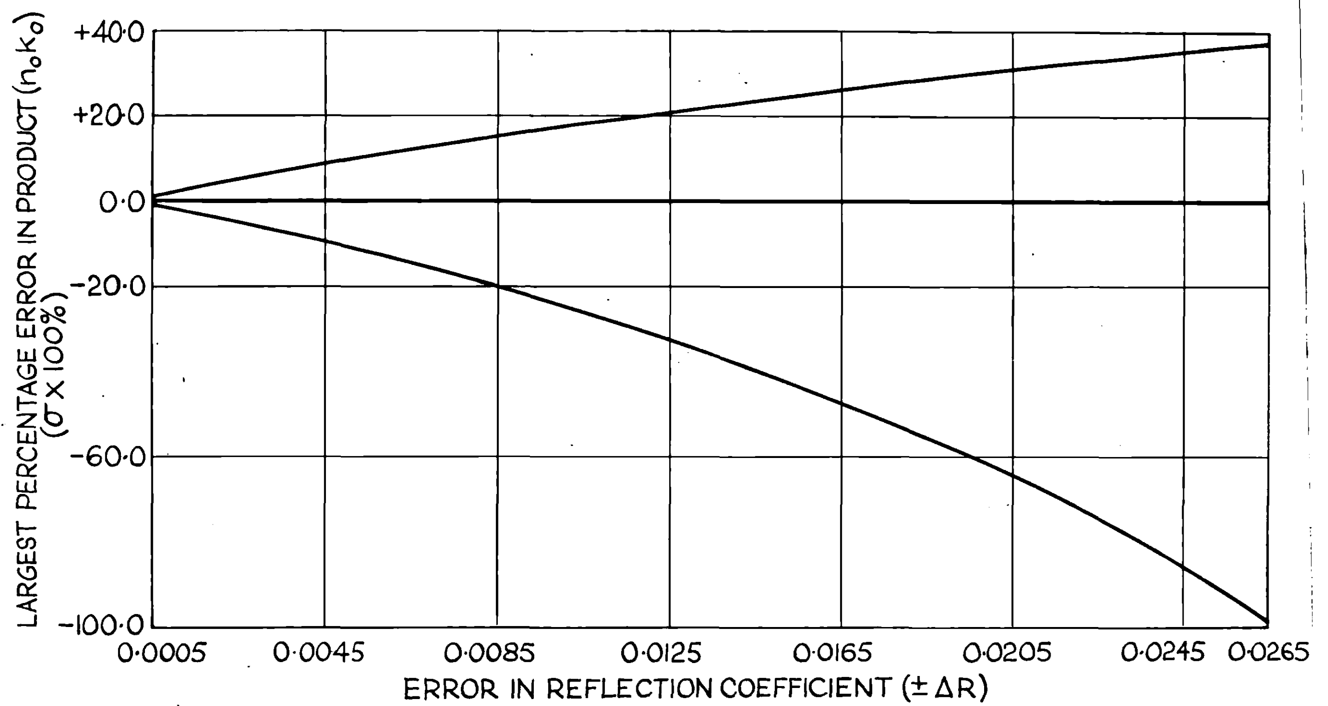

Figure 2.8.4 Variation of σ with ΔR for $n_o = 2.00$, $k_o = 3.00$, $\theta = 74^{\circ}$.

2.9 The case of normal incidence

In this Section we will consider the errors likely to occur in normal incidence reflection methods for obtaining optical constants n_0 and k_0. Such methods measure one reflection coefficient for a range of optical frequencies ω. At normal incidence, $\theta = 0^o$ and $R_{//} = R_{\perp} = R$, and so an ancillary relationship between R and ω is used to obtain n_0 and k_0. A suitable ancillary relationship is based on the Kramers-Kronig (K-K) dispersion relation.

The equations relevant at normal incidence are:

$$n_0 = \frac{(1 - R)}{(1 + R - 2R^{\frac{1}{2}}\text{Cos}\phi)}, \qquad 2.9.1$$

and

$$k_0 = \frac{-2R^{\frac{1}{2}}\text{Sin}\phi}{(1 + R - 2R^{\frac{1}{2}}\text{Cos}\phi)}. \qquad 2.9.2$$

These follow directly from the Fresnel reflectance equations for a single reflecting surface, if we express the complex reflection amplitude in the form $R^{\frac{1}{2}} e^{i\phi}$, where ϕ is the phase change on reflection. The dispersion relation between ϕ at a particular frequency ω_0 and the measured reflection coefficients may be expressed in the form produced by Bode (1945),

$$\phi(\omega_0) = \frac{1}{\pi}\int_0^{\infty} \ln\left|\frac{\omega+\omega_0}{\omega-\omega_0}\right| \frac{d}{d\omega}\,(\ln R_{\omega}^{\frac{1}{2}})\,d\omega \qquad 2.9.3$$

The difficulties associated with this method are well known to those who have used it. In those regions of ω where R is changing rapidly or in regions of singularities in R, the values of n_0 and k_0 deduced often show negative values. From what follows in this Section this fact is not surprising. Calculations based on the considerations of

the foregoing sections show that values of n_0 and k_0 obtained by the (K-K) method are subject to large inherent errors.

'Normal-incidence' reflectance measurements are made at angles as high as 12^0 (Cress and Lapeyre, 1970); at these angles it is assumed $R_{//} = R_{\perp}$. This assumption often injects errors into the method, errors which are larger than those claimed for the measurements of $R_{//}$ and $R_{\perp}$. Table 2.9.1 shows the difference between $R_{//}$ and $R_{\perp}$, for a number of values of the optical constants n_0 and k_0 commonly obtained for metals in the visible range of wavelengths, and for some values of Θ at which normal-incidence measurements are made. The values of $R_{//}$ and $R_{\perp}$ were calculated, using the computer, from the Fresnel reflectance equations (Humphreys-Owen, 1961). At 8^0 incidence and for small values of n the difference between $R_{//}$ and $R_{\perp}$ is small. At 12^0 incidence differences of the order of 0.01 are apparent. From Figure 2.8.2 it can be seen that enormous errors in the deduced values of the product (n_0k_0) could arise with an error $\Delta R = \pm 0.01$ for $\Theta = 12^0$. Even for a small change in reflection coefficient ($\Delta R = \pm 0.001$) there is a large error in the product (n_0k_0). This means that the measured reflection coefficients are insensitive to the values of n_0 and k_0. The following numerical example will emphasize this fact.

When $n_0 = 2.00$ and $k_0 = 3.00$, Table 2.9.1 shows the values of $R_{\perp}$ and $R_{//}$ at $\Theta = 12^0$ are 0.563 and 0.548 respectively. If we assume $\Delta R = \pm 0.001$, $R_{\perp}$ and $R_{//}$ may become, as an extreme example, 0.564 and 0.547 respectively, and the resulting values of n_0 and k_0 will be 0.760 and 1.934. The corresponding value of σ expressed as a percentage is 76%, which shows that a change in n_0 and k_0 of this size will not change the value of the reflection coefficients by more than the uncertainty ΔR. Hence, there is a host of n_0 and k_0 values contained

Table 2.9.1 Differences between $R_\perp$ and $R_\parallel$ at angles close to normal incidence

θ^o	n	k	$R_\perp$	$R_\parallel$	$R_\perp - R_\parallel$
5	1.0	2.0	0.502	0.498	0.004
	1.0	3.0	0.693	0.691	0.002
	1.0	4.0	0.801	0.799	0.002
	2.0	3.0	0.557	0.554	0.003
	2.0	4.0	0.681	0.679	0.002
	3.0	4.0	0.626	0.624	0.002
8	0.3	2.0	0.791	0.787	0.004
	0.3	3.0	0.889	0.887	0.002
	0.3	4.0	0.933	0.931	0.002
	1.0	2.0	0.504	0.496	0.008
	1.0	3.0	0.695	0.690	0.005
	1.0	4.0	0.802	0.798	0.004
	2.0	3.0	0.559	0.552	0.003
	2.0	4.0	0.683	0.677	0.006
	3.0	4.0	0.628	0.622	0.006
12	1.0	2.0	0.509	0.491	0.018
	1.0	3.0	0.698	0.686	0.012
	1.0	4.0	0.804	0.796	0.008
	2.0	3.0	0.563	0.548	0.015
	2.0	4.0	0.686	0.674	0.012
	3.0	4.0	0.632	0.618	0.014

within the range determined by ΔR and, therefore, the substitution of measured reflection coefficients into equations 2.9.1, 2.9.2 and 2.9.3 are likely to lead to erroneous values of n_0 and k_0. The same calculation performed at $\theta = 74^\circ$ gives σ, expressed as a percentage equal to 2·7%.

Ward and Nag (1967) have investigated the sensitivities of some normal-incidence methods used for measuring the optical constants and thickness of absorbing thin films deposited on a substrate of refractive index 1.53. It was shown that none of these methods gave extensive regions of overall high sensitivity to the optical constants. In particular it was shown that for methods involving reflection only the regions of high sensitivity were very small with respect to the optical constants. As the optical thickness (d/λ) became large, i.e. the case of reflection from a single surface was approached, it was shown that those regions shrank even further. The work of Ward and Nag, therefore, implies the same conclusions reached in this Section.

2.10 General Conclusion

The shape of the boundary in ($R_{\parallel}$, $R_{\perp}$, θ) space which includes all possible solutions for n_0 and k_0 from the Fresnel reflectance equations, has been determined. A three-dimensional figure could be constructed from sections of this boundary, some of which are shown in Figure 2.3.2. The overall optimum angle θ, for the determination of n_0 and k_0 from measurements of $R_{\parallel}$ and $R_{\perp}$ has been found to be 74°, and the useful ranges of n_0 and k_0 to which the ($R_{\parallel}$, $R_{\perp}$) method is applicable have been found to be $0 < n_0 < 3.0$ and $0 < k_0 < 3.2$, when $\Delta R = \pm 0.004$.

Furthermore, the angular dependence of the errors in optical constants ($1.0 \leq n_0 \leq 4.0$, $1.0 \leq k_0 \leq 4.0$) obtained from $R_{\parallel}$, $R_{\perp}$ measurements

has been determined, and shown to be large for angles well removed from the optimum about 74°. In particular, it has been shown that reflectances measured at near normal-incidence are inherently insensitive to wide variations in n_0 and k_0. This insensitivity may be a contributory factor to the wide discrepancies observed between the results obtained by near normal-incidence and other methods for optical constants (Robin, 1966).

Experimentally, the optimized ($R_{//}$, $R_{\perp}$) method of measuring optical constants requires only a modest quantity of equipment, and may be readily used for accurate in-situ measurements of surfaces produced in ultra-high, vacuum systems.

Now that Querry has shown how to obtain explicit equations for n and k in terms of the measurables $R_{//}$, $R_{\perp}$ and θ, other methods of obtaining optical constants should now be open to exact analysis, e.g. Avery's method. Following Querry's approach, a possible way of obtaining explicit equations for n and k from any two combinations of measurables obtained at non-normal incidence, is as follows:-

Let X_1 and X_2 be the two reflected measurables; X_1 and X_2 will probably be obtained at two angles of incidence θ_1 and θ_2. From electromagnetic theory it is possible to obtain expressions for X_1 and X_2 in terms of n, k and θ,

$$X_1 = f(n, k, \theta_1)$$

$$X_2 = X_1(P, Q, \theta_1, \theta_2).$$

Expressions for P and Q are given in Querry's paper. It is then necessary to find suitable expressions for P and Q in terms of F, G, θ_1 and θ_2. Expressions for F and G should only be simple linear functions of X_1 and X_2 respectively. For some methods of determining n_0 and k_0 the algebra can be expected to be cumbersome.

CHAPTER 3

STUDIES OF A NEW OPTIMIZED REFLECTION RATIO METHOD FOR OBTAINING n_2 AND k_2 FOR THIN FILMS

Abstract

This Chapter describes how Avery's method of determining the optical constants of single reflecting surfaces has been extended for use with thin films in which multiple, internal reflections occur. The films are assumed to be supported on a dielectric substrate of known refractive index. The ratio $(R_{\parallel}/R_{\perp})$ of two reflection coefficients is measured at two angles of incidence, and the film thickness (d) is determined independently. Optimum angles of incidence for experimental measurement have been determined for $0.2 \leqslant n_2 \leqslant 4.0$, $0.2 \leqslant k_2 \leqslant 4.0$ for many optical film thicknesses (d/λ) in the range $0.01 \leqslant d/\lambda \leqslant 0.25$. The method, when used at these optimum angles, yields n_2 and k_2 accurate to about $\pm$ 0.05 for values of $(d/\lambda) \geqslant 0.05$ provided that angles of incidence are measured to better than $\pm 0.1^{\circ}$, reflection ratios are measured to better than $\pm$ 0.1 and values of (d/λ) are measured to better than $\pm$ 0.005. Computer programmes necessary for computing n_2 and k_2 from experimental data are given.

3.1 Introduction

The optical constants n and k of a metal, semi-conductor or metallic oxide may be obtained from measurements of the ratio of the reflection coefficients $R_{\parallel}$ and $R_{\perp}$, (see Section 1.3). Avery's analysis for obtaining n and k from the experimental data can only be directly applied to reflection at a single interface, so that the method is only useful for bulk specimens or films which are sufficiently thick for internal multiple reflections to be negligible. The

experimental method has, however, certain distinct advantages over other methods involving reflection, notably:

(i) No absolute measurements of light intensity are required provided that the components of light incident on the polarizer in the two planes of polarization (perpendicular and parallel to the plane of incidence) are equal, or in a known ratio. This can be arranged by a suitable depolarizer (Portigal, 1969) or an initial calibration of the polarizer.

(ii) No errors are introduced if the specimen becomes the limiting aperture at high angles of incidence, because the aperture is the same for both components of polarization.

(iii) There is little restriction on the wavelength of the light used, because quarter-wave plates and compensators are unnecessary. Polarizers are now obtainable to cover most parts of the optical spectrum, from ultra-violet to infra-red (Heath, 1967; 1968).

Although the method does not have the same precision as ellipsometry (Avery found that n and k could be obtained to an accuracy of about 4%), the experimental simplicity and the advantages mentioned above, made it worth investigating for possible application to thin films, where in most cases specimen reproducibility is the real limiting factor in experimental accuracy. Optimizing the method with respect to θ has shown that the method is usable even when the experimental precision is only modest. For example, assuming the ratio $(R_{\parallel}/R_{\perp})$ can be measured to within $\pm$ 0.01 at certain optimum angles of incidence, and the film thickness is measured to within $\pm$ 2nm, then n_2 and k_2 ($0.2 \leqslant n_2 \leqslant 4.0$, $0.2 \leqslant k_2 \leqslant 4.0$) can be determined to within about $\pm$ 0.05 for many film thicknesses in the visible range of wavelengths.

3.2 The method of resultant waves to obtain an expression for $R_{\parallel}/R_{\perp}$

Avery quotes an expression directly from electromagnetic theory, for the ratio $(R_{\parallel}/R_{\perp})$ in terms of the optical constants n and k and the angle of incidence θ. For films thin enough for multiple, internal reflections to make a significant contribution to the reflected light, it is no easy matter to derive an expression for $(R_{\parallel}/R_{\perp})$ directly from electromagnetic theory. Instead, separate expressions for $R_{\parallel}$ and $R_{\perp}$ must be obtained and the ratio formed. In computer work, numerical values for $R_{\parallel}$ and $R_{\perp}$ are calculated from the relevant expressions, and the ratio is then computed.

There are several ways of deriving expressions for $R_{\parallel}$ and $R_{\perp}$ at non-normal incidence for thin films on a dielectric substrate situated in air, (Heavens, 1955). One such method, which gives equations for $R_{\parallel}$ and $R_{\perp}$ and is easily coded into FORTRAN IV, computer language is that of "resultant waves" described by Heavens (1955). Hadley and Dennison (1947) have used this method to obtain expressions for $R_{\parallel}$ and $R_{\perp}$ in terms of the optical constants of the film, the geometrical film thickness, the refractive index of the dielectric substrate, the angle of incidence and the wavelength of the incident light. Rather less cumbersome equations than those of Hadley and Dennison have been obtained in the present work by using (n_2-ik_2) instead of (n_2+ik_2), and optical (d/λ) instead of geometrical thickness in a "resultant waves" derivation of $R_{\parallel}$ and $R_{\perp}$.

The following derived quantities were used to obtain the expressions for $R_{\parallel}$ and $R_{\perp}$: see p63

With aid of the above substitutions equations 3.2.1-3.2.6 were derived, from which the ratio $(R_{\parallel}/R_{\perp})$could be obtained.

For the reflection coefficients, $R_{\parallel}$ we have:

$$2u^2 = \left[(n_2^2 - k_2^2 - \sin^2\theta)^2 + 4n_2^2 k_2^2\right]^{1/2} + (n_2^2 - k_2^2 - \sin^2\theta)$$

$$2v^2 = \left[(n_2^2 - k_2^2 - \sin^2\theta)^2 + 4n_2^2 k_2^2\right]^{1/2} - (n_2^2 - k_2^2 - \sin^2\theta)$$

$$P = (n_1^2 - \sin^2\theta)^{1/2}$$

$$Q = (n_3^2 - \sin^2\theta)^{1/2}$$

$$W = u^2 + v^2$$

$$X = \left[u(n_2^2 - k_2^2) + 2vn_2k_2\right] / (n_2^2 + k_2^2)^2$$

$$Y = \left[v(n_2^2 - k_2^2) - 2un_2k_2\right] / (n_2^2 + k_2^2)^2$$

$$P_n = P/n_1^2$$

$$Q_n = Q/n_3^2$$

$$W_n = w/(n_2^2 + k_2^2)^2$$

$$D = d/\lambda$$

$$\alpha = 4\pi u D$$

$$\beta = 4\pi v D$$

$$A_{//} = \left[(W_n/P_n{}^2 + 1)(W_n/Q_n{}^2 + 1) - 4X^2/P_nQ_n\right]\cosh\beta$$
$$+$$
$$\left[2X(W_n/P_n{}^2 + 1)/Q_n - 2X(W_n/Q_n{}^2 + 1)/P_n\right]\sinh\beta$$
$$-$$
$$\left[(W_n/P_n{}^2 - 1)(W_n/Q_n{}^2 - 1) + 4Y^2/P_nQ_n\right]\cos\alpha$$
$$+$$
$$\left[2Y(W_n/P_n{}^2 - 1)/Q_n - 2Y(W_n/Q_n{}^2 - 1)/P_n\right]\sin\alpha$$

3.2.1

$$B_{//} = \left[(W_n/P_n{}^2 + 1)(W_n/Q_n{}^2 + 1) + 4X^2/P_nQ_n\right]\cosh\beta$$
$$+$$
$$\left[2X(W_n/P_n{}^2 + 1)/Q_n + 2X(W_n/Q_n{}^2 + 1)/P_n\right]\sinh\beta$$
$$-$$
$$\left[(W_n/P_n{}^2 - 1)(W_n/Q_n{}^2 - 1) - 4Y^2/P_nQ_n\right]\cos\alpha$$
$$+$$
$$\left[2Y(W_n/P_n{}^2 - 1)/Q_n + 2Y(W_n/Q_n{}^2 - 1)/P_n\right]\sin\alpha$$

3.2.2

$$R_{//} = A_{//}/B_{//} \qquad 3.2.3$$

For the reflection coefficient $R_\perp$ we also have:

$$A_\perp = \left[(W/P^2 + 1)(\ /Q^2 + 1) - 4U^2/PQ\right]\cosh\beta$$
$$+$$
$$\left[2U(W/P^2 + 1)/Q - 2U(W/Q^2 + 1)/P\right]\sinh\beta$$
$$-$$
$$\left[(W/P^2 - 1)(W/Q^2 - 1) + 4V^2/PQ\right]\cos\alpha$$
$$+$$
$$\left[2V(W/P^2 - 1)/Q - 2V(W/Q^2 - 1)/P\right]\sin\alpha$$

3.2.4

$$B_{\perp} = \left[(W/P^2 + 1)(W/Q^2 + 1) + 4U^2/PQ\right]\cosh\beta$$
$$+$$
$$\left[2U(W/P^2 + 1)/Q + 2U(W/Q^2 + 1)/P\right]\sinh\beta$$
$$-$$
$$\left[(W/P^2 - 1)(W/Q^2 - 1) - 4V^2/PQ\right]\cos\alpha$$
$$+$$
$$\left[2V(W/P^2 - 1)/Q + 2V(W/Q^2 - 1)/P\right]\sin\alpha \qquad 3.2.5$$

$$R_{\perp} = A_{\perp}/B_{\perp} \qquad 3.2.6$$

From equations (3.2.3) and (3.2.6) the value of $R_{\parallel}/R_{\perp}$ can be computed, for known values of n_1, n_2, k_2, n_3, θ, d, λ.

In deriving $R_{\parallel}$ and $R_{\perp}$ the following assumptions were made:

(i) The film is optically isotropic with a plane reflecting surface.

(ii) The supporting dielectric substrate has negligible absorption and a thickness much greater than the film.

(iii) There is no difference between the wavelength of the incident and reflected light.

(iv) The optical constants of the film are independent of the angle of incidence.

The final equations for $R_{\parallel}$ and $R_{\perp}$ were written in terms of the following explicit quantities:

(i) The refractive index of the medium in which the incident light travels, (air of refractive index 1.00).

(ii) The refractive index of the substrate used in subsequent experimental work, (float glass microscope slides of refractive index, 1.51). For details of these substrates see Chapter 5.

3.3 Application of the reflection ratio method to thin films

Avery's method of deducing the optical constants n and k of bulk surfaces from reflection ratio measurements has been described in Section 1.3. The same technique was adopted for use with thin films to deduce n_2 and k_2. However, because of the inclusion of the film thickness in the equation for $R_{\parallel}/R_{\perp}$, the arithmetic involved in computing data for the necessary curves is complicated and, therefore, a computer programme was evolved for drawing Avery type curves automatically. The computer programmes were written in FORTRAN IV and "Calcomp" symbolic language for use with the University of London C.D.C. 6600 computer and the associated "Calcomp" plotting facility.

The evolution of this programme is now described. A function subroutine programme was written to compute a value for $R_{\parallel}/R_{\perp}$ for given values of n_2, k_2 sinθ, d and λ, supplied either from data cards or predimensioned arrays. A flowchart for this subroutine (called ROSQ) is shown in Figure 3.3.1; the nomenclature used is that described in Section 3.2. The compilation of programme ROSQ was checked in the following way. A large value of d (d = 200nm) was inserted and the values of $(R_{\parallel}/R_{\perp})$ computed for a number of n_2,k_2 pairs. These $(R_{\parallel}/R_{\perp})$ values were compared with values computed for the same n_2, k_2 pairs using Avery's formula for the reflection ratio. Differences between the two ratio values were less than $\pm$ 0.001. Function subroutine ROSQ was, therefore, assumed to be compiling and executing correctly. A programme was then written, incorporating the subroutine ROSQ, to generate on the Calcomp plotter curves of n_2 versus the ratio $(R_{\parallel}/R_{\perp})$ with k_2 as a parameter for constant θ and d/λ. Values of the parameters used in the programme were:

$$0.9 \leqslant n_2 \leqslant 3.5, \quad 0.9 \leqslant k_2 \leqslant 3.5, \quad 0.010 \leqslant d/\lambda \leqslant 0.200$$

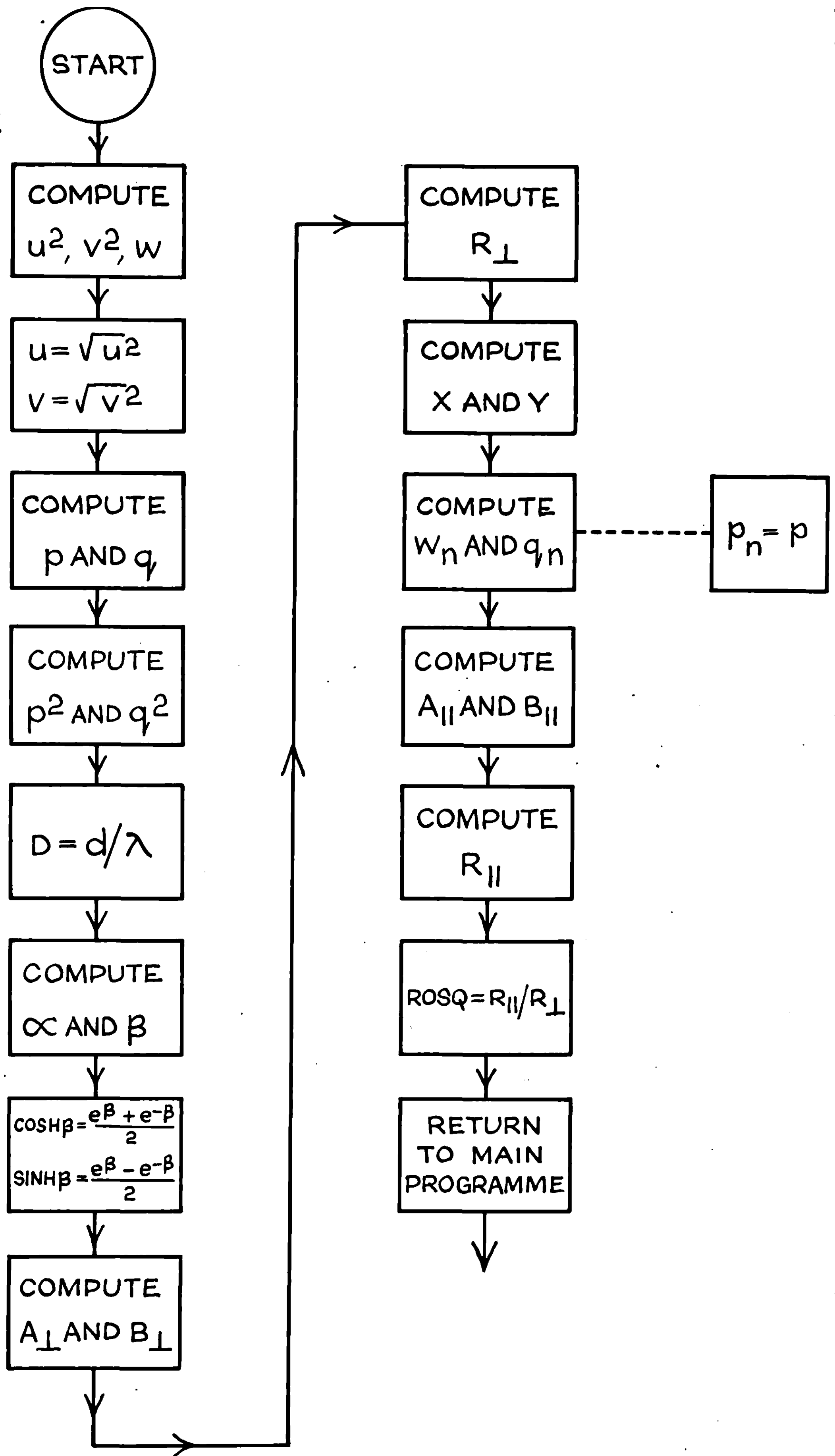

Figure 3.3.1 A flowchart of the computer subroutine ROSQ for computing $R_{\parallel}/R_\perp$.

and any value of θ in the range $0^{o} \leqslant \theta \leqslant 88.0^{o}$. The values of n_2 and k_2 were so chosen because of their relevance to metals in the visible wavelength range. Data cards were used to input the initial value of k_2 and the values of $\sin\theta$ and d/λ. A complete listing of the programme for generating the "Calcomp" curves is given in Appendix II. For illustration purposes, portions of two "Calcomp" curves generated for $d/\lambda = 0.164$ and for $\theta = 61.3^{o}$ and $\theta = 81.3^{o}$, are shown in Figures 3.3.2 and 3.3.3. Such plots are drawn by the plotter to a scale of about 1m x 1.5m, so that graphical error is practically eliminated.

Experimentally, the procedure is the same as that adopted by Avery, except that by determining the two angles of incidence at which measurements may be most sensitively made, further measurements at a third angle (a third angle was recommended by Avery) are rendered unnecessary. The film thickness (d) is determined by multiple beam interferometry. Further experimental details are given in Chapter 4 of this thesis, and some results obtained by the method are given in Chapter 7.

To facilitate the use of the reflection ratio method a further computer programme, which did not rely on graphical output, was written to extract n_2 and k_2 from the measured quantities. This programme allows the computer to carry out Avery's method of extracting n_2 and k_2 from the experimental data. To deduce one n_2, k_2 pair the following set of experimental data is required:

$$(R_{\parallel}/R_{\perp})_{\theta_1} = \text{ROSQ1M},\ \theta_1,\ (R_{\parallel}/R_{\perp})_{\theta_2} = \text{ROSQ2M}$$

θ_2, d, λ and the errors associated with the reflection ratios, $\pm\ \Delta(\text{ROSQ1M})$, $\pm\ \Delta(\text{ROSQ2M})$.

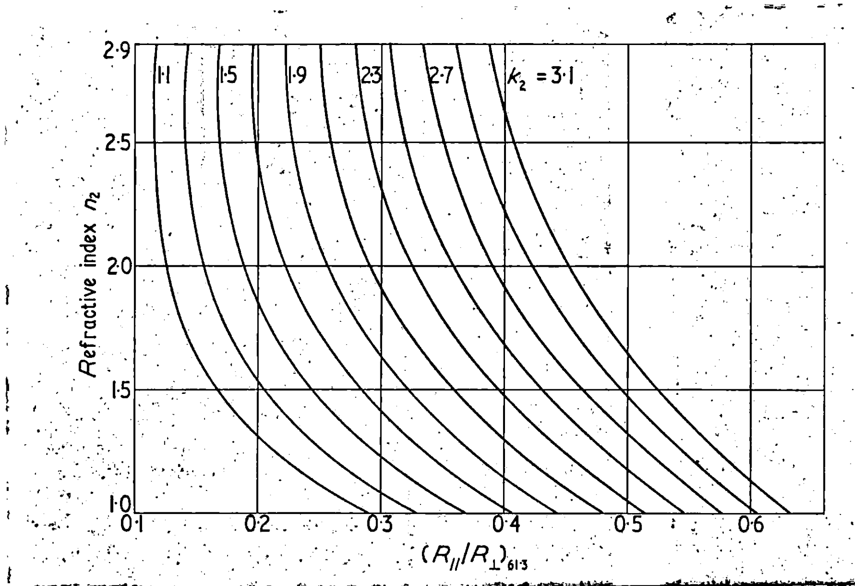

Figure 3.3.2 Portion of 'Calcomp' curves relating $(R_{//}/R_{\perp})$ to n_2 and k_2 for $d/\lambda = 0.164$, $\theta = 61.3^{o}$.

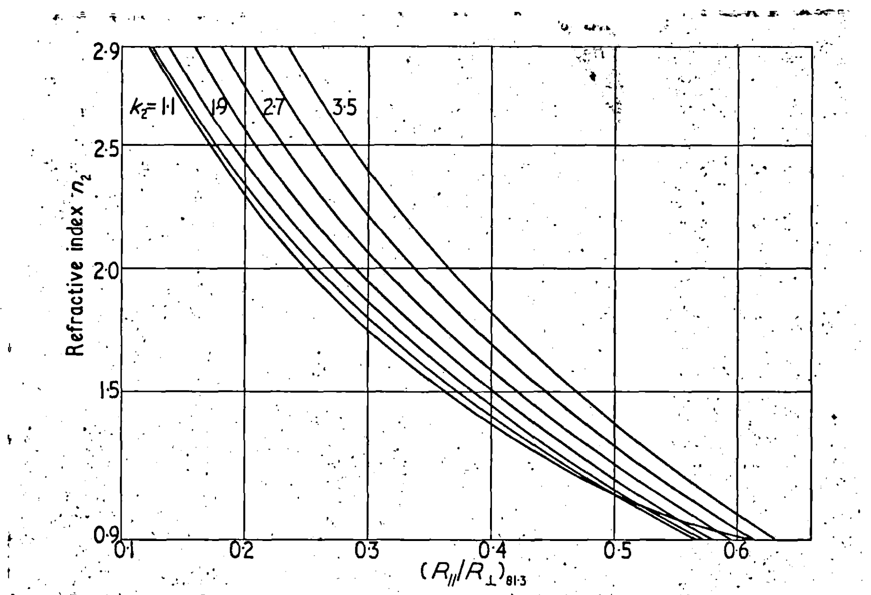

Figure 3.3.3 Portion of 'Calcomp' curves relating $(R_{//0}/R_{\perp})$ to n_2 and k_2 for $d/\lambda = 0.164$, $\theta = 81.3°$.

A value of d/λ is first computed. The programme then selects a possible n_2, k_2 pair for a solution from a suitable range of values, and proceeds to compute the value of $(R_{/\!/}/R_{\perp})_{\theta_1}$ using the function-subroutine ROSQ. The value so obtained is then compared with the experimentally determined value, ROSQ1M. If the difference is greater than the experimental error $\pm\Delta$(ROSQ1M), (Δ(ROSQ1M) is assumed to be equal to Δ(ROSQ2M)), then that particular n_2, k_2 pair is discarded and another is selected for a possible solution. When a n_2, k_2 pair is found, which returns a value of $(R_{/\!/}/R_{\perp})_{\theta_1}$ equal to ROSQ1M within the experimental error, the computer is allowed to store those values of n_2 and k_2. Using values of n_2 and k_2 from the predefined range, the above process is repeated for the experimentally determined quantity ROSQ2M. Each time a pair of n_2, k_2 values is selected as a possible solution, the individual n_2 and k_2 values are compared with those already stored. If the n_2 and k_2 values are equal then they are the required optical constants of the thin film being studied. If no equality is obtained after going through the whole range of n_2 and k_2 for ROSQ2M, then the programme returns to the first n_2 and k_2 range and the procedure is repeated. In this way all the possible combinations of n_2 and k_2 in the ranges used are investigated as possible solutions for both angles of incidence. Output from this programme can consist of a number of n_2, k_2 pairs each reproducing the experimental quantities ROSQ1M and ROSQ2M within the experimental error assigned to them. The programme, therefore, not only extracts n_2 and k_2 from experimental data, but simulates the measurement of ROSQ1M and ROSQ2M. A flowchart of this programme is shown in Figures 3.3.4 and 3.3.5, and should be used in conjunction with the flowchart of Figure 3.3.1. This programme uses only 6,400 words of central memory, but takes about 70 seconds to compute all the

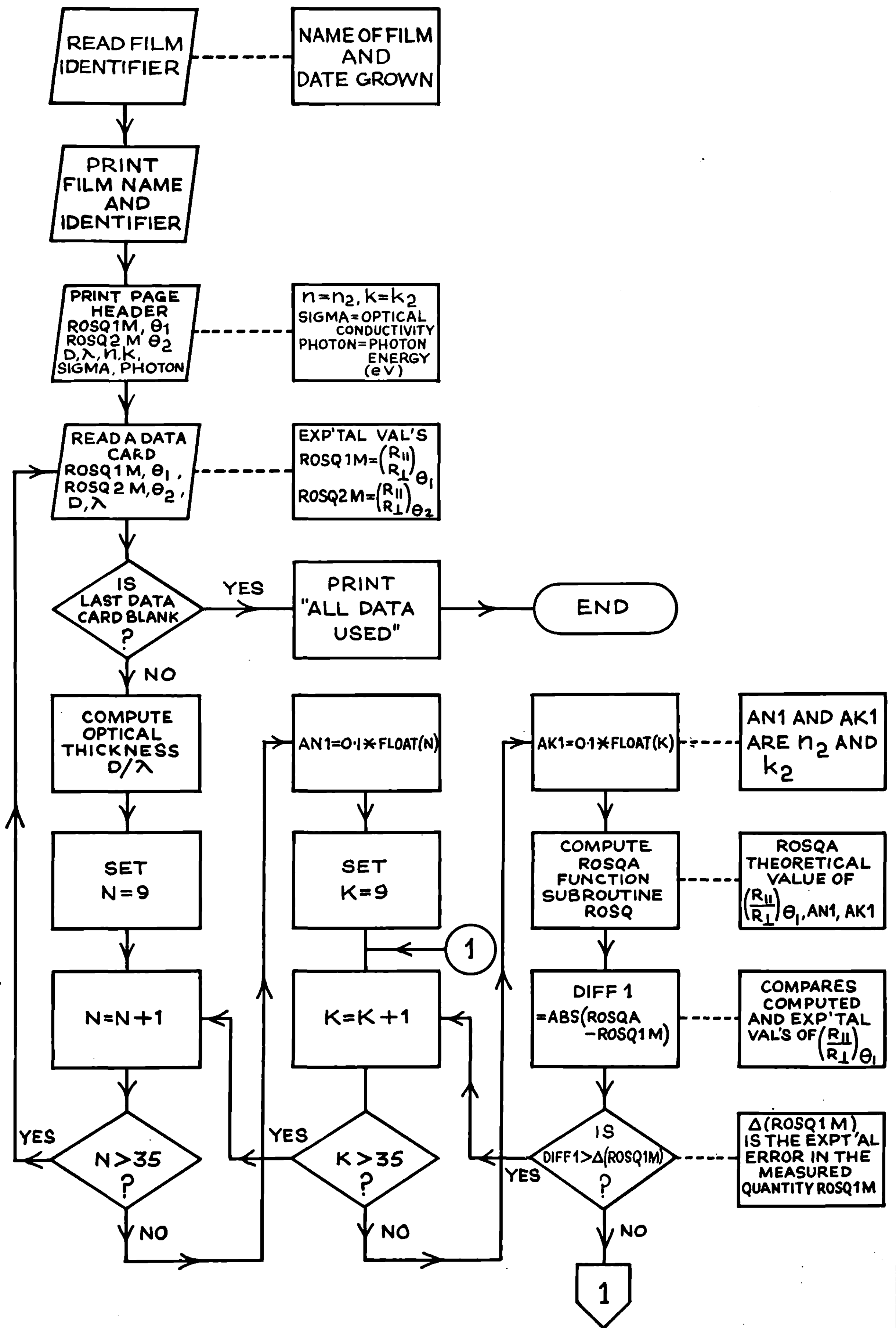

Figure 3.3.4 A flowchart of the computer programme used for deducing n_2 and k_2 values from measured values of $(R_{\parallel}/R_{\perp})$.

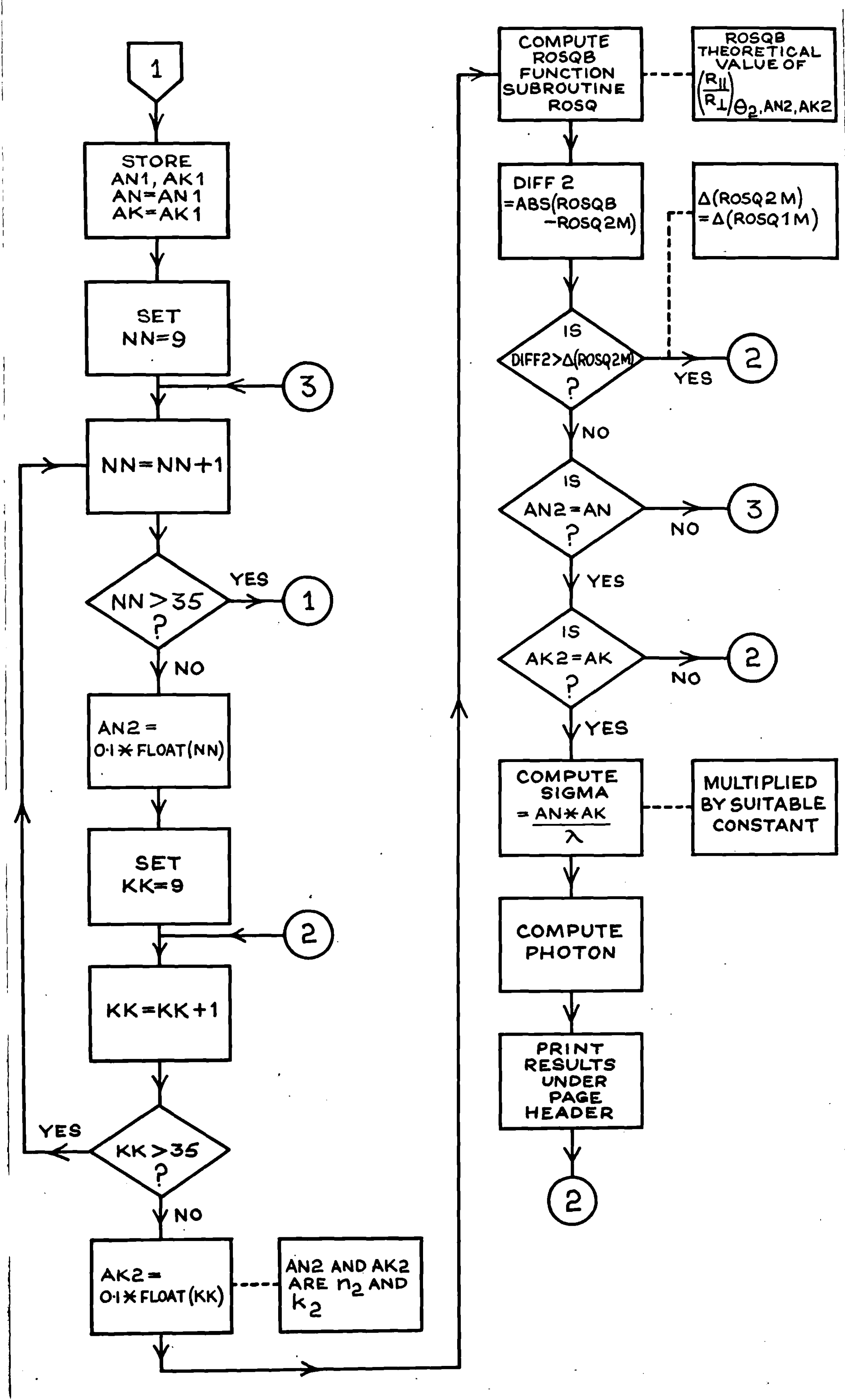

Figure 3.3.5 The flowchart of Figure 3.3.4 continued.

n_2, k_2 pairs associated with one set of experimental data. This programme was used to obtain n_2 and k_2 from some measurements on thin films of nickel and terbium oxide, and these results are given in Chapter 7.

3.4 The optimum angles of incidence for $1.0 \leqslant n_2 \leqslant 4.0$, $1.0 \leqslant k_2 \leqslant 4.0$

Humphreys-Owen (1961) investigated the arithmetical sensitivity of Avery's method to changes in the optical constants, and produced a sensitivity diagram in which $(R_{/\!/} / R_{\perp})_{\theta=60^o}$ was plotted against $(R_{/\!/} / R_{\perp})_{\theta=80^o}$, with n and k as parameters. Such a diagram may be used quantitatively to investigate the sensitivity of $(R_{/\!/} / R_{\perp})$ to changes in n_2 and k_2 for thin films. Figure 3.4.1 shows an enlarged portion of a sensitivity diagram, ($R_{/\!/} / R_{\perp}$ plotted for two arbitrary angles of incidence θ_1 and θ_2) for constant d/λ. Point P has coordinates (n_2, k_2), the optical constants of interest, and lies within the quadrilateral formed by the following lines: constant n_2 +0.05, constant k_2 +0.05, constant n_2 -0.05 and constant k_2 -0.05. It is assumed that the size of the quadrilateral is a measure of the sensitivity of the ratios $(R_{/\!/} / R_{\perp})_{\theta_1}$ and $(R_{/\!/} / R_{\perp})_{\theta_2}$, to the optical constants in the vicinity of n_2 and k_2. A region of good sensitivity is, therefore, one in which large changes in the two reflection ratios produce changes of only $\pm$ 0.05 in n_2 and k_2, that is the area of the quadrilateral is large.

Coordinate geometry gives a formula for the area of such a quadrilateral in terms of the coordinates of the apices. The expression for the area of the quadrilateral illustrated in Figure 3.4.1 is:

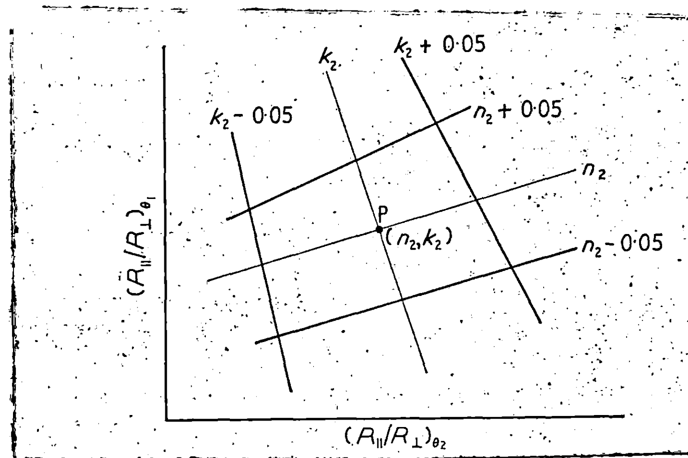

Figure 3.4.1 Basis of calculating the optimum angles of incidence, for a fixed d/λ .

Writing $\rho^2_{\theta_1} = (R_{/\!/}/R_{\perp})_{\theta_1}$

and $\rho^2_{\theta_2} = (R_{/\!/}/R_{\perp})_{\theta_2}$

$$\begin{aligned}
\text{Area} = -\tfrac{1}{2}\Big[& \rho^2_{\theta_2}(n_2 + 0.05,\ k_2 + 0.05)\,\rho^2_{\theta_1}(n_2 - 0.05,\ k_2 + 0.05) \\
& + \rho^2_{\theta_2}(n_2 - 0.05,\ k_2 + 0.05)\,\rho^2_{\theta_1}(n_2 - 0.05,\ k_2 - 0.05) \\
& + \rho^2_{\theta_2}(n_2 - 0.05,\ k_2 - 0.05)\,\rho^2_{\theta_1}(n_2 + 0.05,\ k_2 - 0.05) \\
& + \rho^2_{\theta_2}(n_2 + 0.05,\ k_2 - 0.05)\,\rho^2_{\theta_1}(n_2 + 0.05,\ k_2 + 0.05) \\
& - \rho^2_{\theta_1}(n_2 + 0.05,\ k_2 + 0.05)\,\rho^2_{\theta_2}(n_2 - 0.05,\ k_2 + 0.05) \\
& - \rho^2_{\theta_1}(n_2 - 0.05,\ k_2 + 0.05)\,\rho^2_{\theta_2}(n_2 - 0.05,\ k_2 - 0.05) \\
& - \rho^2_{\theta_1}(n_2 - 0.05,\ k_2 - 0.05)\,\rho^2_{\theta_2}(n_2 + 0.05,\ k_2 - 0.05) \\
& - \rho^2_{\theta_1}(n_2 + 0.05,\ k_2 - 0.05)\,\rho^2_{\theta_2}(n_2 + 0.05,\ k_2 + 0.05)\Big]
\end{aligned}$$

This formula was used in a computer programme to calculate the areas of quadrilaterals for all combinations of θ_1 and θ_2 ($45.0^\circ \leqslant \theta_1 \leqslant 65.0^\circ$; $66.0^\circ \leqslant \theta_2 \leqslant 88.0^\circ$), for fixed values of n_2, k_2 and d/λ. These latter values were chosen from the ranges $1.0 \leqslant n_2 \leqslant 4.0$, $1.0 \leqslant k_2 \leqslant 4.0$ and $0.01 \leqslant d/\lambda \leqslant 0.250$. A computer sorting technique was used for each fixed value of n_2, k_2 and d/λ, to find the combination of θ_1 and θ_2 which generated a quadrilateral with the largest area. Thus for each n_2, k_2 and d/λ investigated two optimum angles of incidence were obtained, one for θ_1 and one for θ_2, at which to measure the ratios $(R_{/\!/}/R_{\perp})_{\theta_1}$ and $(R_{/\!/}/R_{\perp})_{\theta_2}$.

A flowchart of the programme used to compute the optimum angles is shown in Figures 3.4.2, 3.4.3 and 3.4.4. (Function subroutine ROSQ is used in this programme, and so Figure 3.3.1 should also be consulted.) This flowchart is so written that optimum angles will be computed to the nearest degree. There is little loss in sensitivity if such angles are used instead of those computed to the nearest 0.1° provided that, the required angular setting precisions are maintained. A discussion on angular precision is given below. A computer programme designed to compute the optimum angles to the nearest 0.1° required about 250 seconds of computing time per pair of optimum angles chosen. The computing time per pair of chosen optimum angles to the nearest 1° was found to be about 3 seconds.

For each of the chosen optimum angles of incidence a computer subroutine calculated the precision to which angular measurements should be made to obtain n_2 and k_2 to an accuracy of better than $\pm$ 0.05. This subroutine worked simply by incrementing the values of n_2 and k_2 under investigation by + 0.05, and then recomputing the optimum angles for that incremented n_2,k_2 pair. The error introduced in θ_1 and θ_2 was thus obtained. It was assumed that this error would be the same if n_2 and k_2 had been changed by -0.05. Tables 3.4.1, 3.4.2 and 3.4.3 show values of optimum angles of incidence (to the nearest 0.1°) and the necessary setting precisions, for some integer values of n_2 and k_2 and for d/λ = 0.050, 0.100 and 0.150. Tables 3.4.4 and 3.4.5 show the optimum angles of incidence (to the nearest 1°) for the same values of n_2 and k_2 for d/λ = 0.200 and 0.250 respectively.

A study of such tables reveals the following trends:

(i) There is appreciable variation of the optimum angles with n_2 and k_2 for a fixed value of d/λ .

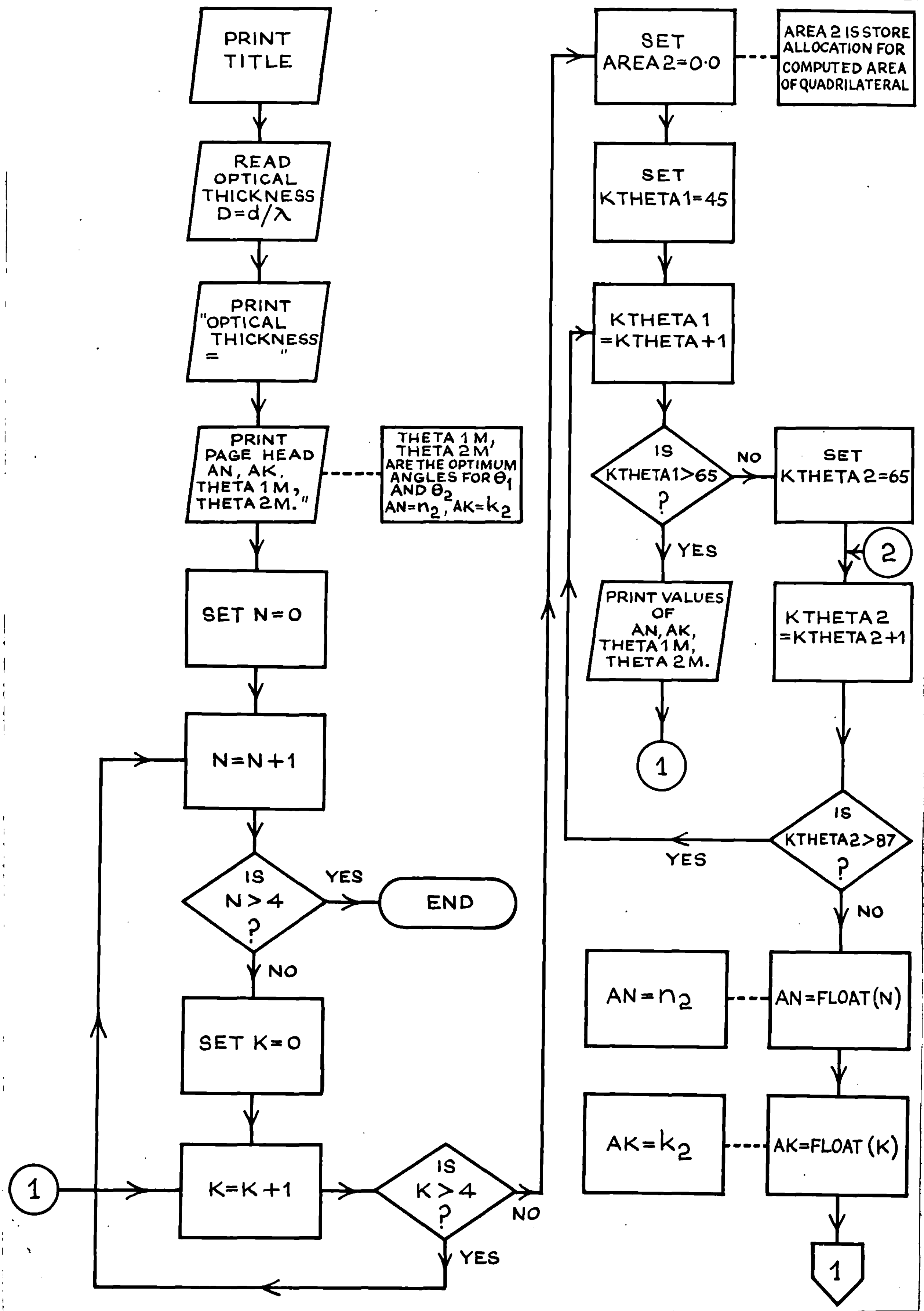

Figure 3.4.2 Flowchart of the computer programme used to calculate the optimum angles of incidence to the nearest 1° ($1 \leqslant n_2 \leqslant 4$, $1 \leqslant k_2 \leqslant 4$, $45 < \theta_1 \leqslant 65$, $66 \leqslant \theta_2 \leqslant 87$)

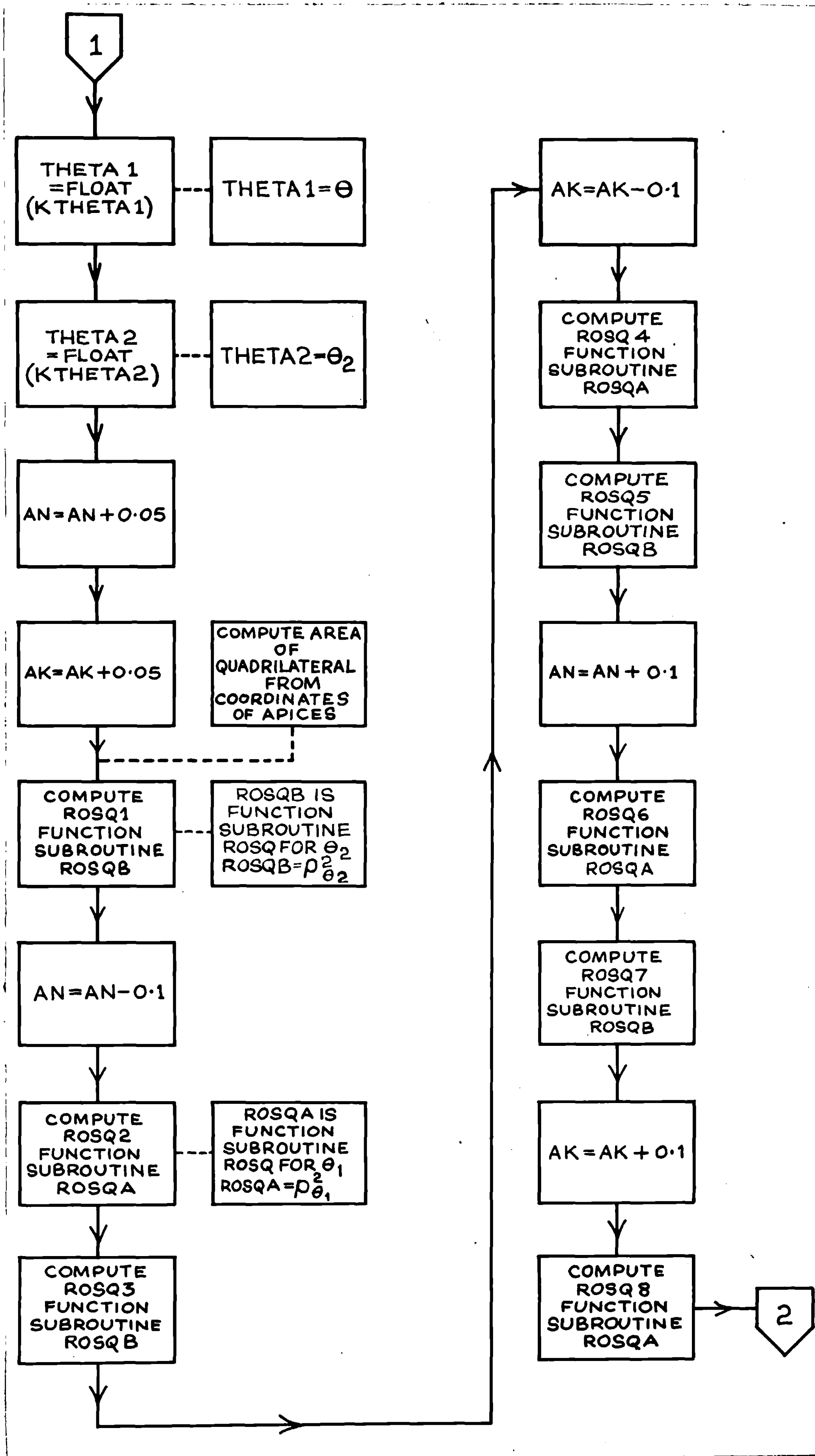

Figure 3.4.3 The flowchart of Figure 3.4.2 continued.

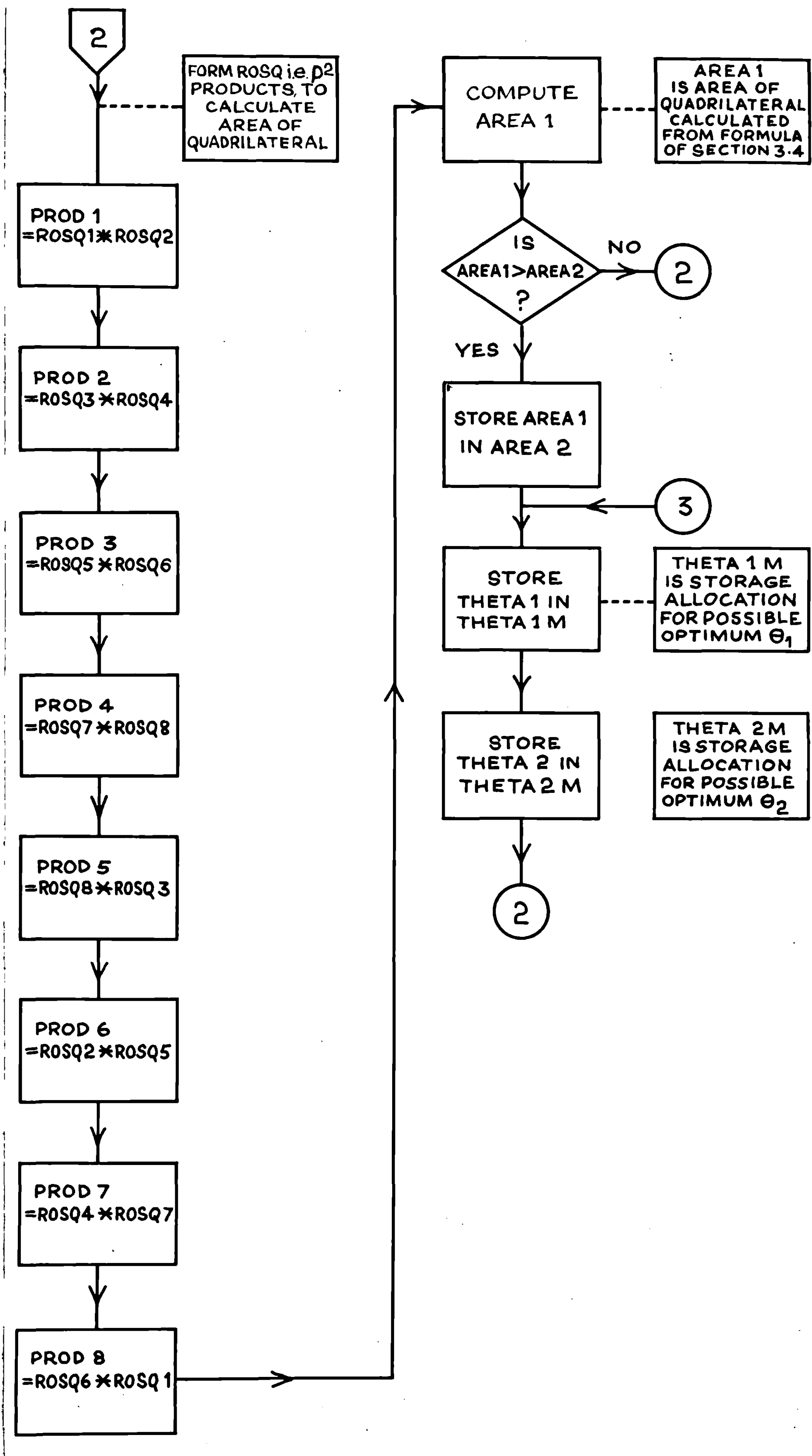

Figure 3.4.4 The flowchart of Figure 3.4.2 concluded.

Table 3.4.1 <u>Values of optimum angles and angular setting precision for $d/\lambda = 0.050$</u>

n_2	k_2	$\theta_1{}^o$	$\theta_2{}^o$	$\pm\Delta\theta_1{}^o$	$\pm\Delta\theta_2{}^o$
1.0	1.0	46.3	76.7	0.7	0.5
1.0	2.0	50.9	80.5	0.5	0.3
1.0	3.0	57.4	82.5	0.4	0.2
1.0	4.0	63.1	83.8	0.3	0.1
2.0	1.0	49.6	81.6	0.6	0.3
2.0	2.0	54.5	83.3	0.5	0.2
2.0	3.0	59.7	84.3	0.4	0.1
2.0	4.0	64.3	85.2	0.2	<0.1
3.0	1.0	55.0	85.5	0.9	0.2
3.0	2.0	59.4	85.9	0.4	0.1
3.0	3.0	63.1	86.2	0.3	<0.1
3.0	4.0	65.0	86.4	0.2	<0.1
4.0	1.0	62.3	87.1	0.2	0.1
4.0	2.0	64.0	87.5	0.3	<0.1
4.0	3.0	65.0	86.6	0.1	<0.1
4.0	4.0	65.0	86.7	<0.1	<0.1

Table 3.4.2 Values of optimum angles and angular setting precision for $d/\lambda = 0.100$

n_2	k_2	θ_1^{o}	θ_2^{o}	$\pm\Delta\theta_1^{o}$	$\pm\Delta\theta_2^{o}$
1.0	1.0	46.1	76.0	0.8	0.5
1.0	2.0	50.7	79.7	0.6	0.3
1.0	3.0	58.5	82.1	0.3	0.2
1.0	4.0	64.4	83.6	0.2	0.1
2.0	1.0	50.0	81.6	0.2	0.3
2.0	2.0	54.0	82.6	0.4	0.2
2.0	3.0	59.4	83.7	0.3	0.1
2.0	4.0	64.3	84.6	0.2	0.1
3.0	1.0	56.1	84.4	0.1	0.1
3.0	2.0	57.3	84.4	0.3	0.1
3.0	3.0	61.1	84.9	0.3	0.1
3.0	4.0	64.8	85.0	0.2	0.1
4.0	1.0	57.0	84.5	0.2	0.1
4.0	2.0	59.1	85.2	0.3	0.1
4.0	3.0	62.6	86.0	0.2	<0.1
4.0	4.0	65.0	86.1	<0.1	<0.1

Table 3.4.3 Values of optimum angles and angular setting precision for $d/\lambda = 0.150$

n_2	k_2	$\theta_1{}^o$	$\theta_2{}^o$	$\pm\Delta\theta_1{}^o$	$\pm\Delta\theta_2{}^o$
1.0	1.0	46.0	74.7	0.8	0.7
1.0	2.0	49.8	79.2	0.6	0.4
1.0	3.0	58.3	81.9	0.3	0.2
1.0	4.0	64.4	83.6	0.2	0.1
2.0	1.0	47.7	80.3	0.4	0.7
2.0	2.0	52.7	82.2	0.4	0.1
2.0	3.0	58.8	83.5	0.4	0.2
2.0	4.0	64.1	84.6	0.3	0.1
3.0	1.0	51.2	82.9	0.7	0.1
3.0	2.0	56.1	84.1	0.4	0.1
3.0	3.0	60.6	84.8	0.4	0.1
3.0	4.0	64.9	85.5	0.3	<0.1
4.0	1.0	61.0	85.0	0.2	0.1
4.0	2.0	60.4	85.5	0.3	0.1
4.0	3.0	63.1	85.8	0.3	0.1
4.0	4.0	65.0	86.2	0.2	<0.1

Table 3.4.4 Values of optimum angles and angular setting precision for $d/\lambda = 0.200$ Optimum angles are to nearest degree

n_2	k_2	θ_1^{o}	θ_2^{o}	$\pm\Delta\theta_1^{o}$	$\pm\Delta\theta_2^{o}$
1.0	1.0	46	74	0.6	0.3
1.0	2.0	49	79	0.5	0.2
1.0	3.0	58	82	0.4	0.2
1.0	4.0	65	84	0.3	0.1
2.0	1.0	46	80	0.3	0.2
2.0	2.0	52	82	0.4	0.2
2.0	3.0	59	84	0.3	0.1
2.0	4.0	64	85	0.2	0.1
3.0	1.0	55	83		
3.0	2.0	57	84		
3.0	3.0	61	85		
3.0	4.0	65	85	$\leqslant 0.2$	$\simeq 0.1$
4.0	1.0	61	86		
4.0	2.0	61	86		
4.0	3.0	63	86		
4.0	4.0	65	86		

Table 3.4.5 Values of optimum angles and angular setting precision for $d/\lambda = 0.250$ Optimum angles are to nearest degree

n_2	k_2	θ_1^{o}	θ_2^{o}	$\pm\Delta\theta_1^{o}$	$\pm\Delta\theta_2^{o}$
1.0	1.0	46	74	0.6	0.4
1.0	2.0	49	79	0.5	0.3
1.0	3.0	58	82	0.4	0.2
1.0	4.0	65	84	0.3	0.1
2.0	1.0	47	80	0.4	0.3
2.0	2.0	52	82	0.3	0.2
2.0	3.0	59	84	0.3	0.2
2.0	4.0	64	85	0.2	0.1
3.0	1.0	55	84		
3.0	2.0	57	84		
3.0	3.0	61	85		
3.0	4.0	65	85	≤ 0.2	$\simeq 0.1$
4.0	1.0	58	85		
4.0	2.0	60	85		
4.0	3.0	63	86		
4.0	4.0	65	86		

(ii) There is some variation of the optimum angles with d/λ for $n_2 \leqslant 2.0$; the variation becomes more marked for $n_2 > 2.0$ especially for $d/\lambda \leqslant 0.150$.

(iii) In general, the higher angle of incidence requires a better setting precision than the lower. A greater degree of precision is required for both angles of incidence for the larger values of n_2 and k_2, ($n_2 \geqslant 3.0$; $k_2 \geqslant 3.0$).

(iv) As d/λ increases, the required angular setting precision becomes smaller. For $d/\lambda \geqslant 0.150$, it appears that angles of incidence measured to within $\pm 0.2^{o}$ do not cause errors in n_2 and k_2 of greater than ± 0.05, (Avery estimated $\pm 0.5^{o}$ as a suitable tolerance to obtain n_2 and k_2 accurate to 4%). For $n_2 > 3.0$ a $\pm 0.1^{o}$ tolerance in the angle of incidence would certainly not cause errors of greater than ± 0.05 in n_2 and k_2.

(v) For $d/\lambda \leqslant 0.150$, greater precision is required for the angular measurements. It is estimated that if the optimum angles of incidence can be measured to better than $\pm 0.1^{o}$, then this should produce changes in n_2 and k_2 of less than ± 0.05.

3.5 The precision required for measurements of d/λ

It should be possible, using multiple beam interferometry, to measure the optical thickness d/λ to within ± 0.005. Assuming the wavelength of the incident light is known precisely, the above tolerance corresponds to an error in the film thickness (d) of between 2nm and 3nm, for the visible range of wavelengths.

A computer programme was written to determine the values of d/λ for which the tolerance of ± 0.005 was insufficient to make errors of n_2 and k_2 fall outside the limits ± 0.05. Values of $1.0 \leqslant n_2 \leqslant 4.0$ and $1.0 \leqslant k_2 \leqslant 4.0$ were investigated for a number of optimum angles of incidence. For a chosen value of d/λ the computer calculated

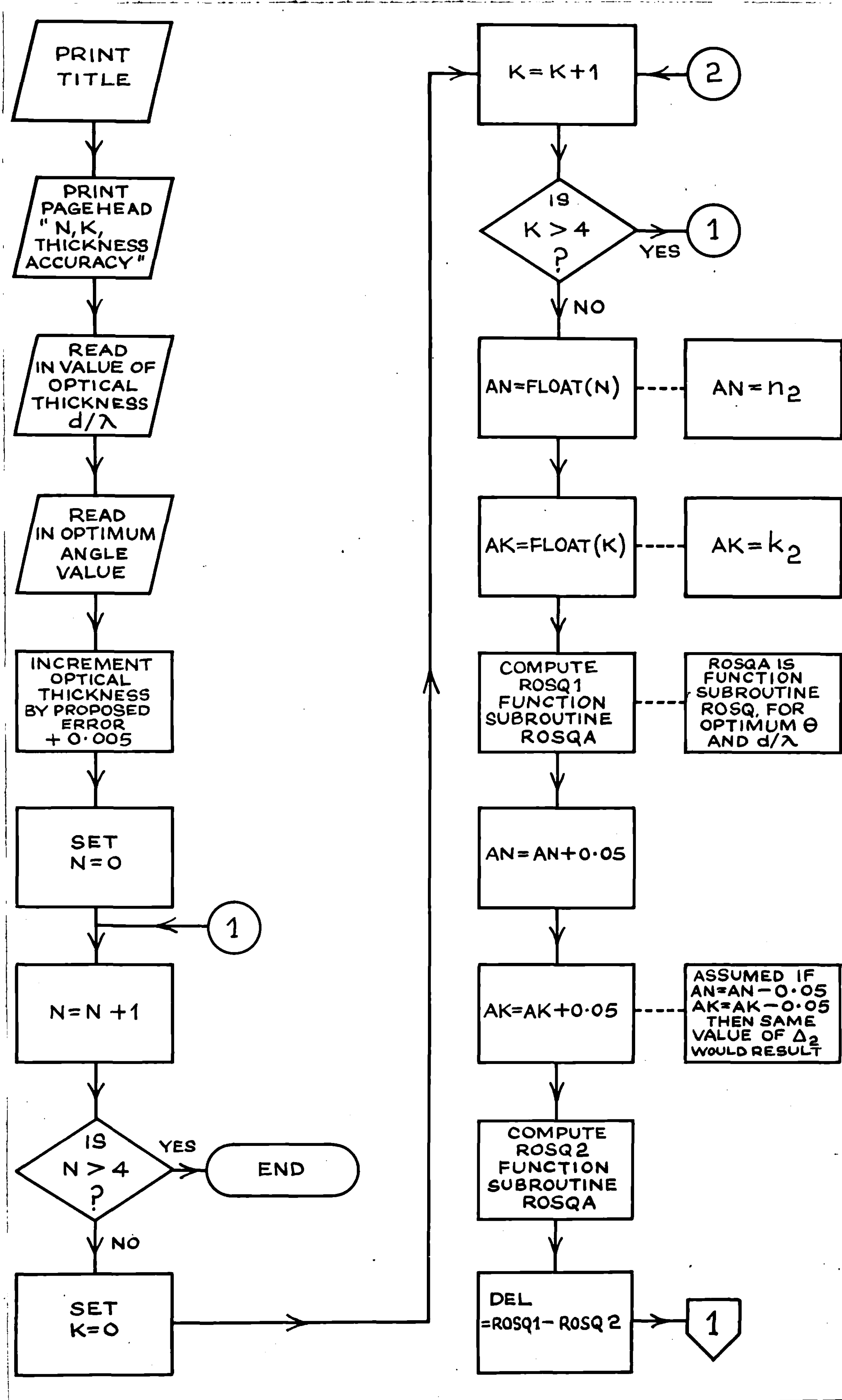

Figure 3.5.1 Flowchart of the programme used to investigate the precision required for d/λ .

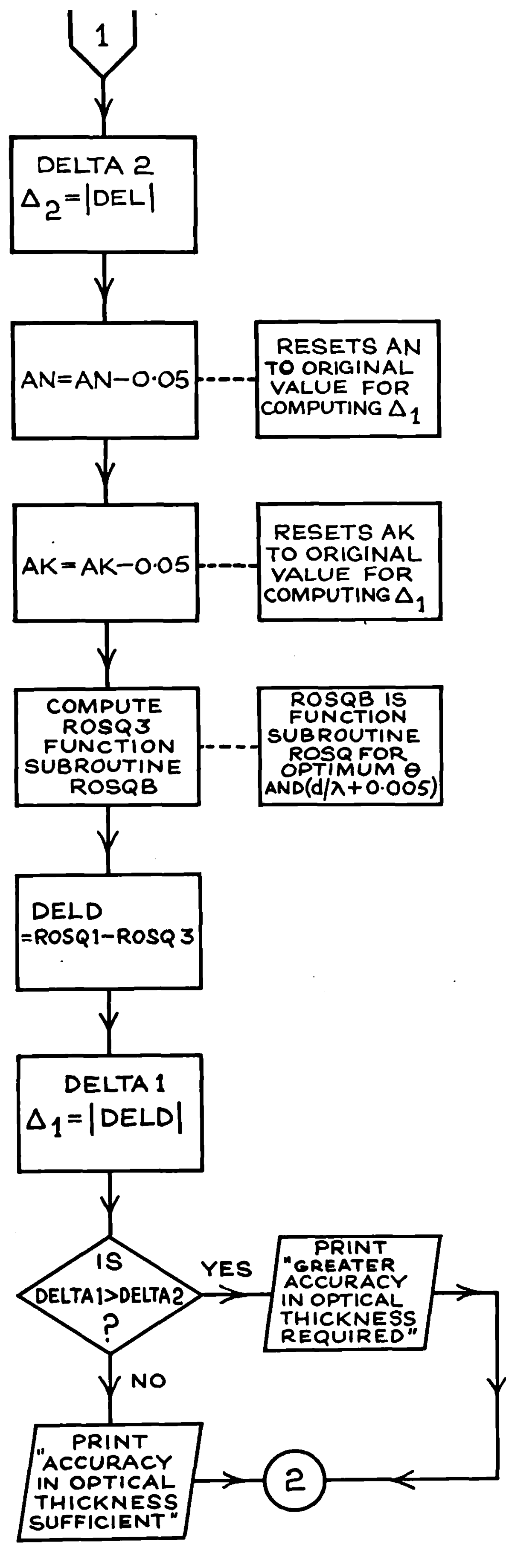

Figure 3.5.2 Flowchart of the programme of Figure 3.5.1 continued.

for fixed optimum θ, n_2 and k_2 the difference Δ_1 given by equation 3.5.1.

$$\Delta_1 = \left| \left[\rho^2(d/\lambda)\right]_{\theta,n_2,k_2} - \left[\rho^2(d/\lambda \pm 0.005)\right]_{\theta,n_2,k_2} \right| \qquad 3.5.1$$

For the fixed θ, n_2 and k_2 and the chosen value of d/λ, the difference Δ_2 given by equation 3.5.2 was also calculated.

$$\Delta_2 = \left| \left[\rho^2(n_2,k_2)\right]_{\theta,d/\lambda} - \left[\rho^2(n_2 \pm 0.05,\ k_2 \pm 0.05)\right]_{\theta,d/\lambda} \right| \qquad 3.5.2$$

Equation 3.5.1 is the difference between two reflection ratios arising from a change in d/λ of $\pm$ 0.005. Equation 3.5.2 is the difference between the two reflection ratios arising out of changes in n_2 and k_2 of $\pm$ 0.05. The quantities Δ_1 and Δ_2 were then compared; if Δ_1 was computed to be less than Δ_2 then the tolerance of $\pm$ 0.005 was deemed sufficient. A flowchart of the computer programme for computing and comparing Δ_1 and Δ_2 for $1 \leqslant n_2 \leqslant 4$, $1 \leqslant k_2 \leqslant 4$, is shown in Figure 3.5.1 and Figure 3.5.2. This programme used function subroutine ROSQ and so Figure 3.3.1 should be consulted also.

The computer results showed that, for measurements at the optimum angles of incidence the tolerance of $\pm$ 0.005 for d/λ was insufficiently accurate for values of $d/\lambda \leqslant 0.050$. This was true for between 85% and 95% of the combinations of n_2 and k_2 investigated, depending on the value of d/λ. For values of $d/\lambda > 0.050$ the above tolerance was found to be sufficiently accurate for at least 70% of the combinations of n_2 and k_2 in the ranges $1.0 \leqslant n_2 \leqslant 4.0$ and $1.0 \leqslant k_2 \leqslant 4.0$. The percentage value again depended on the optical thickness, and increased with increasing d/λ.

3.6 <u>The precision required for measurement of the ratio $R_{/\!/}/R_{\perp}$</u>

It should not be difficult to measure $(R_{/\!/}/R_{\perp})_{\theta_1}$ and $(R_{/\!/}/R_{\perp})_{\theta_2}$ at optimum angles of incidence θ_1 and θ_2 each to within $\pm$ 0.01. The computer programme, which calculated the optimum angles of incidence, also produced values of the necessary tolerances of the two ratios at those angles, in order to achieve errors in n_2 and k_2 of $\pm$ 0.05. Figure 3.6.1, which is similar to Figure 3.4.1, shows the basis of the method of calculating the required tolerances in the reflection ratios for a given n_2, k_2 pair. The apices of the quadrilateral of Figure 3.6.1 correspond to intersections E_1, E_2, E_3 and E_4 with the reflection ratio axes. These intersections represent the changes in $(R_{/\!/}/R_{\perp})_{\theta_1}$ and $(R_{/\!/}/R_{\perp})_{\theta_2}$ caused by changes of $\pm$ 0.05 in n_2 and k_2. Thus E_1 - E_4 represent tolerances defined by $\pm E_n/2$, (n = 1, ...4), in the reflection ratios. It is possible, for certain values of n_2 and k_2, for one member of the (E_1,E_3) pair to be much smaller than the other e.g. $E_3 \ll E_1$. For such cases E_1 would be used to calculate the required tolerance in $(R_{/\!/}/R_{\perp})_{\theta_2}$. This could also apply to the (E_2,E_4) pair. The section of the optimum angle programme (Figures 3.4.2 to 3.4.4) which calculated E_1 - E_4 is shown flowcharted in Figure 3.6.2; its point of insertion into the optimum angle programme is also shown.

Tables 3.6.1 to 3.6.5 show values of the required tolerances, denoted by $\pm\Delta(R_{/\!/}/R_{\perp})_{\theta_1}$ and $\pm\Delta(R_{/\!/}/R_{\perp})_{\theta_2}$, for the two reflection ratios measured at optimum angles for d/λ = 0.050, 0.100, 0.150, 0.200 and 0.250 respectively. From these tables it was found that for $1.0 \leqslant n_2 \leqslant 3.0$, $1.0 \leqslant k_2 \leqslant 4.0$, a tolerance of $\pm$ 0.01 in the measured reflection ratios was sufficient to yield both n_2 and k_2 within $\pm$ 0.05 for all $0.050 \leqslant d/\lambda \leqslant 0.250$. For $3.0 \leqslant n_2 \leqslant 4.0$, measurement of each ratio to $\pm$ 0.005 would be sufficient to allow n_2 and k_2 to be determined within $\pm$ 0.05 for most values of n_2, k_2 and d/λ. It is interesting

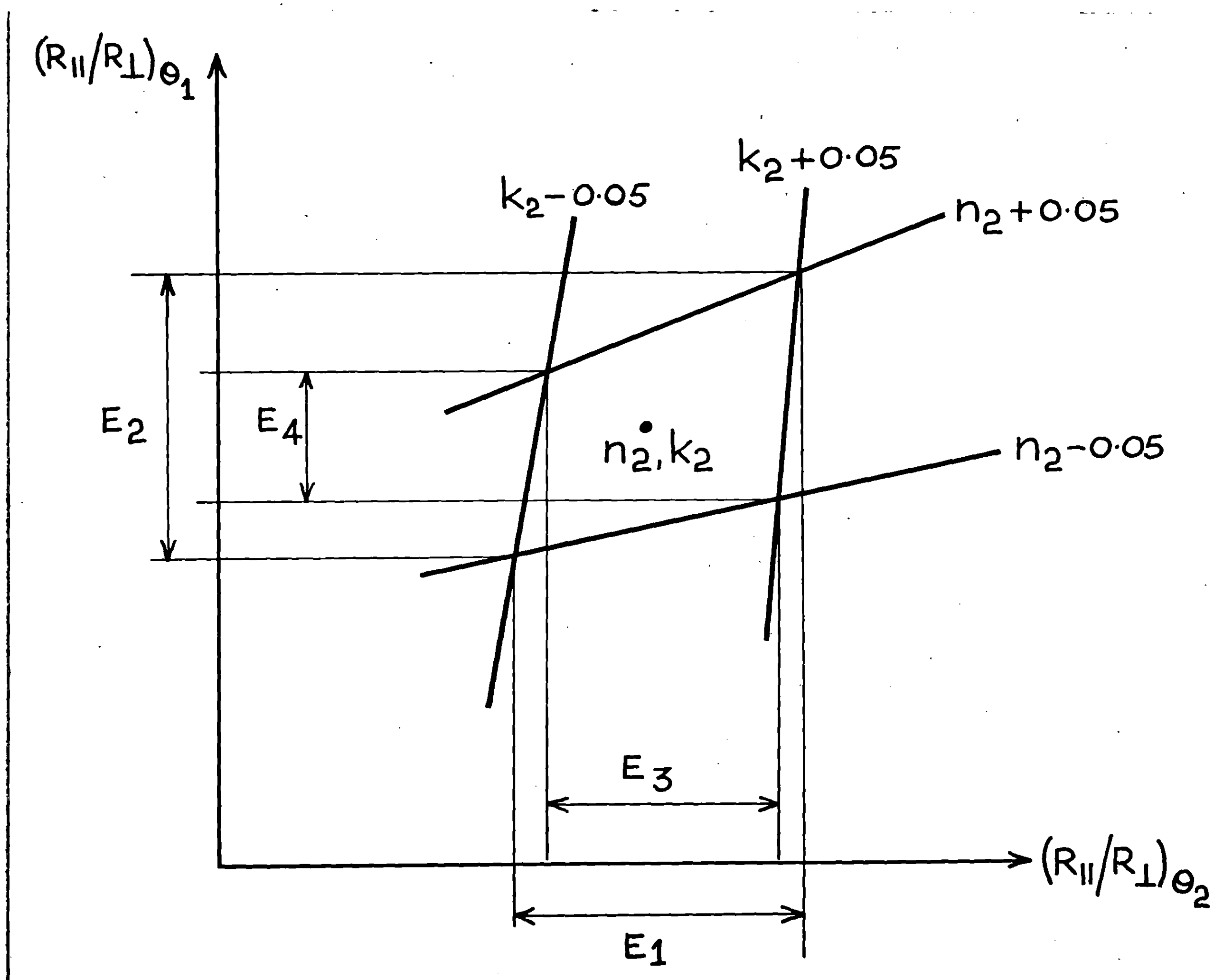

Figure 3.6.1 Basis of method of calculating the tolerances in the reflection ratios.

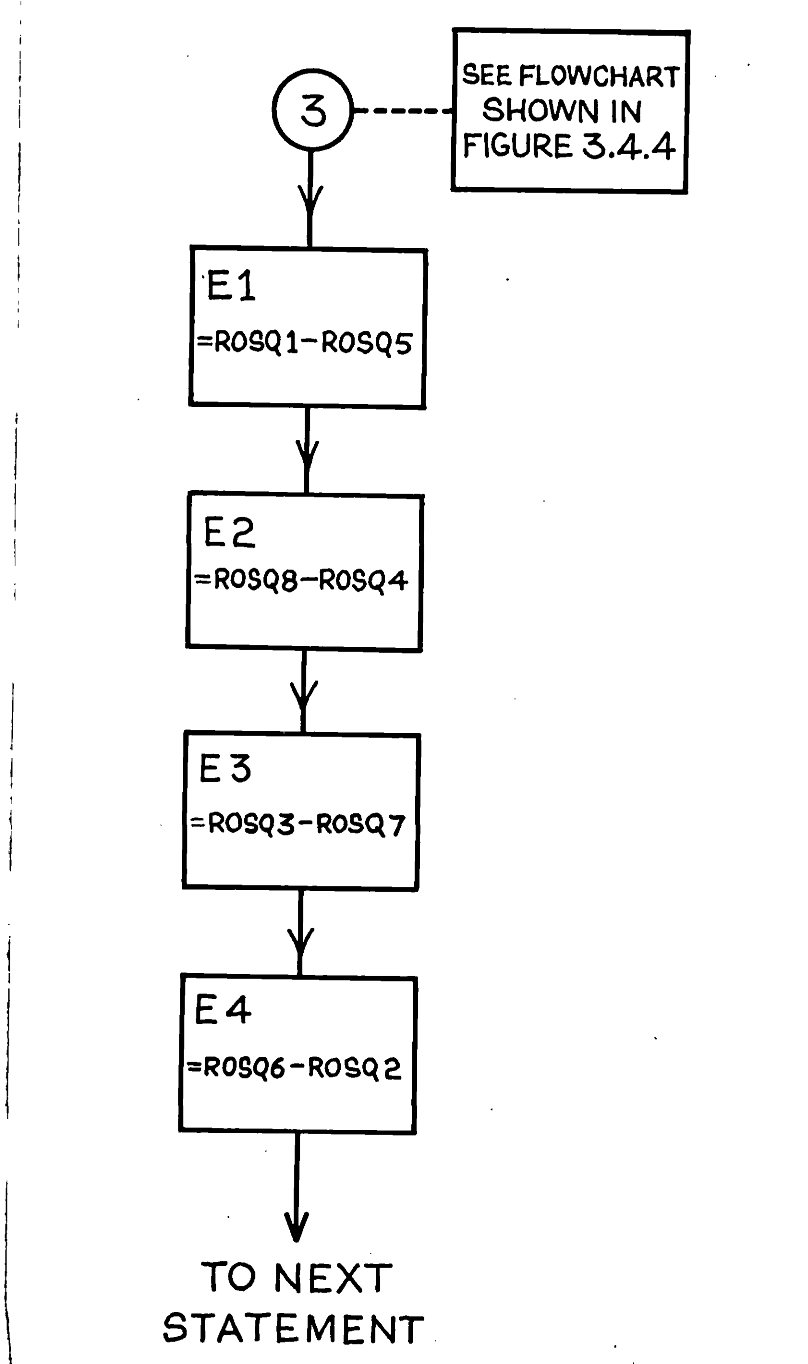

Figure 3.6.2 Flowchart of the programme to compute the required precision in $(R_{//}/R_{\perp})$ to obtain n_2 and k_2 to $\pm$ 0.05. This flowchart to be used with that shown in Figure 3.4.4.

Table 3.6.1 Tolerances, $\Delta(R_{\parallel}/R_{\perp})_{\theta_1}$, $\Delta(R_{\parallel}/R_{\perp})_{\theta_2}$, in the reflection ratios, at optimum angles θ_1 and θ_2 shown in Table 3.4.1, for d/λ = 0.050

n_2	k_2	$\pm\Delta(R_{\parallel}/R_{\perp})_{\theta_1}$	$\pm\Delta(R_{\parallel}/R_{\perp})_{\theta_2}$
1.0	1.0	0.023	0.025
1.0	2.0	0.017	0.014
1.0	3.0	0.015	0.012
1.0	4.0	0.015	0.013
2.0	1.0	0.014	0.014
2.0	2.0	0.010	0.010
2.0	3.0	0.010	0.010
2.0	4.0	0.010	0.009
3.0	1.0	0.011	0.011
3.0	2.0	0.010	0.008
3.0	3.0	0.007	0.007
3.0	4.0	0.006	0.007
4.0	1.0	0.009	0.010
4.0	2.0	0.007	0.007
4.0	3.0	0.006	0.006
4.0	4.0	0.004	0.005

Table 3.6.2 Tolerances, $\Delta(R_{\parallel}/R_{\perp})_{\theta_1}$, $\Delta(R_{\parallel}/R_{\perp})_{\theta_2}$, in the reflection ratios, at optimum angles θ_1 and θ_2 shown in Table 3.4.2 for $d/\lambda = 0.100$

n_2	k_2	$\pm\Delta(R_{\parallel}/R_{\perp})_{\theta_1}$	$\pm\Delta(R_{\parallel}/R_{\perp})_{\theta_2}$
1.0	1.0	0.031	0.025
1.0	2.0	0.022	0.017
1.0	3.0	0.018	0.015
1.0	4.0	0.016	0.013
2.0	1.0	0.015	0.013
2.0	2.0	0.011	0.011
2.0	3.0	0.012	0.010
2.0	4.0	0.012	0.009
3.0	1.0	0.006	0.007
3.0	2.0	0.006	0.006
3.0	3.0	0.007	0.006
3.0	4.0	0.008	0.007
4.0	1.0	0.003	0.002
4.0	2.0	0.004	0.005
4.0	3.0	0.005	0.005
4.0	4.0	0.006	0.005

Table 3.6.3 Tolerances, $\Delta(R_{\parallel}/R_{\perp})\theta_1$, $\Delta(R_{\parallel}/R_{\perp})\theta_2$, in the reflection ratios, at optimum angles θ_1 and θ_2 shown in Table 3.4.3, for $d/\lambda = 0.150$

n_2	k_2	$\pm\Delta(R_{\parallel}/R_{\perp})\theta_1$	$\pm\Delta(R_{\parallel}/R_{\perp})\theta_2$
1.0	1.0	0.031	0.024
1.0	2.0	0.025	0.018
1.0	3.0	0.019	0.016
1.0	4.0	0.016	0.014
2.0	1.0	0.012	0.011
2.0	2.0	0.012	0.010
2.0	3.0	0.013	0.010
2.0	4.0	0.008	0.007
3.0	1.0	0.007	0.008
3.0	2.0	0.008	0.007
3.0	3.0	0.008	0.007
3.0	4.0	0.009	0.007
4.0	1.0	0.012	0.011
4.0	2.0	0.008	0.006
4.0	3.0	0.006	0.006
4.0	4.0	0.006	0.006

Table 3.6.4 Tolerances, $\Delta(R_{\parallel}/R_{\perp})_{\theta_1}$, $\Delta(R_{\parallel}/R_{\perp})_{\theta_2}$, in the reflection ratios, at optimum angles θ_1 and θ_2 shown in Table 3.4.4, for $d/\lambda = 0.200$

n_2	k_2	$\pm\Delta(R_{\parallel}/R_{\perp})_{\theta_1}$	$\pm\Delta(R_{\parallel}/R_{\perp})_{\theta_2}$
1.0	1.0	0.031	0.023
1.0	2.0	0.024	0.018
1.0	3.0	0.019	0.016
1.0	4.0	0.016	0.013
2.0	1.0	0.012	0.011
2.0	2.0	0.012	0.011
2.0	3.0	0.013	0.010
2.0	4.0	0.012	0.009
3.0	1.0	0.012	0.010
3.0	2.0	0.008	0.008
3.0	3.0	0.008	0.007
3.0	4.0	0.009	0.007
4.0	1.0	0.004	0.006
4.0	2.0	0.006	0.005
4.0	3.0	0.005	0.005
4.0	4.0	0.006	0.006

Table 3.6.5 Tolerances, $\Delta(R_{\parallel}/R_{\perp})_{\theta_1}$, $\Delta(R_{\parallel}/R_{\perp})_{\theta_2}$, in the reflection ratios, at optimum angles θ_1 and θ_2 shown in Table 3.4.5, for $d/\lambda = 0.250$.

n_2	k_2	$\pm\Delta(R_{\parallel}/R_{\perp})_{\theta_1}$	$\pm\Delta(R_{\parallel}/R_{\perp})_{\theta_2}$
1.0	1.0	0.031	0.024
1.0	2.0	0.028	0.019
1.0	3.0	0.020	0.016
1.0	4.0	0.017	0.013
2.0	1.0	0.014	0.013
2.0	2.0	0.012	0.011
2.0	3.0	0.013	0.010
2.0	4.0	0.012	0.009
3.0	1.0	0.009	0.009
3.0	2.0	0.008	0.007
3.0	3.0	0.008	0.007
3.0	4.0	0.009	0.007
4.0	1.0	0.007	0.007
4.0	2.0	0.007	0.005
4.0	3.0	0.006	0.004
4.0	4.0	0.006	0.006

to note that for both reflection ratios the required tolerance is about the same.

It was of interest to determine for what values of d/λ Avery's single reflection formula could be accurately used to deduce n_2 and k_2 from the experimental data. The optimum angle programme was modified to include Avery's formula, so that the required calculations could be made for each optimum angle chosen. These further computations showed that for $d/\lambda \gtrsim 0.150$ the values of the two ratios $(R_{\parallel}/R_{\perp})_{\theta_1}$ and $(R_{\parallel}/R_{\perp})_{\theta_2}$, calculated at the optimum angles of incidence from the single reflection formula (see Section 3.2 of this thesis), differed by less than 0.005, i.e. less than the permitted tolerance, $\pm$ 0.01 for $1.0 \leqslant n_2 \leqslant 4.0$ and $2.5 < k_2 \leqslant 4.0$. The same order of difference was found for $1.0 \leqslant k_2 \lesssim 2.5$ and for optical thicknesses, $d/\lambda \gtrsim 0.230$.

3.7 An investigation of the possible use of the optimized, ratio method for weakly absorbing films

It was of practical interest, for subsequent experimental work on a rare-earth metal oxide, to investigate the possibility of using the optimized, reflection ratio method for weakly absorbing films. For the purposes of this thesis a weakly absorbing film is one in which $k_2 < 1.0$. In general, most metal oxide and dielectric thin films have $k_2 < 1.0$. There are several methods for determining the optical constants of weakly absorbing films, e.g. that due to Hadley and Dennison which is described by Heavens (p.210, 1964). This method is capable of about $\pm$ 0.005 accuracy in k_2.

The computational methods described in the preceding Sections of this Chapter, were used to calculate for a number of combinations of n_2 and k_2 ($1.0 \leqslant n_2 \leqslant 4.0$, $0.2 \leqslant k_2 \leqslant 1.0$) the following quantities:

(i) The optimum values for θ_1 and θ_2.

(ii) The necessary precisions in θ_1 and θ_2, $(R_{\parallel}/R_{\perp})_{\theta_1}$ and $(R_{\parallel}/R_{\perp})_{\theta_2}$, to obtain n_2 and k_2 to about $\pm$ 0.05.

(iii) The precision required for the measurement of d/λ, to obtain n_2 and k_2 accurate to $\pm$ 0.05.

(iv) Values of d/λ for which Avery's single reflection formula may be used to deduce n_2 and k_2.

The computations which followed were performed for values of d/λ of 0.05 to 0.25 at 0.05 intervals. The optimum angles and necessary angular precisions are shown in Tables 3.4.1 to 3.4.5. The tolerances in the reflection ratios are shown in Tables ~~3.7.6~~ 3.6.1 to ~~3.7.10~~ 3.6.5. The acceptable precision for the measurement of d/λ, and the values of d/λ for which Avery's formula may be applied, are quoted in the following Section.

3.8 Summary

Avery's (1952) method for obtaining the optical constants (n and k) of a reflecting surface has been extended for use with thin films supported by thick dielectric substrates of known refractive index. If approximate values of the optical constants are known, then optimum angles of incidence may be chosen at which to perform the reflection measurements. The precision to which the measurements must be made to achieve a required accuracy in n_2 and k_2, may also be calculated.

The new method has been investigated for $1.0 \leqslant n_2 \leqslant 4.0$, $0.2 \leqslant k_2 \leqslant 4.0$, $0.01 \leqslant d/\lambda \leqslant 0.250$, and will yield n_2 and k_2 to an accuracy of $\pm$ 0.05 if measurements are obtained to within the following tolerances:

$k_2 \geq 1.0$

(i) Angles of incidence measured to better than $\pm$ 0.1°.

(ii) Optical thicknesses (≥ 0.05) measured to better than $\pm$ 0.005.

(iii) Reflection ratios measured to better than $\pm$ 0.005 for all n_2 and k_2 in the range considered, but if $n_2 \leq 3.0$ measurement to $\pm$ 0.01 is sufficient.

Furthermore, instead of the multiple reflection formula, Avery's single reflection formula may be used, without loss of accuracy, at the required optimum angles for the following values of n_2, k_2 and d/λ :

(i) Optical thicknesses, $d/\lambda \geq 0.150$, $1.0 \leq n_2 \leq 4.0$, $2.5 < k_2 \leq 4.0$.

(ii) Optical thicknesses, $d/\lambda \geq 0.230$, $1.0 \leq n_2 \leq 4.0$, $1.0 \leq k_2 \leq 2.5$.

For $k_2 < 1.0$ the recommended tolerances in the measured quantities are:

(i) Angles of incidence measured to better than $\pm$ 0.1°.

(ii) Optical thicknesses (≥ 0.100) measured to better than $\pm$ 0.005.

(iii) Reflection ratios measured to better than $\pm$ 0.005 for all n_2 and k_2 in the range considered.

CHAPTER 4

A REFLECTOMETER FOR DETERMINING THE OPTICAL CONSTANTS OF OPAQUE AND PARTIALLY TRANSPARENT, ABSORBING FILMS

Abstract

This Chapter starts with a brief review of some previous instrumentation used for determining optical constants n and k. The rest of the Chapter describes a reflectometer which has been designed and constructed from readily available equipment and materials for a relatively low cost. The instrument is a modified circular scale spectrometer. Photomultiplier detection is used to measure reflection coefficients to better than ± 0.006 at pre-set angles of incidence between 21° and 88°. The instrument can yield data, analyzable by a number of methods, from which the optical constants of solid surfaces and thin films may be determined to within ± 0.05. The optical wavelength range covered by the instrument is 400-700nm. A specimen holder and a low temperature optical cell for use with the reflectometer are also described.

4.1 A review of previous instrumentation

Many instruments have been designed and constructed to measure reflection coefficients at non-normal incidence for bulk and thin film specimens. Measurement of optical constants to better than 1% often entails elaborate and expensive equipment (Greef, 1970). This elaboration and expense is often a result of the data acquisition systems employed. It is advantageous if similar performance can be obtained from a simpler and less expensive instrument. This is especially true now that experimentally optimized reflection methods are available. (Miller, Taylor and Julien, 1970; Miller and Taylor, 1971.)

The main requirement of any instrument for measuring reflection coefficients is the ability to determine the incident light intensity and the reflected intensities for known polarizations, without any unknown change in the incident intensity. Practically, there are two methods of ensuring that unknown incident light fluctuations do not occur:

(i) The incident light beam is sampled by a photodetector and the signal is either recorded or fedback to the light source power supply to provide a stable output. Both systems have been employed; the latter is in current use by Davis (1971), who has reported certain difficulties in a private communication with the author of this thesis.

(ii) At the outset every effort is made to provide a stable light output. This can be done by using a tungsten-halide lamp powered from a highly stabilized d.c. power supply. Such a configuration has been used by Pells (1967); the lamp stability was better than $\pm$ 0.1%.

To make measurements of $R_{//}$ and $R_{\perp}$ or $R_{//}/R_{\perp}$ it is necessary to use a polarizer in the incident beam. The basic requirement here is that the polarizer must be such that the beam passing through it suffers no lateral shift on rotating the plane of polarization. Two devices which satisfy this requirement are: high quality polaroid sheet, and the Glan-Thompson prism. A study of the defects which can occur in Glan-Thompson prisms has been made by Moeller and Grieser (1969). Quartz Rochon prisms were used as the polarizer and analyzer in the reflectometer of Pells (1967). The advantage of such prisms is their wide optical transmission range of 200-2700nm. The disadvantage is that the angular separation between the E and O ray is small (typically

1°). Long optical paths are, therefore, needed to remove the unwanted E ray.

If dispersion measurements are required it is necessary to obtain the reflection measurements at a number of known wavelengths. Single, narrow band filters, graded wavelength filters or monochromators can be used to obtain the known wavelengths. Unless the monochromator is of good quality large light losses will occur; interference filters are often better in this respect. A graded wavelength filter when suitably mounted provides a simple and efficient monochromator. Such filters are now obtainable to provide wavelengths from the near ultraviolet to the near infra-red, with half-peak bandwidths of about 20nm.

The choice of detector depends on the wavelength range of interest; photomultipliers are used for the ultraviolet and visible wavelengths and solid state detectors, such as the Pbs cell, are used for the near infra-red where phase sensitive detection is usually used. Recently, a rotating polarizer system with associated phase sensitive detection has been developed by Brahms et al. (1968) for measurements in the vacuum ultraviolet ($\lambda \leqslant$ 250nm). When using a photomultiplier in the d.c. detection mode it is essential that the output from the photomultiplier power supply is stable to at least $\pm$ 0.2%. To reduce the noise level of such a system the photomultiplier cathode voltage can be set at considerably less than the permissible maximum, but still within the linear portion of the characteristic curves of the photomultiplier. Such a technique has been used by Pells (1967).

The optical configuration required to provide the collimated incident beam and subsequent collection of the reflected beam from the specimen surface, can take many forms. Generally, the configurations can be divided into two types: those involving mirror systems, which usually have a reference mirror for obtaining a measure of the incident

intensity, and those which use lens systems. Reflectometers employing mirrors are complicated to design and construct, but have the advantage that they may be used over a considerable wavelength range, from the vacuum ultra-violet to the far infra-red. A typical mirror type reflectometer is that designed and constructed by Potter (1965). This reflectometer uses three mirrors and a gear mechanism for changing the angle of incidence. The instrument is designed to measure the ratio $R_{\parallel} / R_{\perp}$ for a number of incident angles close to the pseudo-Brewster angle of the material, and so there is no need to measure the incident intensity. Simple reflectometers employing lens systems are those due to Avery (1952) and Pells (1967).

A rather novel reflectometer which uses a rotating light pipe instead of mirrors or lenses has been designed and constructed by Endriz and Spicer (1970). The light pipe rotates and samples in turn, the reflected and incident light. Although designed for normal incidence measurements, there appears to be no reason why it could not be used for non-normal angles of incidence. This reflectometer uses a modified, electronic counting system to detect the photomultiplier current; integration times of up to 30 seconds are used. This technique was adopted, presumably to overcome the short-term effects of light source fluctuations.

A further difficulty which can occur when measuring $R_{\parallel}$ and $R_{\perp}$ at two angles of incidence is that the same portion of the photosensitive surface of the detector must be used at both angles, to avoid errors due to variation in photosensitivity across the detector surface. To overcome this problem a diffusing screen is placed in front of the detector, (Kuhn and Wilson, 1950), which in addition overcomes any light polarization effects on the detector sensitivity. When the ratio $R_{\parallel} / R_{\perp}$ is measured, the first of the above problems does not occur.

For the purposes of the experimental work, to be described in this thesis, a simple reflectometer was required, versatile enough to enable data to be obtained for the following experiments:

(i) The evaluation of n and k over the visible wavelength range for opaque, absorbing films, using the ($R_{\parallel}$, $R_{\perp}$) method, and Avery's $R_{\parallel}/R_{\perp}$ method (see Section 1.6).

(ii) The evaluation of the optical constants of partially transparent, thin, absorbing films, using the optimized reflection ratio method described in Chapter 3.

(iii) The evaluation of n and k for visible wavelengths for opaque films below room temperature.

(iv) For preliminary magneto-optical studies of opaque films of gadolinium metal in the ferromagnetic phase.

(The Curie temperature of Gd is $\sim 289^{\circ}K$)

Many of the features of reflectometer design discussed above, were considered in designing the instrument described in the following Section.

4.2 Description of the reflectometer system

4.2.1 The reflectometer

A reflectometer was designed and built for measuring reflection coefficients of metal films, and metal oxide films at non-normal incidence to better than $\pm$ 0.006, using light polarized in planes perpendicular and parallel to the plane of incidence. In addition, using a special optical cell (described in Section 4.2.4), reflection and magneto-optical measurements could be obtained from films at low temperatures, using the same reflectometer. The instrument is a graduated, circular scale spectrometer to which calibrated polaroid heads, a graded wavelength filter (wavelength range 400-700nm), and a

photomultiplier have been added. By means of a special base plate fixed to the spectrometer, specific angular positions of the telescope may be located in steps of 2.5° to cover angles of incidence from 21° to 88°. The light source is a 200 watt quartz iodine lamp which is shrouded in a water cooled housing, and powered by a highly stabilized direct current supply (Farnell Ltd, Type: B30/20) capable of delivering up to 30 amps. The purpose of the shroud is to exclude draughts from reaching the lamp envelope, and to maintain this envelope at the recommended temperature ($400^{\circ}C$). The light output, measured with a photomultiplier, was found to be stable to better than $\pm$ 0.1% and the total drift of the lamp/photomultiplier combination was no more than 1% per hour.

The reflectometer was constructed for use with two types of specimen:

(a) Solid surfaces, and films which are sufficiently thick for multiple reflections to be negligible. If measurements are performed under optimum experimental conditions (Miller, et al., 1970) n and k can be obtained to an accuracy of about $\pm$ 0.05.

(b) Films in which the contribution to the reflected beam from multiple internal reflections is significant. An optimized, reflection ratio method exists for obtaining n_2 and k_2 accurate to about $\pm$ 0.05 (Miller and Taylor, 1971).

In today's financial climate, the cost of any research equipment is an important parameter in its design. The total cost of the reflectometer including materials and photomultiplier was £220; power supplies and a potentiometric recorder cost a further £475. A more detailed description of the instrument is now given.

The essential components of the reflectometer are; a $7\frac{1}{2}$ inch circular scale spectrometer, (Ealing Scientific Ltd., Type No:- A26/4580), with modified collimator and telescope supports, a polarizer, a graded wavelength filter, two slits, a photomultiplier and a metal base. Figure 4.2.1 shows schematically a side elevation of the assembly.

The body B of the spectrometer was fixed coaxially, by means of screws, to a circular duralumin base A of thickness 12mm and diameter 45cm. Radial grooves 42mm long, 2mm deep and V-shaped in cross-section, were milled in the upper face of A, so as to meet the circumference. In all, fifty-seven grooves were cut, the first and last making 42° with the optical axis of the collimator D. These grooves were used to locate the angular position of the telescope.

In order to provide greater working space at the spectrometer table, the collimator was moved outwards and upwards by interposing a duralumin spacer (C in Figure 1) between the collimator and its original support. This spacer could be levelled by means of the existing collimator adjusting screws.

The collimator source slit was adjusted to form a pinhole aperture. Light emerging from the collimator was plane polarized by polaroid mounted in a head E fitted with a circular scale calibrated to 0.1°, (Ealing Scientific Ltd., Polaroid type used in this head is to specification KN36). A slit, (25 x 2mm), cut in a duralumin disc, was fixed between the collimating lens and polaroid, and positioned optically so as to be parallel to the spectrometer axis. An iris diaphragm F was used to adjust the effective slit length. The slit produces a ribbon-like emergent beam from the collimator, which allows measurements to be made at high angles of incidence on small specimens which would otherwise act as limiting apertures, and produce undesirable edge effects. (This limiting aperture problem does not arise when

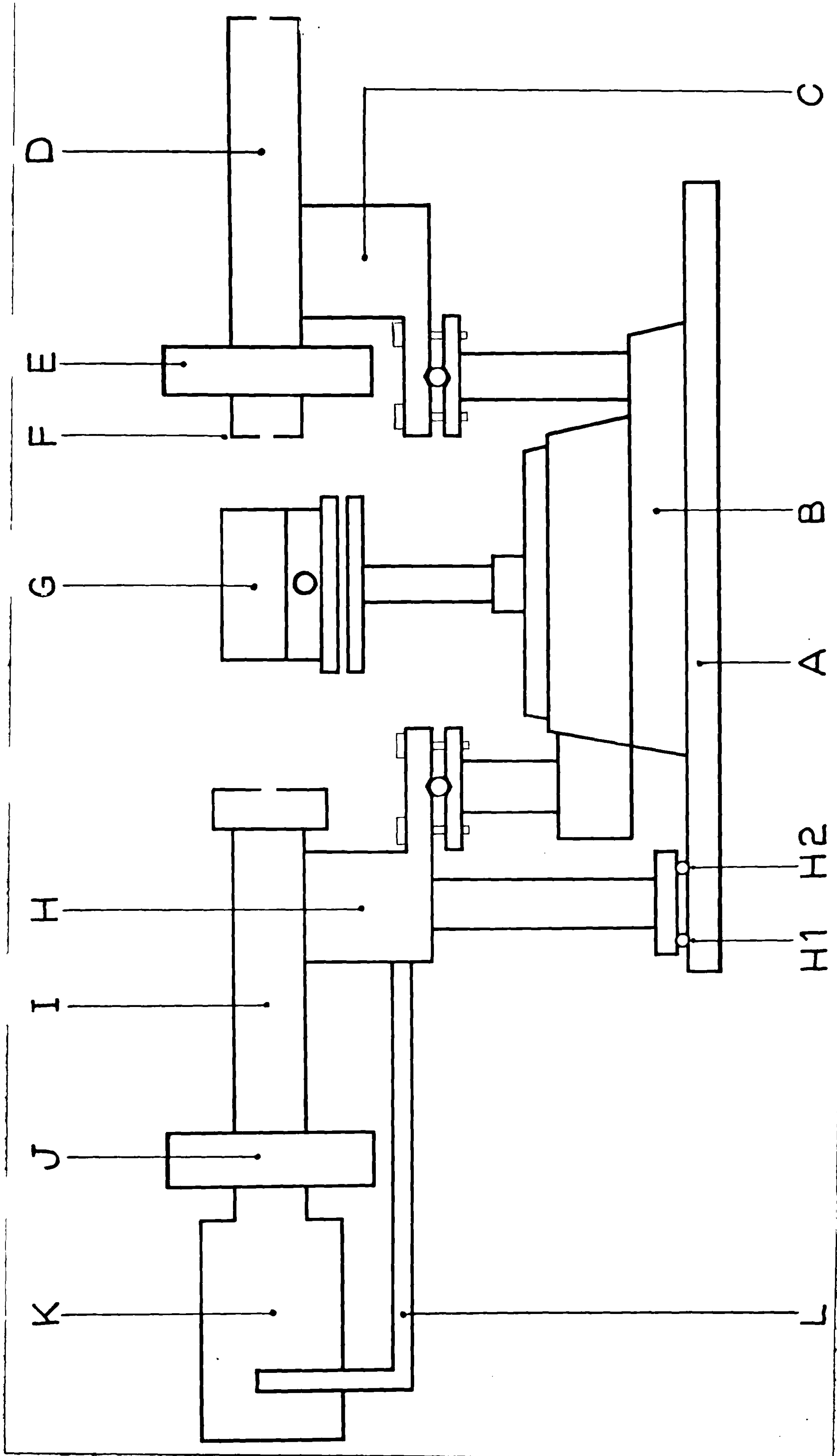

Figure 4.2.1 Schematic side elevation of reflectometer.

Avery's method of determining optical constants is used (Avery, 1952).) For light emerging from the collimator, the plane of incidence at a specimen surface placed parallel to the spectrometer axis is the plane normal to that axis. The absolute alignment of the polarizer, perpendicular and parallel to this plane of incidence, was determined using the method of Rowell et al., (1969). This aligning procedure was carried out for a number of different wavelengths. The absolute alignment differs by 0.2^{o} for the extreme ends of the wavelength range (400-700nm) for both polarization planes.

A substrate holder G was screwed to the existing spectrometer table. Alignment and levelling of the substrate with respect to the incident beam can be achieved by using a fine lateral adjusting screw on G, and the adjusting screws on the spectrometer table. A more detailed description of this substrate holder is given in Section 4.2.2.

The spectrometer telescope (I in Figure 4.2.1), was repositioned in a similar way to the collimator, by means of the duralumin block H. An I-sectioned block of duralumin, with two spring loaded ball bearings H1 and H2 in one end, was fixed at its other end to the underside of H so that H1 and H2 were in contact with the upper face of the base A. When the telescope is rotated H2 remains in contact with A and H1 traverses the milled grooves. H1 and the grooves therefore provide pre-selected angular positions for the telescope. These angular positions are reproducible to within $\pm 0.025^{o}$. The I-sectioned component also provides extra support for the telescope.

The lens in the telescope was replaced by a slit aperture (25 x 1mm) optically aligned with the collimator slit. The telescope eyepiece was replaced by a graded wavelength filter, attached to a horizontal transverse drive and housed in a light-tight duralumin box J. More details of the filter and its housing are described in

Section 4.2.3. A photomultiplier (EMI., Type: 9529B, S10 cathode) with an optically flat end window detects the light transmitted by the filter. The photomultiplier, together with its dynode resistor chain, was magnetically shielded by mu-metal and placed in a duralumin case K, which screwed into the filter attachment. Recommendations, supplied by EMI (1968), for the design of dynode resistor networks were followed when designing a low noise, linear dynode chain for the photomultiplier. The output current from the photomultiplier passes to earth through a 510kΩ high-stability, resistor and the voltage developed across this resistor is the signal recorded. A diffusing screen was mounted in front of and parallel to the photomultiplier window, and separated from it by a cylindrical tube aluminised on the inside. The diffusing screen was a flat disc of flint glass with both faces ground. The purpose of this arrangement is to reduce the sensitivity of the photomultiplier to any changes in polarization or incident beam size. A supporting cradle L for the detector assembly was screwed into the block H.

4.2.2 The substrate holder for measurements in air

The substrate holder (Figure 4.2.2) was constructed from duralumin in two parts, A and B, to accept 76 x 25mm float-glass microscope slides. Part A is a light framework on a solid rectangular base. A glass substrate can be clamped into position on the frame, perpendicular to the spectrometer table top, by two nylon screws C and D. Block B containing bronze bushes to act as guides for steel rods E attached to A, was screwed to the spectrometer table. The lateral position of the specimen, relative to the spectrometer axis, can be adjusted by moving A relative to B by means of a 0.5mm pitch brass screw threaded into A and free to rotate in a bronze bearing in B. This substrate holder, together with the normal spectrometer table levelling screws, allows the surface of a specimen to be brought into coincidence with the rotational axis of the spectrometer.

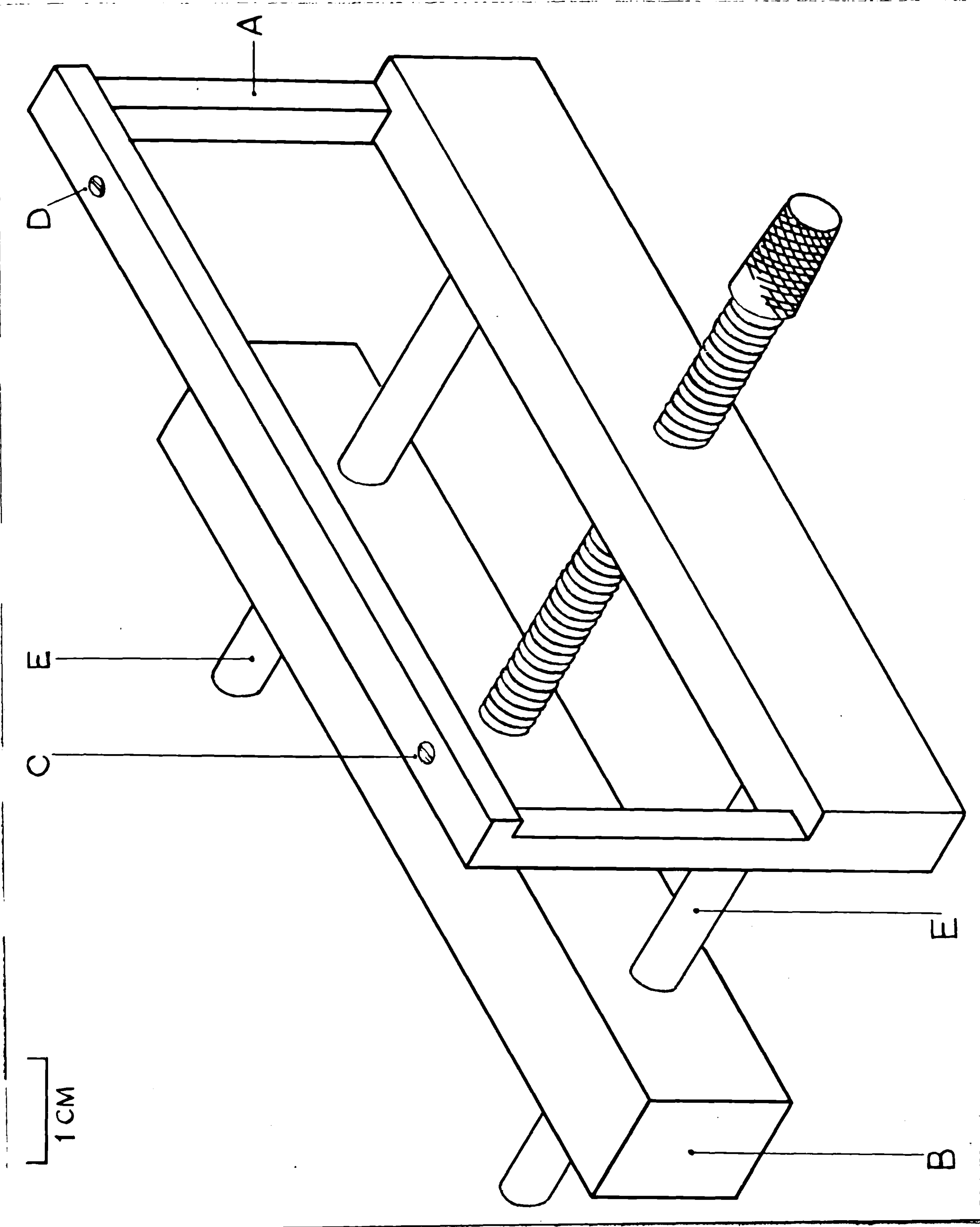

Figure 4.2.2 Isometric drawing of specimen holder for measurements in air.

4.2.3 The graded wavelength filter attachment

The graded wavelength filter (Barr and Stroud Ltd.) used in the reflectometer, permits any desired peak wavelength to be selected within the range 400nm to 700nm, from either the incident or reflected light, by passing the beam through the appropriate part of the filter. The filter is mounted on a glass strip (60 x 25mm), and has half peak bandwidths of 26nm and 32nm at the extreme ends of the wavelength range. In order to achieve these bandwidths, collimated light must fall normally on the filter, and must be of slit width 1mm, with the slit aligned perpendicular to the long dimension of the strip. Transmission for most wavelengths is 40% or greater and only falls to 33% at the extreme ends of the wavelength range. It was these characteristics which made the filter more convenient to use than the monochromators available to the author. A calibration chart is supplied with the filter, which allows the transmitted wavelength to be determined in terms of the distance of the light beam from one end of the filter.

The filter was mounted on a moveable carriage inside a light-tight duralumin box. Figure 4.2.3 is an isometric drawing of the complete filter attachment. A central hole in the front face of the box A allows light passing through the 1mm entrance slit of the telescope tube to fall on the graded wavelength filter B. Two clamps support the filter B in a vertical plane, on the carriage C which can be translated at right angles to the telescope entrance slit by means of a micrometer screw passing between two ground steel guide rails fixed at the two ends of the box A. These guides make sliding contact with the milled faces of the carriage C and prevent any rotation about the micrometer screw. C is carried by the steel shaft D, which is set in bronze bearings in the

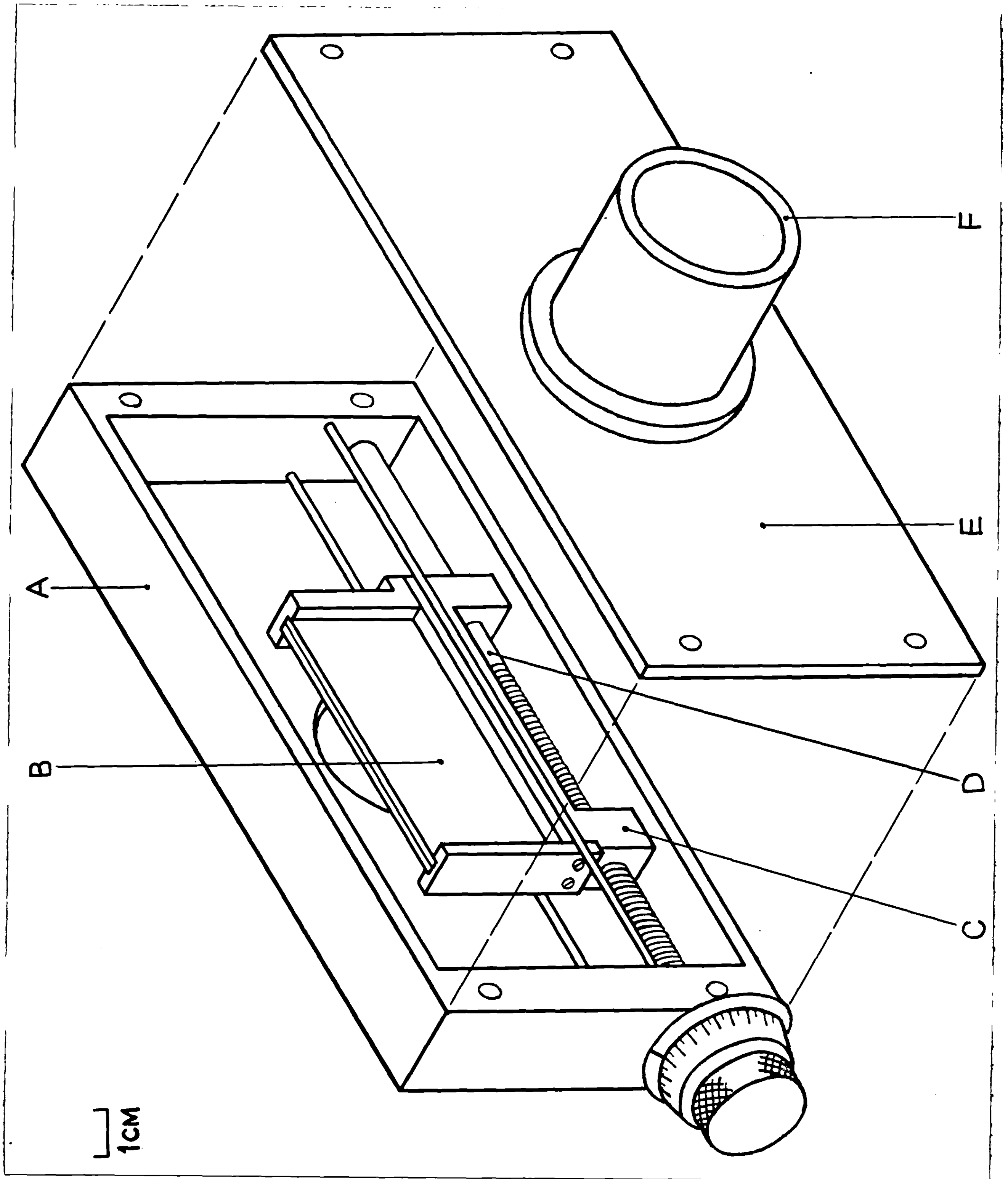

Figure 4.2.3 Isometric drawing of graded wavelength filter attachment.

end walls of A. A micrometer thread of 0.5mm pitch was cut on half of the shaft D and is threaded through one end of the carriage C. The other half of the shaft D passes through a bronze bearing in the other end of the carriage C.

A knurled knob, fixed to a circularly graduated drum, was provided to rotate the shaft D and hence translate the filter B. The circumference of the drum was divided into fifty equal divisions, each of which corresponds to a carriage translation of 0.01mm. A digital counter fixed to the other end of the shaft records complete revolutions of the graduated drum (not shown in Figure 4.2.3). Light transmitted through the filter passes through a central hole in the lid E and into the photomultiplier. The photomultiplier case is screwed into the housing F. Light at a wavelength of 633nm, from a helium-neon laser was used to set the drum and digital counter readings to the calibration data provided. The photomultiplier was used to detect the maximum transmission of the filter corresponding to this wavelength.

4.2.4 The optical cell for measurements at low temperatures

In order to obtain reflection measurements from specimens cooled to well below room temperature it is necessary to prevent atmospheric moisture and CO_2 from condensing onto the cold specimen surface. This may be achieved by surrounding the specimen with a suitable cell either evacuated or filled with a dry, inert gas. Such a cell was designed and constructed so that low temperature optical and magneto-optical studies could be made on gadolinium films. The main features of this cell are described below:-

(i) Reflection measurements can be obtained at a number of angles of incidence so that the optimized methods of Chapters 2 and 3 may be used.

(ii) The cell replaces the existing spectrometer table and fits snugly into the enlarged working space between the spectrometer telescope and collimator.

(iii) Inside the cell a specimen holder, which accepts 76 x 25mm float glass microscope slides, is rigidly connected by a thick copper rod to a liquid nitrogen Dewar outside the cell. Levelling of the specimen is achieved by means of three external screws.

(iv) The cell may be evacuated and afterwards sealed.

Figure 4.2.4 shows a schematic section of the cell and liquid nitrogen Dewar. The base of the cell consists of a spectrometer type table C and D made from duralumin and provided with a brass support rod A. Levelling screws B are provided to tilt the whole cell including the specimen about the spectrometer axis so that optical alignment of the specimen surface can be achieved. Partially inset in the top face of D is a large diameter 'O' ring, and passing through D is the glass vacuum line L, provided with a sealing tap (Acton) L was vacuum sealed into D using the usual 'O' ring method, (this seal is not shown in Figure 4.2.4). The transparent envelope of the cell is a fused quartz (Vitreosil, 066 quality) tube of wall thickness 2.4mm. This tube, manufactured by Thermal Syndicate Ltd., was trepanned from a block of the 066 Vitreosil and highly polished both inside and outside. It was necessary to have the tube prepared in this manner because any imperfections in the walls of the tube would not only distort the beam of light passing through but would also perturb the state of polarization of the beam. Tests showed that drawn tubing of quartz was inferior in these respects than the trepanned tube.

The top H of the cell is also made of duralumin and supports the stainless steel specimen holder F and the polystyrene Dewar assembly J.

Figure 4.2.4 Schematic section of the optical cell and the liquid nitrogen dewar.

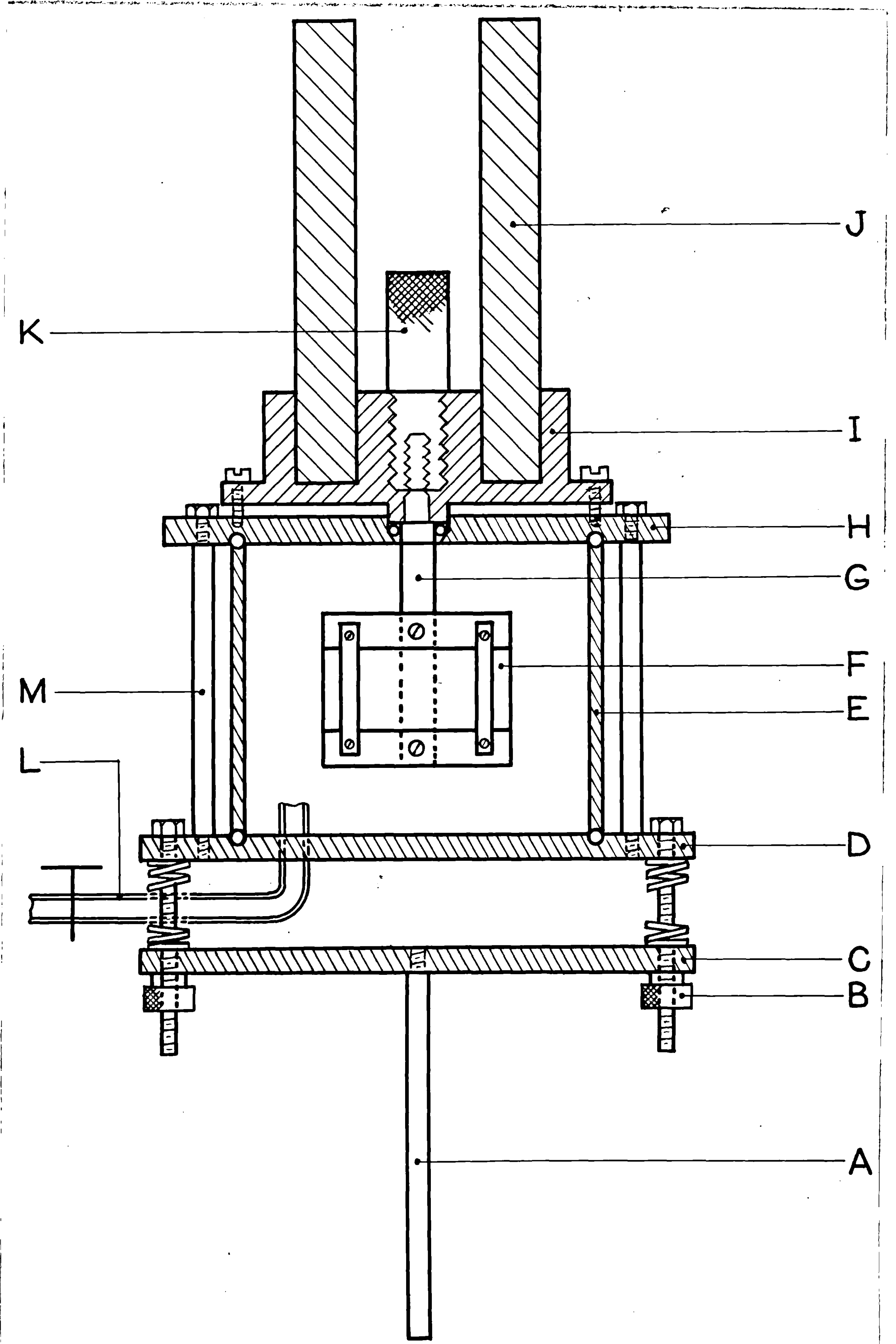
J
K
I
H
G
F
M
E
L
D
C
B
A

F is screwed to a copper rod G which passes through an 'O' ring seal in H into the liquid nitrogen Dewar. Thermal contact is made with the liquid nitrogen by means of the knurled brass plug K, which is tightly screwed into the nylon base I, which in turn is fixed by screws to the top face of H. The lower end of the Dewar fits tightly into this base. A register on the underside of I completes the 'O' ring seal in H, and ensures that the copper rod G is aligned approximately with the axis of the cell. In the underside of H another large diameter 'O' ring was partially inset to provide a vacuum seal with the top end of the tube E.

To assemble the cell, the tube E is placed squarely on the 'O' ring in the top face of D. The top of the cell is then lowered into position so that the other end of E comes squarely into contact with the large diameter 'O' ring in H. Three stainless steel tie-rods screwed into D support the top section of the cell accurately parallel to the bottom section and ensure that the ground ends of the tube E are in good contact with the two sealing 'O' rings.

To evacuate the cell, the vacuum line L is connected to a rotary pump via an activated alumina oxide trap, which minimizes any back streaming of oil from the pump into the cell. The pressure in the cell during the pumping operation is monitored by a Penning gauge-head mounted in the vacuum line between the trap and the cell. The tap in the line L seals the cell from the atmosphere after evacuation. Tests showed that the cell could be evacuated to a pressure of 0.002 torr; after 3 days the pressure rose to $\sim$ 0.05 torr.

The surface temperature of a specimen is measured with a copper/constantan thermocouple sandwiched between a piece of mica and the specimen surface. The wires of the thermocouple are screwed to two electrical feedthroughs in the top face of H (Figure 4.2.4). A d.c. millivoltmeter (Dymar 721) is connected by leads of copper and constantan

to the two feedthroughs, and records the thermal e.m.f. developed by the thermocouple. The thermocouple was calibrated at the following fixed points:

Liquid nitrogen; boiling point	$77^{o}K$
Ether; rapid freezing point	$157^{o}K$
Chloroform; freezing point	$210^{o}K$
Carbon tetrachloride; freezing point	$250^{o}K$
Water; ice point	$273^{o}K$

The ether, chloroform and carbon tetrachloride were 'Analar' quality, the water had been distilled in the laboratory and the liquid nitrogen was oxygen free. A calibration curve of thermocouple e.m.f. against temperature was constructed from these five points. Each thermal e.m.f. could be determined to within $\pm$ 0.1 mV., corresponding to a temperature uncertainty of between $\pm$ 3 and $\pm$ $4^{o}K$. The thermocouple calibration chart is shown in Figure 4.2.5.

4.3 Method of use and some typical results

With this instrument there is no need to set the specimen at the angle or angles of incidence required. The telescope tube is set at the appropriate stop in the base plate and the spectrometer table rotated slowly so that the reflected beam scans across the entrance slit of the detector system: the photomultiplier output is displayed on the chart of a potentiometric recorder (Panax Equipment Ltd. Type:- SREC2P). The signal corresponding to the incident light intensity may be similarly recorded by slowly moving the telescope across the incident beam, with the spectrometer table lowered out of the way. When making the latter measurements with the optical cell it is necessary to raise the whole cell to allow the incident light beam to pass through beneath the specimen holder (see Figure 4.2.4).

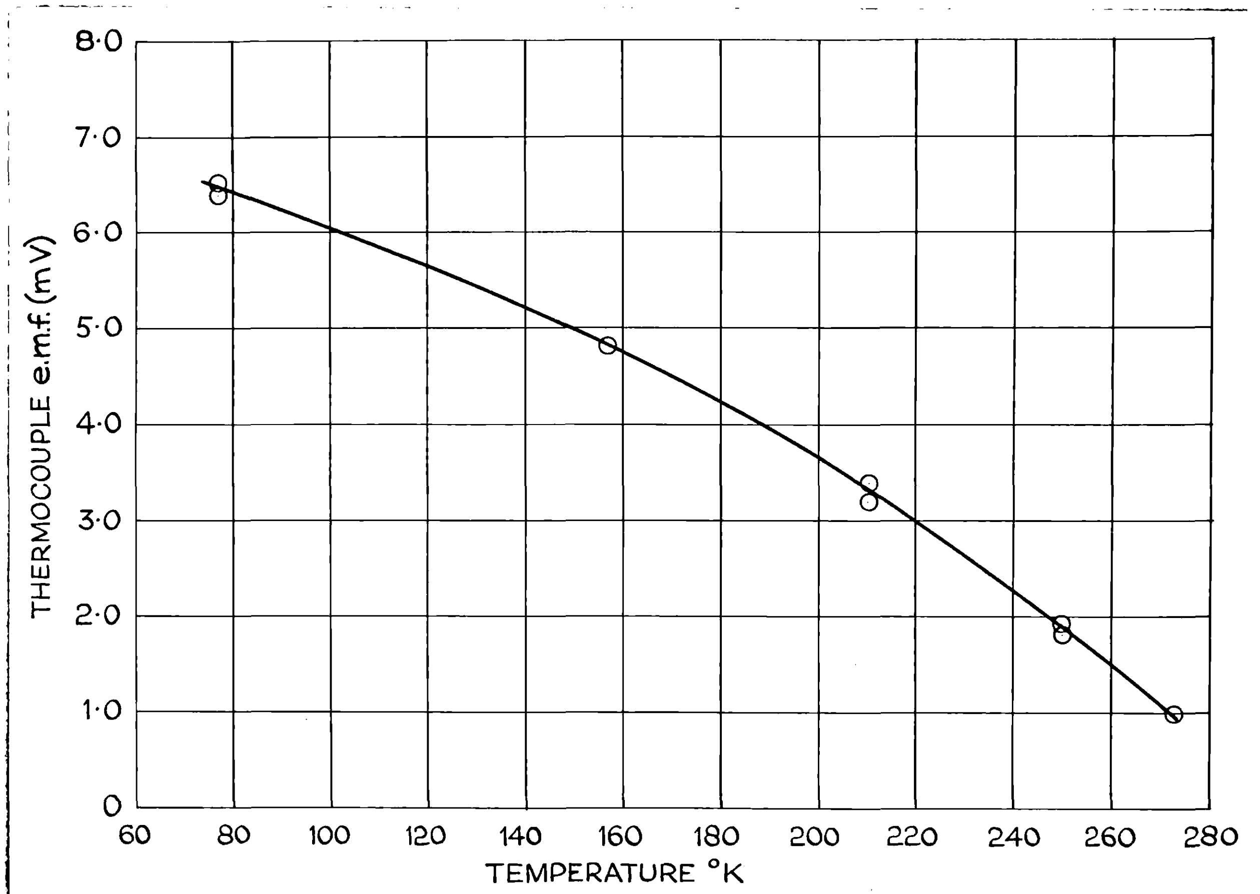

Figure 4.2.5 Copper-constantan thermocouple calibration chart for low temperatures.

In order to keep the noise level in these simple d.c. measurements to a minimum it is necessary that currents $\gtrsim 2\mu A$ are not drawn from the photomultiplier resistor network (E.M.I., 1968). As a consequence of this the input impedance of the recorder must be appreciably greater than the output impedance of the photomultiplier. The recorder used in the experimental work has an input impedance of $11M\Omega$ at balance; the output impedance of the photomultiplier is essentially equal to the anode load resistor value, $510K\Omega$.

Figure 4.3.1 shows an example of chart recordings for incident and reflected light beams, polarized first perpendicular then parallel to the plane of incidence. The peaks are in pairs which correspond to the light scanning once back and forth across the detector slit; the average of each pair of peak heights is later calculated. These recordings were obtained with the chart speed set at 30mm per minute. Because the recorder has a full scale response time of about 1 second, it was necessary to move the incident and reflected light beams sufficiently slowly across the entrance slit of the telescope for the peak photomultiplier output signal to be accurately recorded. A scanning time of between 5 and 10 seconds was found to give reproducible results. The recordings shown in Figure 4.3.1 are in a form suitable for Avery's method of analysis (described in (i) below and Chapter 1), i.e. measurements for perpendicular and parallel polarizations of a particular beam were made in rapid succession so as to minimize the effects of any lamp instability on the intensity of ratios. For Querry's method of analysis (described in (ii) below and Chapter 1), measurements for incident and reflected beams of a particular polarization are measured in rapid succession. These were precautionary measures only because the lamp output was sufficiently stable over the period of time required to obtain the data for $R_{\parallel}/R_{\perp}$ or $R_{\parallel}$ and $R_{\perp}$.

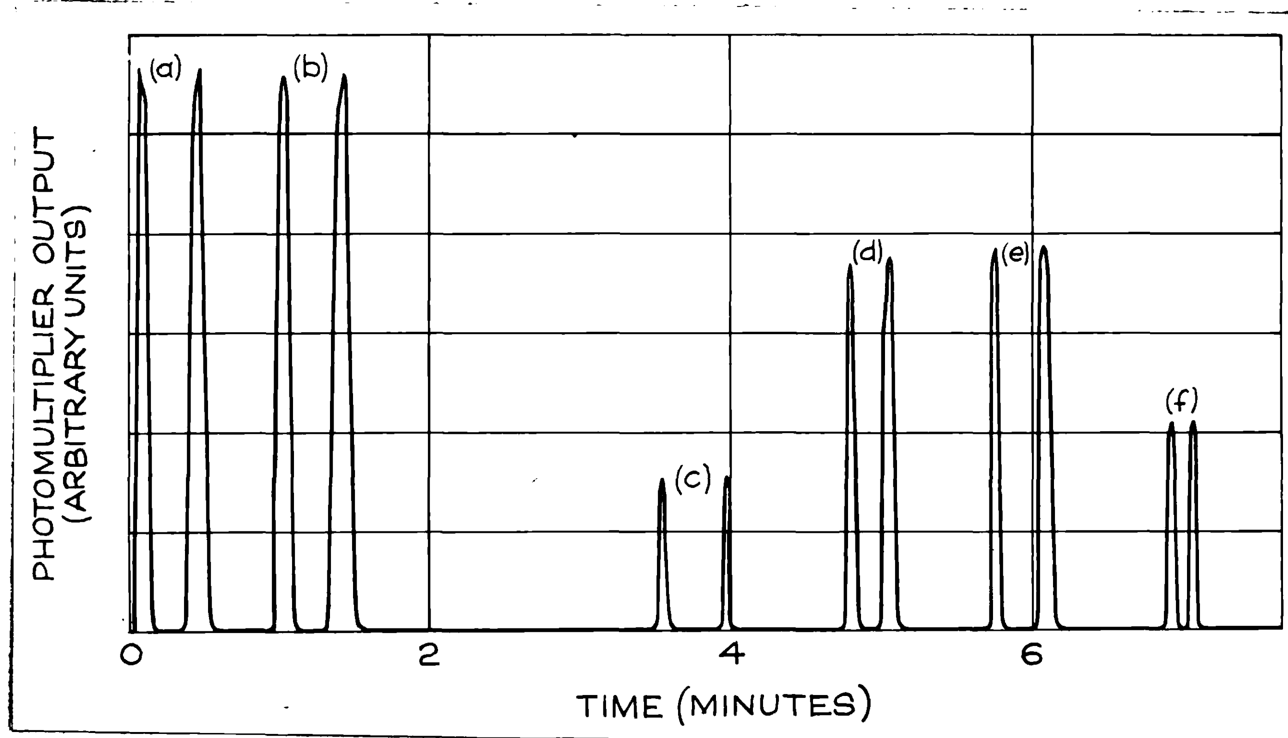

Figure 4.3.1 An example of a chart recording for incident and reflected light; (a) incident beam, polarized perpendicular to plane of incidence, (b) incident beam, parallel polarization, (c) reflected beam at first angle, parallel polarization, (d) reflected beam at first angle, perpendicular polarization, (e) reflected beam at second angle, perpendicular polarization, (f) reflected beam at second angle, parallel polarization.

A number of test experiments were conducted to determine statistically the uncertainties in the measured quantities, $R_{//}$ and $R_{\perp}$, and $(R_{//}/R_{\perp})$. Films of gold and nickel were used. The test experiments measured $R_{//}$ and $R_{\perp}$ twelve times in succession, for a fixed angle of incidence and incident wavelength. From these measurements average values for $R_{//}$ and $R_{\perp}$ were calculated, and for both averages R.M.S. deviations were deduced. There was no case in which the R.M.S. deviation was greater than $\pm$ 0.006 for either $R_{//}$ or $R_{\perp}$, and this, therefore, is a good measure of the worst uncertainty in $R_{//}$ and $R_{\perp}$. Avery type test measurements were made and the uncertainty in $R_{//}/R_{\perp}$ was found to be less than $\pm$ 0.01.

Before making any optical measurements it was necessary to investigate the efficiency of the polaroid used to polarize the incident beam. A measure of the efficiency may be obtained by measuring the intensity transmitted by a crossed polarizer/analyzer pair for light of a known wavelength. However, it should be noted that, because the polarizer and analyzer are both inefficient they will transmit small, unwanted quantities of the orthogonal polarization and thus contribute to the transmitted intensity. It is thus difficult to ascribe an efficiency to either polarizer or analyzer from a measure of this intensity alone. If the observed transmitted intensity with the polarizer and analyzer crossed is simply halved, then to a first approximation this will represent the transmission (ΔIo) of the unwanted polarization for either the polarizer or analyzer. If Io represents the total transmitted intensity for the polarizer or analyzer alone, set with polarization azimuth parallel or perpendicular to the plane of incidence, then (ΔIo/Io) x 100% is the percentage of the unwanted polarization transmitted.

In practice an auxiliary analyzer of polaroid in a calibrated head and mounted in front of the photomultiplier, and a d.c. valve voltmeter (Dymar 721) were used to measure the fraction $\Delta Io/Io$ for the polarizer for a number of wavelengths isolated by the graded wavelength filter. Table 4.3.1 shows values of $\Delta Io/Io$ expressed as a percentage for wavelengths in the range 400-700nm. For wavelengths between 405 and 495nm there is an appreciable quantity of unwanted polarization transmitted, which will introduce an error into each of the observed values $R_{//}$ and $R_{\perp}$. As an extreme example suppose that $R_{//}$ is being measured at a wavelength of 420nm and at an angle of incidence θ for a material with $R_{\perp}$ of 0.800 at θ. From Table 4.3.1 it can be seen that the unwanted polarization ($\Delta Io^{\perp}$ in this case) will have an incident intensity coefficient of 0.004. Consequently 80% of this will be reflected and recorded as a contribution to $R_{//}$; the error in $R_{//}$ will be 0.003. However, this is smaller than the uncertainty of $\pm$ 0.006 in determining $R_{//}$ and $R_{\perp}$.

The reflectometer can be used for measuring reflection coefficients at angles of incidence from 21° to 88°. For films which are sufficiently thick for internal multiple reflections to be negligible, the instrument can yield data suitable for analysis by the following methods:

(i) Avery's method (Avery, 1952): measurement of the ratio $R_{//}/R_{\perp}$ at two angles of incidence.

(ii) Querry's method (Querry, 1969): measurement of $R_{//}$ and $R_{\perp}$ at the optimum angle of incidence 74° (Miller et al., 1970).

(iii) Potter's method (Potter, 1965): measurements of the ratio $R_{//}/R_{\perp}$ at a number of angles of incidence close to the pseudo-Brewster angle for the material.

Table 4.3.1 Percentage of unwanted polarization transmitted by the polarizer used in the reflectometer

Wavelength nm	$\Delta Io/Io$ %
405	0.1
420	0.4
446	0.2
495	0.1
511	0.1
528-687	0.1

For metal and metal oxide films thin enough for the contribution of internal multiple reflections to be significent, the reflection ratio method of Miller and Taylor (1971) is used to obtain n_2 and k_2. In this method, measurements of the ratio $R_{\parallel} / R_{\perp}$ are made at two predetermined optimum angles of incidence; the film thickness is determined independently.

Some n and k values obtained by method (i) above for a thick film of gold (thickness 191nm), evaporated onto float glass from a tungsten boat at a pressure of 5 x 10^{-6} torr, are shown in Table 4.3.2. The gold film was annealed at a temperature of 240°C for about 1 hour at a pressure of less than 5 x 10^{-6} torr. Values of the ratio $R_{\parallel} / R_{\perp}$ were measured to $\pm$ 0.01, angles of incidence to $\pm$ 0.02^{o} and the film thickness was measured to $\pm$ 3nm by multiple beam interferometry. All measurements on the specimen were made in air and the temperature of the film at the time of deposition and measurement was 295°K. The n and k values shown in column 2 of Table 4.3.2 are somewhat different from those reported by Schülz (1954); Philip (1960) obtained values of n and k which were consistently lower than either of those shown in Table 4.3.2. Querry's method, (method (ii) above) was used to obtain some n and k values for the same gold film at wavelengths shown in Table 4.3.2. The valuesof n and k obtained were the same, to within experimental error, as those obtained by Avery's method. For example, for λ = 402nm, Querry's method gave n = 1.59 and k = 1.76; from Avery's method n = 1.55 and k = 1.74.

Two typical curves of the ratio $R_{\parallel} / R_{\perp}$ against angle of incidence for opaque films of gold and iron obtained with the reflectometer, are shown in Figure 4.3.2. Such curves are used in Potter's method (method (iii) above) for determining n and k. This method is not very useful for dispersion type studies because it

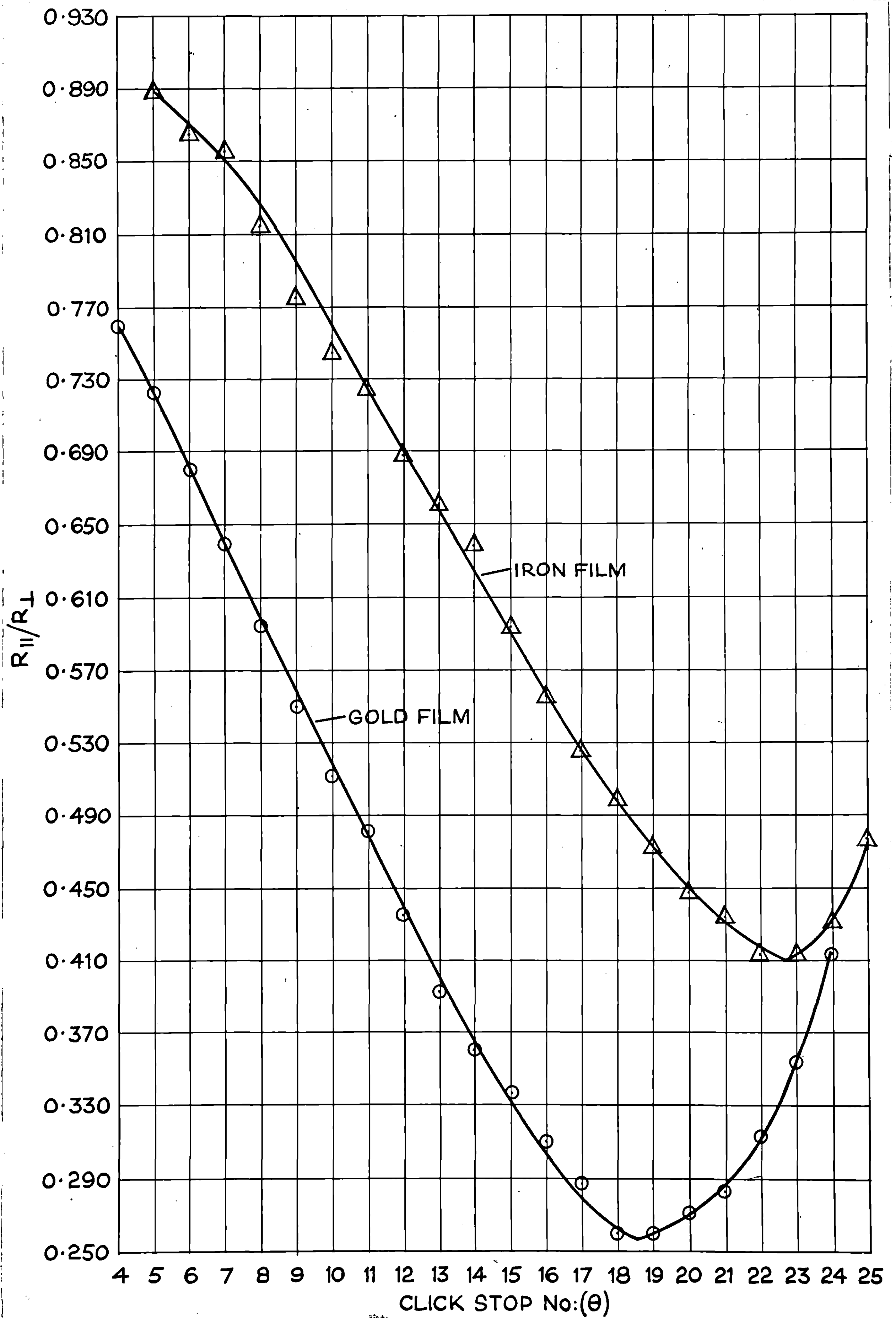

Figure 4.3.2 Typical curves of ($R_{\parallel}/R_{\perp}$) against angle of incidence for opaque films of gold and iron.

Table 4.3.2 Optical constants of a gold film obtained by Avery's method compared with the results of Schülz

Wavelength	This Thesis*		Schülz**	
nm	n	k	n	k
402	1.55	1.74	1.45	-
450	1.48	1.69	1.40	1.88
500	0.94	1.72	0.84	1.84
550	0.39	2.29	0.34	2.37
600	0.30	2.90	0.23	2.97
650	0.23	3.36	0.19	3.50

* n̂ and k are accurate to $\pm$ 0.05 obtained from measurements at θ = 61.3, 68.8, 78.8.

** Schülz (1954).

requires considerable data to deduce one n,k pair. However, this method is included to demonstrate the versatility of the reflectometer.

Some n and k values obtained by the reflection ratio method for a thin film of nickel (thickness 57nm), evaporated onto glass at a pressure of 6×10^{-10} torr, are shown in Table 4.3.3. Reflection coefficients were measured to $\pm$ 0.005, polarization directions to $\pm 0.1^{\circ}$, angles of incidence to $\pm 0.02^{\circ}$ and the film thickness was measured to $\pm$ 2nm by multiple beam interferometry. All measurements on the specimen were made in air and the temperature of the film at the time of deposition and measurement was 293°K. The n and k values shown in Table 4.3.3 are between 10% and 16% lower than the values reported for bulk nickel at 295°K, obtained from measurements in ultra-high vacuum, (Shiga and Pells, 1969).

The reflectometer and accessories described in this Chapter were used in the experiments described in Chapter 7.

Table 4.3.3 Optical constants of nickel film compared with bulk values

Wavelength	Film		Bulk*	
nm	n	k	n	k
402	1.55	2.58	1.79	2.89
436	1.56	2.56	1.82	3.13
486	1.74	3.09	1.93	3.47
546	1.73	3.38	2.07	3.83

* Interpolated values from the results of Shiga and Pells.

CHAPTER 5

SPECIMEN PREPARATION

Abstract

This Chapter describes ordinary high vacuum systems and ultra-high vacuum systems for the thermal evaporation of metals onto float glass microscope slides. Details of evaporation assemblies and evaporation procedures are described for the two types of vacuum system. A method of preparing thin mica substrates for subsequent transmission electron microscopy of evaporated films of metal, is also given.

Introduction

Specimen preparation is essentially concerned with providing a pure specimen, with a plane surface, having the physical properties of the bulk material, - a specimen which can then be used for reflection measurements with the reflectometer and accessories described in Chapter 4. That metallic films often have optical properties which differ significantly from those of bulk specimens has been known for some time, Heavens (p.200, 1955). What is perhaps rather depressing is the large variation ($\sim$20%) in 'optical constant' values which can occur for different films of the same metal, and what is more depressing is the variation in these differences, from observer to observer. However, such variations are also found when determining the optical constants of bulk metal surfaces. All mechanical polishing methods employed to produce such a surface create a disturbed surface layer; electropolishing does not distort the surface but has the disadvantage of leaving impurity films (often of unknown composition) on the surface. Pells and Shiga (1969) have shown that it is possible to obtain considerable variations

(100%) in $\sigma(\omega)$ for a clean, mechanically polished surface, simply by obtaining measurements with the specimen in air and then at a pressure of 10^{-7} torr, (U.H.V. clean system).

The main requirements of a surface intended for optical constant determinations are:-

(i) The specimen surface should be flat, over the area illuminated by the light beam, to a degree such that variations in flatness do not affect the measurements, (see later Section dealing with surface roughness).

(ii) A strain-free surface is also necessary otherwise anisotropies in the surface will produce incorrect values for n and k.

(iii) A clean surface is also important as any film on the surface would greatly affect the reflection from such a surface.

Providing care is taken, evaporated film surfaces comply, to within a reasonable margin, with the above three points.

The high reactivity of the metals under study, Gd and Tb, (Trifonov, 1963) makes thin-film evaporation the only means of preparing good surfaces. Metallurgical polishing techniques have been tried (this author, unpublished) but without any real success. That the resulting evaporated films of Tb and Gd do indeed have the properties of bulk crystalline samples has been verified by Schüler (1963) and Hodgson and Cleyet (1969) in thin film resistivity measurements.

In order to prepare the thin film specimens of Gd and Tb and other metals, three different vacuum evaporation units were available: two ordinary high-vacuum (O.H.V.) and one ultra-high vacuum (U.H.V.). All the films for subsequent optical measurements were deposited onto float-glass substrates. Substrates of microscopically thin mica were

used in electron microscope studies of evaporated films of Tb. Attempts at depositing Gd onto polished, alkali-halide substrates were also made.

5.1 Substrates and their preparation

5.1.1 Float glass

The glass substrates used in the optical experiments described in Chapter 7 were 76 x 25mm float glass microscope slides from Chance-Pilkington Ltd. Some of the properties of this glass are listed below:-

(i) Chemical composition

SiO_2	71.5%
Na_2O	12.5%
CaO	8.1%
MgO	3.5%
Al_2O_3	1.3%
TiO_2	1.8%
Sb_2O_3	1.0%

(ii) Refractive index for the sodium D-doublet 1.52 $\pm$ 0.01. (This figure was checked by the author, using an Anderson-Payne Spinel refractometer, and found to be correct to within $\pm$ 0.01.)

(iii) Thermal coefficient of expansion 80 x 10^{-7} per ^{o}C.

The possible adverse effects of surface roughness on reflectance measurements have been discussed in the literature, with regard to diffuse scattering of reflected light (Bennett and Porteus, 1961), and more recently, with regard to possible anomalies in reflectance near resonant frequencies of the specimen (Berreman, 1970). These resonant reflectance anomalies can occur even when the surface irregularities are much smaller than the wavelength of the reflected radiation, so that diffusely scattered radiation is negligible.

An application of the established theory of light scattering by roughened surfaces shows, for example, that about 2% of an 11.0eV. reflected light beam would be diffusely scattered by a rough surface characterized by a root mean square (R.M.S.) height variation of only ± 1.0nm. This effect drops off rapidly at lower frequencies, and for the frequencies corresponding to visible radiation (1.7eV. to 3.1eV.) is so small that it may be neglected provided the R.M.S. height variation is not too large, (± 3.0nm would be reasonable).

Reductions in reflectance values of considerably greater than 1% at normal incidence, and somewhat larger values at non-normal incidence, may occur as a result of surface-roughness producing resonant reflectance anomalies, especially in the vicinity of the surface plasma frequency. It has been shown theoretically by Berreman (1970) that the normal incidence reflectance of Al may be reduced by ~10% at photon energies close to 11.0eV., if the R.M.S. surface roughness is 0.5nm. At photon energies corresponding to visible radiation (i.e. well removed from the plasma frequency of most metals), R.M.S. height variations of about ± 2.5nm would have negligible effect on reflectance values.

If it is presumed that the evaporated film roughness is not appreciably worse than the roughness of the substrate on which it was deposited (as is the case for most metals), then according to the above theories of diffuse scattering and resonant reflectance anomalies, perturbations in reflectance for visible light reflected from metal films deposited onto substrates with R.M.S. height variations of less than ± 3nm, should be so small as to be unimportant. For optical studies involving visible wavelengths, and very thin films of metal (50nm or less) it is important that the R.M.S. height variation is less than ± 2nm, otherwise the optical thickness cannot be measured to sufficient accuracy (see Chapter 3).

It thus became obvious that R.M.S. height variations of the substrates used in the experimental studies should be less than $\pm$ 2nm over an area of about 1sq.cm. Float glass microscope slides certainly satisfy this demand; Tolansky has used multiple beam interference techniques to show that surfaces of such glass can have height variations of 2nm or less over areas of many sq.cms, and that these variations are gentle undulations in the surface rather than sharp discontinuities. Multiple beam film thickness measurements (Tolansky, 1970), conducted by the present author on films of Ni, Gd and Tb deposited onto float glass in O.H.V. and U.H.V., showed height variations of between $\pm$ 1 and $\pm$ 4nm, for film thicknesses ranging from 20 to 200nm. An example of a multiple beam fringe system at an artificial step in a film of Ni is shown in Figure 5.1.1. This film was deposited onto a clean float glass microscope slide in the U.H.V. system described in Section 5.3.1. The base pressure was 8×10^{-11} torr, the pressure during evaporation was less than 6×10^{-10} torr, and the base pressure was reached 80 seconds after completion of the evaporation. The evaporation rate, calculated from the duration of the evaporation and the measured geometrical film thickness was 100nm per minute. Film thickness measurements were obtained for a sample of 20 fringes covering 75% of the width of the step, (a distance of $\sim$1cm, much greater than the width of the incident light beam used in the reflectometer). Results for the geometrical film thickness showed a scatter of $\pm$ 2.0nm about the mean thickness of 24.5nm, well within the required (R.M.S.) height variation of $\pm$ 2.0nm.

The preparation of the substrates prior to evaporation is now explained. It is necessary to have the substrate surface completely clean: free from grease, dust and moisture, before the metal film is deposited onto it. There exist a host of recipes and techniques

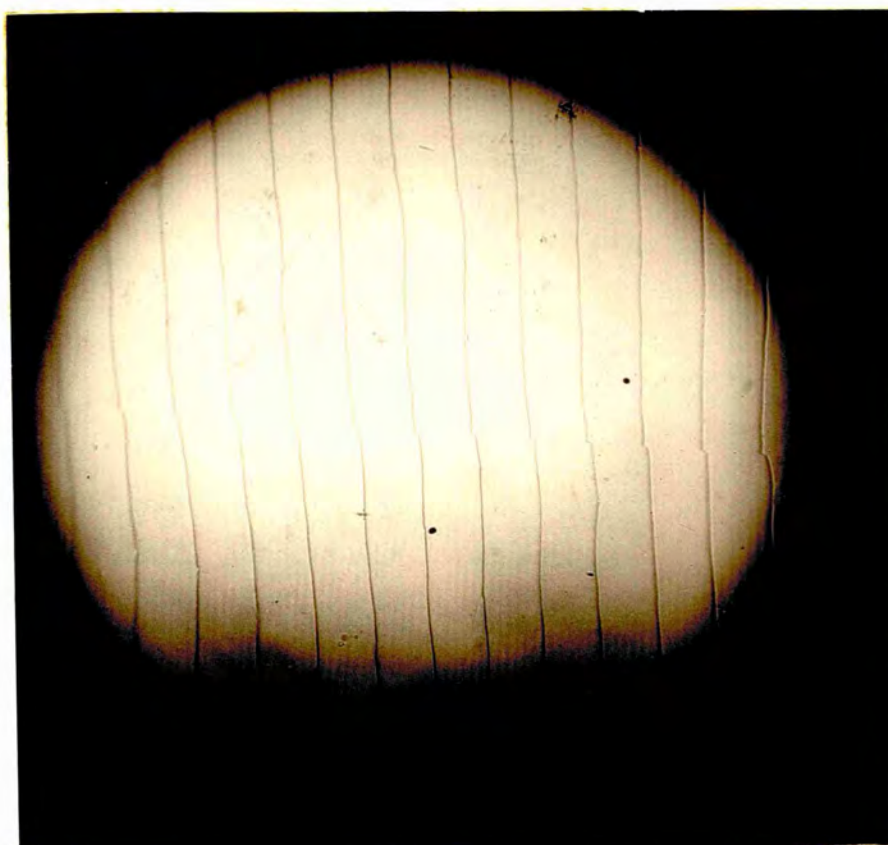

Figure 5.1.1 Multiple beam fringe system at an artificial step in a Ni film deposited in U.H.V. Microscope magnification 30X.

(Anders, p.145, 1967) for cleaning glass substrate surfaces - many were tried. The technique finally adopted, which is simple and efficient, consists of immersing the substrates in a dilute solution of "Decon 75", (manufactured by Medical-Pharmaceutical Developments Ltd.) in such a way that they do not touch one another or the beaker. The beaker, together with the "Decon 75" and substrates is then placed in the tank of an ultrasonic cleaner. Ultrasonic cleaning is continued for about an hour; the beaker is then removed and the "Decon 75" displaced from the beaker by passing a continuous flow of distilled water into the bottom of the beaker. A few tens of litres of distilled water are used in this way to rinse the substrates. The substrates are then withdrawn from the distilled water and left under a tent of paper towels to dry in the air. Using this technique the substrates do not come into contact with the air until the final drying. This procedure prevents the "Decon 75" from evaporating from the substrate and leaving behind a thin, very adhesive film which was shown to be very difficult to remove. In the vacuum system the substrate is further cleaned with a glow discharge for about 5-10 minutes. To relieve any stress in the substrate surface the substrate is heated. In the O.H.V. systems glass substrates are heated to 250°C and maintained at this temperature for about 2 hours by means of a small heating element in the substrate holder (see the following Sections for descriptions of the equipment). The pressure in the system during this annealing process is in the 10^{-6} torr pressure range. In the U.H.V. system the substrates are annealed during the bakeout cycle, during which the pressure is below 10^{-6} torr and the temperature is 280°C. The duration of the bakeout is usually 48 hours and during the latter part the system pressure is in the 10^{-8} torr pressure range.

5.1.2 Mica substrates for electron microscopy

In order to carry out electron microscopic studies of thin films of Tb, very thin specimens of mica were prepared, mounted directly onto copper (200 mesh) electron-microscope grids. These mica specimens were mounted in the O.H.V. systems (to be described below) so that Tb could be evaporated onto them under various pressures, evaporation rates and annealing temperatures. The mica specimens were prepared in the following way.

A small thin sheet of mica is repeatedly cleaved with a pin until thin pieces are obtained too thin for further cleavage with the pin. A selected specimen of this mica is then sandwiched between the adhesive sides of two pieces of sellotape. Slowly pulling apart the two pieces of sellotape induces further cleavage of the mica and, repeated many times, thinner and thinner sections of mica are obtained. In general it is possible to carry out this procedure until the pieces of mica are very difficult to see. The end product is a piece of sellotape covered with a number of pieces of mica, each very thin and usually about 1sq.mm or less in area. The excess sellotape is cut away and this leaves each piece of mica coated with sellotape adhesive. To dilute this coating to a sufficiently low level for electron microscope studies, the mica pieces are immersed in chloroform (500ml of Analar quality) and the suspension gently stirred. Successive small portions of this suspension are filtered through the 200 mesh, copper electron microscope grids using the simple apparatus shown in schematic form in Figure 5.1.2. For each copper grid used the filtering action leaves one or more pieces of mica attached to the grid. Subsequent optical microscopy of the grids allows those to be selected which have one or two mica specimens well separated from each other. The chloroform evaporates from the grids

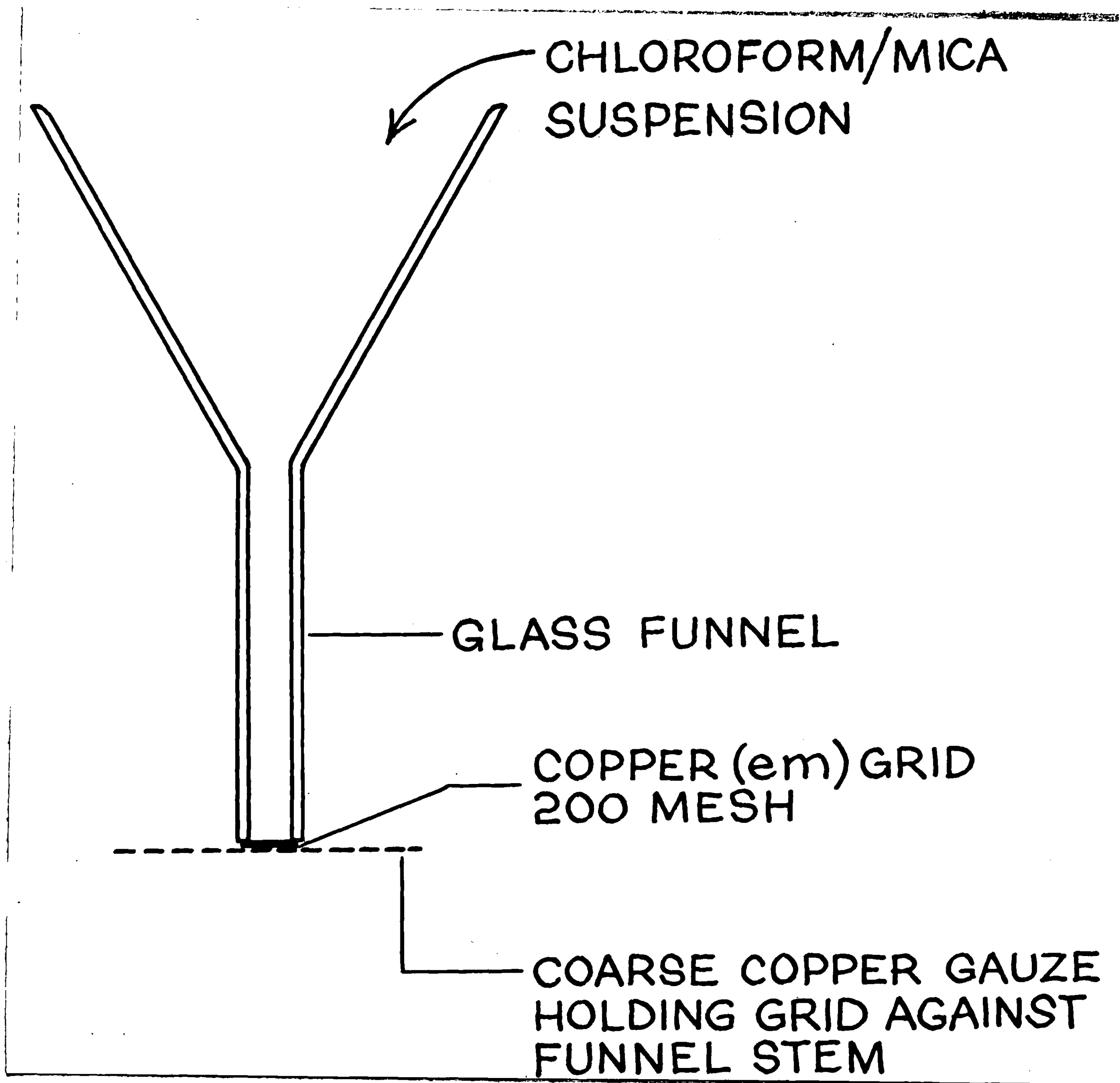

Figure 5.1.2 Method of attaching thin mica specimens to copper electron-microscope grids.

leaving the mica attached to the grid by the very dilute sellotape adhesive. That this adhesive does not produce any electron diffraction is shown in the photograph of a selected area electron diffraction pattern from a typical mica specimen, Figure 5.1.3. The mica pieces adhere to the grids even after heat treatment in vacuum.

5.2 Ordinary high vacuum (O.H.V.) preparation of films

5.2.1 The 12 inch evaporation system for use with tungsten boats and filaments

The 12 inch evaporation system is an Edwards 12EA/424 coating unit. The 12 inch diameter glass bell jar is sealed to the base plate by means of an L-shaped Viton-gasket. This bell jar is evacuated by a water cooled, oil vapour diffusion pump and an Edwards (ED50) 2-stage oil rotary pump. No moisture or oil traps were used. The ultimate pressure of the diffusion pump is better than 5×10^{-6} torr, and the rotary pump is capable of evacuating to at least 0.005 torr. All of the evaporations in this system were performed at pressures below 5×10^{-6} torr. A Pirani gauge is used to measure the backing pressure over the pressure range 0.5-0.001 torr, and a Phillips ionization gauge, incorporated in the evaporation chamber measures pressures in the range 5×10^{-3} to 1×10^{-6} torr. One of the chief residual gases in such a system is oxygen (Caswell, 1961). It was found that when evaporating Tb in this system some of this oxygen could be gettered before commencing the evaporation. To do this the Tb vapour was allowed to deposit over the lower half of the bell jar with the substrate shielded from the vapour source; the chamber pressure always fell during this gettering, usually to the zero on the pressure meter scale.

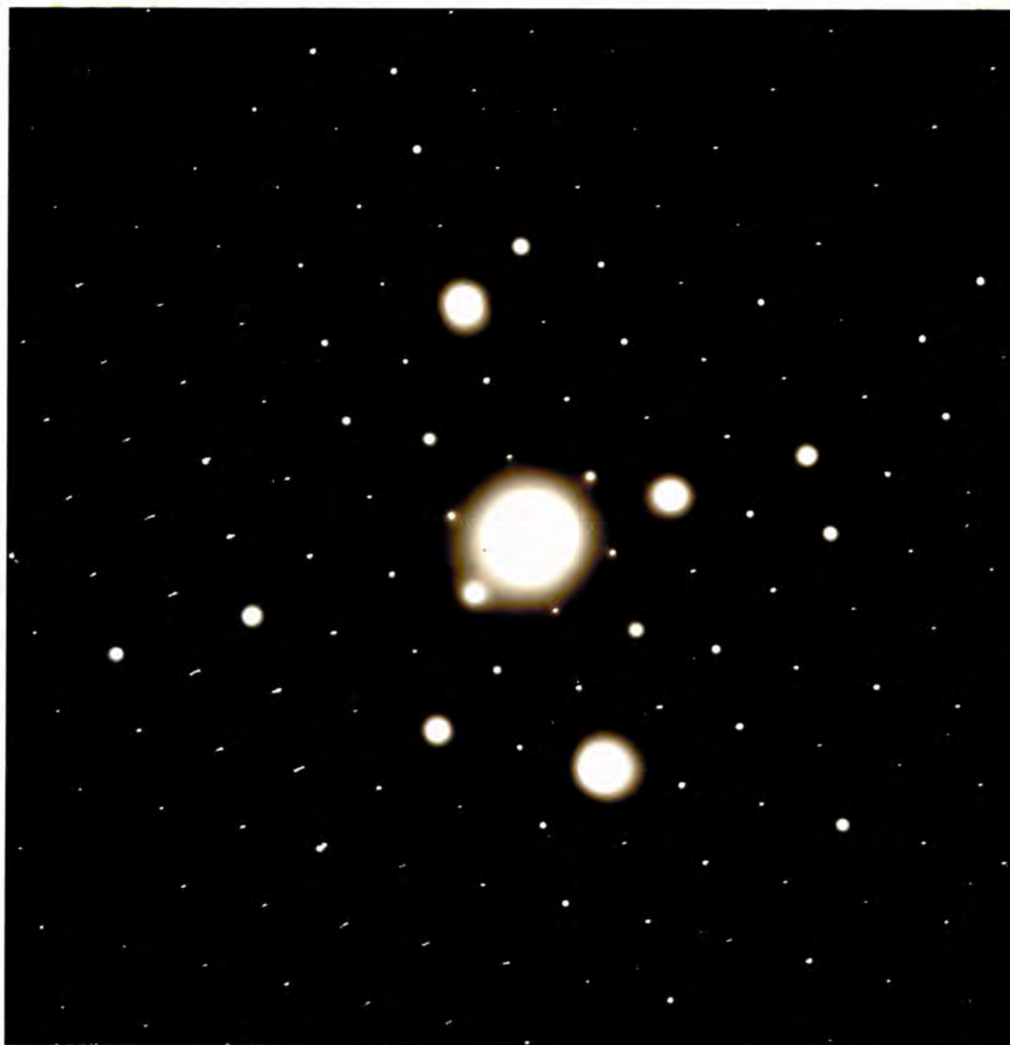

Figure 5.1.3 Selected area electron diffraction produced by a thin, cleaved mica specimen (100kV. electrons).

Electrical feedthroughs, passing through the base plate of the vacuum chamber, provide electrical access to apparatus inside the bell jar. The general features of this apparatus are shown schematically in Figure 5.2.1. Much of the apparatus was constructed from stainless steel and subsequently electropolished (see Appendix III), to provide an extremely clean system. The tungsten filament or boat is connected by stainless steel rods to the heavy current feedthroughs. This filament can be shielded from the substrate by means of a stainless steel shutter, activated from outside the chamber by a vacuum rotary drive. The substrate is held in a stainless steel holder provided with a tungsten heating filament, and the whole is supported by a system of adjustable clamps, so that the height of the substrate above the filament can be set as required. Figure 5.2.1 shows a schematic diagram of the evaporation assembly. The temperature of the substrate can be raised above the ambient temperature by passing about 10 amperes through the flat tungsten heating filament (R.D. Mathid Co.), sandwiched between a thin sheet of mica and a glass slide. A T1-T2 alloy thermocouple, specially calibrated, is used in conjunction with a microammeter (Airmec, Galvamp: Type 391) to measure the surface temperature of the substrate. Figure 5.2.2 shows the substrate holder and heater assembly. The method of calibrating the thermocouple is essentially that due to Miller (1962). Small quantities of 5 low melting point metals with high evaporation temperatures, were placed on the surface of a typical substrate (the substrate holder was orientated so that the substrate surface was uppermost) in vacuo and the temperature of the heater raised, while the metals were observed from outside the bell jar. By raising the temperature very slowly, and thus allowing the establishment of thermal equilibrium in the substrate, the thermocouple

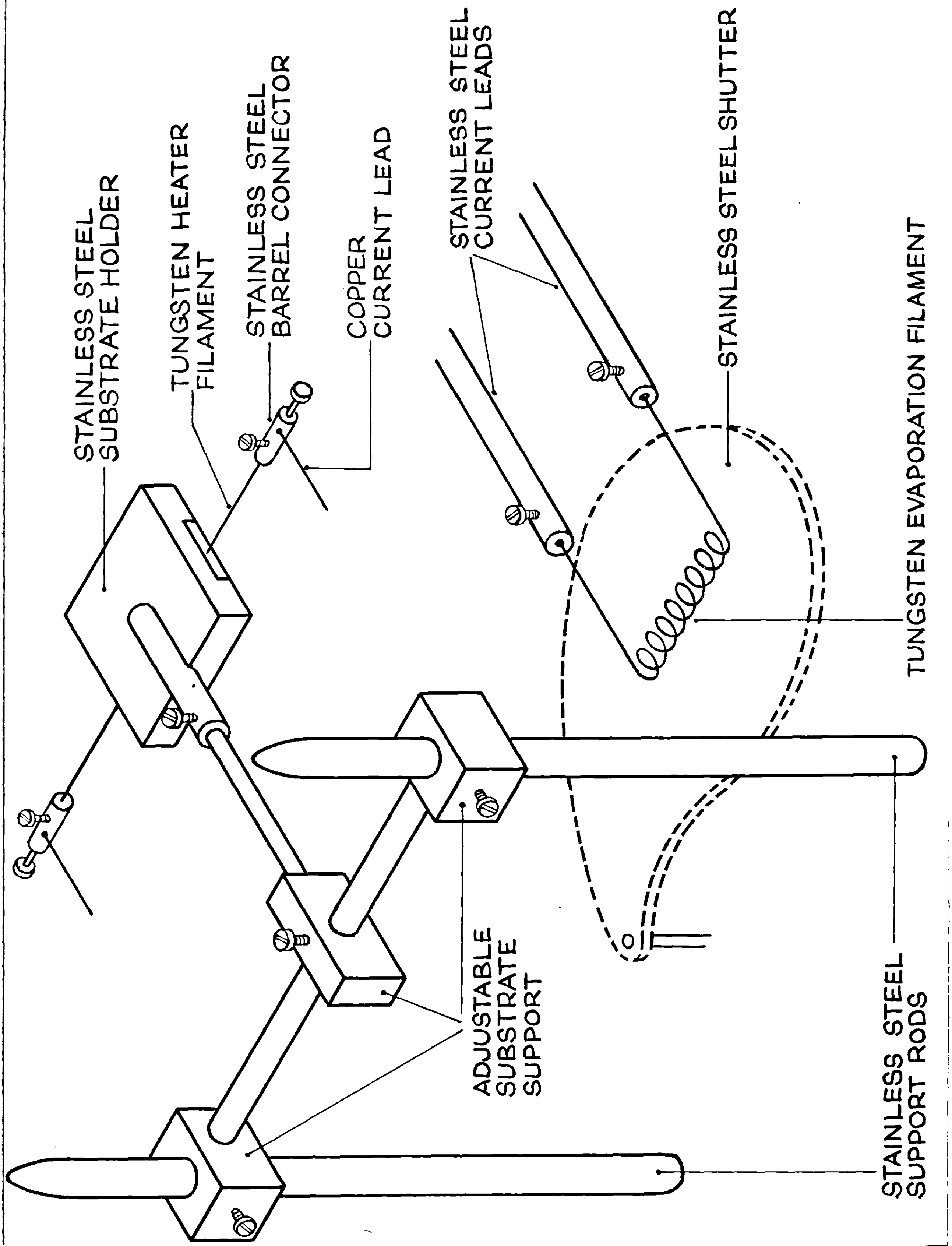

Figure 5.2.1 Evaporation assembly for tungsten filament evaporations: 12" system.

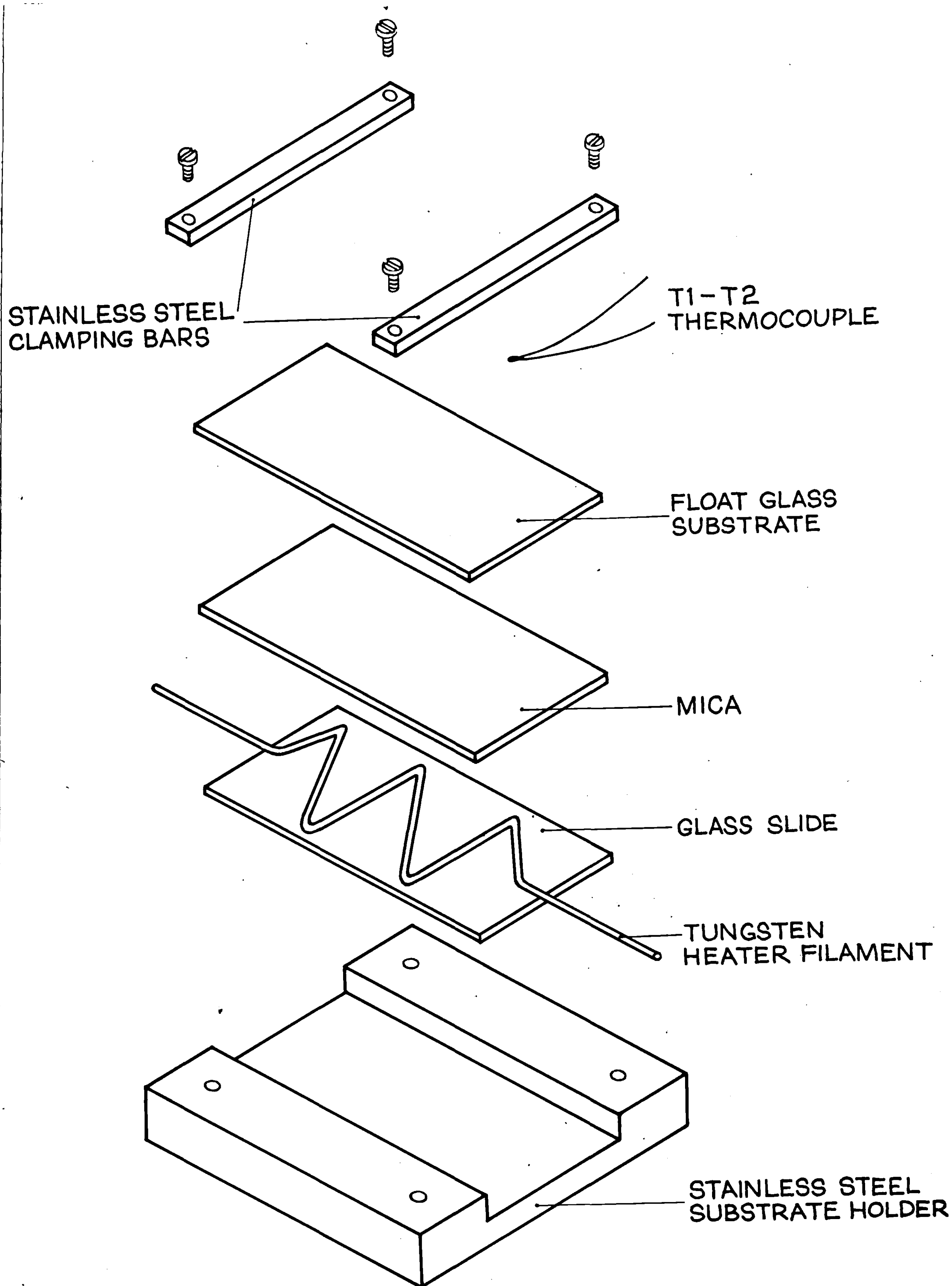

Figure 5.2.2 Substrate holder and heater assembly for 12" O.H.V. system.

reading corresponding to the known melting points could be obtained to $\pm 5^{o}$C. Table 5.2.1 shows the melting points of the metals used in the calibration of the substrate surface temperature. All temperatures mentioned in relation to the annealing of substrates in C.H.V. are true surface temperatures, derived from the observed calibration curve.

Before using a tungsten filament or boat for evaporation it was thoroughly outgassed in vacuo to the base pressure of 5×10^{-6} torr, by passing a current of at least 40 amps through it. After allowing about 20 minutes for the filament to cool it was loaded with the material to be evaporated. In the case of terbium, which was in wire form (1mm diameter), several lengths of wire pushed into the helical filament and about 30 amps of current passed through the wire to premelt the terbium. Successive short bursts of current through the filament outgassed the terbium to the base pressure of 5×10^{-6} torr. For gold evaporations a tungsten boat was used in the manner described by Holland (1958). Details of growth, possible pressure contamination and electron microscopy of films grown in this system are given in Chapter 7.

5.2.2 The electron ring-gun evaporation system

The electron ring-gun evaporation system is housed in a modified Edwards E3 coating unit. The 18 inch diameter, glass bell jar is sealed to the base plate by means of an L-shaped viton gasket. This bell jar is evacuated by a water cooled, oil vapour diffusion pump fitted with a water cooled baffle section to reduce any backstreaming of diffusion pump oil. An Edwards ISC-450B, two stage oil rotary pump is used to provide a low backing pressure (0.001 torr) for the diffusion pump, and is also used to pre-evacuate the bell jar. An

Table 5.2.1

Melting points and evaporation temperatures of the metals used for calibrating the thermocouple

Metal	M.P. °C	Vaporization Temp. °C.
Bismuth	271	698
Indium	157	952
Lead	328	718
Tin	232	1189
Woods Alloy	70	--

activated alumina trap reduces the backstreaming of rotary pump oil into the rest of the system. The ultimate pressure of this diffusion pumped system is about 1×10^{-6} torr. All of the evaporations in this system were performed at pressures between 5 and 9×10^{-6} torr. A Pirani gauge is used to measure the backing pressure over the pressure range 760-0.001 torr, and a Birvac Penning gauge (Model: T2002), incorporated in the evaporation chamber measures pressures to 1×10^{-7} torr.

The Birvac electron ring-gun (Type: RG2) uses electron bombardment to evaporate materials from refractory crucibles. Electron bombardment has been described in general terms by Francombe (1966, pp.40-42). The ring-gun consists of a stainless steel cylindrical, hollow box with one of its ends plane. The other end is conical and each has a hole provided centrally and coaxially with the other. A filament of molybdenum (electron emitter) is in the form of a loop supported at each end of its diameter by suitable connections across which the filament voltage may be applied, (a.c. 10 volts variable to give a maximum filament current of 30 amps). One end of the filament is connected to the box and the other end is insulated from it. The whole assembly is mounted onto posts which insulate it from earth. The other ends of these posts are located onto a table and between this table and the box the variable H.T. voltage from the Birvac ring-gun console (Type: RG) is applied. Beneath the box a small rotating turntable is mounted, capable of holding six cermet (Al_2O_3) type crucibles mounted on molybdenum clips and rotatable from outside the vacuum chamber. Both the turntable and crucible are at earth potential.

The mode of operation of this ring-gun when used for evaporating terbium is briefly explained as follows. When the system was under high vacuum (5×10^{-6} torr) a low voltage was applied to the filament, causing the filament to glow and emit electrons. The negative H.T.

was then applied to the surrounding box. This causes the electrons to be focused by the box onto the crucible. Terbium pieces cut from an ingot (99.9% Tb: Koch-Light Laboratories Ltd.), and placed in the crucible were therefore bombarded through the whole plane end of the cylinder by the emerging electrons. This bombardment resulted first in melting of the terbium and consequently its evaporation, as filament current and H.T. were increased. There was always a pressure burst in the system to 1-2 x 10^{-5} torr, during the initial melting; the pressure afterwards falling to 5-9 x 10^{-6} torr. Terbium evaporated upwards through the gun and, after the gettering procedure (see previous Section), onto the float glass or mica substrate, which was placed in a holder, like that shown in Figure 5.2.2, above the ring-gun crucible. A distance of 30 cms separated the crucible from the substrate. All substrates were annealed in this system, prior to evaporation at $\leqslant 5 \times 10^{-6}$ torr, and for about 2 hours at 250°C. Details of terbium evaporations and subsequent electron microscopy are given in Chapter 7.

5.3 Ultra-high vacuum (U.H.V.) preparation of films

Ultra-high vacuum is concerned with pressures below 10^{-7} torr. Production of U.H.V. requires special apparatus and techniques. Much of this apparatus and many of these techniques have now been included in commercial apparatus designed to achieve pressures in the 10^{-11} torr range. It is therefore not surprising that U.H.V. systems are becoming increasingly popular for producing evaporated films of metals for optical and surface studies. To date the best general text on U.H.V. is that due to Redhead et al. (1968).

5.3.1 General description of U.H.V. system

The U.H.V. system used in the experiments to be described in Chapter 7 was designed by Miller and Taylor (unpublished) and manufactured

by Edwards High Vacuum Ltd. The system was designed for tungsten filament evaporations of metals, in particular gadolinium and terbium, and subsequent in-situ optimized reflection measurements of the evaporated films (Miller et al., 1970).

The system essentially comprises a U.H.V. pumping group together with necessary backing pressure facilities and service chamber complete with baking oven and bake-out controller, mounted on a mild steel, channel-section base, which in turn is supported by massive concrete blocks. The oven, when required, is located on the base by steel pins. The U.H.V. pumping group consists of a "Varian" vac-ion pump connected to an 8 inch diameter conflat flange on the service chamber and a titanium sublimation pump located in the chamber. Instrumentation, control and power supplies to the U.H.V. pumping group and oven are provided from external separately mounted units. All vacuum components are of vacuum brazed, stainless steel construction, leak tested to better than 10^{-11} torr litre/second, and have undergone a degassing bake in vacuo to a temperature of 1050°C for maximum cleanliness. Connecting flanges are to ISO standard throughout and are gold wire sealed, unless otherwise stated. A specification is given below:

Specification and some data

Vacuum Pumps:

Backing line pump:	Edwards two stage (ED250) oil rotary pump, pumping speed 250 l per sec.
Backing line oil vapour trap:	Edwards foreline trap, filled with activated alumina balls (Type: 20-H260-A7)
Vac-ion pump:	Varian model (Type: 912-7008) standard diode vac-ion pump with permanent magnet, pumping speed 140 l per sec.

Titanium sublimation pump:	Vacuum Generators titanium sublimation pump, carrying four individual elements, pumping speed 4000 l per sec.
Cryo-pump:	Liquid nitrogen cooled cylinder in service chamber. Very high pumping speeds for condensable gases.

Service chamber dimensions:

12 inches in diameter and 22.5 inches high.

Feedthrough ports:

Circumferentially placed around service chamber eight 40mm ISO flanged ports, 2 inches effective length. These carry the following components: three optical ports, ionization gauge, evaporation system and evaporation shuttering mechanism. In top of service chamber one Vacuum Generators (TL8) electrical feedthrough and one Vacuum Generators (RD1) calibrated, rotary motion drive, fitted to a goniometer mechanism which was built in the laboratory workshop.

Oven heaters:

Three separate heater elements of 8ft x 5/16 ins. Pyrobar-iconel sheath; each rated at 1.7 kW.

Thermocouple controller:

Copper constantan thermocouple in top of service chamber, connected to a Honeywell thermocouple controller (Type: 02-715).

Optical ports:

Three Vacuum Generators (VP38Q) fused-quartz, end window ports, connected via graded glass seals to standard flanges, each fully bakeable to 400°C.

Vacuum gauges:

Backing line pressures 760 to 0.001 torr:	Edwards Pirani vacuum gauge head M6A/D2405 and a model B5 Pirani vacuum gauge.
Pressures in the range 10^{-3} to 10^{-11} torr:	Edwards model IG4M ionization gauge head and a model 5 ionization gauge. The gauge head is a Bayard-Alpert type.

A schematic plan view of the U.H.V. system is given in Figure 5.3.1.

5.3.2 Details of the main service chamber

The service chamber is of stainless steel argon-arc welded construction and accomodates 8 x 40mm ISO flanged service ports, located in the upper section of the chamber, three of the ports being provided with fused quartz windows, and three ports with a Vacuum Generators (SRD3) uncalibrated rotary drive, a two way 100 amp electrical feedthrough as part of the evaporation assembly, and a model IG4M ionization gauge head, (Blears, 1947) and (Apgar, 1963). This gauge head is nude and projects well into the service chamber so that the effects of tubulation on pressure measurement should be minimal. A 40mm ISO flanged port in the lower portion of the chamber provides for mounting and access to the titanium sublimation pump. The vac-ion pump is connected to the 8 inch diameter conflat flanged port (conflat copper seal), diametrically opposite and the remaining 25mm flanged port provides the connection for a model BV8 bakeable roughing valve with a flanged elbow extension to which is attached the backing line. This backing line consists of the foreline trap and the bakeable valve. The backing line is connected to the oil rotary pump by means of a flexible bellows connection.

A stainless steel liquid nitrogen reservoir is centrally mounted in the pumping chamber immediately above the sublimation pump; the base of this reservoir is curved so that the titanium rods are at the centre of curvature, thus providing a cooled shield for the sublimation pump. Two 3/8 inch stainless steel pipes connect the reservoir to argon arc welded blisters on the external wall of the chamber to provide liquid filling and exhaust connections for the tank.

The upper section of the chamber terminates in a stainless steel, gold wire sealed, blanking flange which is provided with a centrally bored aperture through which passes the spindle of the calibrated rotary

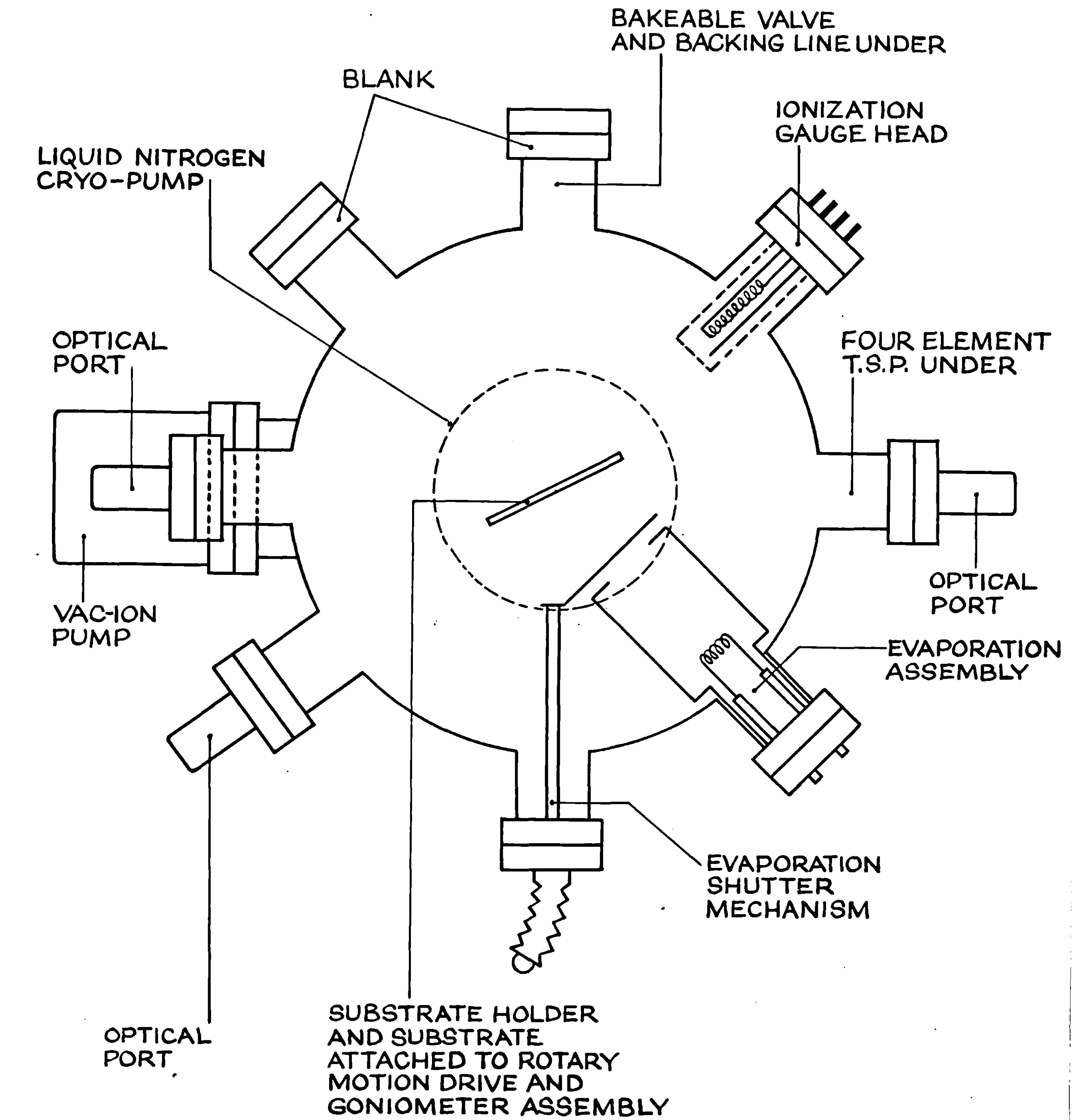

Figure 5.3.1 Schematic plan view of U.H.V. system.

motion drive. Attached to the lower end of this spindle is a stainless steel substrate holder of the same design as that shown in Figure 5.2.2 but without the heater facility. A specially designed goniometer head facilitates levelling of the substrate surface in order to perform in-situ reflection measurements. Three eye bolts are supplied for lifting off and release of the blanking flange.

5.3.3 Details of the U.H.V. pumping group

The U.H.V. pumping group pumps the service chamber to better than 5×10^{-11} torr. The vac-ion pump has a pumping speed capability of 140 l per sec. and essentially comprises an enclosure containing a number of pumping elements located in a strong permanent magnetic field. These elements consist of a multi-cell anode strucutre, positioned between two titanium cathode plates and the pumping action is achieved by supplying a suitable positive voltage (maximum 8 kV) between the anode and cathode from a separate power unit. The pumping process may be divided into two principal mechanisms:

(i) The entrapment in the titanium cathode of molecules accelerated as positive ions, i.e. ionic pumping.

(ii) The sputtering of the cathode surfaces by positive ion bombardment creates 'clean' surfaces onto which chemically active gases can chemisorb or form chemical compounds.

Detailed descriptions of ion pumps may be found in Power (1966).

In the titanium sublimation pump, which consists of four replaceable titanium filaments, the pumping action is achieved by subliming titanium from the electrically heated filaments onto the chamber walls and the liquid nitrogen cooled reservoir base, thus providing a film of clean titanium metal which is then available to

getter gas molecules. In addition, the liquid nitrogen reservoir provides a cryogenic pumping capacity for vapours and gases condensable at liquid nitrogen temperatures and together with the evaporated titanium forms a cryo-getter pump. The action and description of cryogenic systems has been described by Holland (1965).

5.3.4 Details of the U.H.V. electronic control systems and power units

The electronic control systems and power supplies are now described: a Vacuum Generators (Type: BHC2) bake-out control unit is utilized in conjunction with a Varian ion pump power unit (Type: IPS9A), fitted with a bake-out oven control socket, to operate and monitor the three independent oven heater circuits. The bake-out control unit is fitted with a programmeable timer to initiate and time the bake-out. The ion pump discharge current is one of the control parameters for heater operation, thus, if the chamber pressure increases above one of the three pre-selected pressure levels (approximately 10^{-5}, 10^{-6}, 10^{-7}torr), the heater circuits will automatically switch off and subsequently on as the pressure decreases below the pre-selected level. Another control parameter for heater operation comes from the Honeywell temperature indicator/controller which monitors the temperature of the main service chamber and switches off the heater circuits, through the bakeout control unit, when the chamber temperature exceeds a pre-set value (usually 280°C). Thus, in the latter stages of bakeout, when the pressure is below 10^{-7}torr, the Honeywell indicator/controller, controls the heater circuits. The ion-pump power supply unit also incorporates a safety switching circuit to switch off the oven-heaters in the event of the ion-pump over pressure trip operating, pump short circuits, ion-pump high voltage breakdown or vacuum failure. Power supplies for the titanium sublimation pump are from an Edwards (Type: SPS4) power unit. This unit can operate

in one of two modes: automatic or manual. In automatic mode the power supply provides a programmeable time delay (maximum delay 60 minutes) for the current to the titanium filaments and the time for which current flows is approximately 90 seconds. Once the 90 seconds has expired control is passed to the automatic time delay device and current will not flow until the prescribed time delay has elapsed. When the power supply is switched to manual mode the automatic duty cycle and time delay are made inoperative. For automatic and manual modes current through the titanium filaments is controlled manually by means of a Variac and current meter. A Variac controlled a.c. power supply capable of delivering 120 amps was constructed for heating the tungsten filament of the evaporation assembly (see Section 5.3.7 for details of the evaporation assembly).

5.3.5 U.H.V. pressure measurement and the ionization gauge

Ultra-high vacuum pressure measurement is effected by the Edwards (Model IG4M) nude ionization gauge head in conjunction with the Edwards (Model 5) gauge control unit. The IG4M gauge head contains a four electrode assembly and is open to and therefore part of the vacuum system, so that molecules present within the system should be equally present within the electrode structure, (Blears, 1947 and Apgar, 1963). Three of the electrodes are the filament, grid and ion collector. The electrically heated tungsten filament emits electrons and in their transit to the positively biased grid gain sufficient energy to ionize gas molecules upon collision with them. The positive ions thus produced are attracted to the negatively biased collector and the ionization current which results is directly related (to a first approximation) to the pressure in the service chamber. This ionization current is measured and displayed by the Model 5 gauge control unit. At pressures

below 10^{-8} torr there is an appreciable residual current (contained within the total ionization current) which arises from X-rays emitted from the grid striking the collector and causing emission of photo-electrons. The fourth gauge electrode, termed the modulator, enables this residual current to be distinguished from the true gas ion current. A special modulator circuit in the Model 5 gauge control unit allows the true gas ion current, and thus the true pressure, to be measured once the gauge factor has been determined. The gauge factor (0.3 for the particular gauge in use) was determined at pressures above 10^{-8} torr. A complete analysis of the modulated Bayard-Alpert gauge head has been given by Redhead and Hobson (1965).

The Bayard-Alpert gauge is a hot ionization gauge and so will have some effect on the residual gas composition and total pressure inside the service chamber. It is known that such a gauge will itself pump and remit gas. A comprehensive study of the pumping of the rare gases in a Bayard-Alpert gauge has been made by Cobic et al., (1961). A complex situation arises when the gauge is used in the presence of chemically active gases (N_2, H_2, CO, CO_2, CH_4, all of which can occur in U.H.V. systems); chemical adsorption and dissociation occur in addition to the pumping of ions (Alpert, 1962). The combined pumping speeds of a Bayard-Alpert gauge can be as high as 200 l/sec. relative to N_2 (Alpert, 1962). The chemically active gases (N_2, H_2) may interact in or on heated gauge parts to produce other gases. A chemical dissociation occurs at the surface of the hot cathode so that considerable changes in gas composition inside the service chamber could result when the gauge is on. Some possible reactions at the tungsten cathode are:

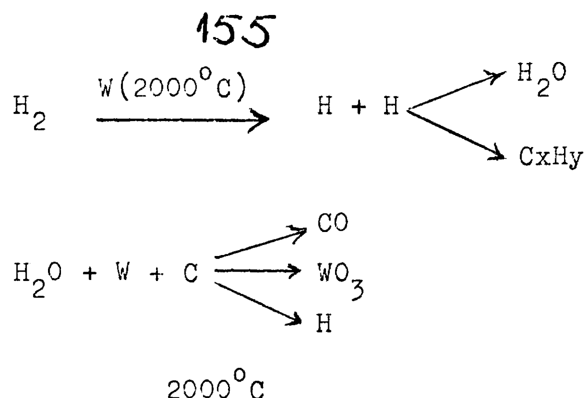

The carbon occurs as impurities in the metals employed in the grid and electrodes of the gauge. Contaminant species, in particular CO, are produced by interaction of atomic hydrogen with the service chamber walls and gauge electrodes, (Singleton, 1967 and Hickmott, 1960).

5.3.6 <u>Residual gas analysis inside the U.H.V. system</u>

There was no available means of obtaining partial pressure measurements of the residual gases present in the U.H.V. system. A knowledge of the gas composition for pressures at which film deposition occurs is important for the analysis of any film surface contamination. All the component parts of a U.H.V. system contribute to the residual gases present at the ultimate pressure of the system. Section 5.3.5 shows how the ionization gauge contributes to the gases present in a U.H.V. system.

Hydrogen is an appreciable constituent of the residual gases present. The mechanisms suggested by various authors as the cause of residual hydrogen in their U.H.V. systems are varied. Davis (1962) located a source of hydrogen in the body of the bakeable U.H.V. valve, and noted that permeation of atmospheric hydrogen through bellows systems might account for the source of residual hydrogen. A bakeable valve and a bellows system form part of the present U.H.V. system. It is also known that outgassing of hydrogen from stainless steel can account for residual hydrogen pressures of 3×10^{-13} torr.

Carbon monoxide and nitrogen are two gases which form the major part of the residual gas composition. They are both readily chemisorbed on system parts. The detailed origins of these two residual gases has not been described. It seems probable, however, that nitrogen represents some residual adsorption or solution of atmospheric nitrogen in system parts. This will almost certainly be the case if the U.H.V. system is let up to atmospheric pressure with dry nitrogen. Gosselin and Bryant (1965) regard hot tungsten filaments, such as those in gauges and evaporation systems, as a possible source of carbon monoxide. It is probable, therefore, that carbon monoxide is present in the U.H.V. system described in this thesis.

Carbon dioxide is not normally found as a major residual gas in laboratory type U.H.V. systems. However, Singleton and Lange (1965) report that carbon dioxide is released from any glass present during bakeout of the system. The present U.H.V. system has glass optical ports and substrate and so carbon dioxide may be present after bakeout, but most of this should condense onto the cooled surface of the cryo-getter pump.

There is usually very little oxygen present in stainless steel U.H.V. systems fitted with sputter ion and cryopumps (Davis, 1962): oxygen is usually undetectable in such systems.

Small partial pressures of the rare gases are to be expected, particularly in an ion pumped system, as a result of thermal re-emission (Davis, 1962), of previously pumped gas. Atmospheric argon enters the system each time it is opened and so accumulates in the ion-pump during the pumping process.

Before baking a U.H.V. system water vapour is a prominent peak in the residual gas spectrum (Hickmott, 1960; Tuzi, 1962), but many workers

have demonstrated that water vapour is not normally a major component of the residual U.H.V. gas spectrum, (Davis, 1962; Klopfer, 1961; Huber, 1966). There is, therefore, no reason to believe that water vapour should be present in the U.H.V. system used in the work described in Chapter 7.

A U.H.V. system having a configuration very similar to that described in this Section has been used by Rozgonyi et al., (1966) for a study of the residual gases present at a total background pressure of 5×10^{-11} torr which is the base pressure of the present U.H.V. system. The details are given below in Table 5.3.1.

5.3.7 Evaporation assembly

Figure 5.3.1 shows the position of the evaporation assembly in the main service chamber. It consists essentially of an electropolished, stainless steel cylinder which fits snugly into one of the chamber service ports and protrudes into the main service chamber. The end protruding into the chamber is provided with a rectangular aperture wide enough to allow evaporant material to deposit onto the substrate, but not so wide to allow evaporant to deposit on the inside of the chamber. An electropolished stainless steel shutter, activated from outside the chamber, can prevent evaporant from reaching the substrate. The evaporation source is a multi-stranded, tungsten helical filament (Mathis & Co.) connected by means of electropolished stainless steel barrel connectors to the copper rods in the flanged electrical feedthrough. Before mounting the filament in the U.H.V. system, it was cleaned and loaded with the metal to be evaporated using the O.H.V. techniques described in Section 5.2.1. Figure 5.3.2 shows a schematic section of the evaporation assembly.

The glass substrate, cleaned in the manner described in Section

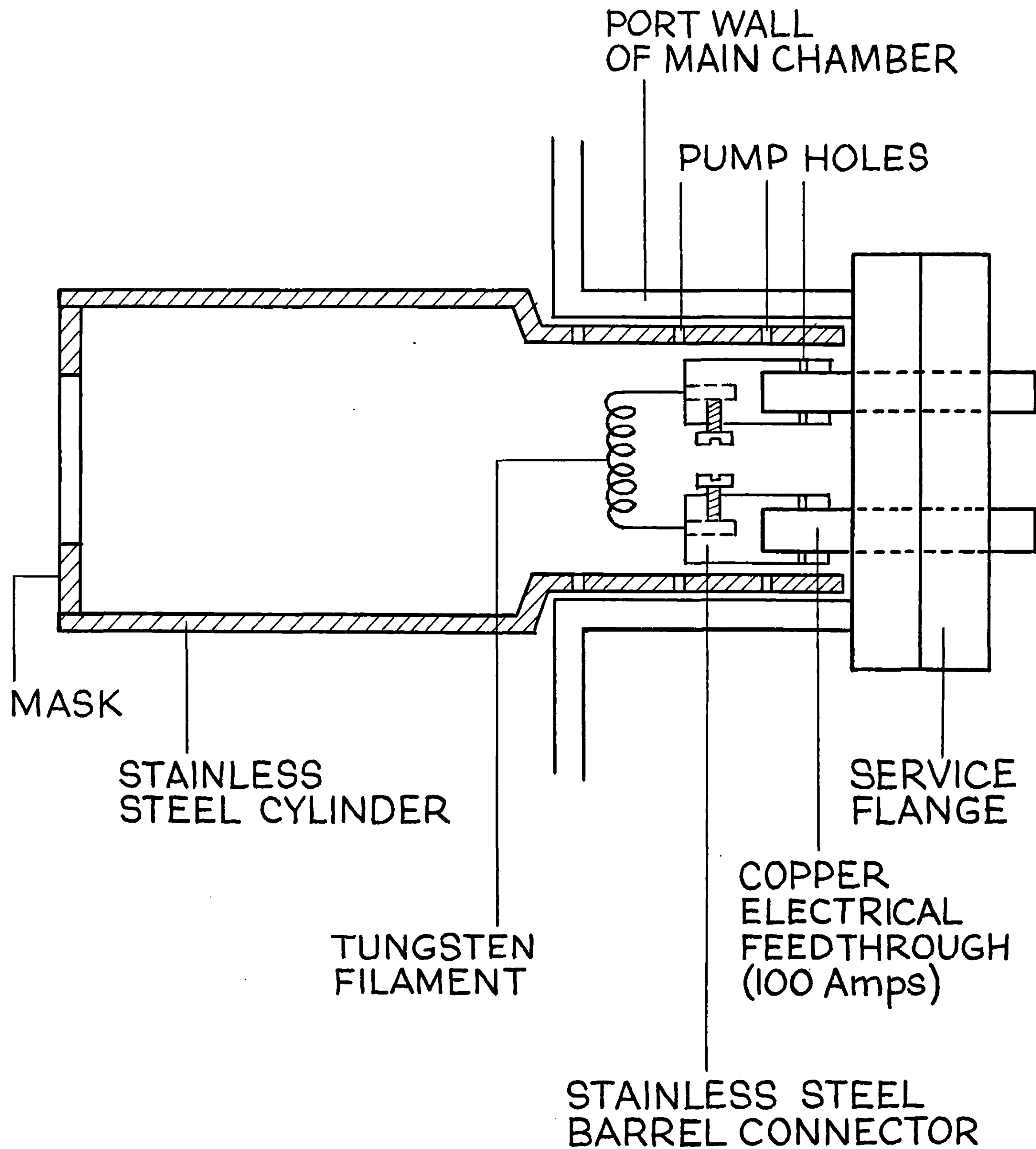

Figure 5.3.2 Schematic section of the evaporation assembly used in the U.H.V. system.

Table 5.3.1 Residual gas analysis in a stainless steel U.H.V. system; Rozgonyi et al.(1966)

Gas Constituent	Partial pressure (units of 10^{-12} torr, equivalent N_2
H_2	7.0
He	0.02
CH_4	2.0
H_2O	0.07
CO)) N_2)	20.0
O_2	0.0
Ar	20.0*
CO_2	0.06
Total background pressure	50.0

* Argon artificially high because apparatus used for argon sputtering. Davis (1962) recorded a partial pressure of 0.1×10^{-12} torr for Argon in an ion pumped stainless steel U.H.V. system.

5.1.1 is clamped into the electropolished stainless steel substrate holder described in Section 5.3.2. The evaporation source to substrate distance is about 18 cms.

5.4 U.H.V. pump-down and evaporation procedures

5.4.1 Pump-down procedure

To begin with the system is rough pumped using the oil rotary pump via the by-pass line until the pressure indicated by the Pirani gauge is about 0.5 torr. The by-pass line is then closed and the system pumped via the foreline trap until the pressure is about 0.001 torr. The ion-pump is then activated by means of the 'start' switch in the ion pump power supply. An ion-pump voltage of about 300V is indicated on the meter. At this stage a glow discharge occurs in the system and the pressure indicated by the Pirani gauge increases to about 0.01 torr. The ion-pump is then switched off if the pressure continues to rise, and is only switched on again when the pressure has fallen to at ~~least~~ most 0.005 torr. The glow discharge occurs again and lasts for between 5 and 10 minutes and then is extinguished. At this stage it is advisable to switch on each titanium sublimation pump filament and run it at 40A for two minutes, to give each filament a preliminary degassing.

After about 15 minutes the ion pump voltage rises to between 2 and 4kV, at which point the bakeable valve is lightly closed. The ion-pump voltage continues to rise and the bakeable valve is then shut firmly. The ion-pump is now pumping the system and the pressure rapidly falls to 10^{-6} torr which is indicated on the ion-pump power supply current/voltage meter. At this pressure the protect and abort circuits for the ion-pump are activated. The bakeout ovens are then assembled around the system and the required bakeout time period is set on the timer of the

bakeout controller. The pressure level trip on the bakeout controller is set at 10^{-6} torr and the Honeywell temperature/controller is set at 280°C. Bakeout is commenced by switching on the heaters. In the latter stages of the bakeout the system pressure as indicated by the ion-pump current is usually less than 5×10^{-8} torr.

After baking for 48 hours, and before the system has completely cooled the ionization gauge is degassed according to the manufacturer's instructions. Once the system has completely cooled to room temperature (~ 22°C) the pressure recorded by the ionization gauge is between 8×10^{-10} torr and 2×10^{-9} torr. With the titanium sublimation pump on and the liquid nitrogen filling the reservoir the pressure recorded by the modulated ionization gauge is below 1×10^{-10} torr; pressures of 3×10^{-11} torr have been recorded.

5.4.2 Evaporation procedure

The evaporation power supply is connected to the evaporation assembly by means of the appropriate electrical feed-throughs. The substrate is manipulated by the rotary drive and goniometer head so that its surface is at right angles to the longitudinal axis of the evaporation cylinder. The shutter is placed between the substrate and the loaded evaporation filament. Outgassing of the loaded filament is achieved by passing current bursts through it by means of the Variac control on the power supply. Starting with bursts of about 10 amps the pressure in the system rises into the 10^{-8} range and is never allowed to go above 1×10^{-7} torr. By gradually raising the value of the current through the loaded filament to the value required for evaporation ($\sim$50 amps.) the filament and contents are outgassed to pressures below 1×10^{-9} torr. For a nickel loaded filament outgassing to 5×10^{-10} torr was achieved and for gadolinium it was found difficult to outgas to below 1×10^{-9} torr.

To evaporate the metal from the filament the current is gradually increased to the evaporation current required, a short pressure burst to about 1×10^{-8} torr usually follows and then the pressure falls rapidly to below 2×10^{-9} torr. At this pressure the shutter is opened and deposition of the film commences, the system pressure is logged throughout the evaporation by means of a chart recorder connected to the appropriate terminals on the ionization gauge control unit. During the evaporation the U.H.V. pumping group is active. The evaporation is stopped by closing the shutter and switching off the evaporation power unit. Evaporation time is recorded by an event marker fitted to the chart recorder and manually operated. Evaporation pressures for nickel were recorded in the pressure range 5 to 8×10^{-10} torr, and 2 to 6×10^{-9} torr for gadolinium. Subsequent film thickness measurement by multiple beam interferometry exterior to the vacuum system showed that the evaporation rates for nickel and gadolinium were greater than 100nm per minute. In all of the evaporations made in this system base pressures were achieved within about 1 minute of the evaporation ending. Base pressures were all below 5×10^{-10} torr. Details of nickel and gadolinium evaporations carried out in this system are given in Chapter 7.

CHAPTER 6

A REVIEW OF THE RARE-EARTH METALS AND SOME PROPOSED EXPERIMENTAL STUDIES

Abstract

The purpose of this Chapter is to review the present state of the art with regard to the optical properties of the rare earth metals, in particular gadolinium and terbium, and the relevance of these properties to recent electronic band structure calculations. In order to extend and clarify previous work on gadolinium and terbium, further experiments are proposed, the results of which are reported in Chapter 7.

6.1 Introduction - a brief review of the rare earth metals

The name 'Rare Earths' is that given to fifteen chemical elements with the atomic numbers 57-71. Because these fifteen elements have similar properties they are usually arranged in some special way in the periodic table of the elements, (see for example Trifonov, 1963). All these elements are typical metals and occur naturally together in ores and minerals. In the elements of the rare earth series there is probably a greater number of interesting features than in any other short, consecutive sequence of elements, (see for example 'Proceedings of the First and Second Rare-Earth Conference, 1960 and 1961 respectively; The Macmillan Company: New York, 1961 and 1962 respectively). These include a somewhat exotic structural behaviour (fcc, bcc and hcp crystal structures occur in this series), the occurrence of superconductivity, six ferromagnetic elements (one of which has a Curie point above room temperature and five of which are also anti-ferromagnetic in certain temperature ranges), four anti-ferromagnetic elements and many unusual characteristics in other

properties (mechanical, thermal, magnetic, optical), which are related to the structural and magnetic behaviour. It is, therefore, not surprising that since the 1950-1960 period when the pure metals became increasingly available (Spedding and co-workers at Iowa University, U.S.A.) the number of investigators and the extent of investigations in this field have grown extremely rapidly. The motivation behind this growth has been varied and is associated partly with technology and partly with attempts to understand the physical properties and their interrelation with one another. There appears to be only one general review article on the rare earth metals (Taylor, 1970) although numerous specific articles have been published. Much useful data on the rare earth metals has been compiled by 'Rare Earth Products Ltd' (1970). A comprehensive bibliography of almost one thousand references on work concerned with the rare earth metals is given in (Kleber and Love, 1963).

6.1.1 Electronic configuration of the rare earth metals

In order to explain the optical properties of the rare earth metals it is necessary to know the electronic configuration of the atoms. Lanthanum is the first element in the series and has an electron structure consisting of a xenon core ($1s^2 2s^2 2p^6 3s^2 3p^6 3d^{10} 4s^2 4p^6 4d^{10} 5s^2 5p^6$) and an outer electron core of $4f^0 5d^1 6s^2$. Cerium is the next element in the series and here we find that the 4f shell has a slightly lower energy than the $5d^1$ state and so the additional electron occupies the 4f shell, thus beginning the progressive population of the 4f level which occurs across the series. The 4f shell, which is situated deeply in the atom, has 14 available electron states, and it is the filling of these states from $4f^0$ for lanthanum (Z = 57) to $4f^{14}$ at lutetium (Z = 71) which characterizes the rare earth series. All of the rare earth metals have the stable, inner xenon core. The rare earth electron structure is given in general by:

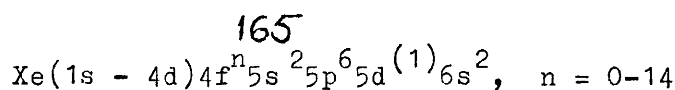

$$Xe(1s - 4d)4f^{n}5s^{2}5p^{6}5d^{(1)}6s^{2}, \quad n = 0\text{-}14$$

The parenthesis for the 5d state is used to indicate that in many of the elements, once the 4f shell contains electrons, the 5d electron is transferred to the 4f shell. However, for some applications such as electronic band structure calculations, the $5d^{1}$ electron is often included in the electronic configuration used even though it is assumed that the neutral atom does not have a $5d^{1}$ electron (Keeton and Loucks, 1968). In Table 6.1.1 the electronic configurations of the rare earth atoms are given. This Table differs from a similar one given by Schüler (1966), for the rare earth metals, which shows that only europium and ytterbium are without 5d-electrons. Whether or not the 5d electron term is included appears to make little significant difference to the results of band structure calculations (Keeton and Loucks, 1968). The Table shows that gadolinium retains the $4f^{7}$ term with the additional electron appearing in the $5d^{1}$ state, as does lutetium with $4f^{14}$, showing that there is a tendency to retain the stable half full or completely full 4f shell structure. In the metallic state the outer electrons ($5d^{1}$ and 6s) are readily removed to become conduction electrons, leaving in general a trivalent ion. Where there is no 5d electron available for conduction then the 4f shell gives up an electron. Valencies of two and four are also possible. It is the 4f shell which dominates many of the properties of the rare earth metals; for example, the 4f electrons give rise to the ferromagnetism observed in gadolinium and terbium.

6.2 The optical and magneto-optical properties of the rare earth metals

It is only within the past decade that there has been any serious attempt to study the optical properties of the rare earth metals. Even now there appears to be no published work on the magneto-optical

properties of the rare-earths. Reasons for this state of affairs are not difficult to find. The surfaces of these reactive metals are easily attacked by the atmosphere, and in some cases even the bulk material is corroded in air, often spontaneously igniting (Johnson and Mathey, 1970). It is not surprising, therefore, that ordinary methods of metallurgical polishing and electrolytic etching fail. Evaporated films of these metals are virtually the only specimens that can provide good enough surfaces for either reflection or transmission spectroscopy. Good, clean vacuum systems are required to prepare such films with the desired degree of purity, and it is preferable if the required optical measurements are obtained in situ. Ultra-high vacuum systems are capable of providing the conditions required for growth and study of rare earth metal films, and these have only recently become commercially available.

In order to prepare metal films by vacuum evaporation techniques, for optical reflection and transmission studies it is necessary that high purity material is used and that it be readily available in a suitable form, e.g. thin wire for tungsten filament evaporations. Again, it is only within the last few years that the rare earth metals have been available commercially, having sufficient purity and in forms suitable for vacuum evaporation. Anotherreason why there has not been much incentive to study the optical properties of the rare earth metals is that electronic band structure calculations are required to interpret the experimentally observed optical dispersion curves ($\sigma(\omega)$ against $\hbar\omega$) and these calculations have only just begun to be published.

The remainder of this Section reviews the present state of the art of experimental and theoretical work, and some suggestions for further work are made.

Table 6.1.1 Basic outer electronic configuration of the rare earth atoms

Element	Symbol	Atomic Number (Z)	No. of electrons			Crystal Structure at 293°K.
			4f	5d	6s	
Lanthanum	La	57	0	1	2	hex.
Cerium	Ce	58	2	0	2	hex.
Praseodymium	Pr	59	3	0	2	hex.
Neodymium	Nd	60	4	0	2	hex.
Prometheum	Pm	61	5	0	2	? *
Samarium	Sm	62	6	0	2	rh.
Europium	Eu	63	7	0	2	bcc.
Gadolinium	Gd	64	7	1	2	hcp.
Terbium	Tb	65	9	0	2	hcp.
Dysprosium	Dy	66	10	0	2	hcp.
Holmium	Ho	67	11	0	2	hcp.
Erbium	Er	68	12	0	2	hcp.
Thulium	Tm	69	13	0	2	hcp.
Ytterbium	Yb	70	14	0	2	fcc.
Lutetium	Lu	71	14	1	2	hcp.

* Radioactive element with a half-life (2 years) produced artificially

Neodymium appears to have been the first rare earth metal to be studied by optical constant techniques. Kern (1957) investigated the optical properties of this metal in the visible wavelength range, and there appears to be no other published work on the optical properties of Nd.

The infra-red reflectivity of a thin film of antiferromagnetic holmium has been measured by Schüler (1964). His data show a temperature dependent anomaly at a photon energy of 0.35eV which has been interpreted as due to interband transitions across the energy gaps created by the antiferromagnetic super-lattice (Taylor, 1970).

Some preliminary studies have been made by Cooper and Redington (1965), of the infra-red optical absorption in thin films of dysprosium, both with and without an applied magnetic field. They observed an anomaly in the absorption dispersion curve at a photon energy of about 0.44eV quite similar to that seen by Schüler for Ho. The optical absorption spectra observed in antiferromagnetic and ferromagnetic Dy were, to a first approximation, identical.

A study of the optical properties of the rare earth metals gadolinium, lutetium, dysprosium, europium and ytterbium was made by Schüler (1966). For his studies he used thin, transmitting and opaque films deposited and measured in U.H.V. (pressures not stated). He used normal-incidence, optical techniques to obtain transmission and reflection coefficients in the photon energy range 0.3-5eV. Optical constant values were deduced for Gd and Lu, and plots of $\sigma(\omega)$ against $\hbar\omega$ obtained; these dispersion curves were essentially the same. The divalent cubic metals Eu and Yb gave dispersion curves similar to one another but distinctly different from those of trivalent Gd and Lu.

Dispersion curves of Eu and Yb showed a striking resemblance to those of Ba and Sr metals. Interpretation of the optical properties of Gd, Lu and Dy in terms of recently published band structure calculations was attempted, and the results were found to be in poor agreement. In addition to studies of the rare earth metals in their paramagnetic state at room temperature, Schüler looked for the effect of magnetic order, occurring at lower temperatures, on their optical properties. Anomalies in the dispersion of $\sigma(\omega)$, associated with either ferromagnetic or periodic electron spin arrangements, were found for Gd, Lu and Ho. Schüler deposited all his films on sapphire substrates (crystalline nature not stated) and assumed the films to be polycrystalline with random orientation.

No further experimental work on the optical properties of the rare earth metals appeared in print until 1969 when Hodgson and Cleyet (1969) reported on the optical absorption bands of Gd in the ferromagnetic and paramagnetic states. The optical constants of Gd were measured by internal reflection from evaporated films of the metal on silica glass prisms, at temperatures above and below the Curie temperature, in the photon energy range 0.50-5.60eV. The Gd films were prepared by vacuum evaporation of 99.9% purity metal from a tantalum boat at deposition pressures of $6\text{-}8\times10^{-8}$torr, and the film coated prisms were subsequently removed to facilitate the reflectance measurements. Film thicknesses were quoted as being in excess of 2000nm, and evaporation rates greater than 200nm per second were also quoted. Hodgson and Cleyet assumed their films to be polycrystalline with a random orientation of crystallites, and no attempt was made to check this assumption. A comparison of their room temperature (293°K) curve for $\sigma(\omega)$ with that published by Schüler (1966) shows that the $\sigma(\omega)$ values of Hodgson and Cleyet are consistently

much smaller. In order to check this discrepancy Hodgson and Cleyet calculated the normal incidence transmission $T(\omega)$ of a film 92.5nm thick from their deduced optical constants, and concluded that the $T(\omega)$ values were in good agreement with those measured directly by Schüler (1966). Somehow, Hodgson and Cleyet persuaded Schüler to revise his $\sigma(\omega)$ values, and when these revised results were compared there was good agreement between the two sets of $\sigma(\omega)$ values. However, differences in positions and sizes of peaks in the $\sigma(\omega)$ against $\hbar\omega$ curve still existed. Blodgett et al. (1966) measured the reflectivity of a thick Gd film for photon energies 1.0-12.0eV. Hodgson and Cleyet (1969) calculated normal incidence reflectivities for their films from the deduced optical constants, and reported that the calculated reflectivities agreed closely with those of Blodgett et al. The work contained in Chapter 2 shows this to be a hazardous procedure, because at normal incidence reflectivities are very insensitive to n and k. Thus, a wide range of n and k values could reproduce normal incidence reflectivities differing amongst themselves by 1% or less. It is, therefore, not surprising that workers using this technique to compare results obtain such good agreement.

A detailed, comparative study of the optical properties of barium (Ba) and strontium (Sr) with those of the rare earth metals Eu and Yb has been made by Endriz and Spicer (1970). This work extends and clarifies that of Schüler (1966) and Müller (1965, 1967) concerning these four metals. Endriz and Spicer performed in-situ reflectance measurements at normal incidence on evaporated films of the metals, and then carried out a Kramers-Krönig analysis of the reflectance data to yield n and k and hence ϵ_1, ϵ_2 and σ to an accuracy of $\pm$ 20%. The photon energy range covered by their measurements was 1.0-11.6eV. Film evaporations were made at rates of 200nm per minute at pressures below 4 x 10^{-8} torr, and

reflectance measurements were obtained at pressures in the 10^{-12} torr range. The substrates were float glass microscope slides. When the results for $\sigma(\omega)$ were compared for the two fcc metals (Sr and Yb) and the two bcc metals (Ba and Eu) good correlation was found to exist between the interband $\sigma(\omega)$ values and the crystal structure. In addition, an excellent interpretative study was made of the $\sigma(\omega)$ dispersion curve using the results of present band structure calculations.

For the rare earth metals La, Ce, Pr, Pm, Sm, Tb and Tm it appears that no optical constants studies have been published, although Schüler (1966) reports that he has made some measurements on Tb.

There are no published results of magneto-optical studies on the rare earth metals, and only one reference even hinting at such measurements has been found (Holmes et al., 1959).

6.2.1 Band structure calculations for the rare earth metals

So far no comprehensive review has been given of the Fermi surface and electronic band structure of the rare earth metals, probably because it is only recently that detailed work has been published.

Early theoretical work (Elliott and Wedgwood, 1963; 1964) attempted to explain the available experimental data on the trivalent rare earth metals by assuming that the three conduction electrons occupy essentially free electron bands. However, it was difficult to explain by means of the free electron model the large saturation magnetization of Gd (Nigh et al., 1963) and especially the large electronic specific heat (Jennings, et al., 1960) of the rare earth metals which indicated a density of states at the Fermi-surface of about eight times that predicted by the free-electron model. This prompted the study of the electronic energy bands in the rare earth metals by more refined techniques, such as the non-relativistic-augmented-plane-wave (APW) method (Slater, 1937; 1953).

One of the first of such calculations on the rare earth metals was performed by Dimmock and Freeman (1964) who calculated the energy curves for the conduction bands of Gd along the major symmetry directions in the first Brillouin zone, and a density of states histogram. They also showed that the Fermi-surface of Gd is extremely anisotropic which helps to explain the anisotropic nature of the electrical and magnetic properties of this metal. These band structure calculations and selection rules for interband transitions (Dimmock et al., 1966) were used by Schüler to successfully interpret the main features of his experimentally obtained $\sigma(\omega)$ dispersion curve.

Freeman et al. (1966) have also reported APW band structure calculations for thulium (Tm) which were nearly the same as those for Gd.

To investigate further the band structure and Fermi-surface of the heavy rare earth metals Gd, Dy, Er and Lu, Keeton and Loucks (1968) carried out relativistic-augmented-plane-wave (RAPW) calculations (Loucks, 1967) for these metals. Keeton and Loucks (1966) had previously suspected that relativistic effects should be included in the band structure calculations of the heavy rare earth metals. It was found that the energy bands for all the elements studied were quite similar, differing only in details, but differing significantly from those calculated by the APW method. Histograms of the density of states for each of the metals are given and the effect on the band structure of using different basic electronic configurations is also reported, (see also Section 6.1.1).

What is probably the most useful band structure calculation for the purpose of explaining the observed optical constants of bcc.Eu has recently been carried out by Freeman et al. (1971), using the APW method. Endriz and Spicer (1970) have used these results to interpret their experimentally observed $\sigma(\omega)$ dispersion curve for Eu.

The electronic band structure of Tb has been calculated using the (RAPW) method by Jackson (1969). In addition a density of states histogram is given and the Fermi-surface is depicted. The energy bands for Tb along symmetry lines in the first Brillouin zone are similar to those calculated by the (RAPW) method for Gd but differ in details. Jackson also reports differences in the calculated band structure of Tb obtained by different workers.

Williams et al. (1966) has obtained some band structure calculations for Ho using the APW method, and Loucks (1966) has reported the Fermi-surface and electronic band structure of yttrium; although not a rare earth metal yttrium has a Fermi-surface closely resembling Gd.

Further theoretical work, including calculations for La, and other rare earth metals has been reported to be in progress (Dimmock and Freeman, 1964).

6.2.2 The optical properties of Gd and Tb

In the preceding two Sections it was shown that the structure in the $\sigma(\omega)$ dispersion curve for Gd films differs in shape and size for different workers. It was decided, therefore, to obtain $\sigma(\omega)$ dispersion curves for Gd films prepared in U.H.V. and measured in-situ and in air, in an attempt to reconcile the apparent differences. The optimized reflection techniques derived in Chapter 2 would be used to determine n and k for opaque films of Gd, with the hope that any $\sigma(\omega)$ structure missed by the techniques used previously would become visible. In addition, because previous workers have assumed that Gd evaporated onto amorphous substrates is polycrystalline, with a random orientation of crystallites, it seemed reasonable to investigate the crystallinity of such films using electron microscopyand reflection X-ray techniques.

In an attempt to interpret the resulting $\sigma(\omega)$ dispersion curve for Gd a technique was adopted whereby the product$\omega\sigma(\omega)$ is compared with a

convolved density of states histogram. Such interpretative techniques have not previously been employed for Gd. This technique is described by Endriz and Spicer (1970) and was used by them in an attempt to correlate their experimental results with existing band structure calculations. In Chapter 7 the theoretical basis of this method of interpretation is given.

Very little attempt has been made previously to investigate any magneto-optical effect in ferromagnetic Gd either in bulk or film form, and some preliminary investigations were, therefore, proposed using experimental methods developed by Krinchik (1959; 1964; 1968; 1969).

It has already been pointed out in the above Sections that no optical constants studies have been published for Tb, and it appears that no work has been published on the vacuum evaporation of Tb. It was, therefore, proposed that the following studies should be made for Tb:-

(i) To evaporate Tb in O.H.V. using (a) a heated tungsten filament and (b) an electron ring-gun evaporation system.

(ii) To study the films so produced using electron microscopy and optical reflection spectroscopy.

(iii) To study any film thickness dependence of the deduced optical constants.

It should be noted that the experimental work on Tb was stopped because of the inability of manufacturers in this country to supply fresh stocks of Tb wire when their existing stocks had run out.

6.3 The optical properties of rare earth oxides

The rare earth oxides have been isolated for some time and their chemical properties studied. There are many technologies in which rare earth oxides are important (Trifanov, 1963). However, it is

only recently that some of these oxides have been prepared in thin film form for optical applications.

Ceric oxide films have been prepared by vacuum thermal evaporation onto heated glass substrates. Such films have a rather strong temperature dependent refractive index; 2.00 at $20^{o}C$ increasing to 2.30 at $350^{o}C$, for $\lambda = 546$ nm. Ceric oxide films have, nevertheless, applications in beam splitters, multilayer filters and anti-reflection coatings, and have a transparency range from 400mμ to 16μ.

Lanthanum oxide has been evaporated from a tungsten boat onto unheated glass substrates, and the films so formed have been found to have a refractive index ranging from 1.72 to 1.75 for $\lambda = 546$nm (SIRA). The films are moderately hard (i.e. are not easily scratched under conditions of normal laboratory use), and find application in dielectric film anti-reflection coatings intended for use with visible light.

Neodymium oxide films can be prepared by thermal evaporation of the oxide from a tungsten boat, in a partial pressure of oxygen (5×10^{-4}torr). The refractive index of these films has been measured (SIRA) at $\lambda = 546$nm and found to be 1.79 ± 0.03. The films are hard with a very low absorption and find application in multilayer coatings.

Vratny (1960) has studied the normal incidence reflectance spectra of terbium oxides with chemical compositions within the range Tb_2O_3 to Tb_4O_7. He obtained the various oxides by heating Tb_4O_7 under different conditions of temperature and vacuum. The samples for reflectance studies were compressed blocks of the powdered oxide. The diffuse reflectance spectra of these oxides were measured in the wavelength range 300nm to 1500nm and an ultra-violet "cut-off" was observed at about $\lambda = 325$nm. A general decrease in reflectance was observed for an increase in the oxygen to metal ratio.

For powdered samples it is very difficult to use Kramers-Krönig analysis to deduce n and k from the normal incidence reflectance data (Johnson, 1952). However, Vratny found it possible to predict certain aspects of the k-dispersion curve.

As a result of this work it seemed reasonable to propose an experiment in which n_2 and k_2 of terbium oxide thin films is measured over a wavelength range 400-700nm, for a variety of film thicknesses. Such work would not only substantiate that of Vratny's, but would provide useful information on thin films of terbium oxide for possible application to thin film, optical devices; e.g. anti-reflection coatings, multilayer filters and beam splitters. It was proposed that the optimized, reflection ratio method of Miller and Taylor (1971) would be used to measure n_2 and k_2.

The results of this work are reported in Chapter 7.

CHAPTER 7

EXPERIMENTALLY OBSERVED OPTICAL AND MAGNETO-OPTICAL PROPERTIES OF EVAPORATED FILMS OF Ni, Gd, Tb and TERBIUM OXIDE

Abstract

This Chapter describes the results of experiments on evaporated films of Ni, Gd, Tb and terbium oxide. Multiple beam interferometry electron microscopy and X-ray reflection spectroscopy have been used to evaluate certain aspects of the growth and crystalline nature of these films. The optical constants n and k of the films have been determined for the wavelength range 400-700 nm, and the resulting $\sigma(\omega)$ dispersion curves for Gd and Tb interpreted using currently available electronic band structure calculations.

For opaque films of Gd in the ferromagnetic state, the ferromagnetic Kerr effect has been investigated and the results compared with existing low temperature optical constants studies.

At the end of this Chapter further work on the optical properties of the rare-earth metals and their oxides is suggested.

7.1 Optical properties of thin films of Ni grown in U.H.V.

In order to obtain experience with the equipment and the techniques for evaluating optical constants it was decided to prepare a number of thin partially-transmitting films of Ni. The films were prepared in the U.H.V. system described in Chapter 5, and the optical constants of these films determined using the optimized-reflection ratio method described in Chapter 3.

To prepare these films Ni wire of 99.99% purity was wound onto a previously cleaned and outgassed tungsten helical filament. The filament was then placed in the O.H.V. system and the Ni wire pre-melted

onto the filament, using the technique described in Chapter 5. The Ni-loaded filament was then mounted in position in the U.H.V. system together with a clean substrate. This substrate had the rear face ground in order to satisfy the condition that no major contribution in the light reflected from the thin film should come from the back-face of the substrate, (see Section 3.2). To facilitate measurement of the film thickness a thin glass cover-slip was sandwiched between one of the substrate holder clamps and the front face of the substrate. This provides a convenient step in the evaporated film for subsequent step height analysis using multiple-beam interferometry.

Using the methods described in Chapter 4 the vacuum system was pumped down and the filament outgassed in readiness for the film evaporation. Evaporation was carried out in the manner described in Section 5.4.2. In all of the Ni evaporations performed in the U.H.V. system base pressures were between 5×10^{-11}torr and 1×10^{-10}torr and evaporation pressures were between 5×10^{-10}torr and 8×10^{-10}torr, and subsequent film thickness measurements showed that evaporation rates were 100nm per minute or greater. Evaporation currents were between 55 and 60 amps. Assuming that residual gas molecules have a unit sticking coefficient and that the residual gas composition was similar to that shown in Table 5.3.1, then it is reasonable to assume that the rate of arrival of Ni atoms at the substrate surface during these evaporations was at least 10^4 times faster than residual gas molecules. Contamination of the film by these molecules during growth is, therefore, minimal.

Unfortunately it was necessary to leave each evaporated film in the vacuum system at the base pressure for about 4 days before commencing the optical measurements. This means that the films were being continually bombarded with residual gas molecules for this period of time. Again, assuming a unit sticking coefficient and the residual

gas composition shown in Table 5.3.1 it would be possible for about 8-10 molecular layers to build up as impurities on the film surface.

The optical constants, n_2 and k_2, for a number of visible wavelengths were measured in air for 4 films of different thicknesses. These thicknesses were, 24.5, 32.6, 44.7 and 57.0nm respectively with observed thickness variations of between $\pm$ 1.5 and $\pm$ 2.5nm. These recorded thickness variations probably include errors arising from measurement of the multiple beam fringes as well as the substrate surface imperfections, and so it is reasonable to assume that these films complied with the surface roughness criteria laid down in Section 5.1.1. The $(R_{\parallel}/R_{\perp})$ measurements were made at angles in the region of 64° and 85°, close to the optimum angles required for films with $n_2 \simeq 2$ and $k_2 \simeq 3$; the ambient temperature at the time of measurement was 294°K, and the values of $(R_{\parallel}/R_{\perp})$ were measured to an accuracy of at least $\pm$ 0.01.

Figure 7.1.1 shows curves of n_2 and k_2 plotted against film thickness for wavelengths of 402, 546 and 656nm respectively. The bulk values of Shiga and Pells (1969) are also shown for comparison, as are those obtained from thick opaque Ni films (Krause and Meyer, 1962). The n_2 and k_2 values were deduced from the experimental data using the graphical technique described in Section 3.2. Subsequent use of the more refined programme for deducing n_2 and k_2 (Section 3.3) showed that the deduced values were accurate to about $\pm$ 0.06, which is not far removed from the accuracy expected. The graphs of Figure 7.1.1 reveal that there is very little variation of n_2 and k_2 with film thickness for the ranges of wavelength and thickness considered. This seems to be in accordance with some recent results for Ni (Nag and Ward, 1971), for near infra-red wavelengths.

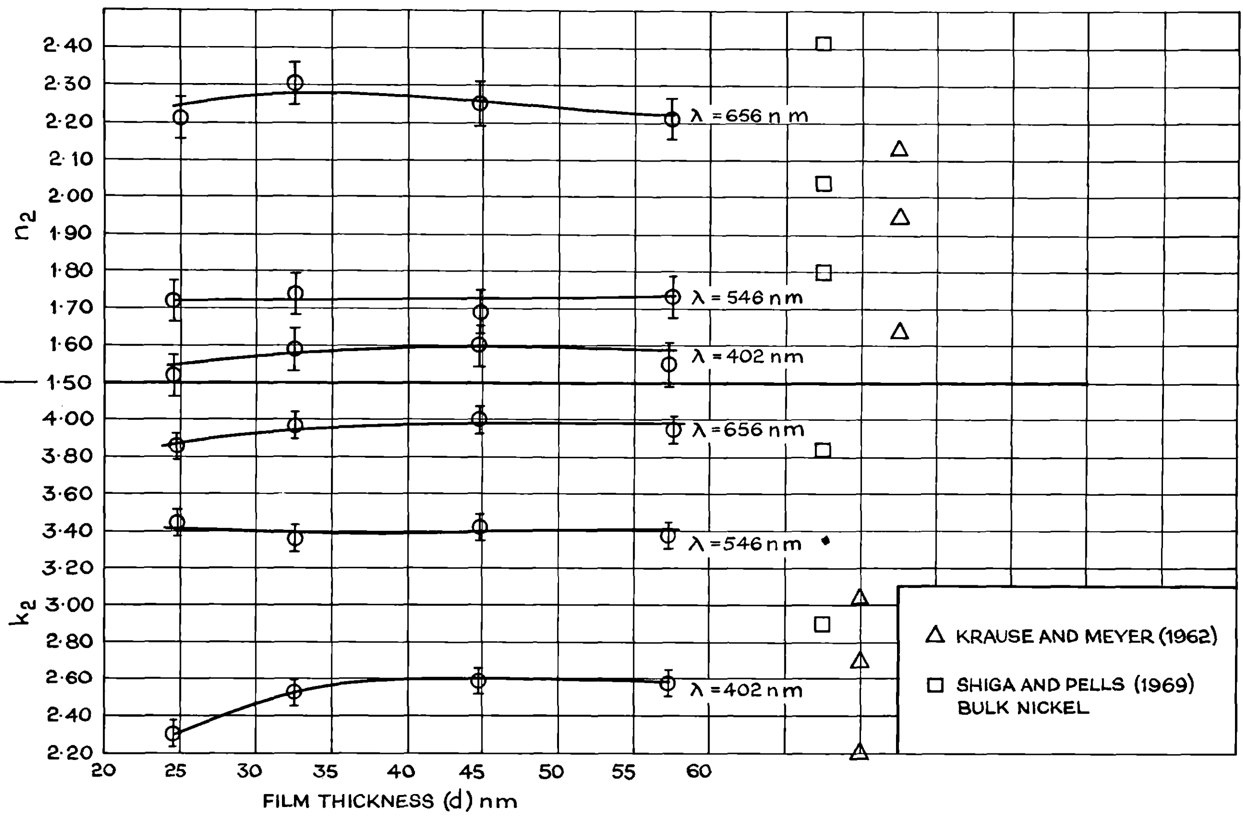

Figure 7.1.1 Thickness dependence of n_2 and k_2 for thin nickel films grown in U.H.V. and measured in air.

7.2 Optical and structural properties of opaque films of Gd grown in U.H.V.

The purpose of this study was to prepare opaque films of Gd by evaporation in the U.H.V. system, and to transfer the films to the optical cell (Section 4.2.4) so that reflection measurements could be obtained with the film in the paramagnetic and ferromagnetic states.

The gadolinium used for evaporation was 99.9% purity wire of 1mm diameter supplied by 'Koch-Light Laboratories' and 'Rare Earth Products Ltd.'. For each evaporation a tungsten helical filament was loaded with Gd and outgassed in the O.H.V. system using the same technique as for Tb wire, (see Section 5.2.1). The loaded filament was inserted in the appropriate port in the U.H.V. system, together with the clean substrate and cover slip and the normal pump down procedure used to evacuate the system to the base pressure of 2 x 10^{-10}torr or better. Before evaporation the filament was outgassed to about 1 x 10^{-9}torr, and the pressure allowed to stabilize in the 10^{-10}torr pressure range before commencing the evaporation. Evaporation of the Gd was carried out in the manner described in Section 5.4.2. Pressures during evaporation of the films were between 2-6 x 10^{-9}torr, and evaporation rates were 100nm per minute or greater. Assuming the Gd atoms and the residual gas molecules to have unit sticking coefficients, then the above evaporation rates and pressures imply that the Gd atoms were arriving at the substrate surface at least 2000 times faster than the residual gas molecules. It is important when evaporating reactive materials such as Gd that the base pressure is reached quickly after the evaporation has ceased. In the case of the Gd evaporations in this system base pressures were achieved within 1 minute of the evaporation ending.

In-situ reflection measurements of each film were commenced 3-5 hours later. During this time period the film could accumulate only a

fraction of a monolayer of residual gas impurity on the surface. Films were kept in the U.H.V. system at pressures below 5 x 10^{-10} torr for periods of up to 48 hours before being transferred to the optical cell. From the residual gas analysis shown in Table 5.3.1 and assuming a unit sticking coefficient, the Gd films could not have accumulated more than 8-10 molecular layers of residual gas atoms during such time periods. It is, therefore, probably safe to assume for the purposes of reflection measurements that, the film surfaces before leaving the U.H.V. system consisted mainly of Gd atoms.

In order to investigate the surface state and crystalline structure of the evaporated films on removal from the U.H.V. system, scanning electron microscopy and X-ray reflection studies were made at the Fulmer Institute. This necessitated transporting the films in an evacuated desiccator to the Institute's laboratories. The films were not stripped from the glass substrates, and two types of film were studied: (a) a film which had been evaporated and stored in the U.H.V. system at room temperature for about 48 hours, (b) a film which had been evaporated and subsequently baked in the U.H.V. system for about 3 hours at a temperature of 150°C and a pressure of about 5 x 10^{-8} torr. The scanning electron microscopy studies were commenced about 2 days after removal of the films from the U.H.V. system and the X-ray reflection data obtained some 3 days later. Both films were estimated, from previous evaporation times to be 120nm thick. Scanning electron microscope photographs of the surface of the films (a) and (b) are shown in Figures 7.2.1a and 7.2.2b respectively. These photographs reveal the following features:

(i) There is no significant detail on the surface of either film.

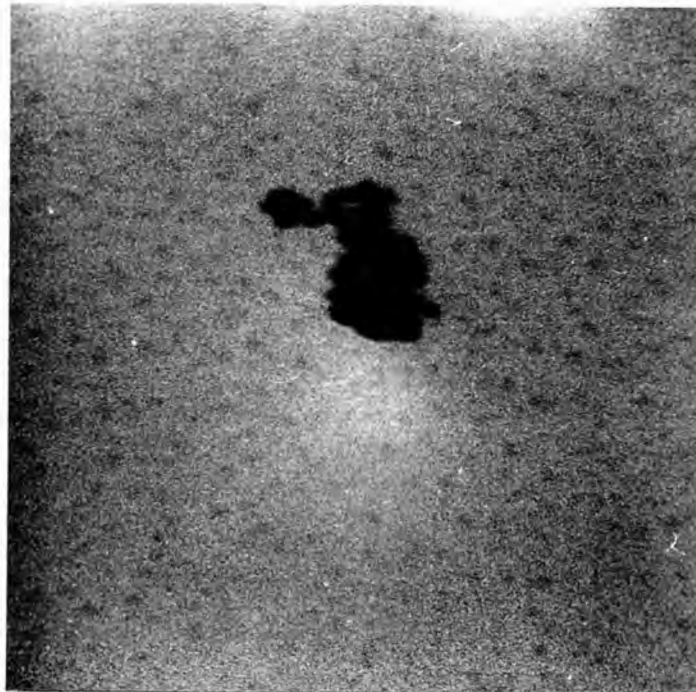

Figure 7.2.1a Scanning electron microscope photograph of a Gd film on a glass substrate. Film thickness 120 nm.

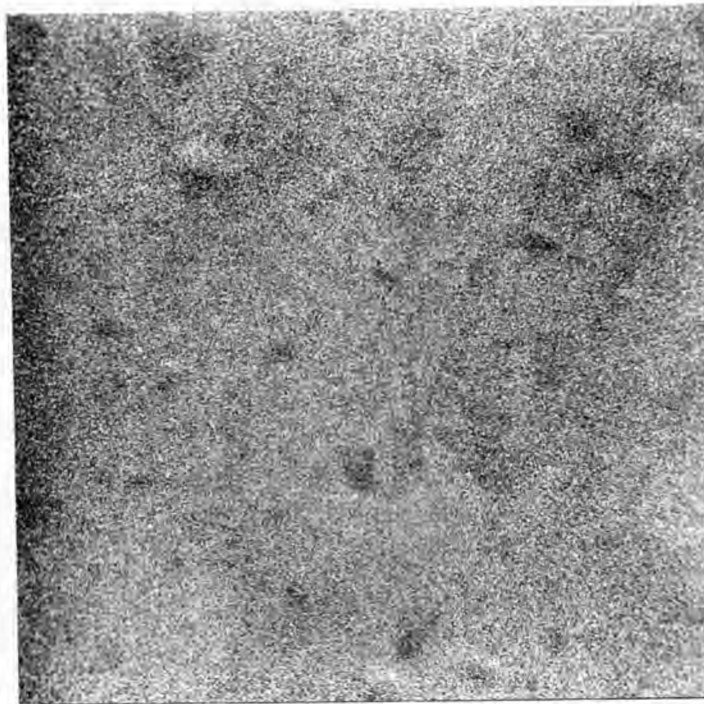

Figure 7.2.2b Scanning electron microscope photograph of a Gd film on a glass substrate.
Heat treated after evaporation for 3 hours at 150°C and at 5×10^{-8} torr.

(ii) One or two minor tears in the films are apparent; these were probably caused by subsequent handling. These tears are the very dark areas in the photographs.

(iii) It was, in fact, found possible to detect some topographic differences between the two films by focussing on the tears in the film surface. Film (a), which had not been heat-treated, shows fine blisters spread uniformly over the film surface. Film (b) which had been heat-treated in the manner described above exhibits a smaller number of considerably larger blisters. It is difficult to obtain from these photographs a measurement of the height of these blisters.

The origin of these film blisters is difficult to explain. Surface blister growth has been observed by Lahiri and Wells (1969) in lead films deposited onto glass substrates. For the lead films it was found that the blisters grew in size as the temperature of the film and substrate was increased, and subsequently shrank again as the temperature decreased: that is, the blister growth was reversible. The explanation given was that blister formation was favoured by compressive stress and the reversal of the growth process was favoured by a change from compressive into tensile stress. It seems reasonable to assume that a blister is a part of the film which has become detached from the substrate surface.

In the present case a plausible explanation of blister growth in the two types of Gd film (a) and (b) can be given. At the time of deposition of the film, the film surface and substrate are both receiving radiation from the evaporation filament. Thus both film and substrate will increase in temperature, the film probably more than the substrate. This fact is vindicated by an experiment which was performed in the O.H.V. system. It was shown that, for the evaporation times used

in preparing the Gd films in U.H.V., the substrate surface temperature could rise to between 40°C and 60°C. The temperature of the film would probably be higher than this. Consequently during the growth process of a Gd film in the U.H.V. system, the film expands more than the substrate and so will be in a compressive stress, thus favouring the formation of surface blisters. After the evaporation has ceased the film and substrate cool, thereby causing a reduction in compressive stress and hence a reduction in the size of the surface blisters. The surface of film (a) would, therefore, be expected to show a large number of small blisters.

Presumably, the surface of film (b) before heat treatment resembled that of film (a). Heat treatment at 150°C would increase the compressive stress in the film, and hence the formation of larger surface blisters, which would arise from the smaller ones linking together. Subsequent cooling would reduce the compressive stress and hence the size of the blisters. The surface of film (b) would, therefore, be expected to contain a smaller number of larger blisters than that of film (a).

X-ray reflection diffraction from the two Gd films (a) and (b) was also obtained. Unfortunately the results gave only a fairly qualitative idea of the crystal structure of the two films. Glancing angle X-ray photographs were taken with Co-Kα radiation from each film. Both films produced weak diffraction patterns showing arced diffractions from a highly textured deposit. All the diffraction arcs from both films could be explained by the h.c.p. structure of Gd metal with a c/a ratio of 1.590. No significant differences could be detected between the diffraction patterns from the two films. It was not possible to make

any detailed measurement of grain size or strain within the films from the X-ray pictures because of the inherent poor quality of the diffraction patterns. However, the observed diffraction patterns were neither unduly broadened (a characteristic of very small crystallites) nor spotty (a characteristic of well oriented films with large crystallites), and from this observation it was estimated that the film grain size was greater than 25nm in a direction perpendicular to the plane of the film and less than 10.5nm in the film plane. It was further found that both films consisted of two crystalline components, one with a (0001) crystallographic plane parallel to the surface and the other with a $(10\bar{1}1)$ crystallographic plane approximately parallel to the surface. A qualitative estimation of the relative intensities of the diffraction arcs showed that the volume of material having the first texture was greater than that having the second.

From these two studies it was possible to make some conclusions about the growth of Gd films on glass substrates at room temperature in the present U.H.V. system. These conclusions are listed below:-

(i) The film surface is not ideally flat: there is certainly some degree of surface roughness. The effect of surface roughness on optical constants determinations has already been discussed in Section 5.1.1.

(ii) Annealing of the evaporated film and substrate at 150°C produces a more uniformly flat surface with only a small number of rough features.

(iii) Evaporation of Gd from a tungsten filament at evaporation rates of 100nm per minute produces films on glass substrates which have a preferred orientation with the c-axis [0001] of the h.c.p. crystallites perpendicular to the plane of the film or nearly so.

There appears to be no evidence for assuming that such films will have a random orientation of crystallites, contrary to the assumptions of Hodgson and Cleyet (1969).

7.2.1 The optical constants of Gd in the paramagnetic state

The Curie temperature of Gd has been variously reported to be in the range 273°K to 289°K. For the purposes of this thesis the evaporated films of Gd are assumed to have a Curie temperature of 289°K. The optical constants of Gd films at room temperature (294-296°K) were, therefore, taken to represent the optical constants of Gd in the paramagnetic state.

The optical constants n and k of Gd films prepared in the manner described in Chapter 5 and in the present Section, were determined using the $(R_{//}, R_{\perp})$ method described in Chapter 2. The reflectometer and the optical cell (Chapter 4) were used to measure $R_{//}$ and $R_{\perp}$ close to the optimum angle of 74°. Optical constants n and k were calculated using Querry's (1969) analytical method, and the errors were estimated using the results obtained in Chapter 2. Film thicknesses were determined after completion of the reflection measurements, using multiple beam interferometry. All the films investigated had a thickness greater than 100nm.

Before commencing any measurements with the optical cell it was necessary to ascertain the errors introduced in $R_{//}$ and $R_{\perp}$ brought about by light passing through the cell walls. It was first necessary to determine the change, if any, in the polarization azimuth for light passing through the cell polarized perpendicular and parallel to the plane of incidence. To do this the telescope arm of the reflectometer was set at 180° to the incident light beam, and an analyzer fitted to

the telescope and crossed with the polarizer. The signal from the photomultiplier was monitored by a d.c. milli-voltmeter, and it was possible to detect changes in the polarization azimuth of 0.2^{o}. The cell was then interposed in the light beam and the collimator stop aperture reduced to limit the size of the beam passing through the cell. The analyzer was then rotated to achieve a minimum photomultiplier signal. This procedure was repeated for a number of wavelengths in the visible region. For the wavelengths investigated there was no difference, to within $\pm 0.2^{o}$, in the analyzer setting with or without the cell in place. It was, therefore, concluded that the transparent wall of the cell did not change the polarization azimuth by more than $\pm 0.2^{o}$. In order to calibrate the cell with respect to Gd the following procedure was adopted. A freshly prepared Gd film was placed in position in the cell and the cell evacuated in the manner described in Chapter 4. Reflection coefficients $R_{\parallel}$ and $R_{\perp}$ were determined for a number of wavelengths at an angle of incidence of 73° 45'. Every effort was made to pass the light through the same parts of the cell for each determination of $R_{\parallel}$ and $R_{\perp}$. Air was then slowly admitted into the cell and the transparent cell wall removed. Measurements of $R_{\parallel}$ and $R_{\perp}$ were repeated as quickly as possible in order to minimize any effects due to film surface changes. A number of such calibrations were made and it was found that the results did not differ by more than the estimated experimental error ($\pm$ 0.006) for $R_{\parallel}$ and $R_{\perp}$. Table 7.2.1 shows values of $R_{\parallel}$ and $R_{\perp}$ obtained with and without the cell for a Gd film 105.3nm thick. From a table such as this corrected values of $R_{\parallel}$ and $R_{\perp}$ could be obtained for subsequent use in deducing n and k.

To illustrate the experimental results the optical constants n and k of a Gd film of thickness 209.7nm are given in Table 7.2.2 for a

Table 7.2.1 Values of R_{11} and $R_{\perp}$ obtained with and without the cell for a Gd film 105.3nm thick. $\theta = 73.75^{\circ}$

Wavelength λ nm.	With cell $R_{\parallel}$	With cell $R_{\perp}$	Without cell $R_{\parallel}$	Without cell $R_{\perp}$	Correction for cell $\%R_{\parallel}$	Correction for cell $\%R_{\perp}$
402	0.245	0.620	0.273	0.688	+11.0	+11.2
430	0.257	0.669	0.285	0.743	+10.8	+11.0
463	0.248	0.701	0.275	0.777	+10.7	+10.9
495	0.253	0.717	0.280	0.794	+10.6	+10.7
528	0.256	0.742	0.283	0.822	+10.5	+10.7
559	0.253	0.736	0.279	0.814	+10.4	+10.6
589	0.249	0.760	0.275	0.842	+10.5	+10.8
619	0.248	0.770	0.274	0.852	+10.6	+10.6
652	0.247	0.779	0.273	0.863	+10.5	+10.7
669	0.244	0.774	0.270	0.858	+10.5	+10.9
687	0.239	0.765	0.263	0.850	+10.1	+11.1

This table should follow p189.

Table 7.2.2 n and k values typical of Gd films grown in the U.H.V. system. Thickness 209.7 nm

nm	n	k
402	1.18	1.78
415	1.17	1.89
430	1.14	1.87
446	1.19	1.95
463	1.31	2.07
479	1.37	2.16
495	1.41	2.17
511	1.42	2.25
528	1.52	2.42
543	1.54	2.42
559	1.57	2.44
574	1.66	2.53
589	1.67	2.60
604	1.69	2.55
619	1.74	2.64
635	1.71	2.60
652	1.76	2.74
669	1.80	2.67
687	1.88	2.80

number of wavelengths in the range 400-700nm. Curves of ϵ_1, ϵ_2 and $\sigma(\omega)$ resulting from this data were plotted against photon energy, and are shown in Figures 7.2.1 and 7.2.2. The reflection coefficients $R_{\parallel}$ and $R_{\perp}$ were each measured to an accuracy of at least $\pm$ 0.006, giving rise to errors in ϵ_2 and $\sigma(\omega)$ of approximately $\pm$ 6-10%, (Miller, Julien and Taylor, 1971). The error in ϵ_1 will, as a result, be about $\pm$ 20%. Figure 7.2.2(a) shows the observed $\sigma(\omega)$ dispersion curves for 3 Gd films having thicknesses in the range 100-200nm. The absolute values of $\sigma(\omega)$ vary by 15-20% from film to film, and this was found to be the variation between other Gd films grown under similar vacuum environments to that shown in Figure 7.2.2(a). Furthermore, this Figure shows that the shapes of the $\sigma(\omega)$ dispersion curves are essentially the same; all show a main peak centred at about 1.8eV, decreasing $\sigma(\omega)$ values with increase in photon energy, and some minor structure in the energy range 2.35-2.7eV. The curves of Figure 7.2.2(a) also show a dependence with evaporation pressure and/or the time period spent in the U.H.V. system prior to commencement of the reflection measurements. The bottom $\sigma(\omega)$ curve which is also plotted in Figure 7.2.2, generally resembles the observed $\sigma(\omega)$ dispersion curves for Gd obtained by Hodgson and Cleyet (1969) and Schüler (1966).

If the $\sigma(\omega)$ dispersion curve (Figure 7.2.2) is compared with that of Hodgson and Cleyet (1969) it will be seen that the present $\sigma(\omega)$ values are between 30-40% lower, and the overall variation is considerably greater. Furthermore, Figure 7.2.2 shows a piece of structure in the $\sigma(\omega)$ curve occurring between 2.35 and 2.65eV, and this seems to be more pronounced than a broad shallow peak occurring between 2.2 and 2.6eV. in the $\sigma(\omega)$ curve reported by Hodgson and Cleyet. The shape of the ϵ_1 curve of Figure 7.2.1 closely resembles the

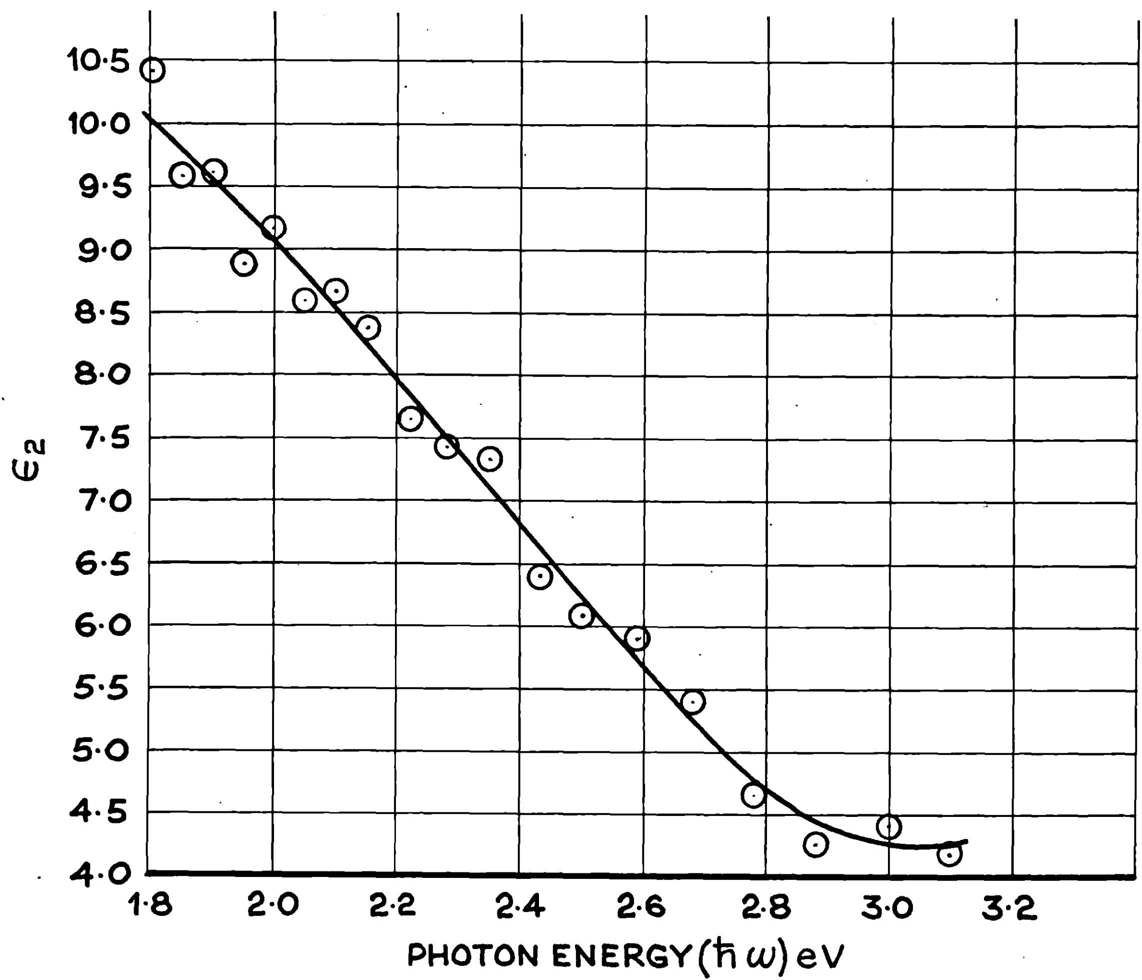

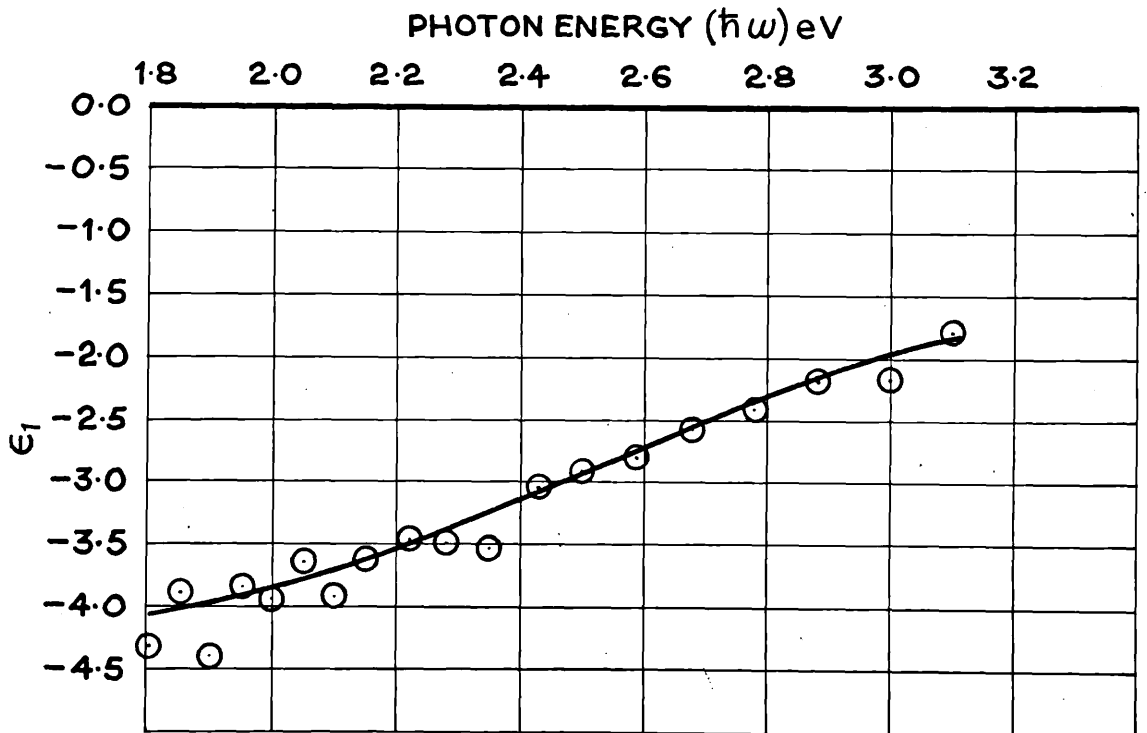

Figure 7.2.1 Optical constants ϵ_1 and ϵ_2 observed for a Gd film. Temperature 295°K.

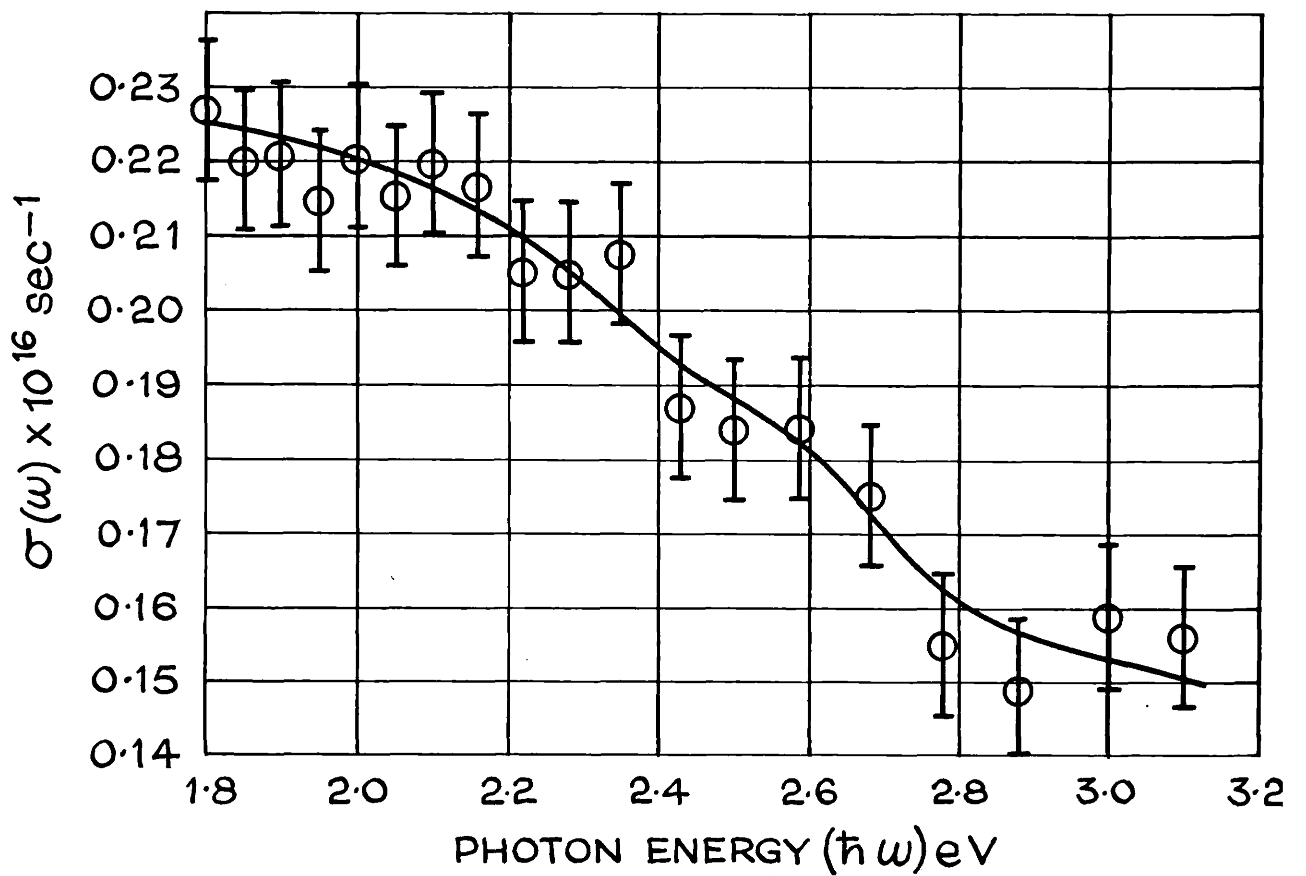

Figure 7.2.2 Optical constant $\sigma(\omega)$ observed for Gd film. Temperature 295°K.

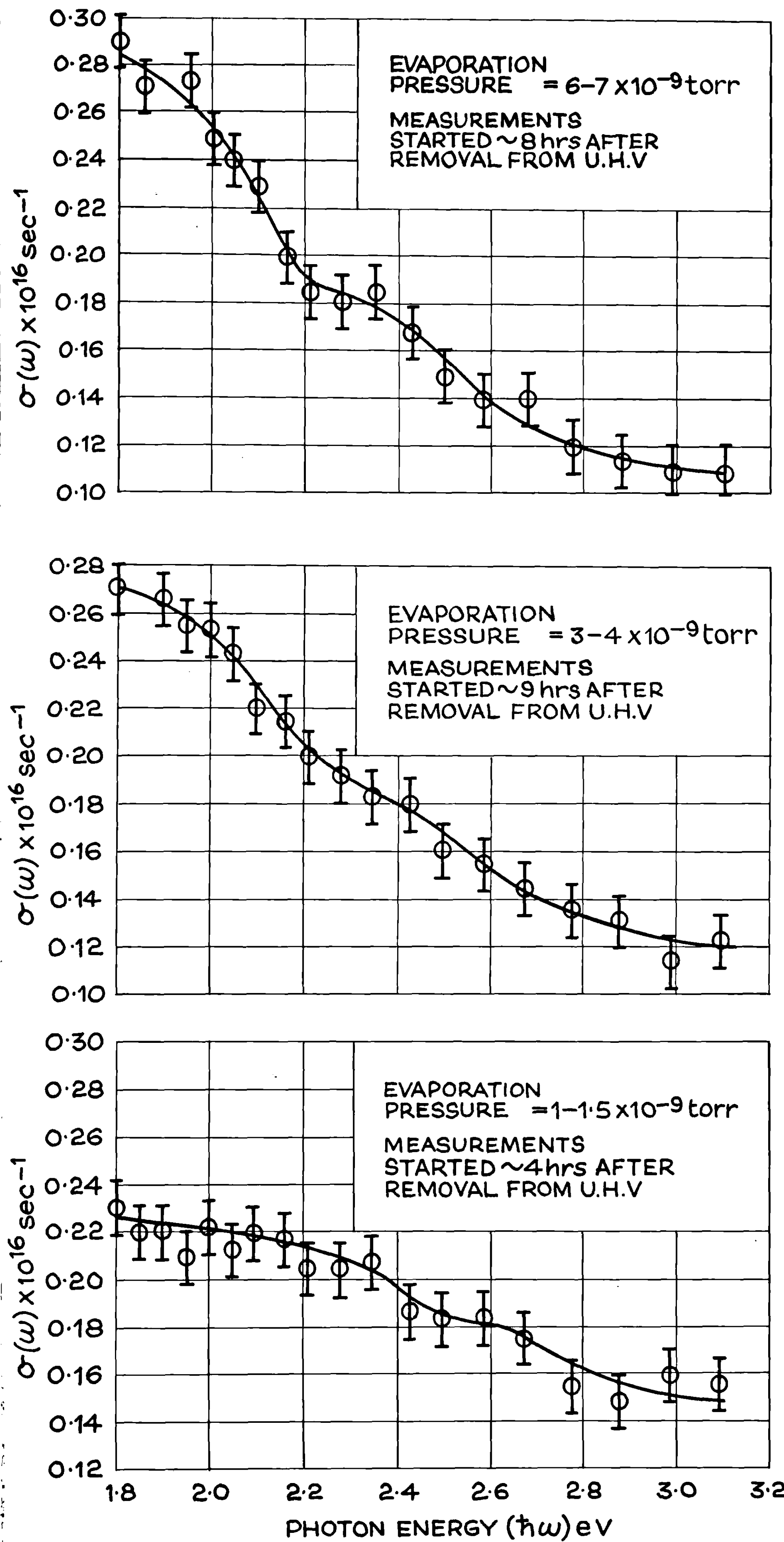

Figure 7.2.2(a) Optical constant $\sigma(\omega)$ observed for 3 Gd films, grown in the U.H.V. system and measured in the optical cell. Temperature 295-297°K.

corresponding portion of Hodgson and Cleyet's curve, and the absolute values are very nearly the same. Over the energy range 2.0-3.0ev. the $\sigma(\omega)$ curve of Schüler (1966) for Gd shows two shallow, but distinct peaks at 2.2 and 2.8eV.

Some preliminary <u>in-situ</u> U.H.V. measurements (Julien, 1971) on the Gd films used in this work produced values of $\sigma(\omega)$ some 15% larger than those shown in Figure 7.2.2, in fact, very close to, and showing about the same overall variation as those of Hodgson and Cleyet (1969). Julien's results appear to imply two pieces of significant structure in the $\sigma(\omega)$ curve centred around 2.2 and 2.55eV. This latter piece of structure appears to confirm that occurring between 2.35 and 2.65eV, shown in Figure 7.2.2. Julien has found a variation of the absolute values of $\sigma(\omega)$ from film to film similar to that reported above.

According to the X-ray data obtained from Gd films grown in the U.H.V. system, it seems certain that the observed optical constants ϵ_1, ϵ_2 and $\sigma(\omega)$ are for Gd crystallites having basal planes perpendicular (or very nearly so) to the plane of incidence of the reflectometer. In the h.c.p. system the basal plane is defined by the 'a' and 'b' crystal axes. Drude (1888) has shown that for a single crystal orientated with the 'a' and 'b' axes perpendicular to the plane of incidence, the reflection coefficients can be expressed as follows:-

$$R_{\perp} = f_1(\theta, \hat{\epsilon}_b) \qquad 7.2.1$$

$$R_{//} = f_2(\theta, \hat{\epsilon}_a, \hat{\epsilon}_c) \qquad 7.2.2$$

Making the assumption that $/\hat{\epsilon}_c/ \gg 1$, equation 7.2.2 becomes,

$$R_{//} = f_2(\theta, \hat{\epsilon}_a) \qquad 7.2.3$$

By making measurements of only $R_{//}$ and $R_{\perp}$ at one angle of incidence it is impossible to determine the absolute values of $\hat{\epsilon}_b$ and $\hat{\epsilon}_a$. However, for Gd there is evidence (Taylor, 1970) that the anisotropy of physical

quantities (e.g. Hall effect, resistivity) in the basal plane is small and, therefore, it is reasonable to put $\hat{\epsilon}_a = \hat{\epsilon}_b$ so that measurements of $R_{//}$ and $R_{\perp}$ at one angle θ will yield $\hat{\epsilon}_a$. Hence, the n and k values shown in Table 7.2.2 and the dispersion curves of Figures 7.2.1, 7.2.2 and 7.2.2a, refer to the basal plane only. Considering the evaporation rates used by Hodgson and Cleyet (200nm per sec. compared with 2 nm per sec. for the present work) it is not surprising that there are differences in the values of $\sigma(\omega)$. With such high evaporation rates the Gd films grown by Hodgson and Cleyet would almost certainly have been polycrystalline with a random orientation of crystallites, in fact as they assumed. Thus their $\sigma(\omega)$ values would be an average over all crystal directions. It can be expected in Gd that there will be a large anisotropy of optical constants between the c-axis and the basal plane, so that interpretation of $\sigma(\omega)$ dispersion curves for polycrystalline material is difficult.

Since Gd is known to be chemically active, it was of interest to see by how much the $\sigma(\omega)$ dispersion curve was distorted for a Gd film exposed to the atmosphere for a period of time. Figure 7.2.3 shows two $\sigma(\omega)$ dispersion curves; one was obtained for a Gd film 4 hours after removing it from the U.H.V. system and the other was obtained for the same film after 50 hours exposure to the atmosphere (temperature 297°K, humidity 50-55%). The $\sigma(\omega)$ values shown are accurate to better than $\pm$ 10%. The shapes of the two curves are similar for photon energies above 2.0eV, and both follow closely that shown in Figure 7.2.2. High energy structure, which in this film occurs in the energy range 2.55-2.75eV, is almost absent in the $\sigma(\omega)$ results for the exposed film. For energies below 2.0eV the two curves of Figure 7.2.3 diverge considerably; the $\sigma(\omega)$ values for the exposed film are considerably

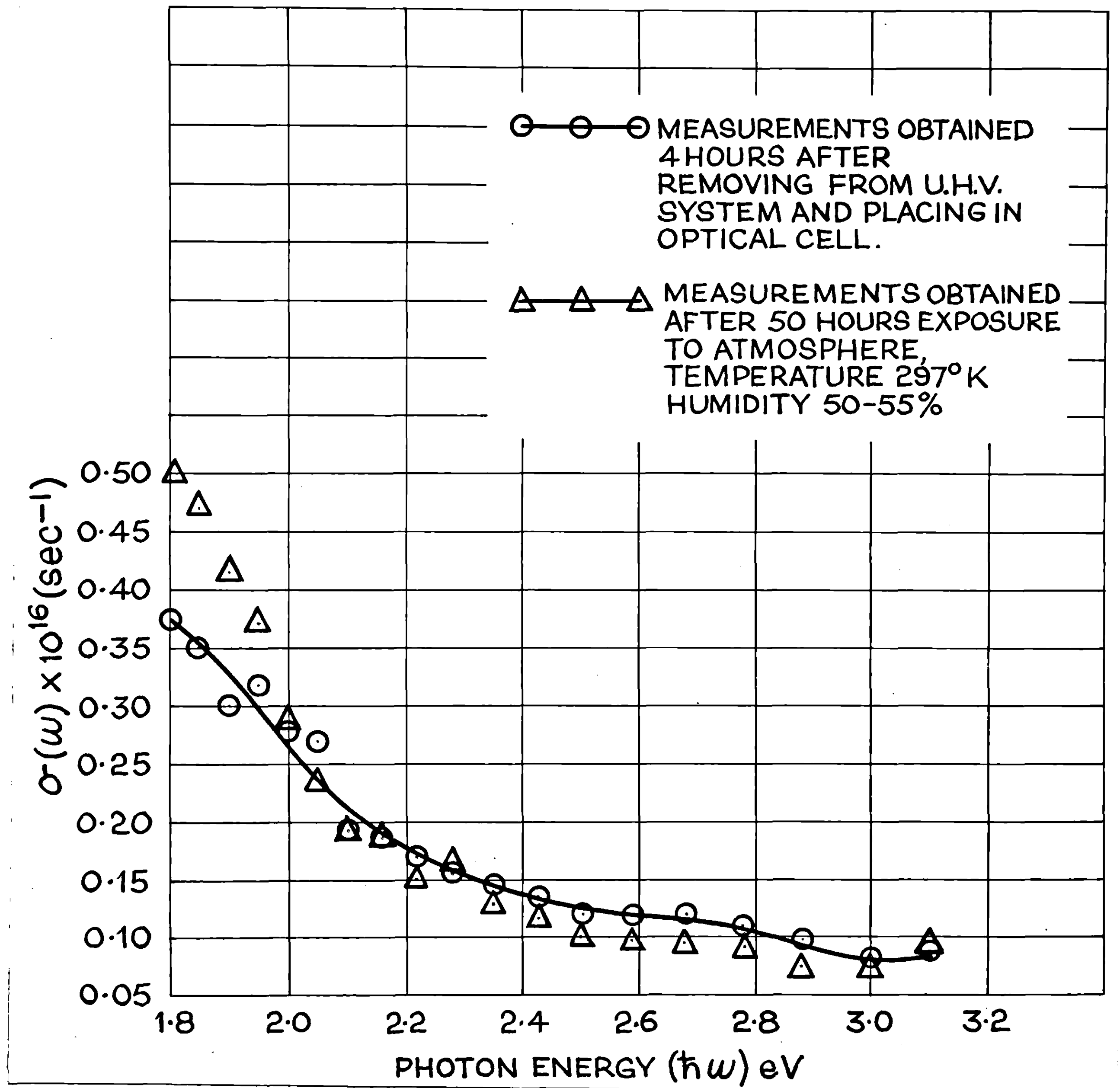

Figure 7.2.3 Optical constant $\sigma(\omega)$ observed for Gd film to show the effects of exposure to atmosphere. Temperature 295°K. to 297°K.

larger than those for the unexposed film. One can conclude, therefore, that exposure of Gd films to the atmosphere for some hours will produce significant changes in the observed optical constants, especially for photon energies below about 2.0eV: distortion and masking of significant $\sigma(\omega)$ structure also results.

Some interpretation of the observed optical properties of paramagnetic films of Gd will now be given: Schüler (1966) and Hodgson and Cleyet (1969) used (APW) band structure calculations in an attempt to interpret their $\sigma(\omega)$ dispersion curves. Cornwall (1965) has calculated the selection rules for allowed, direct transitions between symmetry points in the first Brillouin zone, for the h.c.p. crystal structure. These selection rules were used with the calculated energy bands for Gd (Dimmock and Freeman, 1964) to find the energies associated with possible interband transitions along symmetry lines in the first Brillouin zone. By considering these transitions alone, it is found that many occur in the photon energy range 1.8 to 3.1eV, and these account qualitatively for the general shape of the observed $\sigma(\omega)$ curve. Because the results reported for Gd in this Chapter are for films with a preferred orientation the effect of some of the allowed transitions will be small, because of the symmetry considerations. From a table of possible interband transition energies (Schüler, 1966) it seems likely, therefore, that the shallow peak observed in the $\sigma(\omega)$ curve (see Figures 7.2.2 and 7.2.3) at photon energies between 2.35 and 2.65 $\pm$ 0.1eV. could well be due to transitions along the Γ and A symmetry directions. These transitions have associated energies of 2.8eV.

Any comparison of experimental data with band structure plotted along symmetry lines is obscured by the inability to account for volume effects in the Brillouin zone, that is, direct transitions may occur

within the body of the zone itself. Another method of comparing band calculation and optical constants may be obtained by utilizing the density-of-states calculation for the material of interest. This has been done with some success for b.c.c. europium (Endriz and Spicer, 1970). The basis of the method is the so-called non-direct transition model (Berglund and Spicer, 1964a,b). A non-direct transition is one in which the wave vector $\underline{k}$ is not an important selection rule; for direct transitions $\underline{k}$ must be conserved. In the non-direct transition model the optical matrix elements between all filled states and all empty states of a material are assumed constant so that the product $\omega\sigma(\omega)$ is proportional to the convolution of the filled and empty density of states. This is simply,

$$\omega\sigma(\omega) \propto \int_{E_F}^{E_F+\hbar\omega} N_c(E) N_v(E-\hbar\omega) dE \qquad 7.2.4$$

where N_c denotes the number of states above the Fermi level, i.e. in the conduction band, and N_v denotes the number of states below the Fermi level, i.e. in the valence band. Although the non-direct transition model ignores the $\underline{k}$-conservation selection rule, this assumption may well be justified in a material such as Gd which has strong d band mixing (Dimmock et al., 1966).

In Figure 7.2.4, the convolution of the filled and empty densities of states, calculated using a simple computer programme based on equation 7.2.4 from the density of states histogram given by Keeton and Loucks (1968), is plotted against photon energy ($\hbar\omega$). Also included in the figure for comparison is an experimental plot of $\omega\sigma(\omega)$ against $\hbar\omega$ for the Gd film used for Figure 7.2.2. From the $\sigma(\omega)$ curve of Hodgson and Cleyet (1969) the products $\omega\sigma(\omega)$ were calculated and are also

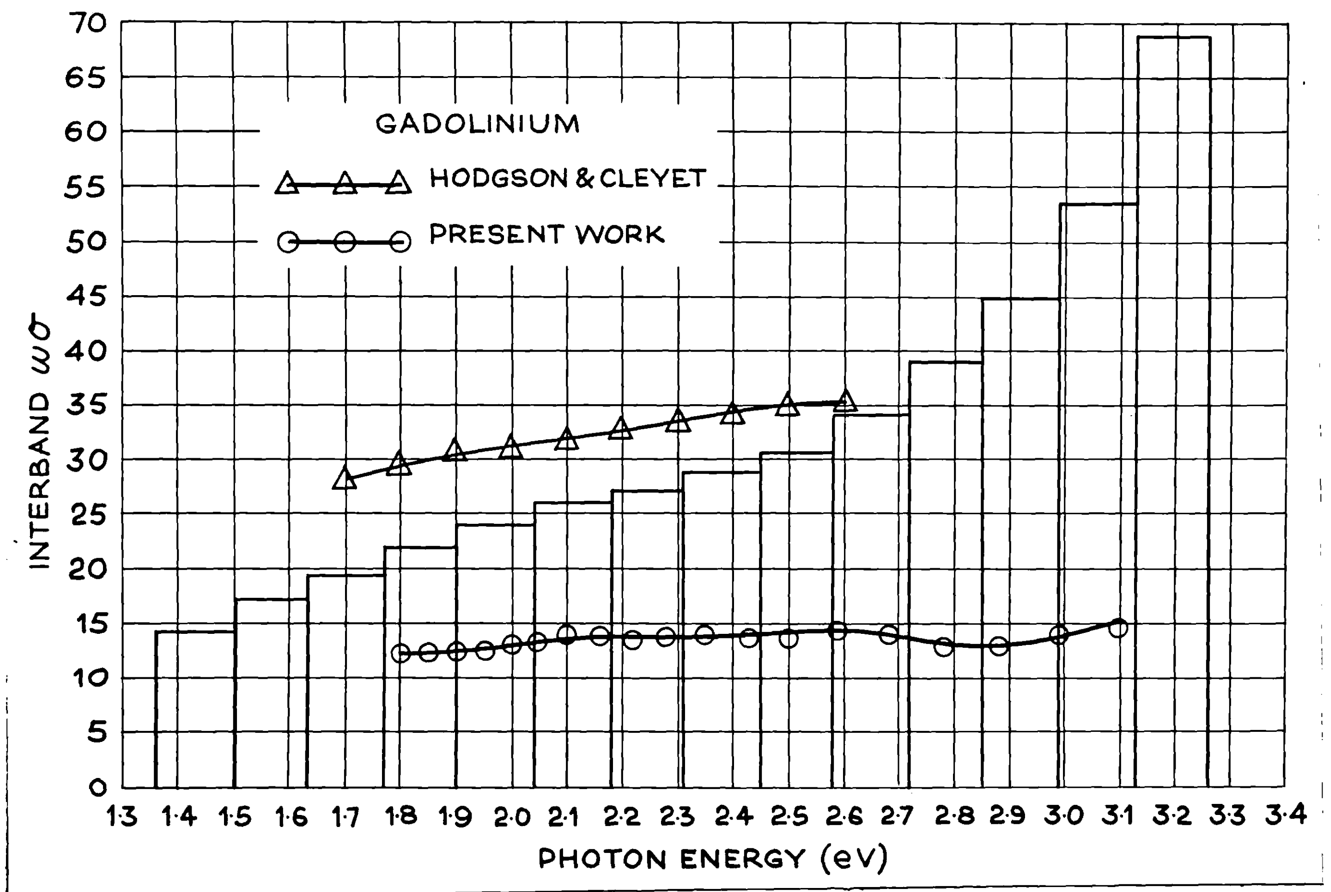

Figure 7.2.4 Calculated histogram of interband $\omega\sigma(\omega)$ against photon energy with experimental curves shown for comparison.

plotted in Figure 7.2.4. The convolved density of states and the $\omega\sigma(\omega)$ products are of an arbitrary scale so that quantitative comparison of ordinates should not be made. Both experimental curves seem to follow the convolved density of states histogram up to about 2.7eV. However, this ceases to be for higher energies. The piece of structure between 2.35 and 2.65eV. in the present experimental curve does not seem to be present in the convolved histogram. It is difficult to say whether or not the present experimental curve would eventually follow the histogram if more observations were made at higher photon energies.

Blodgett et al. (p.251, 1966) have expressed the opinion that non-direct transitions dominate the optical transitions in Gd. From Figure 7.2.4 this would appear to be so for photon energies 1.7 to 2.7eV, but may well be doubtful for higher energies, and non-direct transitions do not appear to explain the $\sigma(\omega)$ structure between 2.35 and 2.65eV. It would appear, therefore, that the main $\sigma(\omega)$ peak observed for Gd is due to a mixture of transitions; direct and non-direct. Any secondary structure observed is almost certainly due to direct transitions.

7.2.2 Some low temperature optical measurements

Measurements of $R_{//}$ and $R_{\perp}$ were obtained for Gd films within the cell at temperatures below the Curie point of 289°K, that is for films in the ferromagnetic state. The cell and its use for low temperature measurements has been described in Chapter 4. The film temperature during the course of measurement varied, typically between 155°K and 170°K. This variation was caused essentially by the rapidly changing level of the liquid nitrogen in the dewar. Lower temperatures than those stated above were achieved but then it was difficult to maintain the film temperature stable, during the course of measurement, to better than about ± 15°K. In order to prevent the glass wall of the cell from

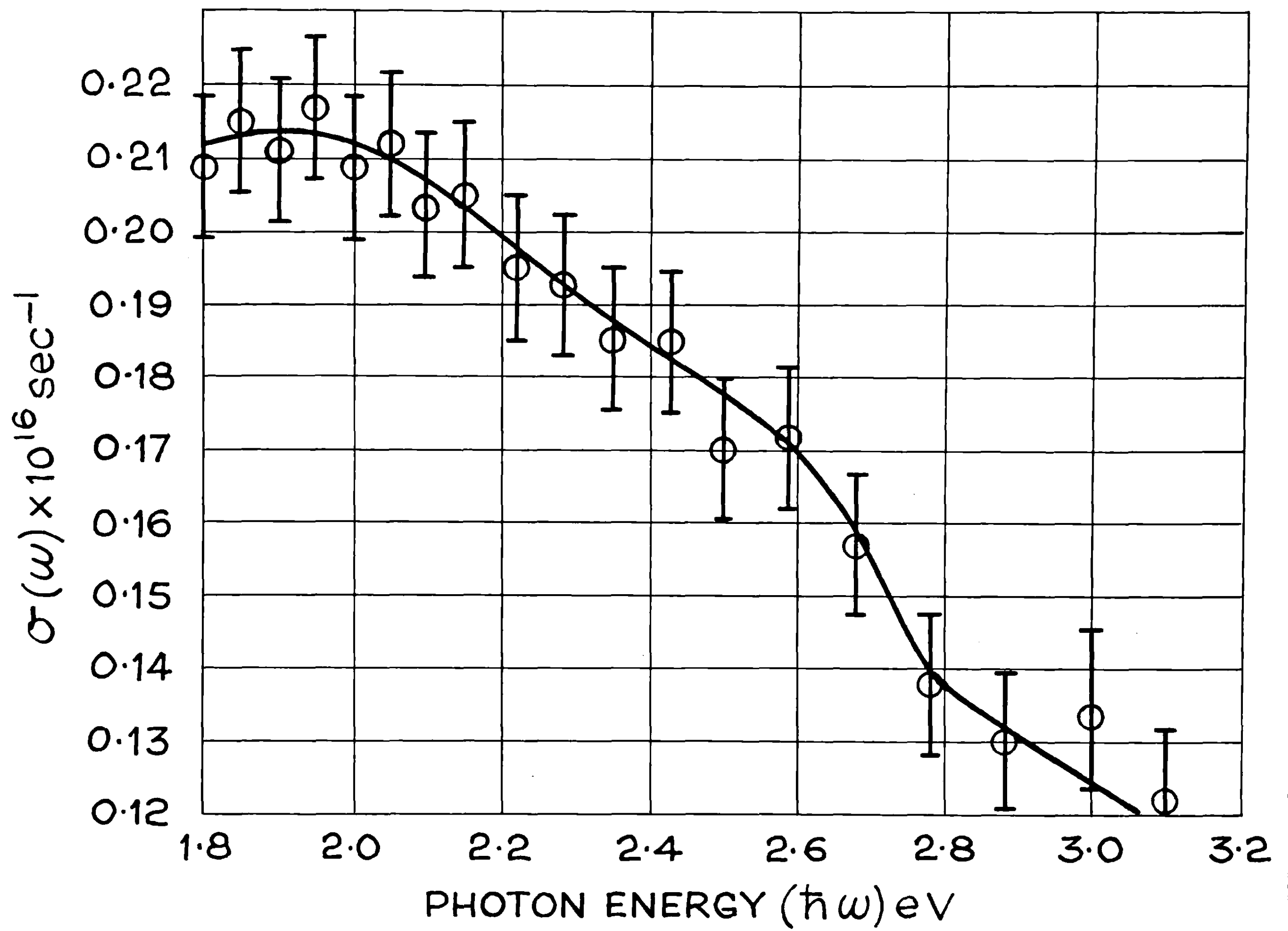

Figure 7.2.5 Optical constant $\sigma(\omega)$ observed for Gd film. Temperature 158-167°K.

"misting up", warm air from a hair dryer was occasionally played onto the cell. Optical constants n, k, and $\sigma(\omega)$ were obtained for wavelengths in the range 400-700nm, using the ($R_{//}$, $R_{\perp}$) method and Querry's analysis.

Figure 7.2.5 shows the observed optical constant $\sigma(\omega)$ plotted against photon energy for a Gd film of thickness greater than 100nm, for a film temperature which varied from 158°K to 167°K during the course of measurement. The reflection measurements obtained at 73.75^{O} were accurate to $\pm$ 0.006 or better, and this gives an error in the observed $\sigma(\omega)$ values of between 6% and 10%. Comparing the low temperature curve with that for 295°K (Figure 7.2.2) shows that, at lower temperatures the main peak has sharpened somewhat and the maximum has shifted from beyond 1.8eV. to about 1.9eV. Hodgson and Cleyet (1969) observed a maximum in the main peak at about 1.8eV for a Gd film at a temperature of 105°K. The $\sigma(\omega)$ structure occurring between 2.35eV. and 2.65eV. in the room temperature curve (Figure 7.2.2) appears to be present in the low temperature curve (Figure 7.2.5), and there appears to be no significant change in shape or position with respect to photon energy. It is difficult to tell what effect lowering the film temperature has on the crystal strucutre or the surface state of the film and it is assumed, therefore, that the $\sigma(\omega)$ curve of Figure 7.2.5 is that of a Gd film having the same crystal structure and surface conditions as one at room temperature. The observed low temperature $\sigma(\omega)$ curves for Gd appear to show no new structure in the ferromagnetic state, which is in agreement with the low temperature curves of Hodgson and Cleyet which shows new $\sigma(\omega)$ peaks occurring at 0.7eV. and 1.1eV. only. Both these peaks are caused by ferromagnetism, and while the peak at 0.7eV. can be satisfactorily explained, that at 1.1eV. has not yet received any theoretical verification.

7.2.3 Some magneto-optical measurements on Gd films

The transverse ferromagnetic-Kerr effect was used to carry out some preliminary investigations of the magneto-optical properties of Gd films in the ferromagnetic state. When examining magneto-optical Kerr effects it is convenient to divide the effect artificially into three, depending on the orientation of the applied magnetic field to the plane of the reflecting surface and the plane of incidence. These three effects are termed the polar, the longitudinal and transverse Kerr effects. The last two effects have in common that the magnetization vector is restricted to the plane of the reflecting surface. For the longitudinal effect, the magnetization also lies in the plane of incidence, whereas for the transverse effect it is perpendicular to the plane of incidence. The transverse effect involves a variation in the component of the light polarized parallel to the plane of incidence, the amplitude of the variation being directly proportional to the magnetization of the surface. It is zero for the demagnetized state. The longitudinal effect is smaller than the transverse effect but is present in the reflected light for both parallel and perpendicular incident polarizations. If we assume the incident light to be polarized parallel to the plane of incidence then the amplitudes of the reflected light polarized parallel and perpendicular to the plane of incidence are given respectively by:

$$A_{//} = r_{//} + \delta r_{//} \qquad 7.2.5$$

and

$$A_{\perp} = k_{\perp} \qquad 7.2.6$$

where $r_{//}$, $\delta r_{//}$ and $k_{\perp}$ are complex quantities and $\delta r_{//}$ represents the transverse effect, $k_{\perp}$ the longitudinal effect and $r_{//}$ is due to normal metallic reflection.

The total intensity I_T of the light reflected at a given θ from the surface of the magnetized specimen is,

$$I_T = (A_{//} A_{//}^* + A_{\perp} A_{\perp}^*) \qquad 7.2.7$$

and it is easy to see that the intensity I_M of that part of the light dependent on the magnetization is,

$$I_M = 2\mathrm{Re}(r_{//} \, \delta r_{//}) \qquad 7.2.8$$

(Re denotes real part)

if second-order magneto-optical terms $(k_{\perp}{}^2)$ are neglected. Thus the requirements for observing the transverse ferromagnetic Kerr effect are:

(i) The incident light is polarized parallel to the plane of incidence.

(ii) The applied magnetic field is in the plane of the reflecting surface and is perpendicular to the plane of incidence.

To obtain a measure of the transverse effect (δ) it is convenient to use the experimental technique developed by Krinchik (1959). Experimentally, the intensities of light reflected from the ferromagnetic surface at some angle of incidence are measured for the magnetized (preferably to saturation) I_S and demagnetized I_D states. The value of δ at the given angle of incidence is obtained directly from,

$$\delta = \frac{I_S - I_D}{I_D} \qquad 7.2.9$$

For measuring δ in the wavelength range 400-700nm for ferromagnetic Gd films, the reflectometer and optical cell described in Chapter 4 were used. To magnetize the film in the reflecting plane and perpendicular to the plane of incidence a Helmholtz-coil system was constructed which fitted snugly around the cell wall and rested on the bottom sealing plate. The dimensions of this coil were such that, when

placed in position, the centre of the coil system was automatically aligned (to within ± 0.5mm) with the plane of the reflecting surface. An axial Hall probe (Scientifica and Cooke Ltd.) clamped to a micromanipulator which in turn was fixed to the reflectometer collimator support, was used to map out the magnetic field produced by the Helmholtz coil system in the vicinity of the film specimen. It was found that the field produced by the coils was extremely uniform; there was no detectable change in field intensity over the width or length of the evaporated film, (approximately 2 x 4 cms). The area of the probe over which the magnetic field was measured was 6 sq. mm, so that the observed magnetic field was certainly uniform down to these dimensions. The probe itself was calibrated by means of a standard magnet which produced a field accurate to ± 2%. With a current of 10 amps flowing through the coil a uniform field over the dimensions given above was produced of value 450 Oe.

The Gd films used in the magneto-optic experiments were grown in the U.H.V. system and so consisted of crystallites with the majority having the c-axis perpendicular to the plane of the film. Thus the applied magnetic field was in the basal plane of these crystallites, and so the observed values of δ refer to this plane only. To a very good approximation, the demagnetizing factor, is zero for a thin film of reasonable extent (cm^2 in area) and magnetized in the plane of the film. If it is assumed that the effective internal field of the film can be obtained by subtracting the average demagnetizing field from the applied field then for the above case the effective internal field is simply equal to the applied field. Nigh et al. (1963) have shown that to produce magnetic saturation along the c-axis of Gd an effective internal

field of 100 Oe. is required at 270°K and a field of >800 Oe. is required at 160°K. For the basal plane to reach saturation 800 Oe. is required at 270°K and 300 Oe. at 160°K. It was felt, therefore, that provided the temperature of the films was lower than 200°K the 450 Oe. produced by the Helmholtz coil would be sufficient to saturate the films in the basal plane.

Figure 7.2.6 shows the observed values of δ for the transverse ferromagnetic Kerr effect for a Gd film at $\sim 180^{\circ}$K. Values of δ were calculated using equation 7.2.9 from the observed quantities I_S and I_D obtained at an angle of incidence of 73.75°. Photomultiplier signals corresponding to I_s and I_d were measured with a 4-digit, digital voltmeter (Solartron Type: LM3). The difference $I_S - I_D$ was small and corresponded to a change in the 4th digit only. Repeating the measurements several times for the same film showed that δ was reproducible to within 15% to 20%.

The $\delta(\omega)$ curve (Figure 7.2.6) shows no significant structure apart from the main peak which has a maximum at 2.10eV. There is some similarity between the shape of this curve and that of the low temperature $\sigma(\omega)$ curve (Figure 7.2.5), although the piece of high energy structure is not present in the $\delta(\omega)$ curve. It seems likely, therefore, that the optical transitions responsible for the overall shape of the low temperature $\sigma(\omega)$ curve are also responsible for the general shape of the $\delta(\omega)$ curve, over this energy range. Unfortunately there is no published work on the magneto-optical properties of Gd and so no comparisons can be made.

7.3 Optical properties of Tb films grown in O.H.V.

Terbium films were grown on float glass microscope slides and thin mica substrates, using the O.H.V. systems described in Chapter 5. For

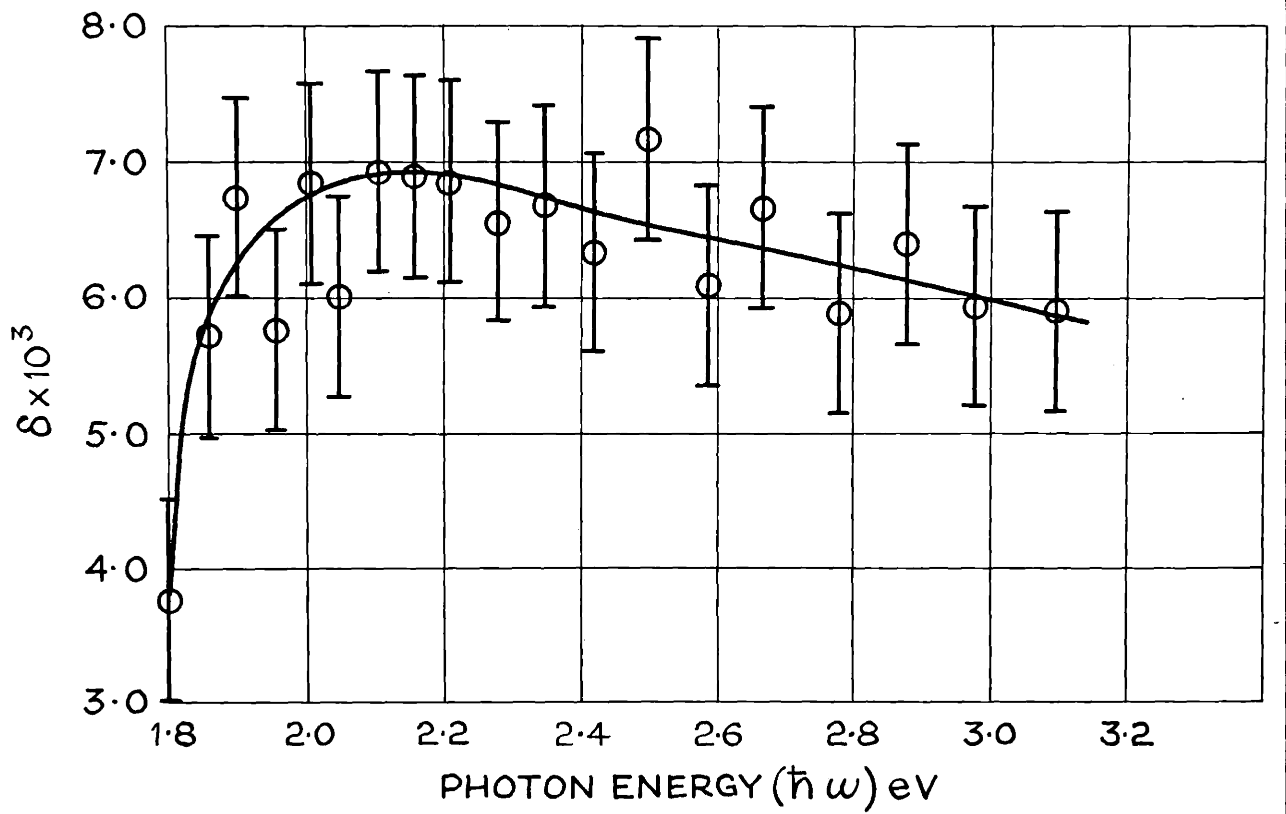

Figure 7.2.6 Ferromagnetic-Kerr effect observed for a Gd film of thickness 210nm. Temperature 180°K. $\theta = 73.75^{o}$. Applied magnetic field = 450 Oe.

the electron ring-gun evaporations a 'cermet' crucible was used. 'Cermet' is a material consisting mainly of Al_2O_3; it was found that the rare-earth metals Gd and Tb when molten dissolved carbon crucibles. The tungsten filaments used for evaporating terbium were loaded with the 99.9% purity Tb wire in the same way as for Gd. In the electron ring-gun evaporation system evaporation pressures were between 6 x 10^{-6}torr and 9 x 10^{-6}torr; in the tungsten filament evaporation system evaporation pressures were below 2 x 10^{-6}torr (see Section 5.2). Evaporation rates for films deposited using the electron ring-gun were generally slower than for films deposited from the tungsten filament. In the former case evaporation rates were between 0.6 and 1.3nm per second, and in the latter evaporation rates of between 1.5 and 2.0nm per second were used.

7.3.1 Tb films deposited onto mica substrates

Films of Tb deposited onto mica substrates, sufficiently thin to transmit electrons, were used to compare the structure of Tb films grown from (a) the electron ring-gun, and (b) the tungsten filament. These experiments were performed in an endeavour to find suitable methods of preparing Tb films for optical constants studies. The method of preparing the small mica substrates has already been described in Section 5.1.2.

A number of these mica substrates were clamped between a clean glass substrate and a mask of molybdenum and mounted in the substrate holder provided with a heater (Figure 5.2.2). The mica was annealed for about 2 hours at a temperature of 150°C and then allowed to cool before evaporating the Tb. The techniques of evaporating from the ring-gun and the tungsten filament have been described in Chapter 5.

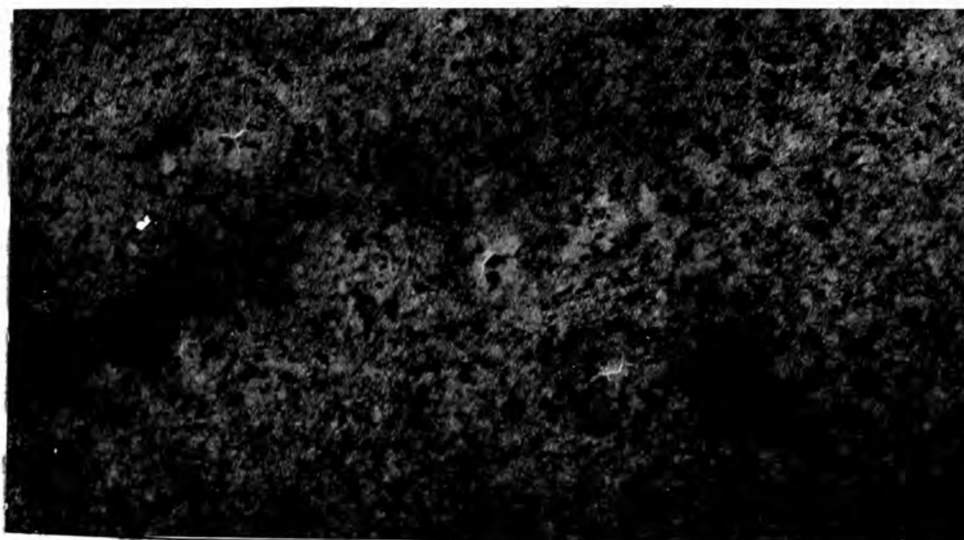

Figure 7.3.1(a) Electron micrograph of Tb film on mica.
Estimated thickness = 31.0nm.
Magnification = 20,000 X.

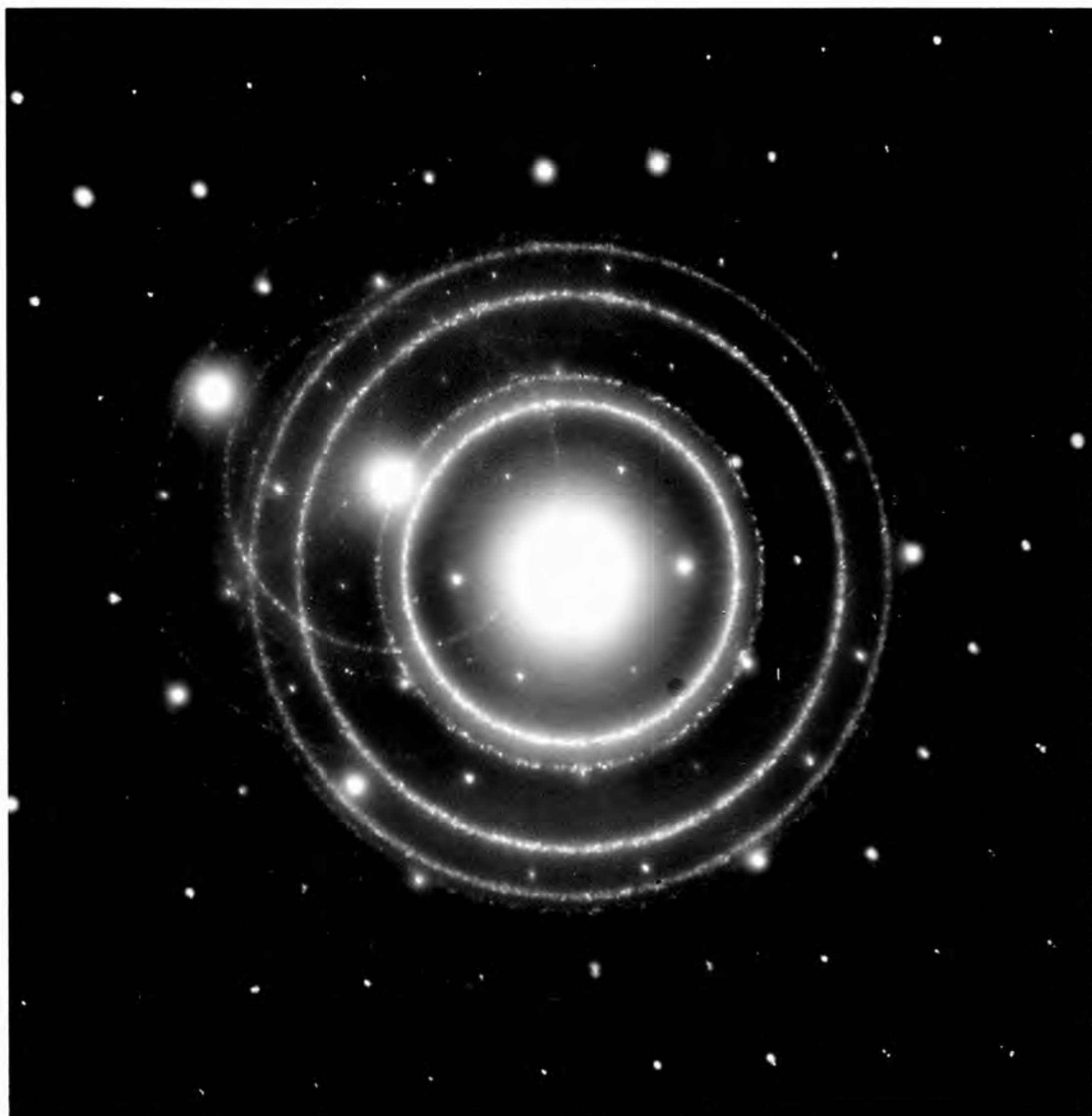

Figure 7.3.1(b) Selected area electron diffraction pattern obtained from the Tb film shown in Figure 7.3.1(a).

Figure 7.3.1 shows an electron micrograph and associated selected area electron diffraction of a Tb film deposited onto mica at room temperature from a tungsten filament in the Edwards (12EA) system. An estimate of the thickness was obtained from a multiple beam interferometric study of the Tb film coating one end of the glass substrate. Similar evaporations were performed in the electron ring-gun evaporation system (Section 5.2.2) and Figure 7.3.2 shows an electron micrograph and diffraction pattern obtained from one of the Tb films on mica. The difference between the two diffraction patterns is most striking. It would appear from these and other observed diffraction patterns that the Tb films deposited in the tungsten filament evaporation system consist essentially of Tb metal.. The diffraction rings (7.3.1b) are quite sharp and are of a granular structure. This shows that the films are essentially randomly polycrystalline with crystallites of the order of 50nm across in the plane of the film. Mica has a pseudo-hexagonal crystal structure and cleaves in the basal plane and, thus, would favour a h.c.p. material depositing with the c-axis perpendicular.to the plane of the film. This tendency is borne out by the observed diffraction patterns. An analysis of the diffraction rings of Figure 7.3.1b using a suitably prepared Bunn chart (Institute of Physics Publication) showed that the majority of the rings could be explained by the Tb metal with the h.c.p. crystal structure. The very faint additional rings which are present could be due to an oxide of Tb.

In complete contrast to the diffraction pattern of Figure 7.3.1b is the diffraction pattern (Figure 7.3.2b) observed for a Tb film deposited in the electron ring-gun evaporation system. Only one very diffuse ring is present, which implies a very small (less than 10nm) crystallite size. The lack of granular structure in the associated micrograph (Figure 7.3.2a) appears to corroborate this fact. Heating the mica substrates to 150°C

Figure 7.3.2(a) Electron micrograph of Tb film on mica, deposited in the electron ring-gun system. Magnification = 16,000 X.

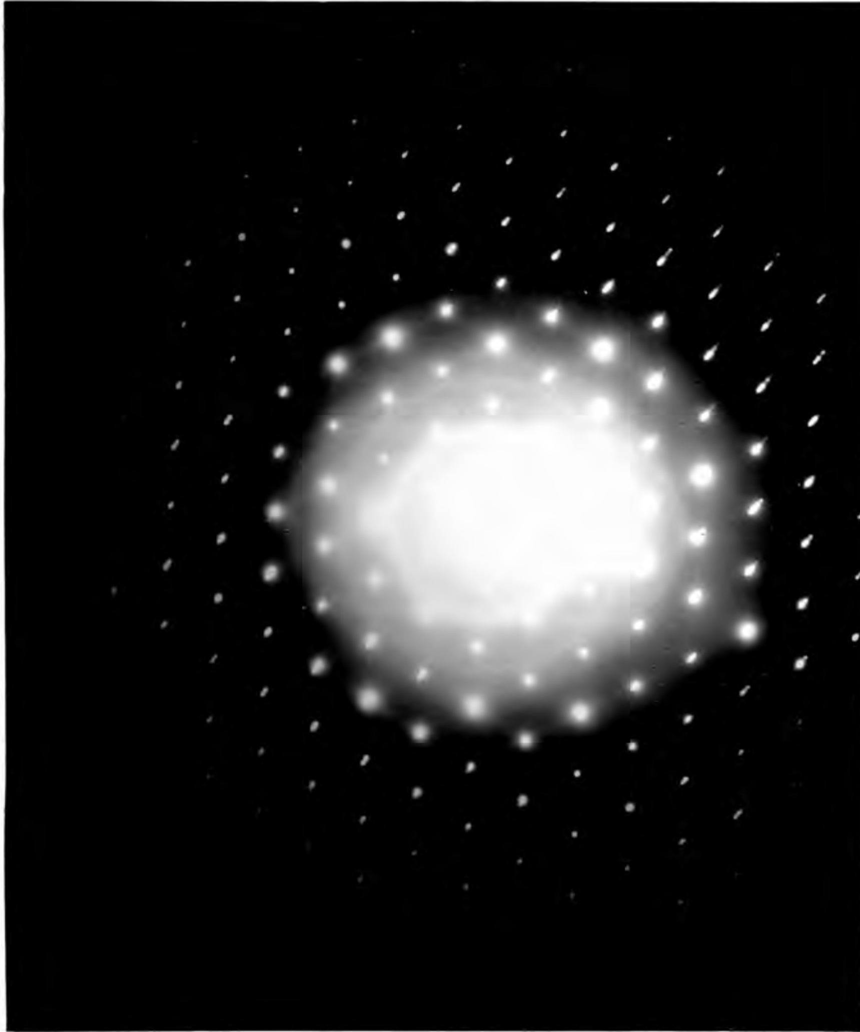

Figure 7.3.2(b) Selected area electron diffraction pattern obtained from the Tb film shown in Figure 7.3.2(a).

and evaporating the Tb onto the hot substrates did not change the observed electron diffraction patterns in anyway. The micrographs of such films were also essentially the same as that shown in Figure 7.3.2a. From these latter experiments it would appear that the Tb films deposited onto mica from the electron ring-gun consist essentially of an amorphous mixture of Tb and possibly terbium oxides and show no tendency to form larger crystals on heated mica substrates. One can only conclude that compared to the tungsten filament evaporation system, the slower evaporation rates, the higher evaporation pressures and the general features of the electron ring-gun system do not favour the deposition of Tb films in O.H.V. On the other hand, it would appear that poly-crystalline films of Tb metal can be successfully deposited in O.H.V. from tungsten filaments. Furthermore, it would seem that mica substrates might prove suitable for epitaxial growth of Tb and perhaps other h.c.p. structured rare-earth metals.

In an endeavour to understand more fully the growth of Tb films in the two O.H.V. evaporation systems a variety of Tb films on glass substrates were prepared for optical constants studies.

7.3.2 Optical constants of Tb films deposited onto glass substrates in O.H.V.

The electron microscope studies of the previous section showed that it was possible to deposit metallic Tb films having little impurity from tungsten filaments in the Edwards 12EA system (Section 5.2.1). Because there are no published values for the optical constants of Tb, it was desirable to obtain some measurements for $\sigma(\omega)$ over the visible wavelength range 400-700nm for Tb films evaporated in O.H.V. from tungsten filaments.

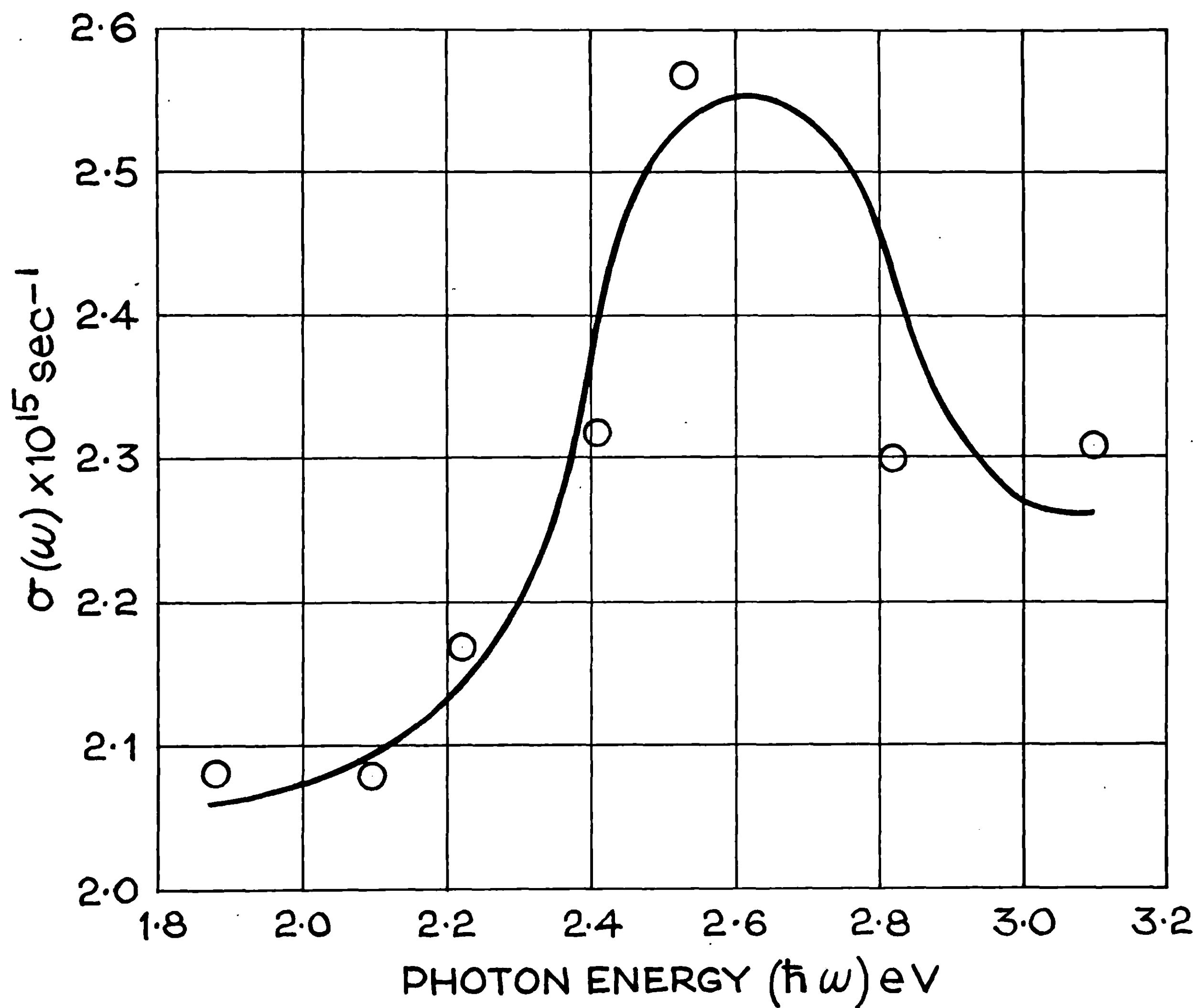

Figure 7.3.3 Optical constant $\sigma(\omega)$ observed for Tb film grown in O.H.V. system. Temperature 294°K. Thickness of film 210nm.

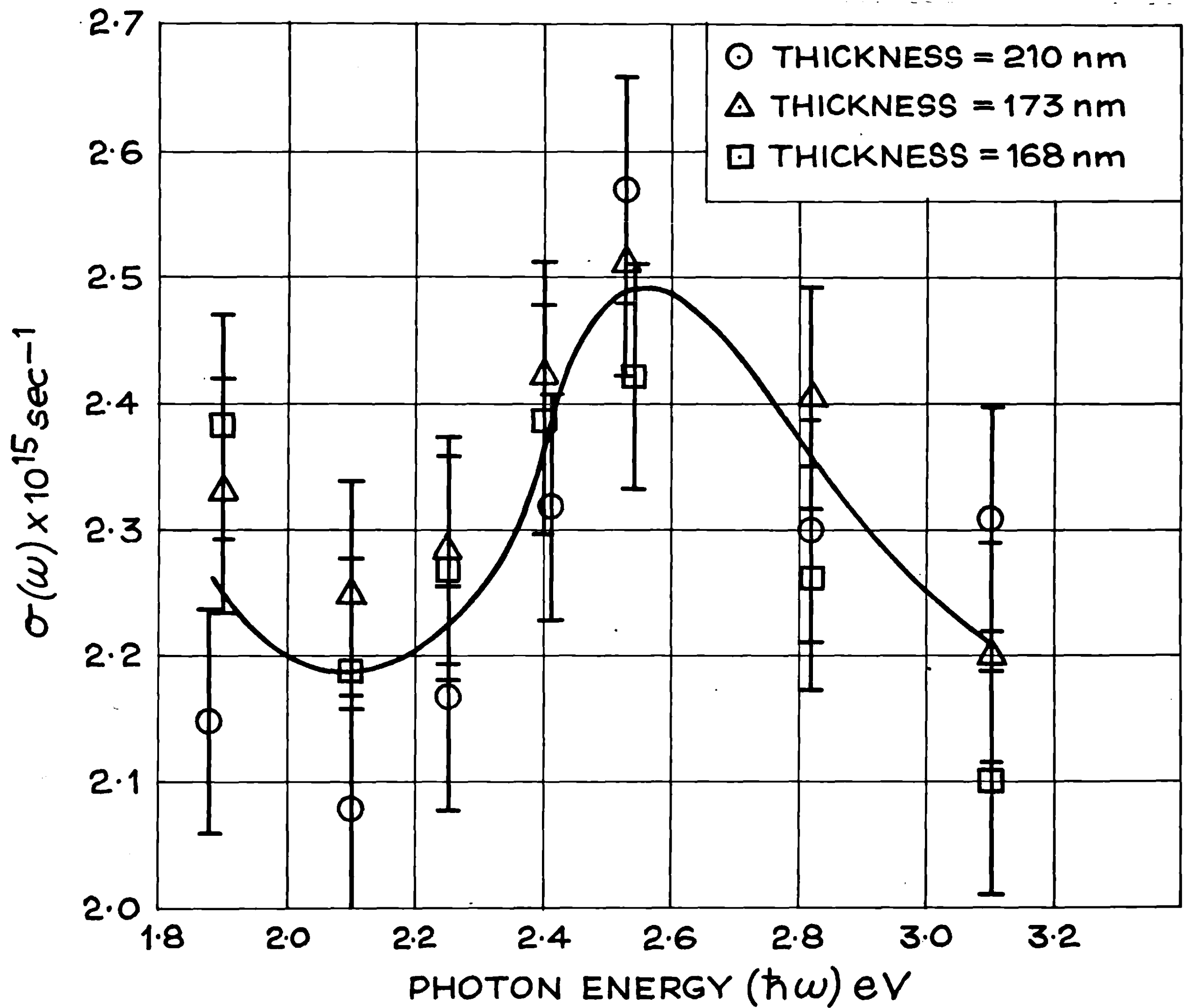

Figure 7.3.3(a) Optical constant $\sigma(\omega)$ observed for 3 Tb films grown in the O.H.V. system. Temperature 294°K. Thicknesses 210, 173 and 168nm.

The optical constants n and k of optically opaque Tb films, prepared in the manner described in Chapter 5, were determined using the ($R_{//}$, $R_{\perp}$) method described in Chapter 2. The films were deposited at room temperature onto float glass microscope slides. The reflectometer (Chapter 4) was used to measure $R_{//}$ and $R_{\perp}$ at 73.75° incidence for films situated in air. Optical constants n and k were calculated using Querry's (1969) analytical method, and the errors associated with $\sigma(\omega)$ were estimated using the results obtained in Chapter 2. Film thicknesses were determined after the reflection measurements were completed, using multiple beam interferometry. All the films investigated had a thickness greater than 150nm and were grown at pressures below 2×10^{-6} torr. Evaporation rates were 2nm per second and evaporation source to substrate distance was 15 cms.

To illustrate the experimental results a $\sigma(\omega)$ dispersion curve is shown in Figure 7.3.3 for a Tb film 210 $\pm$ 5nm thick. This curve was obtained using 7 individual narrow-band, wavelength filters. The reflection coefficients were each measured to an accuracy of $\pm$ 0.006 or better and so $\sigma(\omega)$ has associated errors of between 6 and 10% (Miller, Julien and Taylor, 1971). The absolute value of the optical constant $\sigma(\omega)$ varied by 11% between different films grown in the same vacuum environment, but the shapes of the $\sigma(\omega)$ dispersion curves were essentially the same for the different films. Figure 7.3.3(a) shows a composite plot of $\sigma(\omega)$ for 3 Tb films of thicknesses 168, 173 and 210nm respectively. There was no significant thickness dependence of n, k or $\sigma(\omega)$ for the films investigated with optical thicknesses in the range 150-220nm, neither was there any significant time dependence of the optical constants over the time required for the reflection measurements. All reflection measurements were commenced 15-20 minutes after completion of the evaporation.

The $\sigma(\omega)$ dispersion curve shows a main peak centred at 2.6eV. Curves of a similar shape have been obtained by Schüler (1966) for other rare-earth metals, Lu and Dy. Unfortunately, there are no published details for the optical transitions possible in Tb metal and so no direct comparison can be made between theoretical predictions and the experimental results depicted in Figure 7.3.3. However, it should be possible to predict the allowed optical transitions for Tb from the calculated band structure due to Jackson (1969), and the group-theoretical optical selection rules for h.c.p. structured materials (Cornwall, 1965).

In order to obtain some quantitative verification for the observed $\sigma(\omega)$ dispersion curve for Tb, the product $\omega\sigma(\omega)$ was compared with the convolved density of states histogram calculated from the band structure calculations of Jackson (1969). The computer programme used to perform the required convolution was the same as that used for similar work with Gd. This technique of convolving the densities of states above and below the Fermi level has been described in Section 7.2. In Figure 7.3.4 the convolution of the filled and empty densities of states is plotted against photon energy ($\hbar\omega$) and included in the figure for comparison is an experimental plot of $\omega\sigma(\omega)$ for the Tb film used for Figure 7.3.3. Figure 7.3.4(a) shows a composite of the observed $\omega\sigma(\omega)$ for the 3 films used to obtain Figure 7.3.3(a). The convolved density of states histogram is again included for comparison. The convolved density of states histogram and the $\omega\sigma(\omega)$ values are of an arbitrary scale so that quantitative comparison of ordinates should not be made. The experimental curve seems to follow the convolved density of states histogram throughout the energy range considered. In the experimental curve a slight hump is apparent at 2.6eV. and this seems to be reproduced by the histogram at about 2.4eV. It would

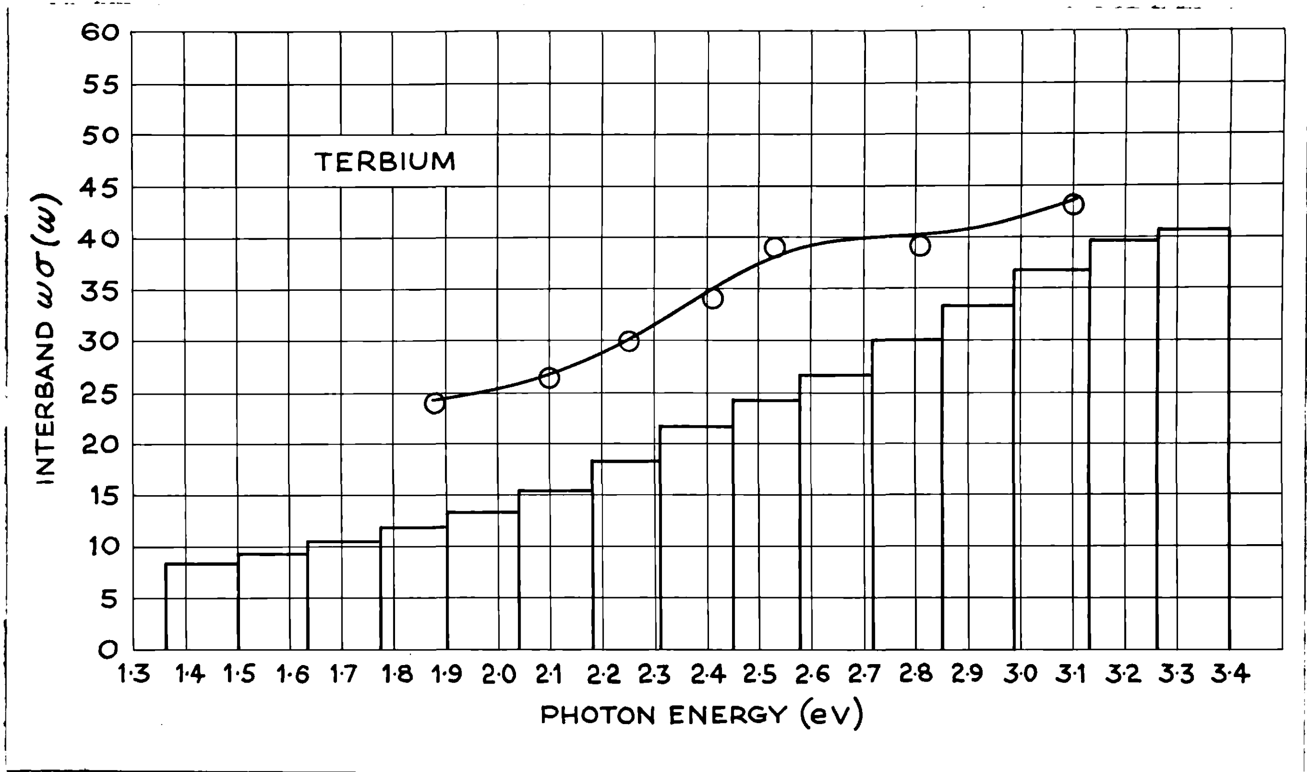

Figure 7.3.4 Observed interband $\omega\sigma(\omega)$ for a Tb film compared with the convolved density of states histogram. Temperature 294°K. Thickness of film 210nm.

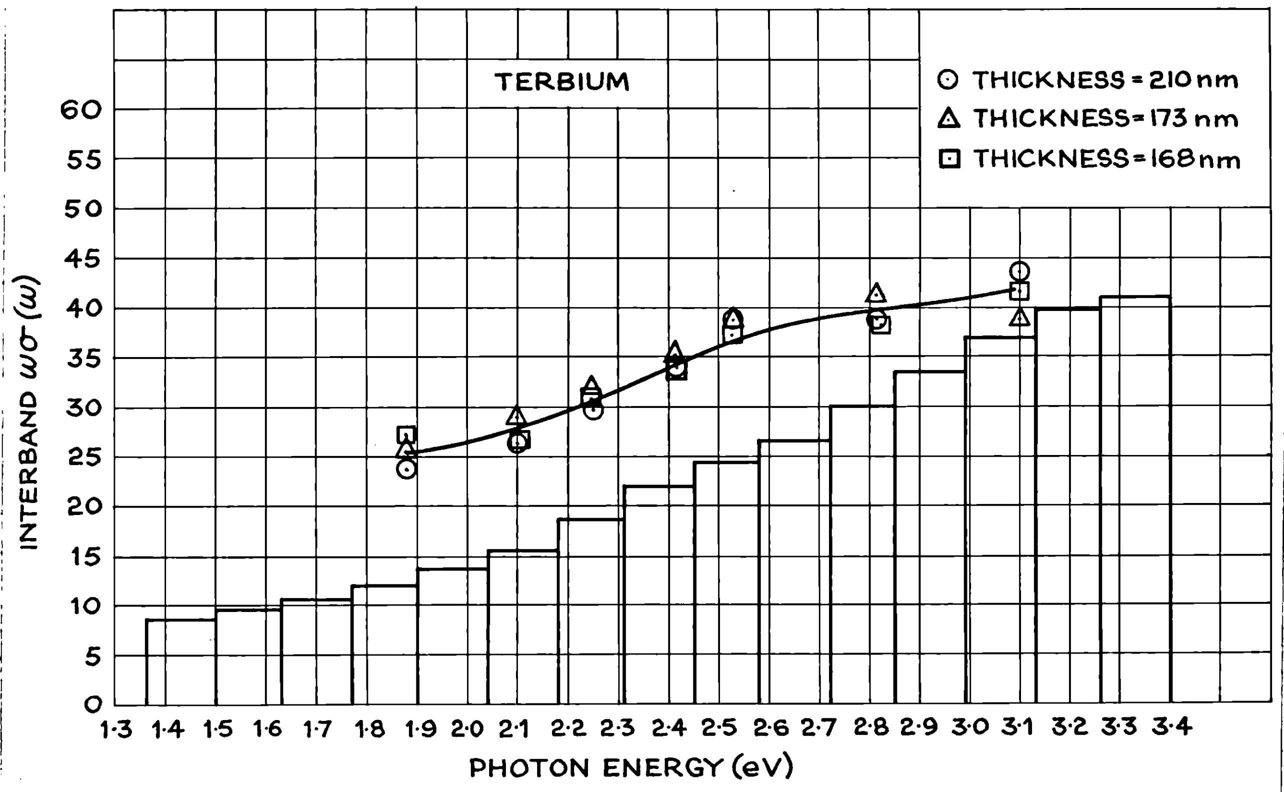

Figure 7.3.4(a) Observed interband $\omega\sigma(\omega)$ for 3 Tb films compared with the convolved density of states histogram. Temperature 294 ^{o}K. Thicknesses 210, 173 and 168nm.

appear, therefore, that as with Gd the main $\sigma(\omega)$ peak observed for Tb can be explained by non-direct transitions. A more detailed experimental investigation of the $\sigma(\omega)$ dispersion curve for Tb will undoubtedly show considerable secondary structure, which can only be explained by direct optical transitions.

In an endeavour to understand the nature of Tb films deposited in the electron ring-gun evaporation system, the optical constants n and k were determined for films deposited onto float glass substrates lightly ground on the back face. The films were prepared in the manner described in Chapter 5. For each film thickness two films were prepared; one for the determination of the optical constants and the other intended for use with multiple beam interferometry to determine the geometrical film thickness. Films were grown with thicknesses in the range 15-210nm, and evaporation rates and pressures used are quoted at the beginning of this Section. The optical constants n and k were determined by the optimized reflection ratio method described in Chapter 3. The fully computational method of evaluating n and k from the measured quantities was used in preference to the graphical method. This programme is described in detail in Chapter 3, and has the advantage over the graphical method of portraying the scatterin n and k values arising from the known errors in the measured reflection ratios. From this computer programme the optical constants of the films investigated were evaluated with accuracies ranging from $\pm$ 0.05 to $\pm$ 0.1, depending on the value of the optical thickness d/λ.

Figures 7.3.5 and 7.3.6 show the observed n and k values for the ring-gun Tb films plotted against film thickness for wavelengths 402 and 546nm respectively.. It can be seen that these films show dielectric type properties, that is $\epsilon_2 = n^2-k^2$ is positive, for film thicknesses

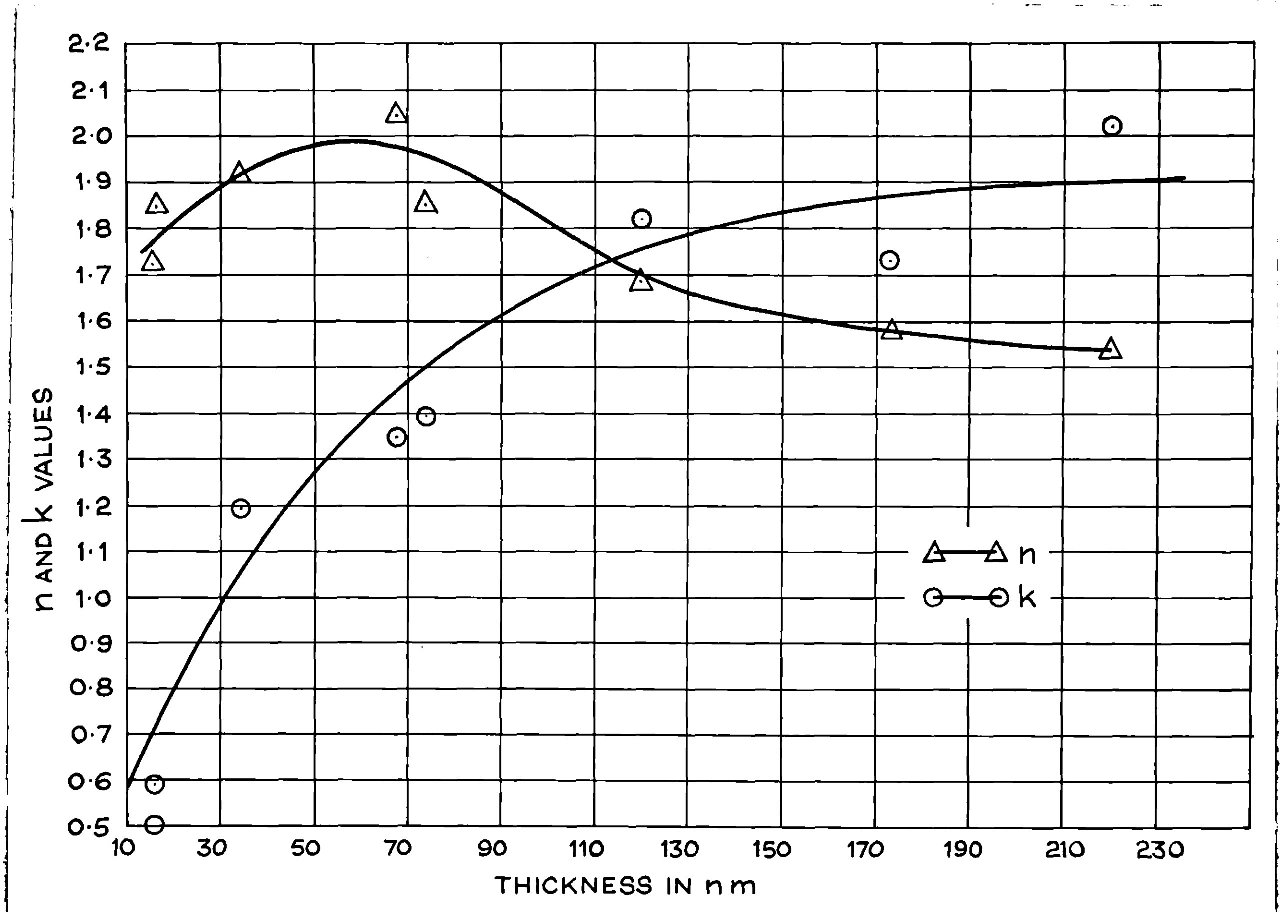

7.3.5 Thickness dependence of n and k for terbium films deposited in the electron ring-gun vacuum system. Wavelength = 402nm. Temperature 293°K.

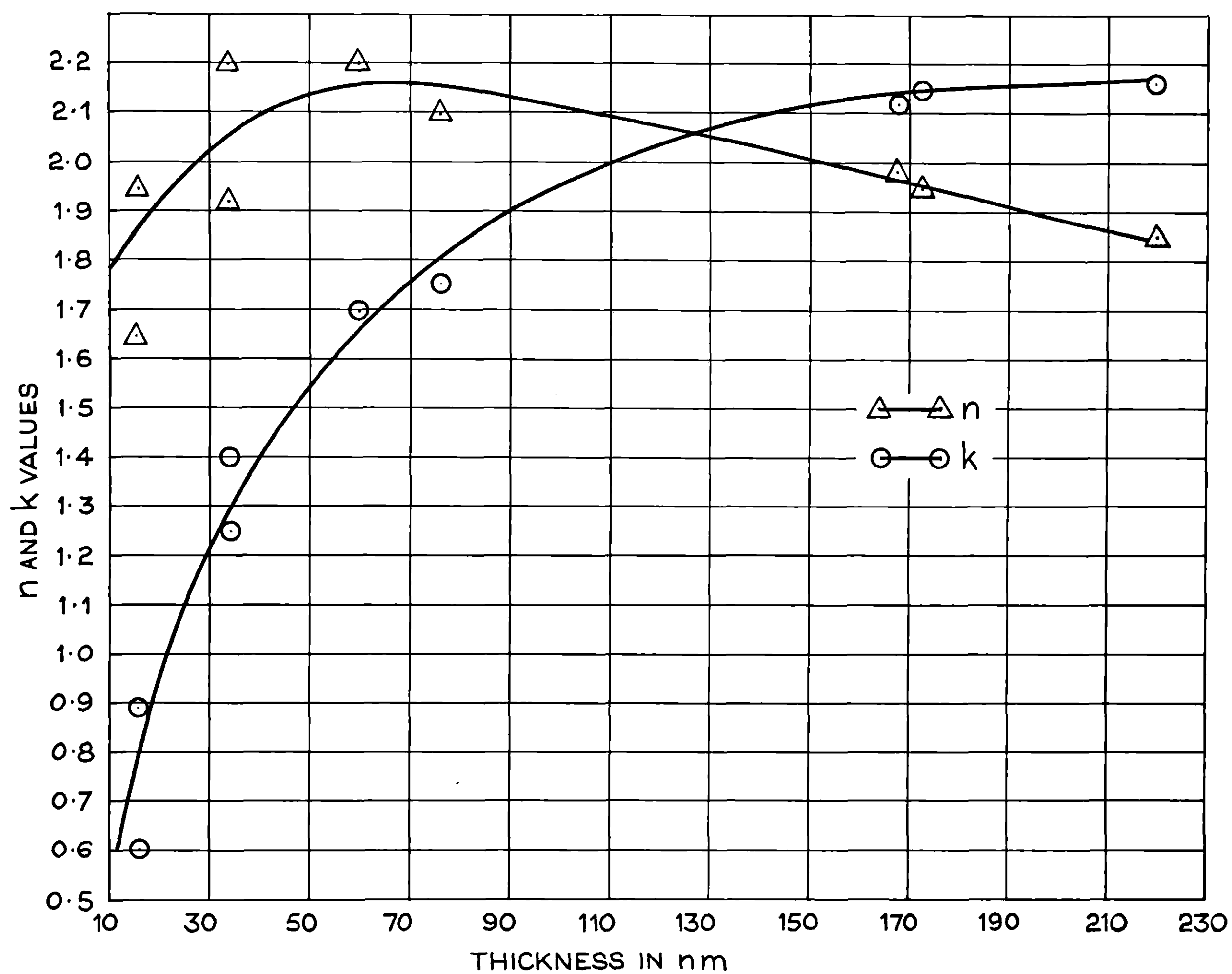

Figure 7.3.6 Thickness dependence of n and k for terbium films deposited in the electron ring-gun system. Wavelength = 546nm. Temperature = 293°K.

below 115nm (Figure 7.3.5) and 127nm (Figure 7.3.6), and only show a tendency to metallic properties above these thicknesses. This appears to corroborate the conclusions of the electron microscopy studies of Section 7.3.1 in which it was suspected that films of thickness less than 100nm consisted essentially of terbium oxides and Tb metal. If the oxide content of such films is appreciable then one would expect the optical properties to show typical dielectric behaviour. One can conclude, therefore, that thin opaque films of Tb grown in the present electron ring-gun system consist of an almost amorphous mixture of Tb metal and terbium oxides. Vratny (1961) has shown that the oxide Tb_2O_3 can form at pressures as low as 10^{-5} torr.

7.3.3 The optical properties of terbium oxide thin films

As the thin terbium films produced in the electron ring-gun evaporation system consisted of oxides of terbium in addition to Tb metal, it seemed a good idea to complete the oxidation process and investigate the optical properties of thin films of terbium oxide. It has already been mentioned in Chapter 6 that very little work on the optical properties of the oxides of terbium has been done. The only work of this nature to date is that of Vratny (1961).

In order to complete the oxidation of the deposited films they were removed from the vacuum system and placed in an oven in air. The oven temperature was increased slowly to $400^{\circ}C$ and maintained at this temperature for 4 hours, and then allowed to cool to room temperature. After this heat treatment it was found that the films changed in appearance from a metallic lustre to a highly transparent coating - typical of dielectric thin films. Multiple beam interferometry showed that the geometrical film thickness always decreased during the oven

treatment, and this decrease always represented something like 10-12% of the original thickness. The oxidized films investigated had thicknesses in the range 30 to 70nm.

The optical constants n_2 and k_2 of the films before and after the oven treatment were determined using the reflectometer (Chapter 4) and the optimized reflection ratio method described in Chapter 3. The reflection measurements were obtained in air.

To illustrate the results obtained, Figure 7.3.7 shows dispersion curves of n_2 and k_2 for a terbium film before and after oven treatment. The n_2 and k_2 values are accurate to between $\pm$ 0.05 and $\pm$ 0.1, and were evaluated using the fully computational method described in Chapter 3. It can be seen that there is a drastic change in both n_2 and k_2 caused by the oxidation process. The values of n_2 have decreased considerably and have become almost independent of wavelength. The change in k_2 is even more marked (lower curve) and shows a strong increase towards the ultra-violet and a small peak at 605nm (2.05eV.). This peak is significant as it appears in the k_2 dispersion curve at 525nm (2.36eV.) for the film before oven treatment, i.e. before full air oxidation. These two peaks represent k_2 maxima in the wavelength range 400-700nm. Vratny (1961) studied the reflectance spectra of terbium oxides having compositions in the range Tb_2O_3 to Tb_4O_7. Without actually calculating optical constants n and k, Vratny was able to predict, to a reasonable degree of approximation, the position of k maxima as a function of oxide composition for the wavelength range 400-600nm. He observed that the position of the k maximum moved to higher photon energies as the oxygen content of the oxide decreased. In fact, this is precisely what is observed in the k_2 dispersion curves of Figure 7.3.7. The chemical composition of the films before and after oxidation was not

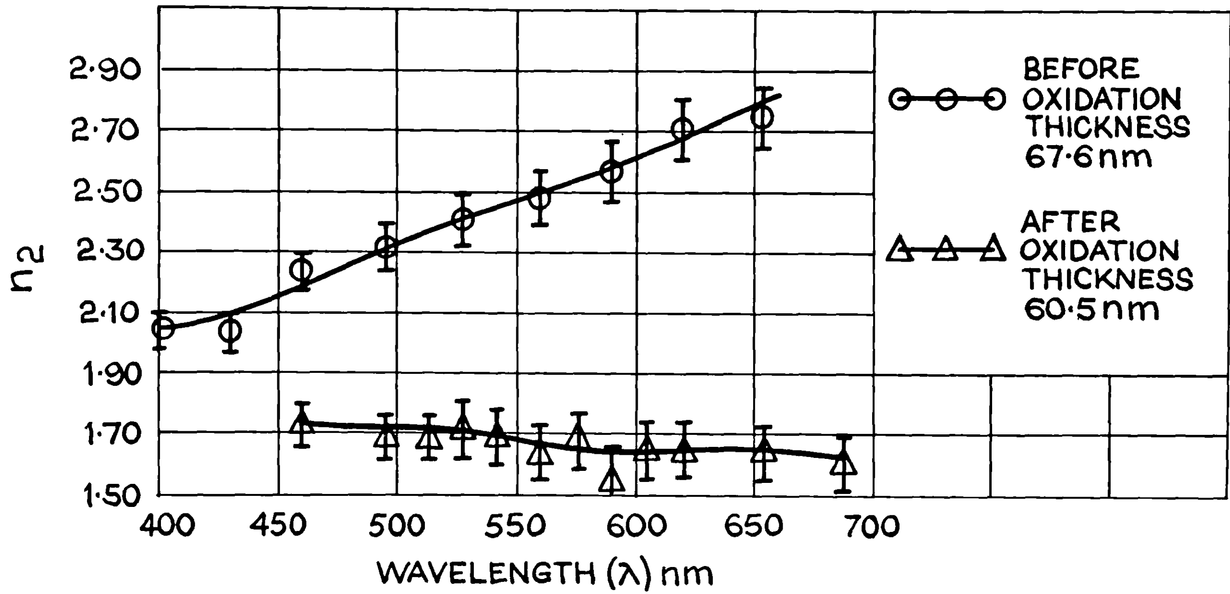

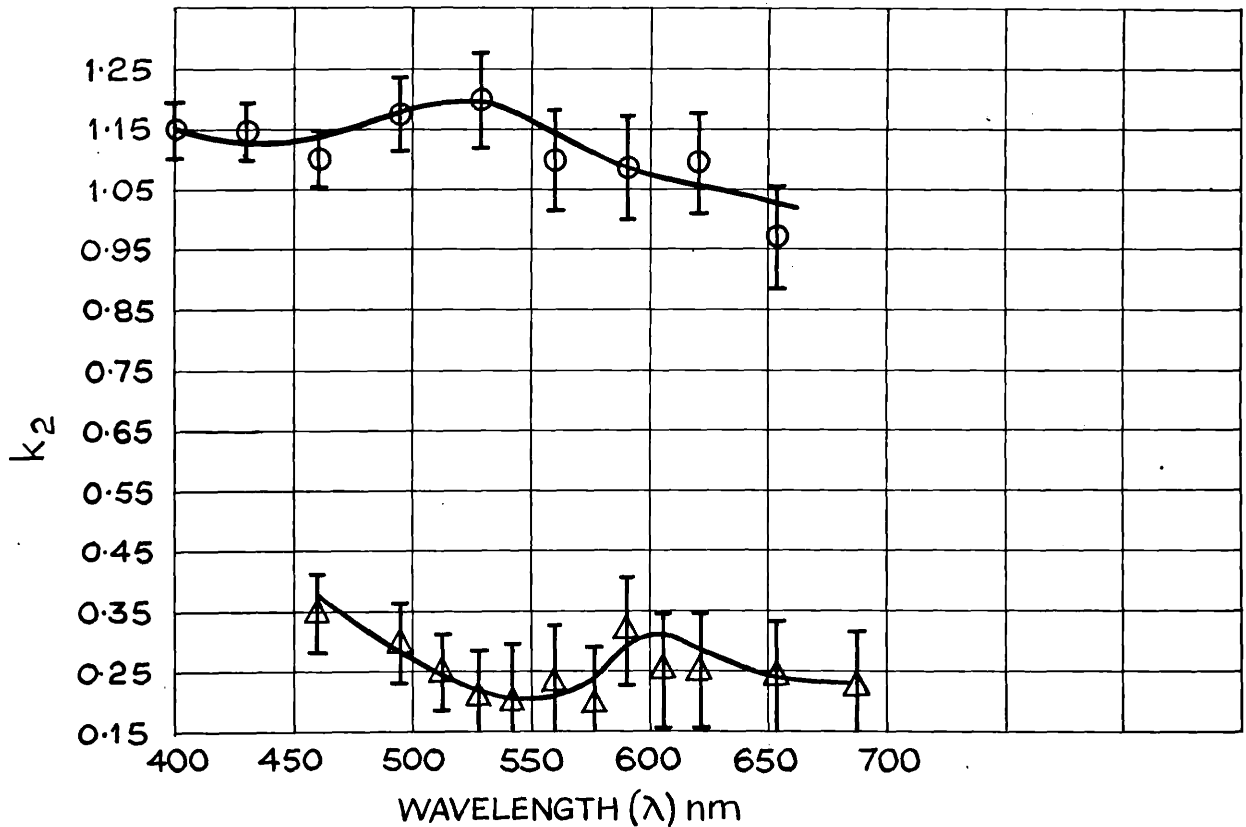

Figure 7.3.7 Observed optical constants n_2 and k_2 against wavelength for a terbium film before and after air oxidation at 400°C. Temperature at time of measurement = 294°K.

determined, but from the evidence of Sections 7.3.1 and 7.3.2 it is certain that the Tb films grown in the electron ring-gun vacuum system consisted of a large proportion of the lower oxides of Tb, possibly Tb_2O_3, although non-stoichiometric compositions are possible under the vacuum conditions present in the ring-gun system. The position of the k_2 maximum at 2.36eV. in the observed dispersion curves for such films would indicate, from Vratny's predictions, the presence of an oxide of Tb with the non-stoichiometric composition $Tb\ O_{1.53}$. Air oxidation of the deposited films at 400°C would favour the production of pure higher oxides of terbium. Vratny predicted that for the oxide of stoichiometric composition Tb_4O_7 the k maximum should occur at a photon energy of 2.17eV. The k_2 maximum at 2.05eV. in the lowest dispersion curve of Figure 7.3.7 would seem to indicate, therefore, that the oxidized films consisted essentially of Tb_4O_7. Other films of different thicknesses were investigated and all gave dispersion curves for the oxidized film very similar to those of Figure 7.3.7, although the reproducibility from film to film was about $\pm$ 0.15 in n_2 and k_2.

It was of interest to plot the optical constant $\sigma(\omega)$ against photon energy for the air oxidized terbium thin film used to produce Figure 7.3.7. This dispersion curve is shown in Figure 7.3.8, and shows a small peak at 2.15eV. and a strong absorption in the near ultra-violet. The small peak at 2.15eV. probably corresponds to the k maximum at 2.17eV. predicted by Vratny for the composition Tb_4O_7. Figure 7.3.8(a) shows $\sigma(\omega)$ dispersion curves for 3 terbium oxide films of thickness 43.2, 50.6 and 60.5nm respectively. A small peak at 2.1eV. occurs for two of the films and at 2.25eV. for the other, and these correspond to the k maximum predicted by Vratny.

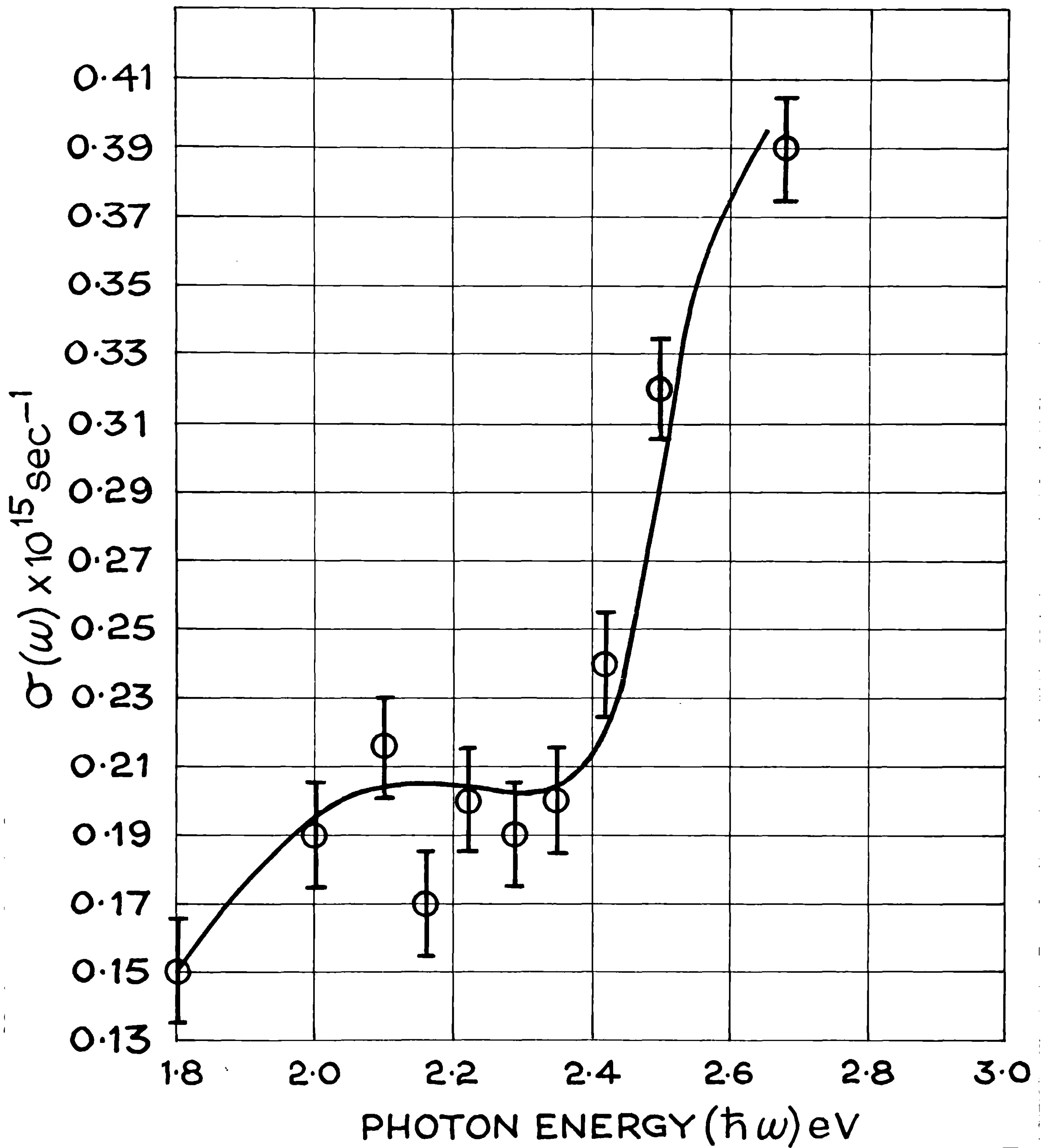

Figure 7.3.8 Optical constant $\sigma(\omega)$ observed for terbium oxide thin film. Temperature 294°K. Film thickness 60.5 nm.

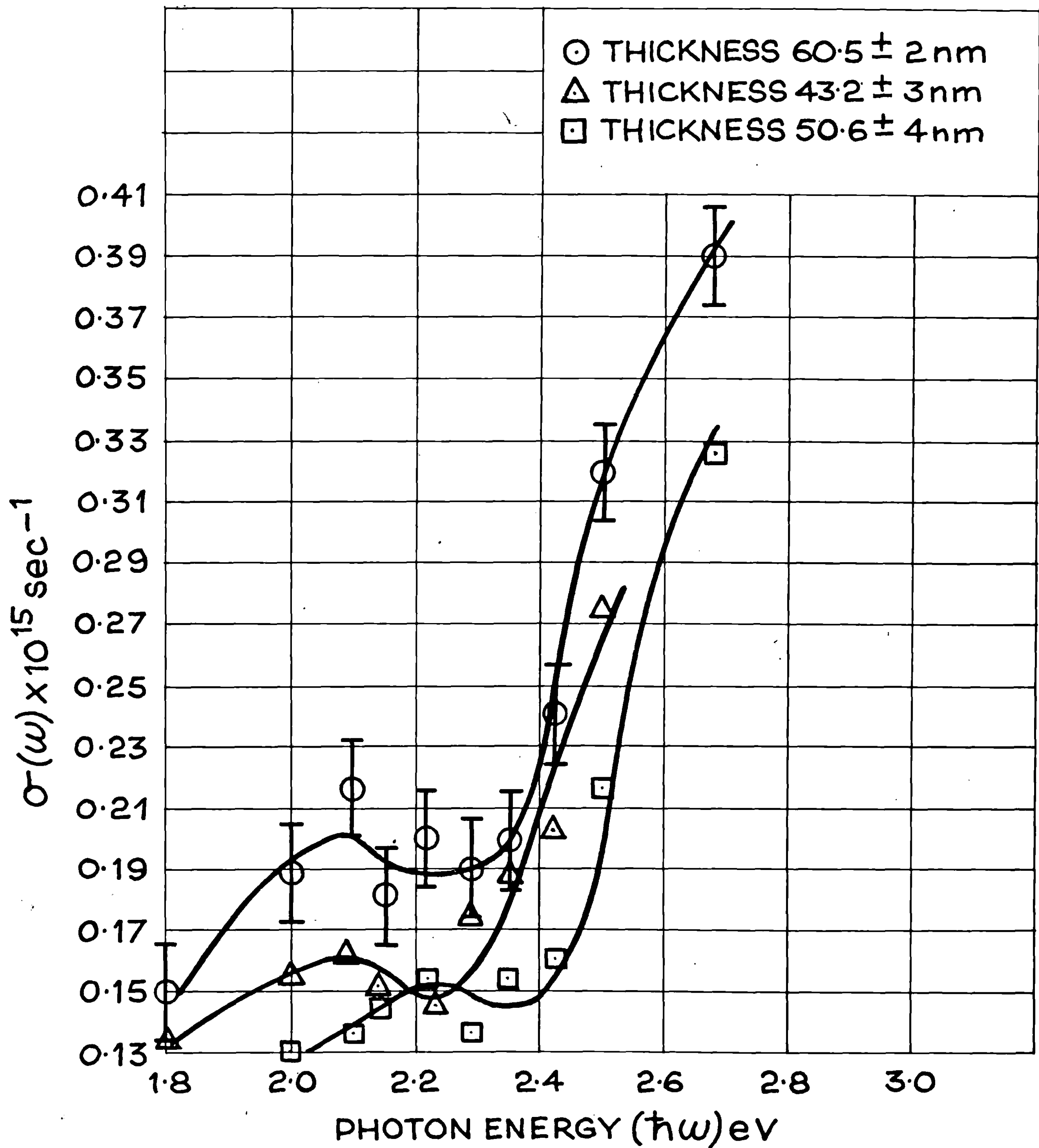

Figure 7.3.8a Optical constant $\sigma(\omega)$ observed for terbium oxide (Tb_4O_7) thin films. Temperature 294°K. Thicknesses 60.5, 43.2, and 50.6nm.

Table 7.3.1 n and k against thickness for terbium oxide films $\lambda = 543nm$

Thickness d/nm ± 3nm	n ± 0.06	k ± 0.07
31.3	1.70	0.20
43.2	1.65	0.20
50.6	1.70	0.13
57.2	1.85	0.15
60.5	1.73	0.21

From a technological point of view the terbium oxide films produced by the air oxidation of terbium films deposited from an electron ring-gun at pressures close to 1×10^{-5} torr seem to be useful. It was found that the terbium oxide films produced were not scratched by normal laboratory handling, and their optical constants in the visible region would make them ideally suitable for beam splitters or hard dielectric coatings for laser-end mirrors. At 543nm, the optical constants of the terbium oxide films in the thickness range 30-60nm were all within the range $1.65 \leqslant n \leqslant 1.85$, $0.13 \leqslant k \leqslant 0.21$, (Table 7.3.1). In Chapter 6 the refractive indices of some other rare-earth oxides are given; all have values of n between 1.7 and 1.8 at 546nm.

7.4 Overall conclusions and further work

Starting with an analytical solution to the generalized Fresnel reflectance equations it has been shown that, by using optimization techniques, suitable angles of incidence can be chosen at which to measure $R_{\parallel}$ and $R_{\perp}$ so that n and k values may be obtained to an accuracy as good as the method will allow. Further computational work showed that normal incidence reflection methods of determining optical constants were subject to large inherent errors, which could give rise to artificial structure in $\sigma(\omega)$ dispersion curves.

For determining the optical constants n_2 and k_2 of thin, partially-transparent films a new optimized reflection-ratio method was devised. Measuring the reflection ratio $(R_{\parallel}/R_{\perp})$ at two "optimum" angles of incidence enable n_2 and k_2 to be determined to an accuracy of $\pm$ 0.05. This method has certain distinct advantages over other reflection methods of determining optical constants of thin films.

In order to investigate the optical and magneto-optical properties of opaque and partially transparent films, a simple but accurate reflectometer was designed and constructed to allow a number of reflection methods to be used to determine optical constants at temperatures above and below room temperature.

The reflectometer and the optimized reflection techniques were used to determine the optical constants of Ni, Gd, Tb and terbium oxide films in the wavelength range 400-700nm.

For Ni films deposited in U.H.V. and measured in air, it was found that there was little significant thickness dependence of the optical constants for film thicknesses in the range 25 to 60nm.

Gd films deposited in U.H.V. and measured in an optical vacuum cell gave $\sigma(\omega)$ dispersion curves which showed significant structure between 2.3 and 2.6eV. This structure can be attributed to direct optical transitions. Further work showed that the main features of the $\sigma(\omega)$ dispersion curve below 2.7eV. could be explained by assuming that non-direct transitions dominated the optical spectrum. For Gd films in the ferromagnetic phase, optical constants and the transverse ferromagnetic Kerr constant were obtained for the wavelength range 400-700nm. A similarity was found between the observed $\sigma(\omega)$ curve and the $\delta(\omega)$ curve. It was also discovered that the Gd films deposited onto glass substrates in the U.H.V. system showed a preferred orientation with the c-axis perpendicular to the plane of the film. Consequently the optical properties observed were relevant to the basal plane of h.c.p. Gd.

The optical properties of Tb metal films deposited in O.H.V. were also studied and a $\sigma(\omega)$ dispersion curve obtained for photon energies 1.8 to 3.1eV. Again, the overall shape of the $\sigma(\omega)$ dispersion curve

for Tb could be explained by assuming that non-direct optical transitions are probable.

A method of preparing terbium oxide (Tb_4O_7) thin films on glass substrates has been devised, and the observed optical properties confirm the predictions of previous work on the oxides of Tb.

Mica substrates have also been investigated as a possible means of obtaining epitaxial films of Tb metal. In order to obtain such films, evaporation rates would have to be high, at least 2nm per second, to overcome oxidation effects in O.H.V. It would be necessary to heat the substrate during film deposition.

Further work is at present in progress on the optical properties of Gd and Tb metal deposited and measured in U.H.V., with a view to elucidating the electronic band structure of these metals. The present work is concerned with using the optimized ($R_{\parallel}, R_{\perp}$) method to obtain $\sigma(\omega)$ dispersion curves for those metals at room temperature. It is hoped that in the near future low temperature in-situ measurements on metal films of Gd and Tb deposited in U.H.V. will help to clarify the electronic band structure of these metals in their ferromagnetic phase.

Transverse ferromagnetic Kerr effect measurements should be obtained for Gd films at photon energies below 1.7eV., with the view to understanding the structure observed in the $\sigma(\omega)$ curves at these energies. In particular the peak at 1.1eV. observed in ferromagnetic Gd should be studied.

More work on the optical constants of the rare-earth oxides is called for, even if only to present data suitable for possible technological applications.

Finally, the author feels that every effort should be made to seek analytical solutions to the methods of obtaining optical constants.

It has been shown in this thesis that it is only when the analytical solution is known that the full capabilities of a method become apparent.

APPENDIX I

List of Symbols

Symbol	Meaning
ϵ_1	The real part of the dielectric constant.
ϵ_2	The complex part of the dielectric constant.
$\hat{\epsilon}$	The complex dielectric constant $\hat{\epsilon} = \epsilon_1 - i\epsilon_2$.
n	The refractive index of a material in bulk or opaque film form.
k	Extinction coefficient of a material in bulk or opaque film form.
n_1	Refractive index of ambient medium.
n_2	Refractive index of a material in thin film form, when the film is partially transparent.
k_2	Extinction coefficient applied to a material in thin film form, when the film is partially transparent.
$\sigma(\omega)$	Optical conductivity at a frequency ω .
ω	Optical frequency.
θ	Angle of incidence.
λ	Wavelength of light in nm.
d	Geometrical film thickness in nm.
Δ	Difference between the phase changes for light polarized parallel and perpendicular to the plane of incidence.
ψ	$\tan^{-1}$ of the ratio of the real amplitude reflection coefficients for light polarized parallel and perpendicular to the plane of incidence.
ϕ	Azimuth angle for polarized light.
$R_{\parallel}$	Reflection coefficient for light polarized parallel to the plane of incidence.
$R_{\perp}$	Reflection coefficient for light polarized perpendicular to the plane of incidence.

Symbol	Meaning
θ_B	Angle of incidence corresponding to the pseudo-Brewster angle.
n_3	Refractive index of a dielectric substrate.
R	Reflection coefficient at normal incidence.
T	Transmission coefficient at normal incidence.
$T_{//}$	Transmission coefficient for light polarized parallel to the plane of incidence.
$T_{\perp}$	Transmission coefficient for light polarized perpendicular to the plane of incidence.
R'	Denotes normal incidence reflection coefficient for light incident on the substrate side of a thin film.
ϕ_R	Total phase change on reflection.
ϕ_T	Total phase change on transmission.
Δn_2, Δk_2, $\Delta(d/\lambda)$ $\Delta\phi$, ΔT, ΔR, $\Delta\theta$	Small changes or errors in the quantities n_2, k_2, (d/λ), ϕ, T, R, θ.
$\hbar\omega$	Photon energy in eV.
$I_o^{\perp}$	Incident intensity for light polarized perpendicular to the plane of incidence.
$I_o^{//}$	Incident intensity for light polarized parallel to the plane of incidence.
ρ^2	Is conveniently used for the ratio $(R_{//}/R_{\perp})$.
$\underline{k}$	The generalized wave vector.
E_F	Fermi energy.
N_C	Number of states in the conduction band.
N_V	Number of states in the valence band.
E	Energy of electronic states.
$A_{//}$	Amplitude (complex) of reflected light polarized parallel to the plane of incidence for a magnetized specimen.

Symbol	Meaning
$A_{//}^{*}$	Complex conjugate of $A_{//}$.
$A_{\perp}$	Amplitude (complex) of reflected light polarized perpendicular to the plane of incidence for a magnetized specimen.
$A_{\perp}^{*}$	Complex conjugate of $A_{\perp}$.
$\delta r_{//}$	Transverse-ferromagnetic Kerr effect.
$k_{\perp}$	Longitudinal-ferromagnetic Kerr effect.
I_T	Is the total intensity of the light reflected at a given θ from the surface of a magnetized specimen.
I_M	Intensity of light reflected, dependent on the magnetization of the specimen.
I_S	Intensity of light reflected from a surface magnetized to saturation.
I_D	Intensity of light reflected from a surface which has been demagnetized.
h.c.p.	Hexagonal close-packed crystal structure.
f.c.c.	Face centred cubic crystal structure.
b.c.c.	Body centred cubic crystal structure.

APPENDIX II

```
      PROGRAM APLOT(INPUT,OUTPUT,TAPE25,TAPE27)
      DIMENSION X(243),Y(243),AN2(243),ROSQ(243),AK2(35),S(1),DL(1)
      DO 1 N=1,241
      Y(N)=0.01*(FLOAT(N-1))+1.10
      AN2(N)=Y(N)
    1 CONTINUE
      READ 100,AK2(1)
  100 FORMAT(F6.0)
      READ 200,S(1)
  200 FORMAT(F7.0)
      READ300,DL(1)
  300 FORMAT(F5.0)
      DO 3 N=1,241
      L=1
      I=1
      K=1
      AN3=1.51
  115 A=AN2(N)*AN2(N)-AK2(K)*AK2(K)-S(L)*S(L)
      B=4.*AN2(N)*AN2(N)*AK2(K)*AK2(K)
      USQ=(A+SQRT(A*A+B))/2.
      VSQ=(-A+SQRT(A*A+B))/2.
      U=SQRT(USQ)
      V=SQRT(VSQ)
      P=SQRT(1.-S(L)*S(L))
      Q=SQRT(AN3*AN3-S(L)*S(L))
      PSQ=P*P
      QSQ=Q*Q
      W=USQ+VSQ
C
C CALCULATE ANUMS
C
      PW1=(W/PSQ)+1.
      PW2=(W/PSQ)-1.
      QW1=(W/QSQ)+1.
      QW2=(W/QSQ)-1.
      UPQ=(4.*USQ)/(P*Q)
      VPQ=(4.*VSQ)/(P*Q)
      UQ=(2.*U)/Q
      UP=2.*U/P
      VQ=2.*V/Q
      VP=2.*V/P
      VDA=4.*3.14159*V*DL(I)
      UDA=4.*3.14159*U*DL(I)
      COSHVDA=(EXP(VDA)+EXP(-VDA))/2.
      SINHVDA=(EXP(VDA)-EXP(-VDA))/2.
      ANUMS1=(PW1*QW1-UPQ)*COSHVDA
      ANUMS2=(UQ*PW1-UP*QW1)*SINHVDA
      ANUMS3=(PW2*QW2+VPQ)*COS(UDA)
      ANUMS4=(VQ*PW2-VP*QW2)*SIN(UDA)
      ANUMS=ANUMS1+ANUMS2-ANUMS3+ANUMS4
C
C         CALCULATE DENOMS
C
      DENOMS1=(PW1*QW1+UPQ)*COSHVDA
      DENOMS2=(UQ*PW1+UP*QW1)*SINHVDA
      DENOMS3=(PW2*QW2-VPQ)*COS(UDA)
      DENOMS4=(VQ*PW2+VP*QW2)*SIN(UDA)
      DENOMS=DENOMS1+DENOMS2-DENOMS3+DENOMS4
```

```
      RPE=ANUMS/DENOMS
C CALCULATE RPA
C THE EQUATION FOR RPA IS OF
C THE SAME FORM AS THAT FOR RPE.
C THE U AND V IN THE COEFFS.
C ARE REPLACED BY X AND Y.
C P CHANGES TO P/(N1)**2.
C BUT N1 = 1.00 SO P WILL
C REMAIN UNCHANGED
C Q CHANGES TO Q/AN3*AN3
C AND WILL BE CALLED QN.
C W GOES OVER TO W/((AN2*AN2+AK2*AK2)**2.)
C AND IS CALLED WN.
C
C CALCULATE XX AND YY.
C
      DIFF=AN2(N)*AN2(N)-AK2(K)*AK2(K)
      SUM=AN2(N)*AN2(N)+AK2(K)*AK2(K)
      XNUM=(U*DIFF)+(2.*V*AN2(N)*AK2(K))
      XX=XNUM/(SUM*SUM)
      YNUM=(V*DIFF)-(2.*U*AN2(N)*AK2(K))
      YY=YNUM/(SUM*SUM)
C
C CALCULATE WN AND QN.
C
      WN=XX*XX+YY*YY
      QN =Q/(AN3*AN3)
      QNSQ=QN*QN
C
C NEW COEFFS. ARE SUFFIXED BY N
C
      PW1N=(WN/PSQ)+1.
      PW2N=(WN/PSQ)-1.
      QW1N=(WN/QNSQ)+1.
      QW2N=(WN/QNSQ)-1.
      XPNQN=(4.*XX*XX)/(P*QN)
      YPNQN=(4.*YY*YY)/(P*QN)
      XQN=(2.*XX)/QN
      XPN=(2.*XX)/P
      YQN=(2.*YY)/QN
      YPN=(2.*YY)/P
C
C CALCULATE ANUMP
C
      ANUMP1=((PW1N*QW1N)-XPNQN)*COSHVDA
      ANUMP2=((XQN*PW1N)-(XPN*QW1N))*SINHVDA
      ANUMP3=((PW2N*QW2N)+YPNQN)*COS(UDA)
      ANUMP4=((YQN*PW2N)-(YPN*QW2N))*SIN(UDA)
      ANUMP=ANUMP1+ANUMP2-ANUMP3+ANUMP4
C
C CALCULATE DENOMP
C
      DENOMP1=((PW1N*QW1N)+XPNQN)*COSHVDA
      DENOMP2=((XQN*PW1N)+(XPN*QW1N))*SINHVDA
      DENOMP3=((PW2N*QW2N)-YPNQN)*COS(UDA)
      DENOMP4=((YQN*PW2N)+(YPN*QW2N))*SIN(UDA)
      DENOMP=DENOMP1+DENOMP2-DENOMP3+DENOMP4
      RPA=ANUMP/DENOMP
```

```
      ROSQ(N)=RPA/RPE
      X(N)=ROSQ(N)
    3 CONTINUE
      CALL START1
      CALL SYMBOL(0.0,20.0,0.28,10HA.J.TAYLOR,0.0,10)
      CALL SYMBOL(0.0,18.0,0.28,22HROYAL HOLLOWAY COLLEGE,0.0,22)
      CALL PLOT(6.0,1.0,-3)
      CALL SCALE(Y(1),24.0,241,1)
      X(242)=0.0
      X(243)=0.02
      CALL AXIS(0.0,0.0,4HROSQ,-4,40.0,0.0,X(242),X(243))
      CALL AXIS(0.0,0.0,9HREF.INDEX,+9,24.0,90.0,Y(242),Y(243))
      CALL LINE(X,Y,241,1,0,1)
C REFILL X ARRAY
      DO 7 K=13,35,2
      AK2(K)=0.1*FLOAT(K)
    7 CONTINUE
      DO 4 K=13,35,2
      DO 6 N=1,241
      L=1
      I=1
      AN3=1.50
   15 A=AN2(N)*AN2(N)-AK2(K)*AK2(K)-S(L)*S(L)
      B=4.*AN2(N)*AN2(N)*AK2(K)*AK2(K)
      USQ=(A+SQRT(A*A+B))/2.
      VSQ=(-A+SQRT(A*A+B))/2.
      U=SQRT(USQ)
      V=SQRT(VSQ)
      P=SQRT(1.-S(L)*S(L))
      Q=SQRT(AN3*AN3-S(L)*S(L))
      PSQ=P*P
      QSQ=Q*Q
      W=USQ+VSQ
C
C CALCULATE ANUMS
C
      PW1=(W/PSQ)+1.
      PW2=(W/PSQ)-1.
      QW1=(W/QSQ)+1.
      QW2=(W/QSQ)-1.
      UPQ=(4.*USQ)/(P*Q)
      VPQ=(4.*VSQ)/(P*Q)
      UQ=(2.*U)/Q
      UP=2.*U/P
      VQ=2.*V/Q
      VP=2.*V/P
      VDA=4.*3.14159*V*DL(I)
      UDA=4.*3.14159*U*DL(I)
      COSHVDA=(EXP(VDA)+EXP(-VDA))/2.
      SINHVDA=(EXP(VDA)-EXP(-VDA))/2.
      ANUMS1=(PW1*QW1-UPQ)*COSHVDA
      ANUMS2=(UQ*PW1-UP*QW1)*SINHVDA
      ANUMS3=(PW2*QW2+VPQ)*COS(UDA)
      ANUMS4=(VQ*PW2-VP*QW2)*SIN(UDA)
      ANUMS=ANUMS1+ANUMS2-ANUMS3+ANUMS4
C
C     CALCULATE DENOMS
C
```

```
      DENOMS1=(PW1*QW1+UPQ)*COSHVDA
      DENOMS2=(UQ*PW1+UP*QW1)*SINHVDA
      DENOMS3=(PW2*QW2-VPQ)*COS(UDA)
      DENOMS4=(VQ*PW2+VP*QW2)*SIN(UDA)
      DENOMS=DENOMS1+DENOMS2-DENOMS3+DENOMS4
      RPE=ANUMS/DENOMS
C CALCULATE RPA
C THE EQUATION FOR RPA IS OF
C THE SAME FORM AS THAT FOR RPE.
C THE U AND V IN THE COEFFS.
C ARE REPLACED BY X AND Y.
C P CHANGES TO P/(N1)**2.
C BUT N1 = 1.00 SO P WILL
C REMAIN UNCHANGED
C Q CHANGES TO Q/AN3*AN3
C AND WILL BE CALLED QN.
C W GOES OVER TO W/((AN2*AN2+AK2*AK2)**2.)
C AND IS CALLED WN.
C
C CALCULATE XX AND YY.
C
      DIFF=AN2(N)*AN2(N)-AK2(K)*AK2(K)
      SUM=AN2(N)*AN2(N)+AK2(K)*AK2(K)
      XNUM=(U*DIFF)+(2.*V*AN2(N)*AK2(K))
      XX=XNUM/(SUM*SUM)
      YNUM=(V*DIFF)-(2.*U*AN2(N)*AK2(K))
      YY=YNUM/(SUM*SUM)
C
C CALCULATE WN AND QN.
C
      WN=XX*XX+YY*YY
      QN =Q/(AN3*AN3)
      QNSQ=QN*QN
C
C NEW COEFFS. ARE SUFFIXED BY N
C
      PW1N=(WN/PSQ)+1.
      PW2N=(WN/PSQ)-1.
      QW1N=(WN/QNSQ)+1.
      QW2N=(WN/QNSQ)-1.
      XPNQN=(4.*XX*XX)/(P*QN)
      YPNQN=(4.*YY*YY)/(P*QN)
      XQN=(2.*XX)/QN
      XPN=(2.*XX)/P
      YQN=(2.*YY)/QN
      YPN=(2.*YY)/P
C
C CALCULATE ANUMP
C
      ANUMP1=((PW1N*QW1N)-XPNQN)*COSHVDA
      ANUMP2=((XQN*PW1N)-(XPN*QW1N))*SINHVDA
      ANUMP3=((PW2N*QW2N)+YPNQN)*COS(UDA)
      ANUMP4=((YQN*PW2N)-(YPN*QW2N))*SIN(UDA)
      ANUMP=ANUMP1+ANUMP2-ANUMP3+ANUMP4
C
C CALCULATE DENOMP
C
      DENOMP1=((PW1N*QW1N)+XPNQN)*COSHVDA
```

```
      DENOMP2=((XQN*PW1N)+(XPN*QW1N))*SINHVDA
      DENOMP3=((PW2N*QW2N)-YPNQN)*COS(UDA)
      DENOMP4=((YQN*PW2N)+(YPN*QW2N))*SIN(UDA)
      DENOMP=DENOMP1+DENOMP2-DENOMP3+DENOMP4
      RPA=ANUMP/DENOMP
      ROSQ(N)=RPA/RPE
      X(N)=ROSQ(N)
    6 CONTINUE
    6 CONTINUE
      CALL LINE(X,Y,241,1,0,1)
    4 CONTINUE
      CALL ENPLOT(46)
      END
```

COMPILER SPACE

APPENDIX III

Electropolishing of Stainless Steel

A suitable solution for electropolishing stainless steel components for high vacuum systems can be made by preparing a saturated solution of chromium-trioxide in orthophosphoric acid at a temperature of 50° - 60°C. This solution is best made in-situ in a stainless steel beaker or tank, so that the walls of the beaker or tank form the cathode of the electropolishing bath. The solution is used at a temperature of $\sim 50^{\circ}$C.

The object to be electropolished is made the anode and is immersed in the solution so that it is symmetrically placed with respect to the beaker walls. This precaution ensures an even polish.

It was found that for the objects described in this thesis a current density of 1 - 2 amps. per. sq. cm. was sufficient to obtain a good polish. Polishing times were of the order of 2 - 5 minutes.

REFERENCES

Abelès, F., 1963, Progr. Opt., 2, 251, Ed., E. Wolf, (Amsterdam: North Holland)

Abelès, F., 1952, Proc. Phys. Soc., B65, 996.

Alpert, D., 1962, Le Vide, 17, 19.

Anders, H., 1967, 'Thin Films in Optics', (London: Focal Press).

Apgar, E., 1963, Proc. 2nd European Vac. Symp., p.233.

Archard, J.F., Clegg, P.L., Taylor, A.M., 1952, Proc. Phys. Soc., 65, 758.

Archer, R.J., 1962, J. Opt. Soc. Am., 52, 970.

Avery, D.G., 1952, Proc. Phys. Soc., B65, 425.

Bennett, H.E., and Porteus, J.O., 1961, J. Opt. Soc. Am., 51, 123.

Berglund, C.N., and Spicer, W.E., 1964a, Phys. Rev., 136A, 1030.

Berglund, C.N., and Spicer, W.E., 1964b, Phys. Rev., 136A, 1044.

Berreman, D.W., 1970, J. Opt. Soc. Am., 60, 499.

Berreman, D.W., 1970, Phys. Rev., 1B, 381.

Blears, J., 1947, Proc. Roy. Soc. (London), A188, 62.

Blodgett, A.J., Spicer, W.E., and Yu, A.Y.C., 1966, "Optical properties and electronic structure of metals and alloys", Ed. F. Abeles (Amsterdam: N. Holland), pp.237-245.

Bode, H.W., 1945, "Network analysis and feedback amplifier design", (New York: van Nostrand).

Born, M., and Wolf, E., 1964, "Principles of Optics", (London: Pergamon).

Brahms, J., Pilet, J., Damany, H., and Chandrasekharan, V., 1968, Proc. Nat. Acad. Sci., 60, 1130.

Callaway, J., 1958, "Electron Energy Bands in Solids", (London: Academic Press).

Caswell, A., 1961, Symposium on the Electric and Magnetic Properties of Thin Metallic Layers, (Lourain).

Cobic, B., Carter, G., and Leck, J.H., 1961, Brit. J. Appl. Phys., 12, 288.

Cobic, B., Carter, G., and Leck, J.H., 1961, Brit. J. Appl. Phys., 12, 384.

Cobic, B., Carter, G., and Leck, J.H., 1961, Vacuum, 11, 247.

Cooper, B.R., and Redington, R.W., 1965, Phys. Rev. Letters, 14, 1066.

Collins, J.R., and Bock, R.O., 1943, Rev. Sci. Instr., 14; 135.

Cornwall, J.F., 1965, For details see Schüler (p.227, 1966).

Davis, E.A., and Mott, N.F., 1970, Phil. Mag., 22, 903.

Davis, E.A., and Shaw, R.F., 1970, J. Non-Crystalline Solids, 2, 406.

Davis, E.A., 1971, Phys. Bull., 22, 81.

Davis, W.D., 1962, Trans. AVS. Vac. Symp., 9, 363.

Dimmock, J.O., and Freeman, A.J., 1964, Phys. Rev. Letters, 13, 750.

Dimmock, J.O., Freeman, A.J., and Watson, R.E., 1966, "Optical Properties and Electronic Structure of Metals and Alloys", Ed. F. Abeles (Amsterdam: N. Holland), pp.237-245.

Ditchburn, R.W., 1955, J. Opt. Soc. Am., 45, 743.

Donovan, T.M., Spicer, W.E., and Bennett, J.M., 1969, Phys. Rev. Letters, 22, 1058.

Dow, J.D., and Redfield, D., 1970, Phys. Rev., B1, 3358.

Drude, P., 1890, Wied, Ann. d. Phys., 39, 481.

Drude, P., 1888, Wied. Ann. d. Phys., 34, 489.

Edmond, J.T., 1966, J. Phys. D. (J. Appl. Phys.), 17, 979.

Ellerbroek, J., 1927, Arch. Neerland., Sci., III, A10, 42.

Elliott, R.J., and Wedgwood, F.A., 1963, 81, 846.

Elliott, R.J., and Wedgwood, F.A., 1964, 84, 63.

E.M.I. Ltd., 1968, E.M.I., Photomultiplier Handbook.

Endriz, J.G., and Spicer, W.E., 1970, Phys. Rev., 2B, 1466.

Francombe, M.H., 1966, "The use of thin films in physical investigations", Ed. J.C. Anderson, (London: Academic Press).

Freeman, A.J., Dimmock, J.O., and Watson, R.E., 1966, Phys. Rev. Letters, 16, 94.

Freeman, A.J., Dimmock, J.O., and Frudyna, A.M., Phys. Rev. (to be published).

Gosselin, C.M. and Bryant, P.J., 1965, J. Vac. Sci. and Technol., 2, 293.

Greef, R., 1970, Rev. Sci. Instr., 41, 532.

Hadley, L.N. and Dennison, D.M., 1947, J. Opt. Soc. Am., 37, 451.

Hadley, L.N., Curves obtainable from L. Hadley, Colorado State University, Colorado.

Heavens, O.S., 1965 "Optical Properties of Thin Solid Films" (London: Butterworths).

Heavens, O.S., 1964, "Physics of Thin Films", 2, 193. Ed. G. Hass, (London: Academic Press)

Heavens, O.S., 1960, Reports on Progress in Physics, 23, 1. Ed. A. C. Stickland (London: Institute of Physics).

Herman, F. and van Dyke, J.P., 1968, Phys. Rev. Letters, 21, 1575.

Herschkowitsch, M., 1931, Ann. d. Phys., 10, 993.

Hickmott, T.W., 1960, J. Appl. Phys., 31, 128.

Hirsch, P.B., Howie, A., Nicholson, R.B., Pashley, D.W., Whelan, M.J., 1965, "Electron Microscopy of Thin Crystals", (London: Butterworths).

Holland, L., 1958, "Vacuum Deposition of Thin Films", (London: Chapman and Hall).

Hodgson, J.N. and Cleyet, B., 1970, J. Phys. C. (Solid State Phys.), 2, 97.

Huber, W.K., 1966, Le Vide, 21, 202.

Humphreys-Owen, S.P.F., 1961, Proc. Phys. Soc., 77, 949.

Hunter, W.R., 1965, J. Opt. Soc. Am., 55, 1197.

Ives, H.E. and Briggs, H.B., 1936, J. Opt. Soc. Am., 26, 238.

Jackson, C., 1969, Phys. Rev., 178, 949.

Jennings, L.D., Miller, R.E. and Spedding, F.H., J. Chem. Phys., 33, 1849.

Johnson, P.D., 1952, J. Opt. Soc. Am., 42, 978.

Julien, L.S., 1971, Unpublished, see reference Miller et al. (1971).

Julien, L.S., 1971, Unpublished results obtained in the U.H.V. system described in this thesis.

Keeton, S.C., and Loucks, T.L., 1966, Phys. Rev., 146, 429.

Keeton, S.C., and Loucks, T.L., 1968, Phys. Rev., 168, 672.

Kent, C.V., and Lawson, J., 1937, J. Opt. Soc. Am., 27, 117.

Kern, E., 1957, Z. Physik, 148, 38.

Kleber, E.V., and Love, B., 1963, "Technology of Scandium, Yttrium and the Rare-Earth Metals", (London: Pergamon Press).

Klopfer, A., 1961, Vakuum Technik., 10, 113.

Krinchik, G.S., 1959, Fiz. Metal. Metalloved., 7, 181.

Krinchik, G.S., and Chetkin, M.V., 1959, Sov. Phys. JETP., 36, 1368.

Krinchik, G.S., 1964, J. Appl. Phys. (U.S.A.), 35, 1089.

Krinchik, G.S., and Gushchin, V.S., 1969, Sov. Phys. JETP., 29, 984.

Krinchik, G.S., and Artem'eV, V.A., 1968, Sov. Phys. JETP, 26, 1080.

Krinchik, G.S., and Gushchin, V.S., 1969, Sov. Phys. JETP, 29, 984.

Kuhn, H., and Wilson, B.A., 1950, Proc. Phys. Soc., B63, 745.

Lahiri, S.K., and Wells, O.C., 1969, Appl. Phys. Letters, 15, 234.

Lindquist, R.E., and Ewald, A.W., 1963, J. Opt. Soc. Am., 53, 247.

Loucks, T.L., 1966, Phys. Rev., 144, 504.

Loucks, T.L., 1967, "Augmented Plane Wave Calculations", (New York: Benjamin).

McCrackin, F.L., Passaglia, E., Stromberg, R., and Steinberg, H.L., "Measurement of the thickness and refractive index of very thin films and the optical properties of surfaces by ellipsometry", 1963, J. Res. Nat. Bur. Std., 67A, 363.

Malé, D., 1950, C.R. Acad. Sci., (Paris), 230, 1349.

Miller, R.F., 1962, Ph.D. Thesis, p.71, University of London.

Miller, R.F., 1965, Brit. J. Appl. Phys., 16, 353.

Miller, R.F., Taylor, A.J., and Julien, L.S., 1970, J. Phys. D. (J. Appl. Phys.), 3, 1957.

Miller, R.F., Julien, L.S., and Taylor, A.J., 1971, J. Phys. D. (J. Appl. Phys.), 4, 1100.

Miller, R.F., and Taylor, A.J., 1971, J. Phys. D. (J. Appl. Phys.), 4, 1419.

Moeller, C.E., and Grieser, D.R., , Appl. Opt., 8, 206.

Müller, W.E., 1965, Phys. Letters, 17, 82.

Müller, W.E., 1967, Phys. Kondensierten Materie, 6, 243.

Nag, A., and Ward, L., 1971, J. Phys. D: Appl. Phys., 4, 829.

Nigh, H., Legvold, S., and Spedding, F.H., 1963, Phys. Rev., 132, 1092.

O'Bryan, H.M., 1936, J. Opt. Soc. Am., 26, 122.

Pells, G.P., 1967, J. Sci. Instr., 44, 997.

Pells, G.P., and Shiga, M., 1969, J. Phys. C. (Solid State Phys.), 2, 1835.

Pfestorf, F., 1926, Ann. d. Phys., 81, 906.

Potter, R.F., 1965, Appl. Opt., 4, 53.

Power, B.D., 1966, "High Vacuum Pumping Equipment", (New York: Reinhold).

Querry, M.R., 1969, J. Opt. Soc. Am., 59, 876.

'Rare Earth Products Ltd.,' 1970, A Catalogue of rare earth metals, available from 'Rare Earth Products Ltd.' Widnes, Lancashire.

Redhead, P.A., and Hobson, J.P., 1965, Brit. J. Appl. Phys., 16, 1555.

Redhead, P.A., Hobson, J.P., and Kornelsen, E.V., 1968, "The Physical Basis of Ultra-High Vacuum", (London: Chapman and Hall).

Robin, S., 1966, "Optical Properties of Metals and Alloys", Ed. R. Abelès, p.208, (Amsterdam: North Holland).

Rowell, R.L., Levit, A.B., and Aval, G.m., 1969, Appl. Opt., 8, 1734.

Schopper, H., 1952, Z. Phys., 131, 215.

Schüler, C., 1963, Z. Angew. Physik., 15, 218.

Schüler, C.C., 1964, Phys. Letters, 12, 84.

Schüler, C.C., 1966, "Optical Properties and electronic structure of metals and alloys", Ed. F. Abelès, pp.221-236, (Amsterdam: North Holland).

Schulz, L.G., 1954, J. Opt. Soc. Am., 44, 357.

Sell, D.D., 1971, Appl. Opt., 9, 1926.

Shiga, M., Pells, G.P., 1969, J. Phys. C. (Solid State Phys.), 2, 1847.

Simon, I., 1951, J. Opt. Soc. Am., 41, 336.

Singleton, J., and Lange, W.J., 1965, J. Vac. Sci. and Technol., 3, 354.

Singleton, J.H., 1967, J. Vac. Sci. and Technol., 4, 103.

S.I.R.A., Results obtained by M.J. Shadbolt, S.I.R.A. Institute, Chislehurst, Kent.

Slater, J.C., 1937, Phys. Rev., 51, 846.

Slater, J.C., 1953, Phys. Rev., 92, 603.

Spicer, W.E., and Donovan, T.M., 1970, J. Non-Crystalline Solids, 2, 66.

Taylor, K.N.R., 1970, Contemp. Phys., 11, 423.

Tolansky, S., "Multiple beam interferometry of surfaces and films", (Oxford: University Press).

Tolansky, S., 1970, "Multiple beam interference microscopy of metals", Cha. 10, (London: Academic Press).

Tomlin, S.G., 1968, J. Phys. D: Appl. Phys., 1, 1667.

Tool, A.Q., 1910, Phys. Rev., 31, 1.

Tousey, R., 1939, J. Opt. Soc. Am., 29, 235.

Trifonov, D.N., 1963, "The Rare Earth Elements", (London: Pergamon Press).

Tuzi, Y., 1962, J. Phys. Soc. (Japan), 17, 218.

Vasicek, A., 1960, "Optics of Thin Films", (Amsterdam: North Holland).

Vratny, F., 1961, J. Chem. Phys., 34, 1377.

Ward, L., and Nag, A., 1967, J. Phys. D: Appl. Phys., 18, 277.

Ward, L., and Nag, A., 1967, J. Phys. D: Appl. Phys., 18, 1629.

Williams, R.W., Loucks, T.L., and Mackintosh, A.R., 1966, Phys. Rev. Letters, 16, 168.

Winterbottom, A.B., 1955, "Optical Studies of metal surfaces", (Trondheim: Bokhandel).

R.H.C. LIBRARY

ACKNOWLEDGMENTS

I gratefully acknowledge the help of my supervisor, Dr. R.F. Miller, who has given much encouragement and able assistance throughout the work described in this thesis. His help with finding the necessary finances to enable the experimental work to be done is also gratefully acknowledged.

My thanks are also due to my colleague, Mr. L.S. Julien; we have shared some stimulating conversations covering certain aspects of the work described in this thesis.

I would also like to thank the following technicians:

Mr. R. Elton and Mr. G. Hayward for constructing the reflectometer and the accessories that went with it.

Mr. J. Williams for help with the work on terbium and terbium oxide.

Mr. M. Thyer for some lighthearted and not so lighthearted suggestions on how to deposit thin films in ordinary high vacuum. His help with the multiple beam interferometry is also appreciated.

Finally I would simply like to thank Miss H.B.L. Glover-Thierens.

Thanks are also due to people outside College.

Mrs. C. Smith has done an excellent job in typing the thesis.

I would also like to thank the Science Research Council for an S.R.C. Studentship and the Paul Instrument Fund for finances to purchase equipment.

The optimum angle of incidence for determining optical constants from reflectance measurements

R. F. MILLER, A. J. TAYLOR and L. S. JULIEN

Department of Physics, Royal Holloway College, University of London, Englefield Green, Surrey

MS. received 9th July 1970

Abstract. The shape of the boundary enclosing analytical solutions to the generalized Fresnel reflectance equations for n and k in terms of reflectances and angle of incidence has been investigated and the optimum angle of incidence for experimental measurement determined to be 74°. The distribution of reflectance values for fixed n and k for which the method is accurate to within $\pm 0{\cdot}05$ has been deduced to be $n<3{\cdot}0$ and $k<3{\cdot}2$.

1. Introduction

In order to investigate the optical constants of metals, it was desired to determine n, the refractive index, and k, the extinction coefficient, by measuring the reflectances $R_{\parallel}$ and $R_{\perp}$ of light polarized respectively parallel and perpendicular to the plane of incidence, at an angle of incidence θ. The generalized Fresnel equations correlating these quantities have been solved analytically by Querry (1969) for all angles except 0° and 45° and can therefore be used to evaluate n and k as required.

Since the experimental method consists of measuring $R_{\perp}$ and $R_{\parallel}$ for a given θ, it is of interest (*a*) to determine which value or values of θ give the best sensitivity to changes in n and k, and (*b*) for what ranges of n and k the method is experimentally useful. In the following discussion, it is shown that Querry's analysis can be extended by examining the boundary values for $R_{\perp}$, $R_{\parallel}$ and θ which satisfy Fresnel's equations. The useful range of n and k to which the method can be applied is obtained by plotting $R_{\perp}$ and $R_{\parallel}$ for a series of fixed n and k, at the optimum θ.

2. Determination of the boundary, in ($R_{\perp}$, $R_{\parallel}$, θ) space, enclosing values which satisfy Fresnel's equations

Querry's solution to the Fresnel reflectance equations may be summarized as follows: Making the substitutions

$$F=\frac{(R_{\perp}+1)}{(R_{\perp}-1)} \tag{1}$$

$$G=\frac{(R_{\parallel}+1)}{(R_{\parallel}-1)} \tag{2}$$

and putting

$$Q=\frac{(F-G)\sin\theta\cot 2\theta}{GF+(1-F^2)\cos^2\theta-1} \tag{3}$$

$$P^2=-Q^2-2FQ\cos\theta-\cos^2\theta \tag{4}$$

into Fresnel's reflectance equations in the form

$$R_{\perp}=\frac{(Q-\cos\theta)^2+P^2}{(Q+\cos\theta)^2+P^2} \tag{5}$$

$$R_{\parallel}=R_{\perp}\frac{(Q-\sin\theta\tan\theta)^2+P^2}{(Q+\sin\theta\tan\theta)^2+P^2} \tag{6}$$

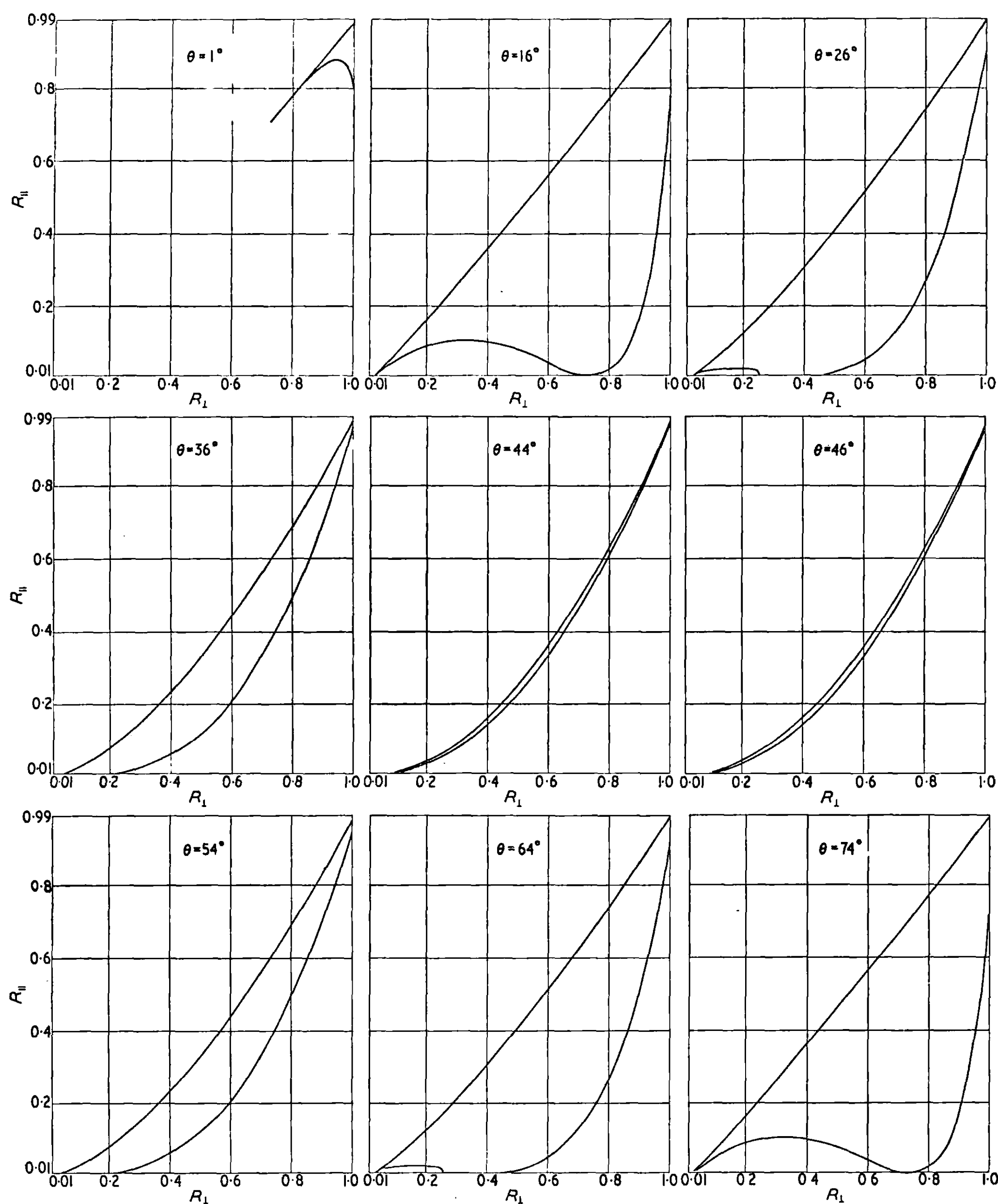

Figure 1. Boundaries enclosing all possible solutions to the Fresnel reflectance equations.

then

$$(Q^2-P^2)=n^2-k^2-\sin^2\theta \tag{7}$$

and

$$QP=nk \tag{8}$$

F and G are functions of the observables $R_{\perp}$ and $R_{\parallel}$ only. Therefore P and Q can be calculated for a given θ, and by substituting in (7) and (8), n and k are obtained.

Equation (3) shows Q to be real, and therefore real n and k are only obtained for real P in (8). It follows that solutions satisfying the Fresnel equations are only obtained for $P^2>0$. The condition $P^2=0$ delineates a boundary for these solutions, and it is readily shown that on one side of this boundary P is indeed imaginary, i.e. the boundary does not merely indicate a zero minimum value for P^2. Substituting for Q from (3) into (4) we get:

$$P^2=-\left(\frac{(F-G)\sin\theta\cot 2\theta}{GF+(1-F^2)\cos^2\theta-1}\right)^2-\frac{2F\cos\theta(F-G)\sin\theta\cot 2\theta}{GF+(1-F^2)\cos^2\theta-1}-\cos^2\theta. \tag{9}$$

Rearranging,

$$\begin{aligned}P^2=&G^2\{\sin^2\theta\cot^2 2\theta+F^2\cos\theta(\cos\theta-2\sin\theta\cot 2\theta)\}\\&+G[2F\cos\theta(\cos\theta-\sin\theta\cot 2\theta)\{(1-F^2)\cos^2\theta-1\}\\&+2F\sin\theta\cot 2\theta(F^2\cos\theta-\sin\theta\cot 2\theta)]\\&+F^2\sin^2\theta\cot^2 2\theta+2F^2\cos\theta\sin\theta\cot 2\theta\{(1-F^2)\cos^2\theta-1\}\\&+\cos^2\theta\{(1-F^2)\cos^2\theta-1\}^2.\end{aligned} \tag{10}$$

P^2 is thus a quadratic function of G, which changes sign when

$$aG^2+bG+c=0 \tag{11}$$

where a, b and c are the functions of F and θ indicated by equation (10). The solutions of (11), when transformed to the $(R_\perp, R_\parallel, \theta)$ space, via (1) and (2), bound the region for which all real n and k values may be obtained. This boundary also represents the condition $k=0$, since if

$$P^2=\tfrac{1}{2}[\{(n^2-k^2-\sin^2\theta)^2+4n^2k^2\}^{1/2}-(n^2-k^2-\sin^2\theta)]=0 \tag{12}$$

then

$$4n^2k^2=0 \tag{13}$$

and therefore

$$k=0 \tag{14}$$

i.e. the boundary values of $R_\perp$ and $R_\parallel$ are those corresponding to perfect dielectrics.

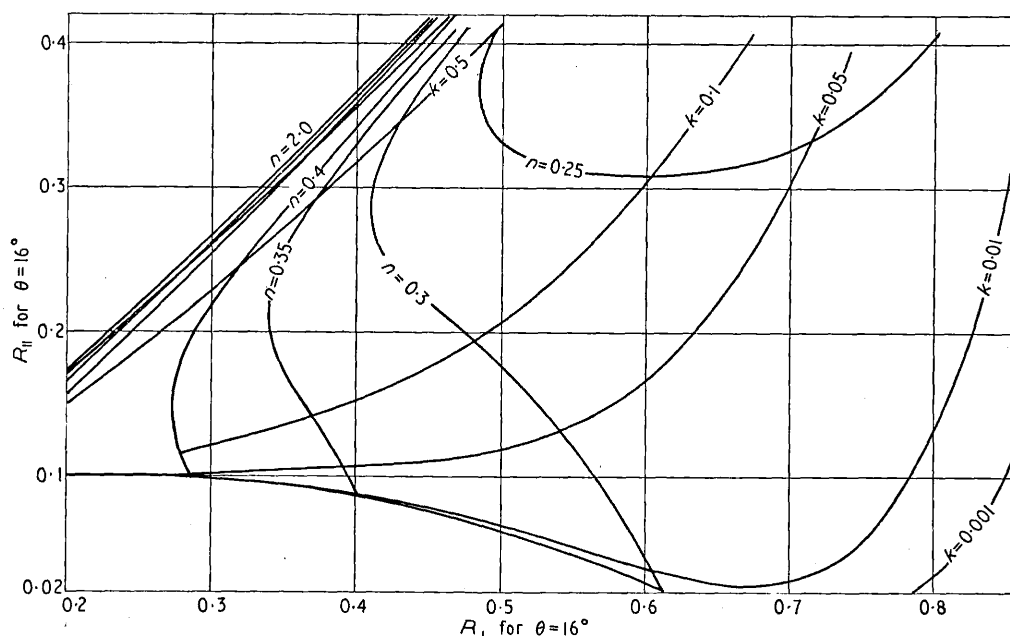

Figure 2. Distribution of n and k loci for $\theta=16°$.

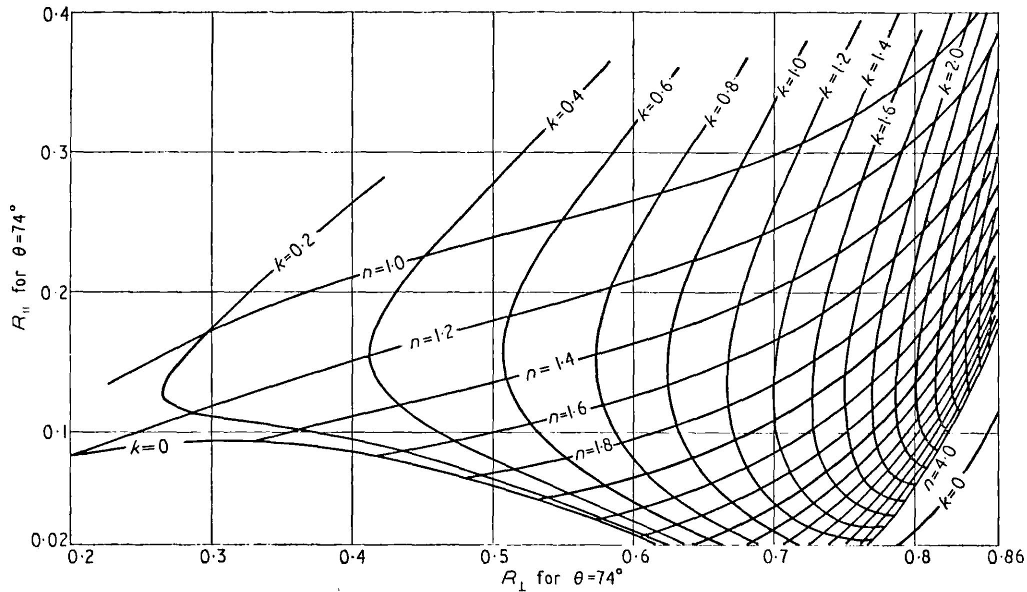

Figure 3. Distribution of n and k loci for $\theta=74$ °.

Figure 1 shows sections of the boundary within which solutions for real n and k exist, for a range of angles θ between 0 and 90 °, obtained by computer, using the $P^2 \geqslant 0$ condition. Loci have also been plotted of $R_{\perp}$ and $R_{\parallel}$ values for which n or k are fixed, and it is found that the distributions of these n and k loci are similar within the ranges $0° < \theta < 45°$ and $45° < \theta < 90°$ (figures 2 and 3).

The 'bunching' of n and k loci which occurs near the upper boundary for $0° < \theta < 45°$ changes to the lower boundary for $45° < \theta < 90°$ as θ passes through 45 °. This bunching is associated with high values of n, and arises from the rapid approach of Q to $+\infty$ as Q changes sign:

$$(Q^2)_{P^2=0} = n^2 - k^2 - \sin^2 \theta. \tag{15}$$

If the $Q>0$ boundary is close to one of the $P^2=0$ solutions, then $k^2 \to 0$ in (15). For $(Q^2)_{P^2=0}$ to go to $+\infty$, n^2 must tend to $+\infty$.

3. Sensitivity of n and k to $R_{\perp}$ and $R_{\parallel}$

All points ($R_{\perp}$, $R_{\parallel}$) generated by all possible n and k, for a given θ, are contained in the area enclosed by the $P^2=0$ boundary transformed to the $R_{\perp}$, $R_{\parallel}$ plane. The most sensitive measurements of n and k can therefore be performed for angles θ such that this area is largest, since the largest change in $R_{\perp}$ and $R_{\parallel}$ will be produced at these angles for a given change in n and k. Numerical integration shows that the maximum area, and therefore the best values of θ, occurs at 16 ° and 74 ° (figure 1). Empirical observation, rather than exact analysis, has previously indicated the most sensitive angle to be about 70 ° (Humphreys-Owen 1961). The area of the bounded region is in any case stationary with respect to θ at 16 ° and 74 °, and therefore small changes in θ near these values will not greatly affect the results.

The distributions of n and k loci within the bounded regions at the best angles demonstrate the ranges of n and k to which the method may usefully be applied. In figure 2, for $\theta=16$ °, the loci corresponding to values of n and k which are of practical interest are so close together that accurate determination from measurements of $R_{\perp}$ and $R_{\parallel}$ are impossible. Figure 3 shows 74 ° to be practically useful, the distribution being such that $R_{\perp}$ and $R_{\parallel}$ are sensitive to n and k values normally observed.

The precise range of n and k for which the method is acceptably sensitive can be found by determining the $R_\perp$ and $R_\parallel$ values for which an acceptable uncertainty in n and k produce a typical experimental uncertainty in $R_\perp$ and $R_\parallel$. Assuming n and k are required within $\pm 0{\cdot}05$, and the reflectances are measurable to within $\pm 0{\cdot}004$, the method is found to be applicable for $n < 3{\cdot}0$ and $k < 3{\cdot}2$. This region of usefulness is included in figure 3.

4. Conclusion

The shape of the boundary in $(R_\perp, R_\parallel, \theta)$ space, which includes all possible solutions for n and k from the Fresnel reflectance equations has been determined. Consequently the optimum angle θ, for the determination of n and k, from measurements of $R_\perp$ and $R_\parallel$ has been found to be 74°, and the useful ranges of n and k to which the method is applicable have been found to be $n < 3{\cdot}0$ and $k < 3{\cdot}2$.

Acknowledgments

We wish to thank Dr F. G. Kingston for assistance with the computing, and the Science Research Council for an SRC Studentship (AJT).

References

Querry, M. R., 1969, *J. Opt. Soc. Am.*, **59**, 876–7.
Humphreys-Owen, S. P. F., 1961, *Proc. Phys. Soc.*, **77**, 949–57.

J. Phys. D: Appl. Phys., 1971, Vol. 4. Printed in Great Britain

An analysis of the errors in optical constants obtained from reflectance measurements

R. F. MILLER, L. S. JULIEN and A. J. TAYLOR

Department of Physics, Royal Holloway College, University of London, Englefield Green, Surrey

MS. received 2nd March 1971

Abstract. For n and k in the ranges $1{\cdot}0 \leqslant n \leqslant 4{\cdot}0$, $1{\cdot}0 \leqslant k \leqslant 4{\cdot}0$, a computer study has been made of the way in which large errors in n and k may arise from errors in reflection coefficients, when the latter are measured at angles of incidence other than 74°. It is shown, as an example, that at near normal incidence errors in the product nk of $\pm 76\%$ are possible for $n = 2{\cdot}00$, $k = 3{\cdot}00$ when the measured reflection coefficient is in error by $\pm 0{\cdot}001$.

1. Introduction

In a previous paper (Miller *et al.* 1970) the general solution to the Fresnel reflectance equations (Querry 1969) was used to obtain an optimum angle of incidence, 74°, for measuring optical constants n and k from reflectance measurements. We now investigate in more detail how changes in the values deduced for n and k, produced by small changes in the measured reflection coefficients $R_\perp$ and $R_\parallel$, depend on the angle of incidence θ. $R_\perp$ and $R_\parallel$ are the respective reflection coefficients for incident light polarized perpendicular and parallel to the plane of incidence. The values of n and k were selected to be in the ranges $1{\cdot}0 \leqslant n \leqslant 4{\cdot}0$, $1{\cdot}0 \leqslant k \leqslant 4{\cdot}0$ (ie values relevant to the optical properties of metals in the visible region). Computer programs, written for a CDC 6600 computer, allowed a study of a large number of combinations of the parameters concerned. In particular, reflection coefficients measured near normal incidence have been shown to be insensitive to changes in n and k. Specific examples are used to illustrate our work.

2. Method for error investigation

The basis of the method is shown in figure 1. For an arbitrary value of θ, the bounded region in the $(R_\perp, R_\parallel)$ plane includes all values of $R_\perp$ and $R_\parallel$ which will give solutions to the Fresnel equations. A point P within this boundary is related to unique values of the optical constants n_0 and k_0 via the generalized Fresnel reflectance equations. If there is an uncertainty in the reflection coefficients of $\pm\Delta R$, then the extreme deviant values of optical constants, n and k, will be obtained from points lying on the perimeter of a square of edge $2\Delta R$ drawn with P as centre. These values of n and k are computed for 400 equally spaced points on the perimeter, assuming $\Delta R = \Delta R_\perp = \Delta R_\parallel$, independent of $R_\perp$ and $R_\parallel$.

The product of the optical constants nk was chosen as a suitable parameter for the investigation because of its relevance to band structure calculations. The fractional error in the product $n_0 k_0$ for a point on the square is given by

$$\sigma = \frac{n_0 k_0 - nk}{n_0 k_0}.$$

Products nk for which σ took the largest positive and negative values were determined using a computer search technique. The values of σ associated with these nk products represent the maximum positive and negative errors resulting from uncertainties $\pm\Delta R$ in the reflection coefficients.

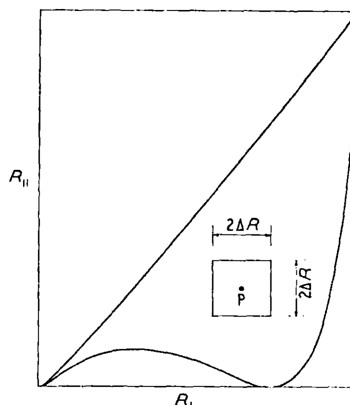

Figure 1. Boundary enclosing all possible solutions to the Fresnel reflectance equations, for an arbitrary value of θ.

3. Angular dependence of σ

The method described in the previous section was used to calculate σ for a large number of combinations of n_0 and k_0 in the ranges $1\cdot0 \leqslant n_0 \leqslant 4\cdot0$, $1\cdot0 \leqslant k_0 \leqslant 4\cdot0$ and for angles of incidence in the range $0 < \theta < \pi/2$ ($\theta \neq \pi/4$). We choose $n_0 = 2\cdot00$ and $k_0 = 3\cdot00$ to typify our results. The point $n_0 = 2\cdot00$, $k_0 = 3\cdot00$ lies close to the upper boundary of the valid region in ($R_{\perp}$, $R_{\parallel}$) space for values of $\theta < \pi/4$, and close to the lower boundary for values of $\theta > \pi/4$ (see figures 1, 2 and 3 of our previous paper).

Figure 2 shows the variation with θ of the largest positive and negative percentage errors in the product n_0k_0 for $\Delta R = \pm 0\cdot000\,05$. The latter value appears to be the best accuracy currently obtained in reflectance measurements. The two broad minima (figure 2) are in accordance with the results shown in our previous paper which clearly identified two regions of maximum sensitivity at $\theta = 16°$ and $\theta = 74°$. Furthermore, the shallower of the two minima occurs for large θ (shown in our previous paper to be that region of θ most sensitive for the determination of optical constants from reflectance measurements in the range $n_0 \leqslant 3\cdot0$ and $k_0 \leqslant 3\cdot2$). This broad shallow minimum indicates the existence of a large range of θ at which accurate determinations of n_0 and k_0 may be made. Catastrophic behaviour occurs as θ approaches $0°$ and $45°$: σ increases significantly and, beyond the points at which the curves are discontinued, the possibility exists of values of $R_{\perp}$ and $R_{\parallel}$,

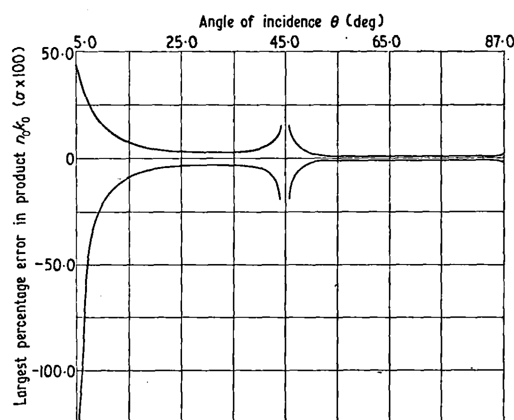

Figure 2. Angular dependence of the largest percentage error in the product n_0k_0 (ie $\sigma \times 100\%$, for $\Delta R = \pm 0\cdot00005$, $n_0 = 2\cdot00$, $k_0 = 3\cdot00$).

within the range $\pm\Delta R$, to produce non-valid solutions to the Fresnel equations (eg negative values for k).

For a modest degree of accuracy $\Delta R=\pm 0{\cdot}001$ and the same optical constants $n_0=2{\cdot}00$ and $k_0=3{\cdot}00$, figure 3 shows a shape similar to figure 2. However, the minima have sharpened and there is a dramatic increase in σ as θ approaches 0° and 45°. Parts of the

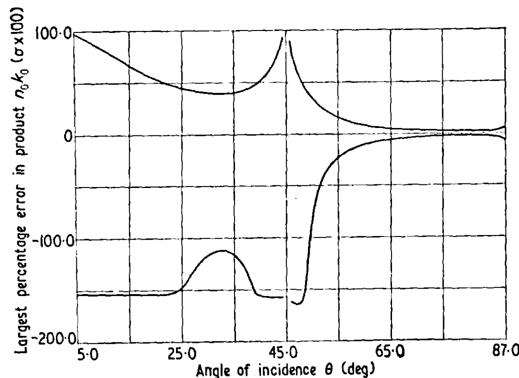

Figure 3. Angular dependence of the largest percentage error in the product n_0k_0 (ie $\sigma\times 100\%$, for $\Delta R=\pm 0{\cdot}001$, $n_0=2{\cdot}00$, $k_0=3{\cdot}00$).

negative curve in figure 3 show little variation with σ for $\theta<45°$. In our previous paper (Miller *et al.* 1970) we have shown that for $\theta=16°$ the point $n_0=2{\cdot}00$, $k_0=3{\cdot}00$ will be near to a boundary in the $R_{\parallel}$, $R_{\perp}$ plane. We showed that close to such a boundary $n\rightarrow\infty$, $k\rightarrow 0$. Further numerical work showed that the product nk passes through a maximum near this boundary. For $\Delta R=\pm 0{\cdot}001$, $n_0=2{\cdot}00$, $k_0=3{\cdot}00$, the perimeter of the test square approaches the ($R_{\parallel}$, $R_{\perp}$) boundary and therefore the computer search technique locates the above maximum for certain values of θ. From figure 3 it is seen that the maximum in the nk product maintains a fairly constant value in this range of θ. Even so, the individual errors associated with n_0 and k_0 may still increase rapidly. For different values of n_0 and k_0 our work indicates that the general shape of the σ against θ curves remains the same, but differs only in detail.

Previous work has indicated that $\theta=74°$ is the best angle for determining optical constants from reflectance measurements. In figure 4 the angular positions at which minimum σ

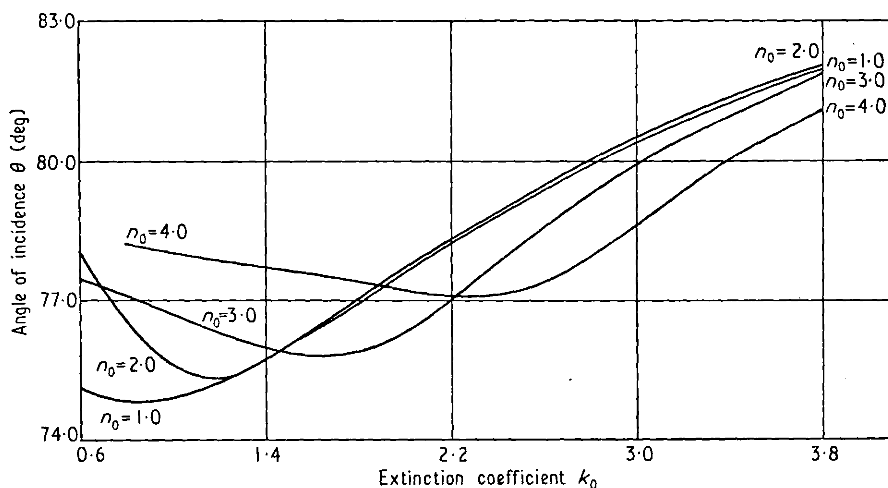

Figure 4. Angles for which the value of σ is smallest for $\Delta R=\pm 0{\cdot}001$.

occur have been plotted for a number of combinations of n_0 and k_0 for $\Delta R = \pm 0{\cdot}001$. If, for example, $n_0 = 2{\cdot}00$ and $k_0 = 3{\cdot}00$, figure 4 shows 80·5 ° to be the angle of incidence for greatest sensitivity. If this angle is used instead of the 'optimum' 74 °, figure 3 shows the gain in accuracy in $n_0 k_0$ to be only 0·5 %.

4. Variation of σ with ΔR

It was of practical interest to see how the value of σ varied with known errors ΔR in the reflection coefficient. Figure 5 shows the results of this study for the optimum angle 74 ° and for $n_0 = 2{\cdot}00$ and $k_0 = 3{\cdot}00$. For ΔR less than $\pm 0{\cdot}005$ the positive and negative portions of the graph are symmetrically placed about the line $\sigma = 0$, and σ varies linearly with ΔR. Above this value of ΔR the negative portion of the curve varies more rapidly, owing to the 'bunching' effect of the constant n and k curves shown on a plot of $R_\perp$ against $R_\parallel$ at 74 ° (see figure 3 of our previous paper).

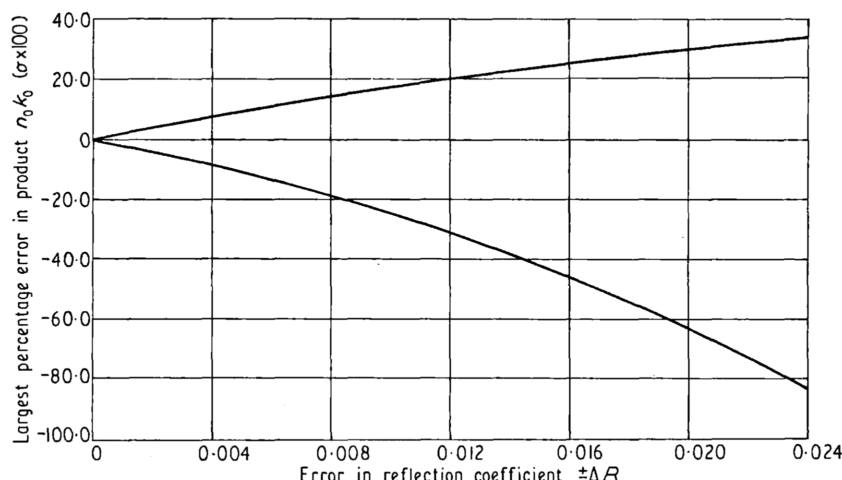

Figure 5. Variation of σ with ΔR for $n_0 = 2{\cdot}00$, $k_0 = 3{\cdot}00$, $\theta = 74$ °.

5. Normal incidence measurements

In this section we shall consider the errors likely to occur in normal incidence reflection methods for obtaining the optical constants n_0 and k_0. Such methods measure one reflection coefficient for a range of optical frequencies ω. At normal incidence $R_\perp = R_\parallel = R$ and an ancillary relationship between R and ω is used to obtain n_0 and k_0. A suitable method is based on the Kramers–Kronig (KK) dispersion relation.

The equations relevant at normal incidence are

$$n_0 = \frac{1-R}{1+R-2R^{1/2}\cos\phi} \tag{1}$$

and

$$k_0 = \frac{-2R^{1/2}\sin\phi}{1+R-2R^{1/2}\cos\phi}. \tag{2}$$

These follow directly from the Fresnel reflectance equations if we express the complex reflection amplitude in the form $R^{1/2}\,e^{i\phi}$, where ϕ is the phase change on reflection. The dispersion relation between ϕ at a particular frequency ω_0 and the measured reflection coefficients may be expressed in the form (Bode 1945, p. 335)

$$\phi(\omega_0) = \frac{1}{\pi}\int_0^\infty \ln\left|\frac{\omega+\omega_0}{\omega-\omega_0}\right| \frac{d}{d\omega}(\ln R_\omega{}^{1/2})\,d\omega. \tag{3}$$

The difficulties associated with this method are well known. Calculations based on the considerations of the foregoing sections show that values of n_0 and k_0 obtained by the KK method are subject to large inherent errors.

'Normal incidence' measurements are made at angles as high as 12° (Kress and Lapeyre 1970); at these angles it is assumed $R_{\perp}=R_{\parallel}$. For $\theta=12°$, figure 3 shows that for a small change in reflection coefficient ($\Delta R=\pm 0{\cdot}001$) there is a large error in the product n_0k_0. This means that the measured reflection coefficients are insensitive to the values of n_0 and k_0. The following numerical example will emphasize this fact.

When $n_0=2{\cdot}00$ and $k_0=3{\cdot}00$, the values of $R_{\perp}$ and $R_{\parallel}$ at $\theta=12°$ are 0·563 and 0·548 respectively. If we assume $\Delta R=\pm 0{\cdot}001$, $R_{\perp}$ and $R_{\parallel}$ may become, as an extreme example, 0·564 and 0·547 respectively, and the resulting values of n_0 and k_0 will be 0·760 and 1·934. The corresponding value of σ expressed as a percentage is 76%, which shows that a change in n_0 and k_0 of this size will not change the value of the reflection coefficients by more than the uncertainty ΔR. Hence, there is a host of n_0 and k_0 values contained within the range determined by ΔR and therefore the substitution of measured reflection coefficients into equations (1), (2) and (3) are likely to lead to erroneous values of n_0 and k_0. The same calculation performed at $\theta=74°$ gives σ, expressed as a percentage equal to 2·7%.

6. Conclusions

The angular dependence of the errors in optical constants ($1{\cdot}0\leqslant n_0\leqslant 4{\cdot}0$, $1{\cdot}0\leqslant k_0\leqslant 4{\cdot}0$) obtained from reflectance measurements has been determined, and shown to be large for angles well removed from the optimum region about 74°. In particular, it has been shown that reflectances measured at near normal incidence are inherently insensitive to wide variations in n_0 and k_0. This insensitivity may be a contributory factor to the wide discrepancies observed between the results obtained by near normal incidence and other methods for optical constants (Robin 1966, p. 208).

Acknowledgments

We wish to thank the Science Research Council for an SRC studentship awarded to one of us (AJT).

References

Bode, H. W., 1945, *Network Analysis and Feedback Amplifier Design* (New York: Van Nostrand).
Kress, K. A., and Lapeyre, G. J., 1970, *J. Opt. Soc. Am.*, **60**, 1681–4.
Miller, R. F., Taylor, A. J., and Julien, L. S., 1970, *J. Phys.* D: *Appl. Phys.*, **3**, 1957–61.
Querry, M. R., 1969, *J. Opt. Soc. Am.*, **59**, 876–7.
Robin, S., 1966, *Optical Properties of Metals and Alloys*, ed. F. Abelès (Amsterdam: North Holland).

J. Phys. D: Appl. Phys., 1971, Vol. 4. Printed in Great Britain

Optical constants of thin films by an optimized reflection ratio method

R. F. MILLER and A. J. TAYLOR

Department of Physics, Royal Holloway College, University of London, Englefield Green, Surrey

MS. received 3rd May 1971

Abstract. A new method for determining optical constants n and k, for thin absorbing films supported by a dielectric substrate, has been devised. Measurement of the ratio of two reflection coefficients $R_{\parallel}/R_{\perp}$ is made at two angles of incidence, and the film thickness d is determined independently. Optimum angles of incidence for experimental measurement have been determined for $1{\cdot}0 \leqslant n \leqslant 4{\cdot}0$ and $1{\cdot}0 \leqslant k \leqslant 4{\cdot}0$ for many optical film thicknesses d/λ in the range $0{\cdot}01 \leqslant d/\lambda \leqslant 0{\cdot}25$. The method, when used at these optimum angles, yields n and k accurate to $\pm 0{\cdot}05$ for values of $d/\lambda \geqslant 0{\cdot}05$, providing angles are measured to better than $\pm 0{\cdot}1°$, reflection ratios are measured to better than $\pm 0{\cdot}01$ and values of d/λ are measured to better than $\pm 0{\cdot}005$.

1. Introduction

The refractive index n and extinction coefficient k ($n-ik$ is the complex refractive index) of a metal may be obtained from measurements of the ratio of the reflection coefficients $R_{\parallel}$ and $R_{\perp}$ for incident light polarized respectively parallel and perpendicular to the plane of incidence (Avery 1952). Avery's analysis can only be directly applied to reflection at a single interface, so that the method is only useful for bulk specimens or films which are sufficiently thick for internal multiple reflections to be negligible. The experimental method has, however, certain distinct advantages over other methods involving reflection, notably:

(i) No absolute measurements of light intensity are required, provided that the components of light incident on the polarizer in the two planes of polarization are equal or in a known ratio. This can be arranged by a suitable depolarizer (Portigal 1969) or an initial calibration.

(ii) No errors are introduced if the specimen becomes the limiting aperture at high angles of incidence, because the aperture is the same for both components of polarization.

(iii) There is little restriction on the wavelength of the light used, because quarter-wave plates and compensators are unnecessary. Polarizers are now obtainable to cover most parts of the optical spectrum, from ultraviolet to infrared (Heath 1967, 1968).

Although the method does not have the same accuracy as ellipsometry (Avery quoted n and k to 4%), the experimental simplicity, and the advantages mentioned above, make it worth investigating for possible application to thin films. We have used optimization techniques to show that the method is usable even when the experimental accuracy is only modest. Assuming the ratio $R_{\parallel}/R_{\perp}$ can be measured to within $\pm 0{\cdot}01$ at certain optimum angles of incidence, and the film thickness measured to within ± 2 nm, then n and k ($1{\cdot}0 \leqslant n \leqslant 4{\cdot}0$, $1{\cdot}0 \leqslant k \leqslant 4{\cdot}0$) can be determined to within $\pm 0{\cdot}05$ for many film thicknesses.

2. Application of the reflection ratio method to thin films

Avery quotes an expression for the ratio $R_{\parallel}/R_{\perp}$ in terms of the optical constants n and k and the angle of incidence θ. Curves relating $R_{\parallel}/R_{\perp}$ to n and k are then drawn for three

angles of incidence chosen so that measurements of $R_{\parallel}/R_{\perp}$ are made on both sides of the pseudo-Brewster angle for the material. From these curves possible n and k values can be obtained, which are then plotted with n and k as axes. Three curves result which should, theoretically, intersect at a point, the coordinates of which are the optical constants of the material.

For films thin enough for multiple internal reflections to make a significant contribution to the reflected light it is no easy matter to derive an expression for $R_{\parallel}/R_{\perp}$. Instead, separate expressions for $R_{\parallel}$ and $R_{\perp}$ must be obtained and the ratio formed. There are some ways of deriving expressions for $R_{\parallel}$ and $R_{\perp}$ at non-normal incidence for thin films on a dielectric substrate situated in air (Heavens 1955). One such method, which gives equations for $R_{\parallel}$ and $R_{\perp}$ easily coded into FORTRAN IV computer language, is that of 'resultant waves' described by Heavens (1955, pp. 59–62). Hadley and Dennison (1947) have used this method to obtain expressions for $R_{\parallel}$ and $R_{\perp}$ in terms of the optical constants of the film, the geometrical film thickness, the refractive index of the dielectric substrate, the angle of incidence and the wavelength of the incident light. Our equations for $R_{\parallel}$ and $R_{\perp}$ derived by this method are slightly less cumbersome, but similar to those of Hadley and Dennison, and are therefore omitted.

In deriving $R_{\parallel}$ and $R_{\perp}$ the following assumptions were made:

(i) The film is optically isotropic, with a plane reflecting surface.
(ii) The supporting dielectric substrate has negligible absorption and a thickness much greater than the film.
(iii) There is no difference between the wavelength of the incident and reflected light.
(iv) The optical constants of the film are independent of the angle of incidence.

The final equations for $R_{\parallel}$ and $R_{\perp}$ were written in terms of derived quantities expressed as functions of the following:

(i) The refractive index of the medium in which the incident light travels (air of refractive index 1·00).
(ii) The optical constants n_2, k_2 of the film.
(iii) The optical thickness d/λ (d is the geometrical film thickness, λ is the wavelength of the incident light).
(iv) The angle of incidence θ.
(v) The refractive index of the substrate, used in subsequent experimental work (glass of refractive index 1·51).

In an experimental investigation of the thickness dependence of n_2 and k_2 it is necessary to produce many curves of the Avery type, and in view of the laborious task of drawing these by hand a computer program was evolved so that the curves could be drawn automatically by a computer plotter (Calcomp version). The program generated curves of n_2 against the ratio $R_{\parallel}/R_{\perp}$ with k_2 as a parameter, for constant θ and d/λ. Values used in the program were $1{\cdot}0 \leqslant n_2 \leqslant 3{\cdot}5$, $1{\cdot}0 \leqslant k_2 \leqslant 3{\cdot}5$, $0{\cdot}010 \leqslant d/\lambda \leqslant 0{\cdot}200$ and any value of θ in the range $0° < \theta \leqslant 88{\cdot}0°$. Portions of two Calcomp curves generated for $d/\lambda = 0{\cdot}164$ and for $\theta = 61{\cdot}3°$ and $\theta = 81{\cdot}3°$ are shown in figures 1 and 2. Such plots are drawn to a scale of about 1 m × 1·5 m so that graphical error is practically eliminated.

Our experimental procedure is the same as that adopted by Avery, except that, by determining the two angles of incidence at which measurements may be most sensitively made, further measurements at a third angle are rendered unnecessary. The film thickness d is determined by multiple beam interferometry.

3. The optimum angles of incidence

Humphreys-Owen (1961) investigated the arithmetical sensitivity of Avery's method to changes in the optical constants, and produced a sensitivity diagram in which $(R_{\parallel}/R_{\perp})_{\theta=60°}$ was plotted against $(R_{\parallel}/R_{\perp})_{\theta=80°}$, with n and k as parameters. Such a diagram may be used quantitatively to investigate the sensitivity of $R_{\parallel}/R_{\perp}$ to changes in n_2 and k_2 for thin

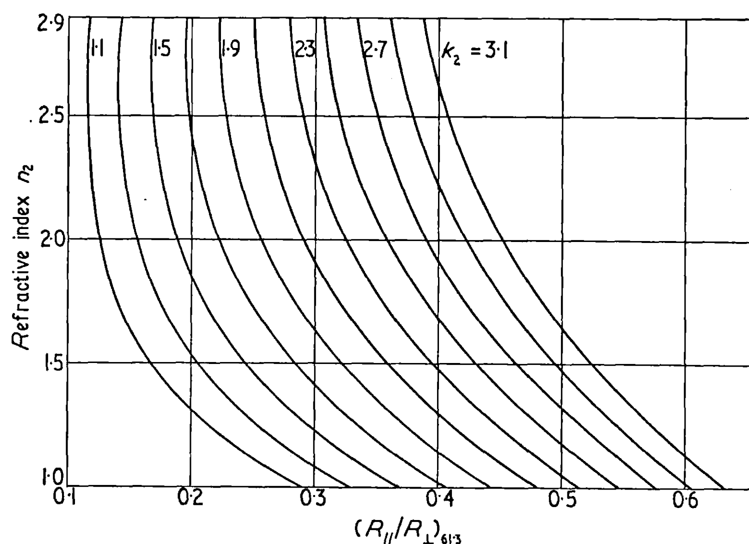

Figure 1. Portion of Calcomp curves relating $R_{\parallel}/R_{\perp}$ to n_2 and k_2 for $d/\lambda=0{\cdot}164$, $\theta=61{\cdot}3°$.

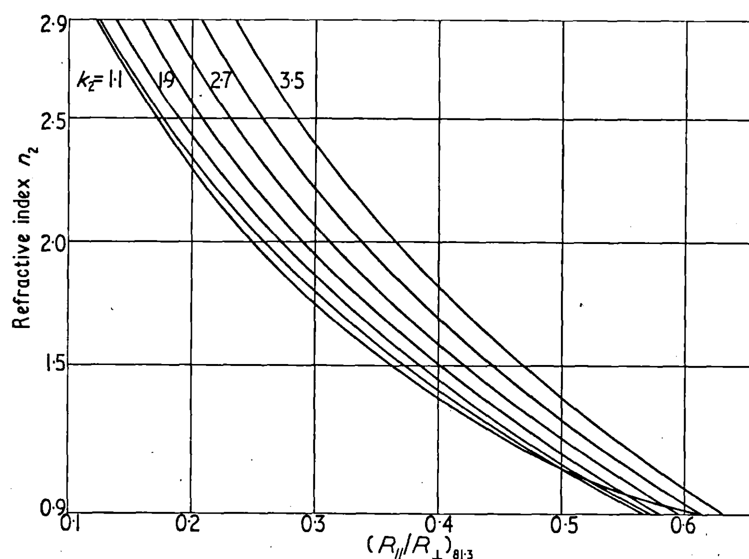

Figure 2. Portion of Calcomp curves relating $R_{\parallel}/R_{\perp}$ to n_2 and k_2 for $d/\lambda=0{\cdot}164$, $\theta=81{\cdot}3°$.

films. Figure 3 shows an enlarged portion of a sensitivity diagram ($R_{\parallel}/R_{\perp}$ plotted for two arbitrary angles of incidence θ_1 and θ_2) for constant d/λ. Point P has coordinates (n_2, k_2), the optical constants of interest, and lies within the quadrilateral formed by the following lines: constant $n_2+0{\cdot}05$, constant $k_2+0{\cdot}05$, constant $n_2-0{\cdot}05$ and constant $k_2-0{\cdot}05$. It is assumed that the sides of the quadrilateral are linear over these small changes in n_2 and k_2. The area enclosed by the quadrilateral is a measure of the sensitivity of the ratios $(R_{\parallel}/R_{\perp})_{\theta_1}$ and $(R_{\parallel}/R_{\perp})_{\theta_2}$ to the optical constants in the vicinity of n_2 and k_2. A region of good sensitivity is, therefore, one in which large changes in the two reflection ratios produce changes of only $\pm 0{\cdot}05$ in n_2 and k_2; that is, the area of the quadrilateral is large.

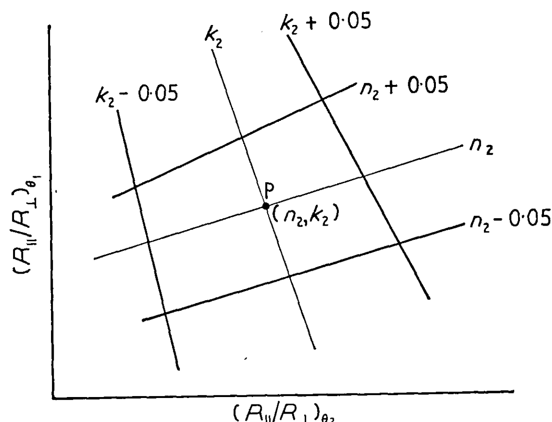

Figure 3. Basis of calculating the optimum angles of incidence for a fixed d/λ.

Coordinate geometry gives a formula for the area of such a quadrilateral in terms of the coordinates of the apices. This formula was used in a computer program to calculate the areas of quadrilaterals for all combinations of θ_1 and θ_2 ($45{\cdot}0° \leqslant \theta_1 \leqslant 65{\cdot}0°$, $66{\cdot}0° \leqslant \theta_2 \leqslant 88{\cdot}0°$) for fixed values of n_2, k_2 and d/λ. These latter values were chosen from the ranges $1{\cdot}0 \leqslant n_2 \leqslant 4{\cdot}0$, $1{\cdot}0 \leqslant k_2 \leqslant 4{\cdot}0$ and $0{\cdot}010 \leqslant d/\lambda \leqslant 0{\cdot}250$. A computer sorting technique was used, for each fixed value of n_2, k_2 and d/λ, to find the combination of θ_1 and θ_2 which generated a quadrilateral with the largest area. Thus, for each n_2, k_2 and d/λ investigated, two optimum angles of incidence were obtained at which to measure the ratios $(R_{\parallel}/R_{\perp})_{\theta_1}$ and $(R_{\parallel}/R_{\perp})_{\theta_2}$. For each of these optimum angles of incidence a computer subroutine calculated the precision to which angular measurements should be made to obtain n_2 and k_2 to an accuracy of better than $\pm 0{\cdot}05$. Tables 1 and 2 show values of optimum angles of incidence and the necessary setting precisions, for some integer values of n_2 and k_2, for $d/\lambda = 0{\cdot}050$ and $d/\lambda = 0{\cdot}100$.

A study of a number of such tables revealed the following trends:

(i) There is appreciable variation of the optimum angles with n_2 and k_2 for a fixed value of d/λ.

(ii) There is little variation of the optimum angles with d/λ for $n_2 \leqslant 2{\cdot}0$; the variation becomes more marked for $n_2 > 2{\cdot}0$.

Table 1. Values of optimum angles and angular setting precision for $d/\lambda = 0{\cdot}050$

n_2	k_2	θ_1 (deg)	θ_2 (deg)	$\pm\Delta\theta_1$ (deg)	$\pm\Delta\theta_2$ (deg)
1·0	1·0	46·3	76·7	0·7	0·5
1·0	2·0	50·9	80·5	0·5	0·3
1·0	3·0	57·4	82·5	0·4	0·2
1·0	4·0	63·1	83·8	0·3	0·1
2·0	1·0	49·6	81·6	0·6	0·3
2·0	2·0	54·5	83·3	0·5	0·2
2·0	3·0	59·7	84·3	0·4	0·1
2·0	4·0	64·3	85·2	0·2	<0·1
3·0	1·0	55·0	85·5	0·9	0·2
3·0	2·0	59·4	85·9	0·4	0·1
3·0	3·0	63·1	86·2	0·3	<0·1
3·0	4·0	65·0	86·4	0·2	<0·1
4·0	1·0	62·3	87·1	0·2	0·1
4·0	2·0	64·0	87·5	0·3	<0·1
4·0	3·0	65·0	86·6	0·1	<0·1
4·0	4·0	65·0	86·7	<0·1	<0·1

Table 2. Values of optimum angles and angular setting precision for $d/\lambda=0{\cdot}100$

n_2	k_2	θ_1 (deg)	θ_2 (deg)	$\pm\Delta\theta_1$ (deg)	$\pm\Delta\theta_2$ (deg)
1·0	1·0	46·1	76·0	0·8	0·5
1·0	2·0	50·7	79·7	0·6	0·3
1·0	3·0	58·5	82·1	0·3	0·2
1·0	4·0	64·4	83·6	0·2	0·1
2·0	1·0	50·0	81·6	0·2	0·3
2·0	2·0	54·0	82·6	0·4	0·2
2·0	3·0	59·4	83·7	0·3	0·1
2·0	4·0	64·3	84·6	0·2	0·1
3·0	1·0	56·1	84·4	0·1	0·1
3·0	2·0	57·3	84·4	0·3	0·1
3·0	3·0	61·1	84·9	0·3	0·1
3·0	4·0	64·8	85·0	0·2	0·1
4·0	1·0	57·0	84·5	0·2	0·1
4·0	2·0	59·1	85·2	0·3	0·1
4·0	3·0	62·6	86·0	0·2	<0·1
4·0	4·0	65·0	86·1	<0·1	<0·1

(iii) In general, the higher angle of incidence requires a better setting precision than the lower. A greater degree of precision is required for both angles of incidence for the larger values of n_2 and k_2 ($n_2 \gtrsim 3{\cdot}0$, $k_2 \gtrsim 3{\cdot}0$).

(iv) As d/λ increases, the required angular setting precision becomes smaller. For $d/\lambda > 0{\cdot}150$, it appears that angles of incidence measured to within $\pm 0{\cdot}3^\circ$ do not cause errors in n_2 and k_2 of greater than $\pm 0{\cdot}05$. (Avery estimated $\pm 0{\cdot}5^\circ$ as a suitable tolerance.)

(v) For $d/\lambda \lesssim 0{\cdot}150$, greater precision is required for the angular measurements. We estimate that if the optimum angles of incidence can be measured to better than $\pm 0{\cdot}1^\circ$ then this should produce changes in n_2 and k_2 of less than $\pm 0{\cdot}05$.

4. The precision required for measurements of d/λ

We have estimated that it should be possible, using multiple beam interferometry, to measure the optical thickness d/λ to within $\pm 0{\cdot}005$. Assuming the wavelength of the incident light is known precisely, the above tolerance corresponds to an error in the film thickness d of between 2 nm and 3 nm, for the visible range of wavelengths.

A computer program was written to determine the values of d/λ for which the tolerance of $\pm 0{\cdot}005$ was insufficient to make errors in n_2 and k_2 fall outside the limits $\pm 0{\cdot}05$. Values of $1{\cdot}0 \leqslant n_2 \leqslant 4{\cdot}0$ and $1{\cdot}0 \leqslant k_2 \leqslant 4{\cdot}0$ were investigated for a number of optimum angles of incidence. For a chosen value of d/λ the computer calculated, for a fixed optimum angle θ, n_2 and k_2, the difference Δ_1 given by

$$\Delta_1 = \left| \left(\frac{R_\parallel(d/\lambda)}{R_\perp(d/\lambda)}\right)_{\theta,n_2,k_2} - \left(\frac{R_\parallel(d/\lambda \pm 0{\cdot}005)}{R_\perp(d/\lambda \pm 0{\cdot}005)}\right)_{\theta,n_2,k_2} \right|. \qquad (1)$$

For the fixed θ, n_2 and k_2 and the chosen value of d/λ, the difference Δ_2 given by equation (2) was also calculated:

$$\Delta_2 = \left| \left(\frac{R_\parallel(n_2, k_2)}{R_\perp(n_2, k_2)}\right)_{\theta,d/\lambda} - \left(\frac{R_\parallel(n_2 \pm 0{\cdot}05, k_2 \pm 0{\cdot}05)}{R_\perp(n_2 \pm 0{\cdot}05, k_2 \pm 0{\cdot}05)}\right)_{\theta,d/\lambda} \right|. \qquad (2)$$

The quantities Δ_1 and Δ_2 were then compared: if Δ_1 was computed to be greater than Δ_2 then an accuracy better than $\pm 0{\cdot}005$ was required in the measurement of d/λ; if Δ_1 was computed to be less than Δ_2 then the tolerance of $\pm 0{\cdot}005$ was deemed sufficient.

The computer results showed that, for measurements at the optimum angles of incidence, the tolerance of $\pm 0{\cdot}005$ for d/λ was insufficiently accurate for values of $d/\lambda \lesssim 0{\cdot}050$. This

was true for between 85% and 95% of the combinations of n_2 and k_2 investigated, depending on the value of d/λ. For values of $d/\lambda > 0{\cdot}050$ the above tolerance was found to be sufficiently accurate for $1{\cdot}0 \leqslant n_2 \leqslant 4{\cdot}0$ and $1{\cdot}0 \leqslant k_2 \leqslant 4{\cdot}0$.

5. The precision required for measurement of the ratio $R_{\parallel}/R_{\perp}$

The two ratios $(R_{\parallel}/R_{\perp})_{\theta 1}$ and $(R_{\parallel}/R_{\perp})_{\theta_2}$ at optimum angles of incidence θ_1 and θ_2 should be capable of being measured to within $\pm 0{\cdot}01$. The computer program, which calculated the optimum angles of incidence, also produced values of the necessary tolerances of the two ratios at those angles, in order to achieve errors in n_2 and k_2 of $\pm 0{\cdot}05$. Tables 3 and 4 show these tolerances, denoted by $\pm \Delta(R_{\parallel}/R_{\perp})_{\theta_1}$ and $\pm \Delta(R_{\parallel}/R_{\perp})_{\theta_2}$, for $d/\lambda = 0{\cdot}050$ and 0·100 respectively. Similar tables were produced for other values of d/λ in the range $0{\cdot}050 \leqslant d/\lambda \leqslant 0{\cdot}250$. From these tables it was found that for $1{\cdot}0 \leqslant n_2 \lesssim 3{\cdot}0$ and $1{\cdot}0 \leqslant k_2 \leqslant 4{\cdot}0$, a tolerance of $\pm 0{\cdot}01$ in the measured reflection ratios was sufficient to yield both n_2 and k_2

Table 3. Tolerances in the reflection ratios, at optimum angles θ_1 and θ_2 shown in table 1, $\Delta(R_{\parallel}/R_{\perp})_{\theta_1}$, $\Delta(R_{\parallel}/R_{\perp})_{\theta_2}$ for $d/\lambda = 0{\cdot}050$

n_2	k_2	$\pm \Delta(R_{\parallel}/R_{\perp})_{\theta_1}$	$\pm \Delta(R_{\parallel}/R_{\perp})_{\theta_2}$
1·0	1·0	0·023	0·025
1·0	2·0	0·017	0·014
1·0	3·0	0·015	0·012
1·0	4·0	0·015	0·013
2·0	1·0	0·014	0·014
2·0	2·0	0·010	0·010
2·0	3·0	0·010	0·010
2·0	4·0	0·010	0·009
3·0	1·0	0·011	0·011
3·0	2·0	0·010	0·008
3·0	3·0	0·007	0·007
3·0	4·0	0·006	0·007
4·0	1·0	0·009	0·010
4·0	2·0	0·007	0·007
4·0	3·0	0·006	0·006
4·0	4·0	0·004	0·005

Table 4. Tolerances in the reflection ratios, at optimum angles θ_1 and θ_2 shown in table 2, $\Delta(R_{\parallel}/R_{\perp})_{\theta_1}$, $\Delta(R_{\parallel}/R_{\perp})_{\theta_2}$ for $d/\lambda = 0{\cdot}100$

n_2	k_2	$\pm \Delta(R_{\parallel}/R_{\perp})_{\theta_1}$	$\pm \Delta(R_{\parallel}/R_{\perp})_{\theta_2}$
1·0	1·0	0·031	0·025
1·0	2·0	0·022	0·017
1·0	3·0	0·018	0·015
1·0	4·0	0·016	0·013
2·0	1·0	0·015	0·013
2·0	2·0	0·011	0·011
2·0	3·0	0·012	0·010
2·0	4·0	0·012	0·009
3·0	1·0	0·006	0·007
3·0	2·0	0·006	0·006
3·0	3·0	0·007	0·006
3·0	4·0	0·008	0·007
4·0	1·0	0·003	0·002
4·0	2·0	0·004	0·005
4·0	3·0	0·005	0·005
4·0	4·0	0·006	0·005

within $\pm 0{\cdot}05$ for all $0{\cdot}050 \leqslant d/\lambda \leqslant 0{\cdot}250$. For $3{\cdot}0 < n_2 \leqslant 4{\cdot}0$, measurement of each ratio to $\pm 0{\cdot}005$ would be sufficient to allow n_2 and k_2 to be determined within $\pm 0{\cdot}05$ for most values of n_2, k_2 and d/λ. It is interesting to note that for both reflection ratios the required tolerance is about the same.

Further calculations showed that for $d/\lambda \gtrsim 0{\cdot}150$ the values of the two ratios $(R_{\parallel}/R_{\perp})_{\theta_1}$ and $(R_{\parallel}/R_{\perp})_{\theta_2}$, calculated at the optimum angles of incidence from the single reflection formula (Avery 1952) and the multiple reflection formula (Hadley and Dennison 1947), differed by less than $0{\cdot}005$ for $1{\cdot}0 \leqslant n_2 \leqslant 4{\cdot}0$ and $2{\cdot}5 < k_2 \leqslant 4{\cdot}0$. The same order of difference was found for $1{\cdot}0 \leqslant k_2 \lesssim 2{\cdot}5$ and for optical thicknesses $d/\lambda \gtrsim 0{\cdot}230$.

6. Conclusion

Avery's (1952) method for obtaining the optical constants of a reflecting surface has been extended for use with thin films supported by thick dielectric substrates. If approximate values of the optical constants are known, then optimum angles of incidence may be chosen at which to perform the reflection measurements.

The new method has been investigated for $1{\cdot}0 \leqslant n_2 \leqslant 4{\cdot}0$, $1{\cdot}0 \leqslant k_2 \leqslant 4{\cdot}0$ and $0{\cdot}01 \leqslant d/\lambda \leqslant 0{\cdot}250$ and will yield n_2 and k_2 to an accuracy of $\pm 0{\cdot}05$ if measurements are obtained within the following tolerances:

(i) Angles of incidence measured to better than $\pm 0{\cdot}1°$.
(ii) Optical thicknesses ($\geqslant 0{\cdot}050$) measured to better than $\pm 0{\cdot}005$.
(iii) Reflection ratios measured to better than $\pm 0{\cdot}005$ for all n_2 and k_2 in the range considered, but if $n_2 \lesssim 3{\cdot}0$ measurement to $\pm 0{\cdot}01$ is sufficient.

Furthermore, instead of Hadley and Dennison's formula, Avery's formula may be used at the required optimum angles for the following values of n_2, k_2 and d/λ:

(i) Optical thicknesses $d/\lambda \gtrsim 0{\cdot}150$, $1{\cdot}0 \leqslant n_2 \leqslant 4{\cdot}0$, $2{\cdot}5 < k_2 \leqslant 4{\cdot}0$.
(ii) Optical thicknesses $d/\lambda \gtrsim 0{\cdot}230$, $1{\cdot}0 \leqslant n_2 \leqslant 4{\cdot}0$, $1{\cdot}0 \leqslant k_2 \lesssim 2{\cdot}5$.

Acknowledgments

We wish to thank the Science Research Council for a Postgraduate Studentship awarded to one of us (AJT).

References

AVERY, D. G., 1952, *Proc. Phys. Soc.* B, **65**, 425–8.
HADLEY, L. N., and DENNISON, D. M., 1947, *J. Opt. Soc. Am.*, **37**, 451–65.
HEATH, D. F., 1967, *Instrums exp. Tech.* (USA), **4**, 930–1.
—— 1968, *Appl. Opt.*, **7**, 455–9.
HEAVENS, O. S., 1955, *Optical Properties of Thin Solid Films* (London: Butterworth).
HUMPHREYS-OWEN, S. P. F., 1961, *Proc. Phys. Soc.*, **77**, 949–57.
PORTIGAL, D. L., 1969, *Appl. Opt.*, **8**, 838–9.